Characterisation of Elastomers for Dynamic Sealing Applications

Barnabas Harvey Keelan Shaw

Submitted in partial fulfilment of the requirements of the Degree of Doctor of Philosophy.

I.   ABSTRACT

One of the most extreme applications for elastomer materials is in sealing applications within the oil and gas sector. These applications often feature high strains, high strain rates, wide temperature ranges, contact with water and organic solvent mixes all of which can take place at large pressures. Attempting to understand and model just one of these effects would be difficult enough but to understand their full complexity when they are all acting in parallel is even more challenging. However, this thesis aims to lay the foundational work to build an all-encompassing model to help understand the behaviour of the elastomer materials that are found in mud motor stators.

The work presented here focusses on material characterisation, static fracture and cyclic fatigue analysis over a range of temperatures together before and after ageing at high temperatures and in organic solvents. The materials used are typical compound formulations used in the oil and gas industry that use hydrogenated acrylonitrile butadiene rubber (HNBR) as the base polymer. However, there is only limited published research on the response of HNBR compounds to the extreme environments that are seen in these applications, their fatigue and tear behaviour and in particular the origins of their high levels of mechanical toughness.

This thesis develops appropriate material characterisation models and then explores the different cyclic fatigue properties for both unaged and aged samples. This shows a complicated fatigue response frequently incorporating an increase in toughness after ageing. By examining changes to the hysteresis with ageing as well as changes to tearing type crack growth behaviour and by utilising X-ray diffraction techniques, it is possible to start to propose possible mechanisms that explain the surprisingly good performance of HNBR compounds in these types of extreme environment.

II. DECLARATION

I, Barnabas Shaw, confirm that the research included within this thesis is my own work or that where it has been carried out in collaboration with, or supported by others, that this is duly acknowledged below and my contribution indicated. Previously published material is also acknowledged below.

I attest that I have exercised reasonable care to ensure that the work is original, and does not to the best of my knowledge break any UK law, infringe any third party's copyright or other Intellectual Property Right, or contain any confidential material.

I accept that the College has the right to use plagiarism detection software to check the electronic version of the thesis.

I confirm that this thesis has not been previously submitted for the award of a degree by this or any other university.

The copyright of this thesis rests with the author and no quotation from it or information derived from it may be published without the prior written consent of the author.

Signature:

Date: **01/11/19**

CONFERENCE PROCEEDINGS

POSTER PRESENTATIONS

RUBBERCON 2016, June 2016, Tampere, Finland

International Rubber Conference 2016, October 2016, Kitakyushu, Japan

ORAL PRESENTATIONS

North European PhD Seminar Conference 2017, May 2017, Dresden, Germany

10th European Conference on Constitutive Models for Rubbers (ECCMR X), September 2017, Munich, Germany

International Rubber Conference 2017, October 2017, Cleveland, USA

International Rubber Conference 2018, September 2018, Kuala Lumpur, Malaysia,

International Rubber Conference 2019, September 2019, London, England

III.   ACKNOWLEDGEMENTS

I would firstly like to thank Prof. James Busfield for his incredible supervision and support throughout my PhD journey. His combination of academic excellence, humour, patience and kindness are second to none and I am extraordinarily fortunate to have met and been supervised by him. Prof. Busfield enabled his whole research team including myself to travel, attend and take part in numerous scientific conferences in all parts the world. This provided me with an excellent experience of being part of the scientific community by sharing and discussing work with the current leading elastomeric researchers. This thesis would not have been possible without him and I cannot be more thankful.

My deepest thanks go to my sponsor company and team at Schlumberger Cambridge Research Centre for providing financially and intellectually to this project. A team that featured Dr Joachim Sihler, Dr Jakub Jarabek and Dr Julien Ramier. In particular, I want to thank Dr Ramier for his constant involvement in my project, concern for its direction and for help proof reading. I also want to thank Dr Claire Wilshaw for such generous supervision while working and spending time at the Cambridge Research Centre as well as helping proof reading. Finally, another particular thanks to Dr Samba Ba at Katy Research Centre whose knowledge of the application helped steer and ground this project tremendously.

My colleagues working the Soft Matter Group at Queen Mary University provided endless support both academically and as friends. I would not have enjoyed this project nearly as much without them. In particular I want to thank Dr Richard Windslow, Dr Yinping Tao and Dr Fransesca Carleo for not only being great friends to travel the world with, but also providing great support throughout the PhD process. My thanks also to Mr Travis Hohenberger and Mr William Kyei-Manu for proofreading this work.

Finally I want to thank my family and friends who have supported me without question throughout the whole process. There are too many to mention by name, however, without their company, friendship and prayers, I would not have managed to complete this course. Most importantly, I want to thank my mother, father, sister, brother in law and niece. My mother, father, and sister have loved and supported me every second of my 27 years of age. I could not be more fortunate to have them by my side. This is for them.

CONTENTS

IV. LIST OF ABBREVIATIONS

ACN	Acrylonitrile
ASTM	American Society of Testing and Materials
BOP	Blow-out preventer
CV	Conventional vulcanisation
DSC	Differential Scanning Calorimetry
EDS	Energy-Dispersive X-ray Spectroscopy
EV	Efficient vulcanisation
FEA	Finite Element Analysis
FFKM	Prefluorinated Elastomers
FKM	Fluorinated Elastomers
FTIR	Fourier Transform Infrared Spectroscopy
HNBR	Hydrogenated Acrylonitrile Butadiene Rubber
IR	Synthetic Polyisoprene
NBR	Nitrile Butadiene Rubber
NR	Natural Rubber
PHR	Parts per hundred rubber
QMUL	Queen Mary University of London
SBR	Styrene Butadiene Rubber
SEF	Stored Energy Function
SEV	Semi-efficient vulcanisation
SIC	Strain-Induced Crystallisation
TGA	Thermogravimetric Analysis
XRD	X-ray Diffraction

V. LIST OF SYMBOLS

A	Physical Creep Rate
A	Area
A_t	Crack growth constant for region 2
B	Chemical Creep Rate
B	Material Constant in region 3
B_s	Static material constant
b	Width
b	The number of active bonds per unit volume
C	Creep strain dependence of the effective creep strain rate
C_A	Arbitrary Constant
C_{10}	Yeoh Model Constant first order
C_{20}	Yeoh Model Constant second order
C_{30}	Yeoh Model Constant third order
c	Crack length
c	Centi
c_0	Additional amount of crack growth
Δc	Increment of crack growth per cycle
d	Diameter of a crack tip
d_b	Diameter of a strained crack tip
d_0	Minimum possible crack tip diameter
D	Diffusion coefficient
E	Constant
$erf(x)$	Function Error
F	Force
$f(t)$	Function of t
G	Shear Modulus
ΔG	Free energy change
g	Grams
ΔH	Change of Enthalpy

Hz	Hertz
h	Thickness of Specimen
h	Longitudinal length of a pure shear sample
I	Strain Invariant
J	Joule
J_b	Bond rupture energy
K	Kelvin
k	Boltsmann's Constant
k	Strain dependent term
k	Kilo
k_z	Rate constant due to ozone
kg	Kilograms
L	Distance between the clamped regions of a trouser test piece
l	Length
l_0	Unstrained distance between clamped region in a pure shear test
l_m	Length in a network
M	Mega
M_c	Average chain molecular weight
m	Metre
m	Stress dependence of the effective creep strain rate
m	Material Constant: Ogden Roxburgh model
mins	Minutes
dm	Amount of liquid
mm	Millimetre
N	Newton
N	Number of chains in a unit of volume
N	Number of Cycles
n	Number of chain links
$[O_3]$	Ozone concentration
Pa	Pascal

Q	Normalized Heat Flow
R	Steady-state fatigue crack growth rate per cycle
R_{gas}	Gas Constant
R_z	Crack growth rate in region 1
r	Distribution of distance between crosslinks
r	Material constant: Ogden Roxburgh model
r_t	Radius of a semi-circle
S	Entropy
ΔS	Change of Entropy
s	Second
T	Temperature
T	Tearing Energy
T_c	Critical Tearing energy
T_0	Threshold Tearing Energy
T_g	Glass Transition Temperature
t	Thickness
t	Time
dt	Increment of time
t_{90}	Time to 90% delta torque
ts2	Time at 2-point rise
U	Internal Energy
U_{dev}	Current deviatoric strain energy density
U_{dev}^m	Maximum deviatoric strain energy density
U_A	Elastic strain energy in region A
V	Volume
W	Elastically stored energy function
W_0	Minimum elastic stored energy
w_0	Width
x	Displacement
x	Arbitrary Constant

X	A letter describing the curing in carbon black nomenclature
Y	Mean particle diameter in carbon black nomenclature
ZZ	Structure of carbon black in carbon black nomenclature

GREEK ALPHABET AND OTHER

α	Angular Distance
β	Material Constant in region 3
β_s	Static material constant
°	Degree
°C	Degrees Celsius
λ	Stretch
ρ	Density
σ	Stress
ε_B^{cr}	Effective creep strain rate in Network B
λ_B^{cr} `	Normal creep strain in Network B
θ	Angle
ξ	Length of a molar unit
η	Damage Variable

VI.   LIST OF FIGURES

VII.   LIST OF TABLES

1. AIM OF THE STUDY

Downhole tools used in the oil and gas industry often encounter harsh and extreme environmental conditions. Rock formations and other difficulties such as drilling in areas where vertical access to the reservoir is difficult can often make it problematic to always drill vertically. One solution used by the oil and gas industry to overcome this is by using a directional drill known as a mud motor. These are positive displacement pumps that transfer fluid pressure into mechanical energy to turn a drill [Schlumberger, 2004]. These are placed in the drill string and subsequently often come into contact with these harsh conditions including high temperatures, mixtures of organic solvents and water, high pressures and either cyclic or static mechanical loads. Depending on the well they are used in and the motor driver, motors can fail within just a few days of use. Over 90% of these failures occur as a result of the failure of their elastomeric stator. There is a general lack of an accurate understanding of the mechanical forces in the elastomeric stator and how the elastomer behaves under these extreme mechanical and environmental conditions.

Some work has been published on positive displacement motor modelling such as that from [Zhang. J et al, 2014] and [Han. C et al, 2014] from South-West Petroleum University in China. These studies consider only the elastomeric stator and the research has significant short comings. The finite element modelling techniques used have simplistic constitutive equations for the materials which will struggle to capture the real environmental and mechanical effects that positive displacement motors experience. However, to tackle these problems is not a trivial task. For most elastomer products, the environmental and the mechanical properties are interconnected. In practice there are many coupled effects present in this problem, and a significant effort must be taken to analyse the interdependencies carefully.

As a result, the primary objective of this PhD project was to gain a greater understanding into these topics to build a foundation where improved elastomer models can be developed, and their failure modes can be better predicted and extended. To do this, suitable constitutive models must be derived that can start to predict and understand the behaviour of these elastomers under these conditions.

Chapter 2 begins by giving a brief overview of basic elastomer knowledge including natural and synthetic elastomers, how they are vulcanised, a basic understanding of elastic and viscoelastic

behaviour and how they are compounded with different additives to improve their performance. A basic conclusion and understanding on how each section connects to the oil and gas industry is given as the chapter develops.

Chapter 3 goes into more detail focusing on the behaviour that is of most interest in this study. These topics include the static and cyclic crack growth behaviour of elastomers and the various different ageing mechanisms. All of this work addresses the fatigue and ageing issues that arise when HNBR materials are used in a positive displacement motor. Detailed descriptions of the understanding of the strain energy release rate also known as the tearing energy and how to measure it are given together with a description of how it might be affected by temperature and elastomer compound composition. Descriptions of oxidation and other ageing mechanisms are also given. However, a key issue is that many of these studies have not been focussed on materials that are used for oil and gas applications. This justifies why this investigation into how cyclic crack growth behaviour and different ageing mechanisms affect Hydrogenated Acrylonitrile Butadiene Rubber (HNBR) materials is required at this time.

Chapter 4 provides the understanding how different tests on the materials have been undertaken. A detailed description of a positive displacement motor called a mud motor is given with a description of its operating conditions and failure modes. The typical oil and gas formulations used throughout this body of work are given together with details of their basic mechanical characterisation.

Chapter 5 investigates how four typical oil and gas HNBR elastomer formulations change their fatigue crack growth behaviour in response to different pre-ageing conditions including exposure to elevated temperatures and the presence of an organic solvent. The four materials are all characterised in fatigue also at elevated temperatures and after significant post curing. The results are then examined further through material characterisation techniques to investigate differences between the four formulations as well as the changes that are introduced by ageing.

Chapter 6 then extends the work further by probing in more detail the origin of the large mechanical toughening behaviour found in HNBR. This is done through a combination of a static tearing tests over a wide range of tearing rates and temperatures. This data is then used to further analyse the fatigue work in the previous chapter. Insight into how to exploit this

toughening behaviour is explored as well as trying to understand the detailed mechanism of the toughening by using x-ray diffraction.

Chapter 7 provides a concise summary and outline future work that is required to further extend and develop this work further.

2. INTRODUCTION TO ELASTOMERIC MATERIALS

The aim of this chapter is to provide a basic overview of elastomeric materials. This will cover their origins, common elastomeric materials and their ingredients and their basic elastic and viscoelastic nature. This will then lead to the next chapter which will go into more details about the specific elastomeric behaviours and research focused in this body of work.

2.1. ORIGIN

Since the discovery of the vulcanisation process, polymers that can exhibit large strain elasticity have become widely adopted in a wide variety of different applications in the automotive engineering, civil engineering and the oil and gas sectors to name a few. Polymers with exceptional abilities to elastically deform, in some cases, up to strains of 1000% and return to their original shapes are commonly called rubbers or elastomers. The word 'rubber' was originally used by the chemist Joseph Priestly in 1770 who noted that that this material could remove or "rub" pencil marks from paper [Memmler, 1934]. Therefore, the word rubber initially described any material demonstrating this type of behaviour. Today, rubber like materials have many diverse uses and rubber is commonly used to refer to many types of large strain elastic materials that have properties that are broadly similar to those of natural rubber.

Another term used to describe these types of material is elastomer. While this term is sometimes used to describe synthetic forms of rubbery materials, it is not restricted to that group as 'elastomer' describes any "macromolecular material which returns rapidly approximately to its initial dimensions and shape after substantial deformation by a weak stress and release of the stress." [ISO, 1382:2012, Rubber-Vocabulary, 2012]. In practice, a rubber has an additional requirement that it "can be modified to a state in which it is essentially insoluble (but can swell) in boiling solvent …. and which in its modified state cannot be easily remoulded to a permanent shape by the application of heat and moderate pressure." In practice this implies that a rubber must contain crosslinks whereas to be an elastomer this is not an essential requirement. However, in practice the terms rubber and elastomer are considered interchangeable. In some specific cases though for example there is a preference for specific wording such as when "rubber-like elasticity" is being used [Treloar. L. R. G, 1975].

The stress-strain response of elastomeric material in tension is distinctly non-linear as seen in figure 1.
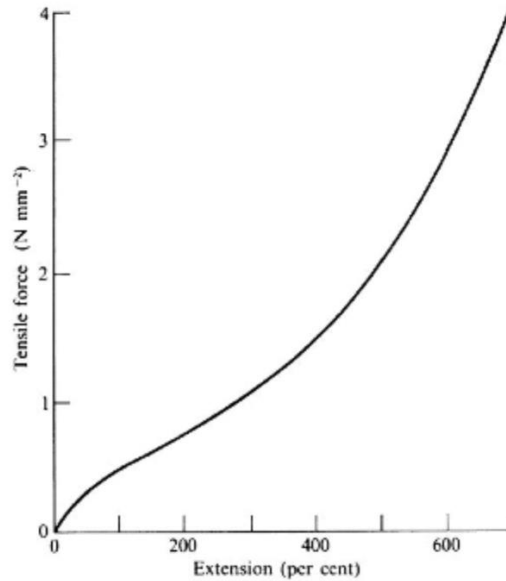
Figure 1: Force vs extension plot of natural rubber [Treloar. L.R.G, 1975]

Hooke's law therefore does not apply to these materials except at very small strains, for example at less than 1% strain. This means that descriptions of the behaviour that specify the Young's modulus have to be used at specific strains. By way of comparison the Young's modulus of a typical rubber materials at 1% strain would be about 1 Nmm^{-2} which is five orders of magnitude smaller than the value of 207 x 10^3 Nmm^{-2} measured for a typical steel.

2.2. NATURAL AND SYTHETIC RUBBERS

2.2.1. NATURAL RUBBER (NR)

Natural rubber is a hydrocarbon polymer predominantly composed of cis-1,4-polyisoprene except at the molecular chain ends. It is produced from the latex of the Hevea Brasiliensis tree. Certain preservatives are added to the latex before coagulation as stabilisers, for example, ammonia, formaldehyde and sodium sulphite. The macromolecules of NR have a stereo-regular structure that enable the polymer chains to form crystallites at low temperatures. These form at a maximum rate at approximately -25°C, a temperature above the glass transition temperature T_g that is approximately -70°C. NR also forms crystallites when undergoing strain, known as strain-induced crystallisation (SIC). This is a phenomenon not found in all types of rubber. However, rubbers that undergo SIC feature much higher tensile strength and crack growth resistance at large deformations [Allen. P, Jones. K, 1988].

There is also a synthetic version of polyisoprene (IR). The cis-1,4 microstructure is not as consistent as it is with NR, with the molecules having between 95% and 98% cis structure depending on whether it was produced anionically or by Ziegler-Natta polymerisation. However, IR features a lower tensile strength than NR probably due to an inhibition of the strain induced crystallisation.

2.2.2. SYTRENE BUTADIENE RUBBER (SBR)

First synthesised in Germany in the 1930s due to a shortage of NR, Styrene-Butadiene Rubber (SBR) is a copolymer of styrene and butadiene and is the most widely used synthetic elastomer. Typically tyre compounds contain approximately 23% styrene content. SBR is synthesised via free-radical polymerisation. Its T_g is approximately -55°C. Due to its random copolymer structure, it does not strain crystallise and has much weaker mechanical properties compared to NR. However, SBR is typically reinforced with fillers such as carbon black that reinforce its properties so it behaves similarly to NR. They are used in many engineering applications but most commonly in the tire industry.

2.2.3. ACRYLONITRILE-BUTADIENE RUBBER (NBR) AND HYDROGENATED NITRILE-BUTADIENE RUBBER (HNBR)

Acrylonitrile-Butadiene Rubber (NBR) is a copolymer of acrylonitrile (ACN) and 1,3-butadiene where the ACN content can be controlled and is often varied between 18%-50%. It was first manufactured by Konrad and Tshunkur through free radical emulsion polymerisation [Eduard. T, Erich. K, 1934]. Due to its acrylonitrile content and polar nature, NBR is often used in applications that require higher chemical resistance to oil and fuel. Increasing the ACN content increases the chemical and heat resistance, the strength and T_g but reduces the rebound resilience and gas permeability. It is often used in applications that require high levels of resistance to oil and fuel such as seals and hoses [Gent. A. N, 2001].

However, due to the unsaturation of butadiene, NBR can be susceptible to ageing though oxygen, ozone and heat attack. To counter these issues, NBR can be significantly hydrogenated to make a more expensive but more chemically inert material hydrogenated nitrile-butadiene rubber (HNBR) where the hydrogenation process makes the polymer typically 96% hydrogenated shown in figure 2. HNBR is used in similar applications to NBR; however, it can

be used in more demanding applications that require, for example, better tensile strength, elongation at break, and heat resistance, with maximum operating temperatures up to 150°C rather than 120°C for NBR. This makes HNBR a preferred choice for oil and gas applications, and specifically for this work, the mud motor stator.

The ability for HNBR to crystallise is a recent on going debate. The arguments for HNBR exhibiting crystallinity effect focus around its ACN content. As identified by [Hayashi, S, Sakakida, H, Oyama, M, and Nakagawa, T. 1991], at low ACN contents HNBR can consist of repeated units of tetramethylene spaced between the ACN units. Then developed by [Kobatake, T, Kodama, K, and Hayashi, S, 1997] who found that chains with five or more repeating units of tetramethylene allowed the ability for HNBR to strain crystallise, similarly to NR. By increasing ACN content, these units were spaced further from each other preventing crystallinity. The ability for high ACN HNBR materials to crystallise has also been investigated more recently by [Severe, G and White, J. L, 2000]. By using x-ray diffraction (XRD) and differential scanning calorimetry (DSC), they found that high ACN content HNBR materials formed crystals due to sequential tetramethylene and ACN units, forming ordered structures. This topic however is still under debate.
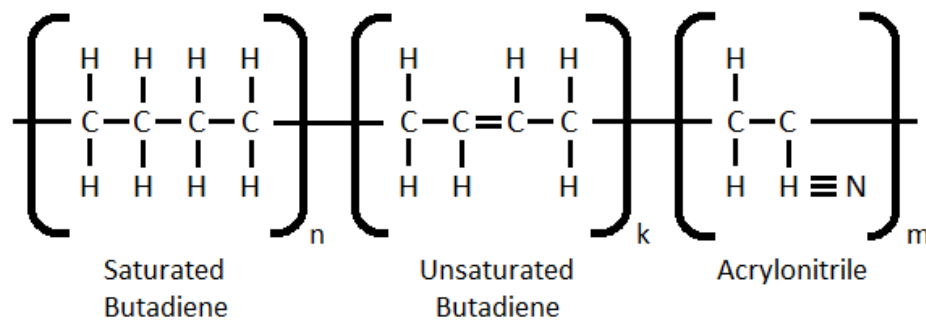
Figure 2: Chemical structure of HNBR. Adapted from [Windslow. R. J, 2018]

2.2.4. FLUOROELASTOMERS

Fluoroelastomers are a distinct class of elastomers that are designed for even more extreme applications. They are also typically more expensive however. Some examples of fluoroelastomers include FKM, FFKM and FEPM, all with engineered subtypes. They are made in an emulsion process to protect the carbon backbone with the large fluorine atoms.

Formulations vary on application; however a typical formulation involves the copolymerising of the fluorinated analogues of ethylene and propylene.

Fluoroelastomers have high resistance to thermal degradation (up to 300°C), high chemical ageing resistance, high resistance to nonpolar materials including oils and low gas permeability. These elastomers are used in oil and gas applications but due to their high price are only used for the most extreme applications.

2.3. VULCANISATION

Before elastomers can be used in an engineering application, they are mixed with different ingredients following specific compound formulations and then vulcanised. The process of vulcanisation, also known as curing or crosslinking, is a process by which chains are chemically linked together to form a three-dimensional network. Before crosslinking, they are referred to more often as a high molecular weight liquid. Polymer chains are physically entangled, however they can readily disentangle under the application of a stress and flow like a very viscous fluid. After vulcanisation, chemical crosslinks form that increase modulus and tensile strength of the whole system, whilst decreasing permanent set and hysteresis during loading.

Curing characteristics of an elastomer formulation can be measured using a rheometer. A typical curing response with helpful definitions can be seen in figure 3. This is done by placing an uncured elastomer sample in a heated and pressurised cavity, which contains a circular serrated disk. As the disk oscillates under the application of heat and pressure, the curing process starts. Throughout the cure cycle, the torque is measured with respect to time. The resulting graph indicates which of three types of curing: marching or creeping, plateau and reversion takes place. A plateau cure indicates that at t_{100}, the time it takes to reach 100% delta torque, the ratio of making and breaking chemical crosslinks is equal. A marching cure indicates that more crosslinks are being made than broken over extended time frames, and a reversion cure indicates more crosslinks are being broken than made. To avoid an undesired cure characteristic such as marching or reversion, materials are often cured to t_{90} which is the time it takes to reach 90% of delta torque. In practice the parts that are produced do not cool down immediately to room temperature the moment they are removed from the hot mould. So some additional curing always takes place after the part has been demoulded.

There are two main types of curing systems widely adopted in the rubber industry namely peroxide and sulphur cure systems.
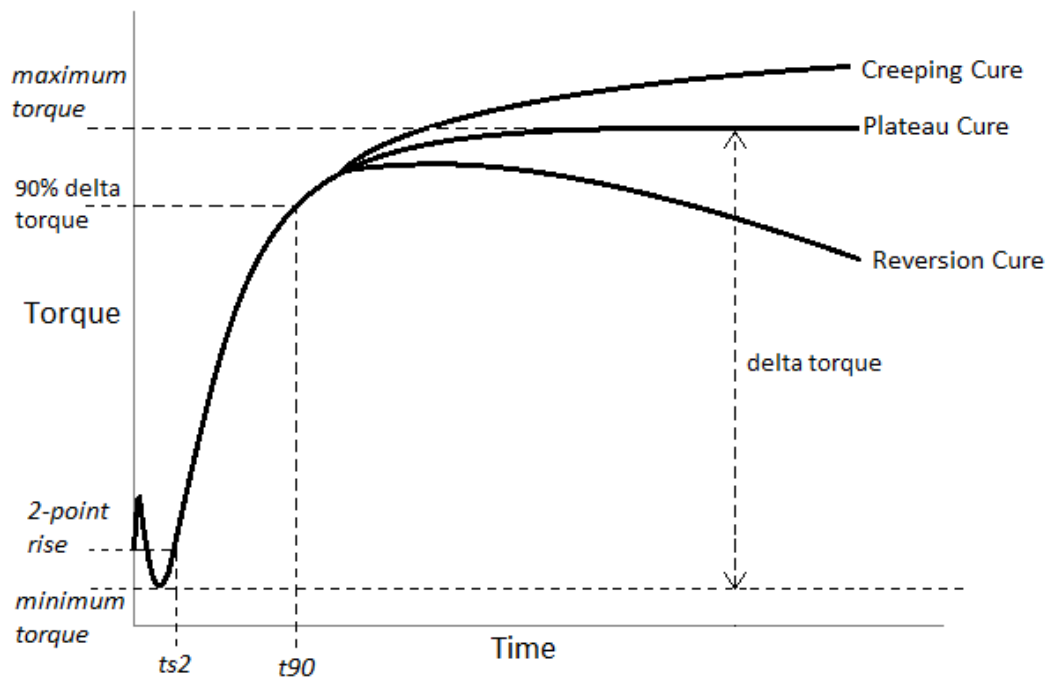
Figure 3: A typical rheometer response of uncured rubber. Adapted from [Dluzneski. P. R, 2001]

2.3.1 SULPHUR CURE

The most common curing system uses sulphur curing. Crosslinking with just sulphur is quite inefficient. For every crosslink, 40-55 sulphur atoms are combined with the rubber with structures ranging between polysulfide linkages, dangling sulphur fragments and cyclic sulphides. Some of the sulphur is not involved in crosslinking between polymer chains and leads to networks that are unstable and have poor ageing resistance. Therefore, three types of sulphur curing have been developed to manage the efficiency of vulcanisation using a ratio of sulphur to accelerators: efficient vulcanisation (EV), semi-efficient vulcanisation (SEV) and conventional vulcanisation (CV). As the amount of sulphur atoms per crosslink increases, the stability of the sulphur bond decreases. EV systems predominantly generate less sulphur atoms per crosslink and therefore generate sulphur bonds that are generally more stable and have a higher resistance to chemical and thermal ageing. CV systems on the other hand have less stable sulphur bonds that conversely enable the elastomer to have higher strength and fatigue

properties due to the flexibility of the polysulphide bonds and their ability to recombine under strain once yielded [A.N. Gent, 2012].

Despite sulphur cured elastomer featuring high levels of toughness, they often struggle to withstand high temperature and ageing environments. Therefore, they are predominantly used for applications requiring low resistance to these factors.

2.3.2 PEROXIDE CURE

A peroxide curing system builds carbon-carbon crosslinks within an elastomer via a free-radical mechanism. These systems can be used to cure saturated or unsaturated elastomers as well as diene elastomers. The process of peroxide curing can be summarized into three basic reactions: homolytic cleavage, hydrogen abstraction and radical coupling.

As strong carbon-carbon bonds are generated, this leads to an elastomer that shows good ageing resistance and low compression set. It is therefore often a preferred method of curing in the oil and gas industry due to its increased ability to resist high temperatures and ageing.

2.4. THERMODYNAMICS OF ELASTOMERS

In 1805 Gough first observed two thermoelastic phenomena in rubber that were:

1. Rubber retracts reversibly upon heating under constant load.
2. Rubber heats up on stretching and cools down when it is retracted.

These effects have come to be known as the Gough-Joule effect after Joule reconfirmed them in 1859 [Gough. J, 1805] [Joule. J.P, 1858].

Based on the first and second laws of thermodynamics, a statistical thermodynamic analysis has been developed to explain these thermoelastic effects. The first expression represents tension, F, as a sum of the change of internal energy, U, and change in entropy, S with a change in length l, at a specified temperature, T, and volume, V:

$$F = \left(\frac{\partial U}{\partial l}\right)_{T,V} - T\left(\frac{\partial S}{\partial l}\right)_{T,V} \tag{2.1}$$

The entropy change per unit length can be found experimentally by finding the force whilst varying the temperature and keeping the length constant:

$$\left(\frac{\partial S}{\partial l}\right)_{T,V} = -\left(\frac{\partial F}{\partial T}\right)_{L,V} \tag{2.2}$$

The combination of Equation 2.1 and 2.2 leads to Equation 2.3:

$$\left(\frac{\partial U}{\partial l}\right)_{T,V} = F - T\left(\frac{\partial F}{\partial T}\right)_{L,V} \tag{2.3}$$

When the above experiment is adjusted to keep extension ratio constant instead of constant length, the influence of thermal expansion is eliminated for unstrained rubber [Treloar. L. R. G, 1975].

2.4.1 STATISTICAL NETWORK THEORY

The statistical theory is a theory used to understand elasticity of long chain molecular networks based on certain assumptions [Treloar. L. R. G, 1975]:

1. No volume change occurs
2. An affine deformation of the network, meaning chains deform proportionally to the bulk system
3. The entropy of the whole system equals the sums of the entropies of each individual chain within that system. These chains are then dealt with as having a 'Gaussian' distribution of end to end chain lengths.

The entropy of an individual chain is given by:

$$S = C_A - \frac{3\mathrm{k}r^2}{2nl_m^2} \tag{2.4}$$

where C_A is an arbitrary constant, k is the Boltzmann's constant, r is the distribution of distance between crosslinks, n is the number of chain links of length l_m in a network.

By summing the entropy of each individual chain, the change in entropy of the whole system is given as:

$$\Delta S = -\frac{1}{2}N\mathrm{k}(\lambda_1^2 + \lambda_2^2 + \lambda_3^2 - 3) \tag{2.5}$$

where ΔS is the change in entropy of the network per unit volume under deformation, N is the number of chains per unit volume in the rubber network and λ_1, λ_2 and λ_3 are the three principal extension ratios. The principal extension ratios are ratios of stretched to unstretched

lengths along perpendicular (principal) axes. From the second law of thermodynamics it can be derived for rubber that:

$$W = -T\Delta S \tag{2.6}$$

By substituting (2.5) into (2.6) we achieve:

$$W = \frac{1}{2}G(\lambda_1^2 + \lambda_2^2 + \lambda_3^2 - 3) \tag{2.7}$$

where:

$$G = NkT = \rho R_{gas}\frac{T}{M_c} \tag{2.8}$$

Were W is the elastically stored energy function (SEF), T is the absolute temperature, G is the shear modulus, ρ is the density, R_{gas} is the gas constant and M_c is the average chain molecular weight between two crosslinks. This type of Gaussian treatment is valid up to moderate extensions, above which a non-Gaussian treatment is used [Treloar. L. R. G, 1975].

2.4.2 PHENOMENOLOGICAL THEORY

The phenomenological theory is another approach to deriving strain energy density developed by Mooney and Rivlin [Mooney, M. 1940] [Rivlin. R. S, 1948] using experimental stress vs strain data of rubber using a mathematical modelling approach. It starts with two assumptions for Rivlin's large strain elasticity theory:

1. The rubber is assumed to be incompressible and is isotropic in its unstrained state.
2. Upon deformation, no volume change occurs. Isotropy requires that the function W shall be symmetrical with respect to the three principal extension ratios λ_1, λ_2 and λ_3.

Based on the assumptions and arguments of symmetry, Rivlin expressed the strain energy function (SEF) in terms of three strain invariants, defined as:

$$I_1 = \lambda_1^2 + \lambda_2^2 + \lambda_3^2 \tag{2.9}$$

$$I_2 = \lambda_1^2\lambda_2^2 + \lambda_1^2\lambda_3^2 + \lambda_2^2\lambda_3^2 = \lambda_1^{-2} + \lambda_2^{-2} + \lambda_3^{-2} \tag{2.10}$$

$$I_3 = \lambda_1^2\lambda_2^2\lambda_3^2 \tag{2.11}$$

Rivlin derived through mathematical reasoning the form of the strain energy function should follow this series expansion:

$$W = \Sigma_{i=0, j=0}^{\infty} C_{ij}(I_1 - 3)^{\mathrm{i}}(I_2 - 3)^{\mathrm{j}}$$

(2.12)

By making i=1 and j=0, the equation becomes the Neo-Hookean SEF. By adding the first two terms of this equation, the Mooney SEF can be found:

$$W = C_1(I_1 - 3) + C_2(I_2 - 3)$$

(2.13)

Later, Yeoh [Yeoh. O. H, 1990] expanded on this approach to generate a useful SEF for use with filled rubbers:

$$W = C_{10}(I_1 - 3) + C_{20}(I_1 - 3)^2 + C_{30}(I_1 - 3)^3$$

(2.14)

Yeoh deduced this function based on I_1 only as he observed that for filled rubbers working at engineering strains, $\frac{\partial W}{\partial I_1}$ becomes relatively larger than $\frac{\partial W}{\partial I_2}$ and is independent of I_2. The Yeoh function is a preferred SEF for many purposes and for many applications as it has the ability to capture strain behaviour very reliably using only one of set of test data, for example tensile data. However, this function struggles to capture the significant small strain nonlinearities encountered with highly filled compounds and so is typically used in large strain applications.

2.5 VISCOELASTICITY

The elastic nature of elastomers occurs as a result of the ability for single bonds to rotate freely and so change configuration during loading to reach an equilibrium [Gough. J, 2000]. Temperature has a large effect on the elastic nature of elastomers. As temperature is decreased, the ability for these bonds to rotate is decreased until a point where they can no longer rotate. This transition in behaviour occurs for most polymers over a temperature range of approximately 25°C. This region is called the glass transition temperature or T_g. Below this temperature, the elastomer can no longer change configuration freely due to a reduction in free volume. As a result at low temperatures polymers become brittle. This therefore means the force deformation plot of an elastomer is very dependent on temperature, and not only does the behaviour of an elastomer change drastically below the T_g but it can also be expected, when referring to equation (2.8), that above the glass transition temperature that an unfilled rubber will increase in modulus with the addition of temperature.

Elastomer properties are not only significantly dependent on temperature, but they also exhibit rate dependent effects as can be seen in figure 4. This is generally thought to be as a result of an

internal viscosity between polymer chains, the polymer chains and the other ingredients such as fillers and between the filler particles themselves. As a result, phenomena such as stress relaxation, creep, hysteresis, compression set and heat generation can be commonly found in rubber materials and they become more significant in engineering compounds that contain fillers [Gent. A. N, 2001].

Strain Rate Change
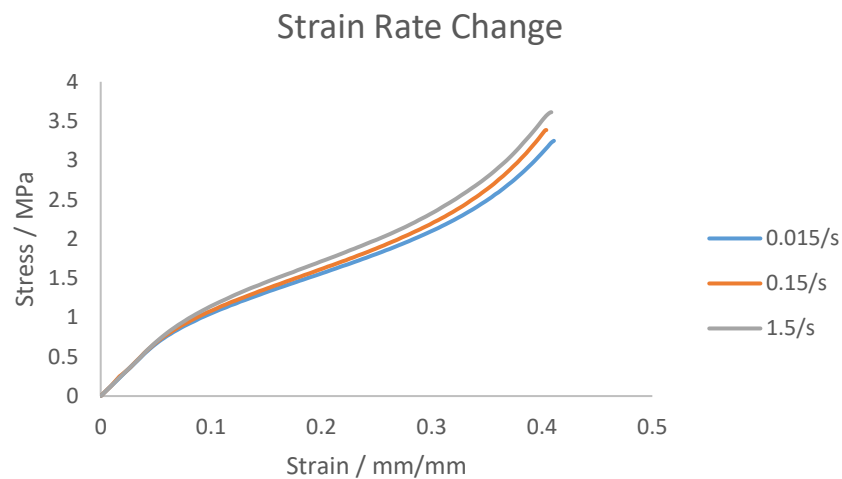
Figure 4: Stress vs strain plot showing the Influence of strain rate on elastomeric materials [Tunnicliffe. L and Busfield. J. J. C, 2015]

2.5.1 STRESS RELAXATION AND CREEP

Stress relaxation and creep are time-dependent relaxation phenomena observed in elastomers. First investigated by [Mooney, M, Wolstenholme, W. E, and Villars, D. S, 1944] and [Mooney, M, and Wolstenholme, W. E, 1952], these phenomena are complex problems. Creep is the increase of deformation under constant load, figure 5, and stress relaxation is the reduction of stress under constant deformation, figure 6.
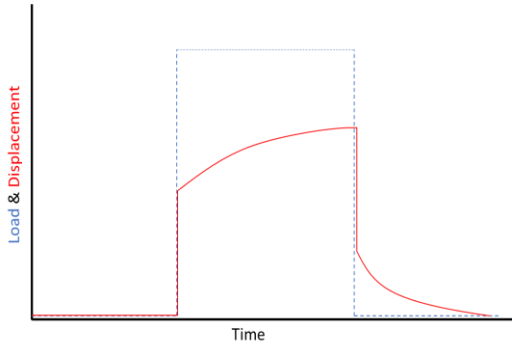
Figure 5: Creep behaviour.
Adapted from [Tunnicliffe. L, 2015]
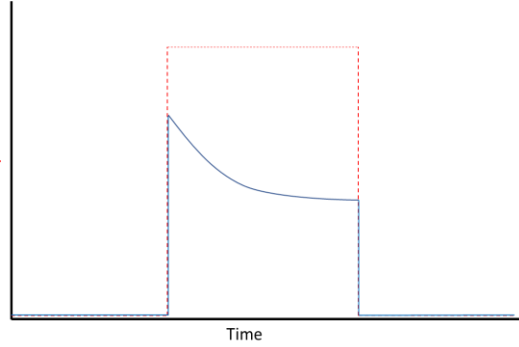
Figure 6: Stress relaxation behaviour.
Adapted from [Tunnicliffe. L, 2015]

As can be seen, the load or displacement vs time curve can easily quantify the degree of relaxation; however, the understanding behind these phenomena is quite complex. Both relaxations are expressed as percentage changes:

$$\text{Stress Relaxation} = \frac{\sigma_0 - \sigma_t}{\sigma_0} \times 100\% \qquad (2.15)$$

$$\text{Creep at Time } t = \frac{x_t - x_0}{x_0} \times 100\% \qquad (2.16)$$

The degree by which the elastomer has relaxed and remains deformed is known as set, a permanent deformation that is not recovered. The relaxation from both of these reactions is reduced after vulcanisation when compared to the behaviour of the uncured compound. A large basis of this behaviour occurs due to disentanglement of polymer chains.

Stress relaxation is very important when designing for sealing applications. As seals are required to maintain a sealing force over their entire lifetime. Relaxation of this force limits their effectiveness as seals and therefore may require them to be replaced.

Creep is important for many applications such as bridge bearing in civil engineering or engine mounts for the automotive industry. There are both physical and chemical mechanisms present as the polymer chains both reorder their configurations and chemically change their structure as well. The physical creep rate decreases over time whereas the chemical creep rate is approximately linear with time at a constant temperature. This can be characterised as:

$$creep\ (\%) = A \log_{10}\left(\frac{t}{t_0}\right) + B(t - t_0) \qquad (2.17)$$

36

where A is the physical creep rate and B is the chemical creep rate [Gent. A. N, 2001].

2.5.2 HYSTERESIS

Hysteresis contributes to imperfect elasticity and is an energy dissipation process. If the material were to exhibit perfect elasticity, the loading and unloading curves would be the same. However, this is often not the case. As can be seen in Figure 7, for a rubber containing a significant amount of filler, the unloading curve of an elastomer that experiences hysteresis unloads down an alternative load-extension path with an apparently lower Young's modulus. Another viscoelastic phenomenon that can be seen from this graph is set. This is the difference in length between the specimen before loading and after unloading.
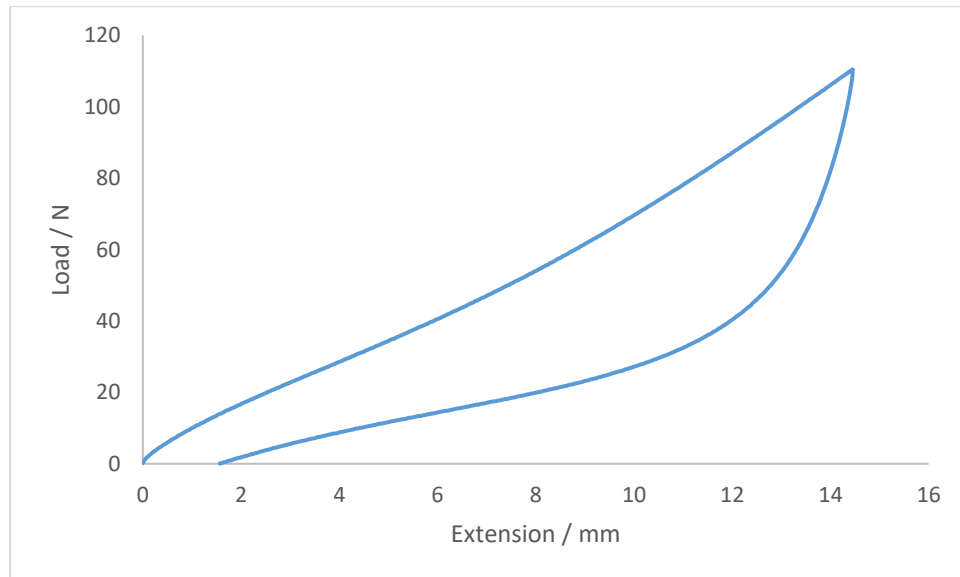
Figure 7: One cycle of a tensile test of a highly filled HNBR rubber

The value of the energy dissipated due to hysteresis is calculated as the difference in area below a loading and unloading cycle on a force versus extension plot. Samples with particulate fillers such as carbon black exhibit increased hysteresis. Elastomers that are closer to their glass transition temperature also exhibit increased hysteresis. Process aids like plasticisers are used to lower T_g and therefore can reduce hysteresis.

Hysteresis can play a important role in the role of crack propagation of elastomeric samples. Lake [Lake, G. J, 1995] [Lake, G. J, 2003] suggests that hysteresis is a mechanism that can lead to crack tips blunting, especially for strain crystallising materials, causing knotty tearing.

2.5.3 CYCLIC STRESS SOFTENING

Cyclic stress softening is a phenomenon where elastomers become progressively softer with each loading cycle. Mullins [Mullins. L, 1947] first investigated this with natural rubber in uniaxial tension and discovered the Mullins effect which is an idealised, theoretical representation of the effect. This is shown in figure 8.
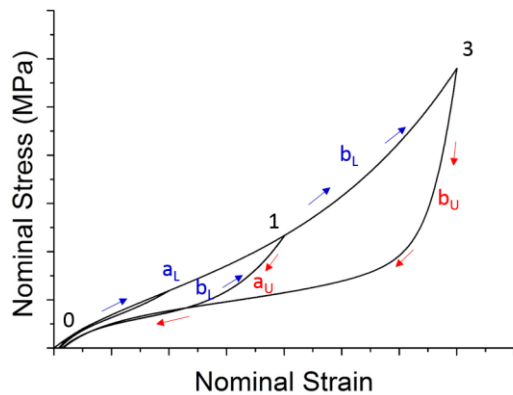
Figure 8: The Idealised Mullins effect.
Adapted from [Carleo. F, 2018]
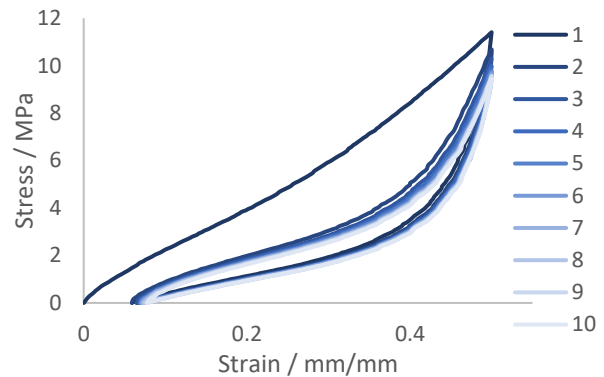
Figure 9: Cyclic stress softening shown in a highly filler HNBR rubber

For increasing strains per cycle, the idealised Mullins effect shows that the loading curve follows the unloading path from the preceding cycle until the maximum strain from the previous cycle (Point 1) is reached. It then follows the virgin loading path (between Points 1 and 3). However, from Figure 9 we can see that the behaviour of these materials is not quite as described in the idealised case as the loading curve does not follow exactly to the previous unloading curve and shows some level of recovery.

The fundamental understanding of this behaviour is still a significant subject of debate in the literature. However, the leading understanding of this behaviour stems from rubber-filler particle linkage ruptures, molecular slippage at the fillers, breakdown of filler-filler interactions, breakdown and reformation of crosslinks or the disentanglement of polymer chains and crosslinks [Blanchard, A, Parkinson, D, 1952] [Houwink, R, 1956] [Kraus, G, Childers, C and Rollmann, K, 1966]. With this in mind, cyclic stress softening is found to be much greater in rubber compounds that incorporate particulate reinforcement such as carbon black.

2.6 MODELLING

2.6.1 HYPERELASTICITY

Finite element analysis is used throughout modern day engineering analysis and this is true for the elastomer industry. Much research has been done into constitutive modelling of rubber in the last 30 years and often papers are released that review these different models such as [Boyce. M. C and Arruda E. M, 2000] or [Dal, H. Badienia, Y. Acikgoz, K. and Denli, F. A, 2019]. To account for both material and geometric non-linearities, strain energy functions are commonly used to model the ideal hyperelastic behaviour of rubbery materials. These usually take the form of a relationship between elastically stored energy and strain invariants of the specimen. There are two main approaches to construct strain energy functions [Flory. P. J, 1953]. These are the statistical, physics-based theory and the phenomenological theory. Statistical theory aims to predict large strain hyperelasticity based on macromolecular network structure. The statistical Gaussian model (2.7) previously introduced is the most elementary of these. Alternatively, phenomenological theories aim to model hyperelasticity from a mathematical curve fitting perspective. Examples include the 8 chain model from Arruda & Boyce [Arruda. E.M and Boyce. M. C, 1993] and Rivlin's invariant-based elasticity theory for a phenomenological approach [Rivlin. R. S, 1948].

2.6.2 VISCOELASTICITY

Today, modelling viscoelasticity is where many significant challenges remain when simulating elastomers.
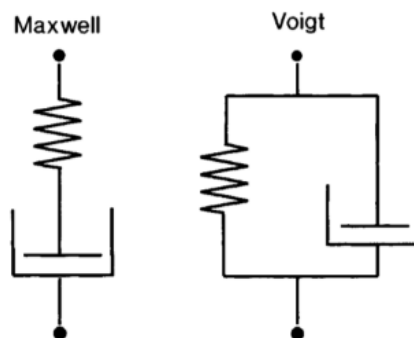
Figure 10: Phenomenological representation of Maxwell and Voigt models [Treloar. L. R. G, 1975]

Phenomenological approaches are used in which elastomer behaviour is related to springs for

elastic effects and dashpots for viscous effects. The origins of these approaches can be understood from the elementary Maxwell and Voigt models shown in figure 10. The models can describe specific types of linear viscoelastic behaviour, with the Maxwell model usually used to describe stress relaxation and the Voigt model usually used to describe creep.

For a more complicated viscoelastic model that is able to include a combination of viscoelastic behaviours, the Bergstrom Boyce model [Bergstrom. J. S and Boyce. M. C, 1998], shown in figure 11, is a non-linear viscoelastic material model that can be used to predict strain-rate dependence, hysteresis, cyclic stress softening as well as the linear viscoelasticity described above. A rheological representation of the model shows that there are two network streams: network A representing the equilibrium response, or the elastic response at low strain rates, and network B representing the viscoelastic contribution. This model is based upon the Doi and Edwards theory of reptation [Doi. M and Edwards. S. F, 1986].
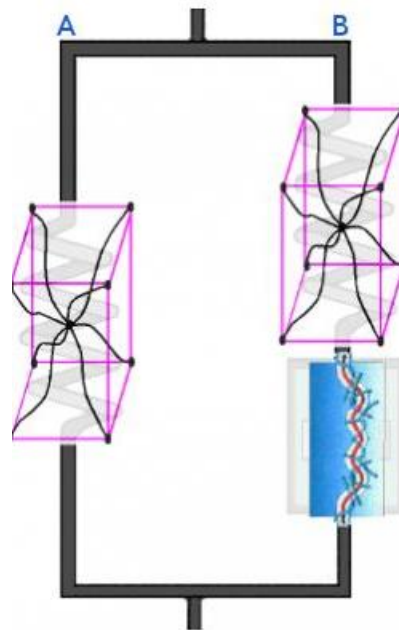
Figure 11: Phenomenological representation of the Bergstrom Boyce model [Bergstrom. J. S, 2019]

One example of this model and methodology being used is the work by [Tunnicliffe. L and Busfield. J. J. C, 2015] which features modelling of elastomer compounds used for oil and gas. In this case a curve fitting analysis determined that the most suitable hyperelastic model to use was the one proposed by Yeoh [Yeoh. O. H, 1990] and which is given in equation 2.14. This is a

cubic model using three elastic constants and only depends on the first strain invariant. The Yeoh model defines network A in the Bergstrom-Boyce model. Network B is defined by the three elastic constants from the Yeoh model as well as four viscoelastic parameters that make up the creep-strain rate equation [Dassault Systemes, 2014]:

$$\varepsilon_B^{cr} = A[\lambda_B^{cr} - 1 + E]^C(\sigma_B)^m \qquad (2.18)$$

Where m is a positive exponent characterising the stress dependence of the effective creep strain rate of Network B, C is an exponent restricted to [-1,0] characterising the creep strain dependence of the effective creep strain rate in Network B and A is a constant for expressing effective creep strain rate. In addition to these parameters ε_B^{cr} is the effective creep strain rate in Network B, $\lambda_B^{cr} - 1$ is the normal creep strain in Network B and σ_B is the effective stress in Network B. E is not calibrated and is fixed at 0.01. This model also requires characterisation data through mechanical testing which is then calibrated through a software called MCalibration. This form of the model does not include a temperature dependence. Therefore, calibrations were done at five different temperatures according to [Tunnicliffe. L and Busfield. J. J. C, 2015]

2.6.3 STRESS SOFTENING EFFECT

There are several models that discuss modelling stress softening. One model by Miehe [Miehe. C, 1995] investigates introducing damage parameters into the model. This involves a discontinuous damage as well as a continuous damage parameter. Combined, they contribute to the cyclic stress softening. The discontinuous damage parameter is dependent on the maximum elongation encountered by the material whereas the continuous damage depends on the entire strain history.

2.7 FILLERS

Particulate fillers are usually added to elastomer formulations to improve elastomer performance, increasing desired properties such as wear resistance or fatigue resistance by about 10 times in some cases. Carbon black and silica are the two most common reinforcement fillers.

The two primary ways reinforcement fillers are controlled is the quantity and size of particulates. Small particles have high surface area enabling more area to interact with the elastomer and closer particle-particle spacing. Two more important aspects are structure and

surface chemistry. As particles are added to the elastomer, they coagulate to form aggregates that take irregular structures. A high structure means large void volume within the space it takes up. In most cases, reinforcement is enhanced by using materials with a high structure and stronger filler rubber interactions.

2.7.1 CARBON BLACK

Carbon blacks are the most commonly used reinforcement fillers. They are produced by combustion of vaporised hydrocarbons whilst controlling conditions such as time, temperature and quench time to produce carbon black particles of different sizes and properties. An ASTM (American Society of Testing and Materials) classification was created to generate a nomenclature for categorising carbon black particles, usually in the form of XYZZ where:

- X is a letter describing the curing, either N for normal cure or S for slow cure.
- Y is a number between 1 and 9 corresponding to mean particle diameter where smaller numbers indicate smaller diameters. The smaller the diameter of the particle, the higher the reinforcement but due to the increased filler-filler interactions the dispersion becomes more difficult.
- ZZ are numbers that indicate the structure of the carbon black, where the smaller the number the lower the structure. Particles with high structures form aggregates easily during compounding and moulding.

Carbon black becomes chemically and physically linked to the rubber during shear mixing. Carbon black primarily increases strength and viscoelasticity but also improves processability by reducing melt elasticity. It is very effective for strengthening elastomers that do not strain crystallise, for example SBR.

2.7.2 SILICA

Silica is the second most commonly used reinforcing filler. It can be produced via acidification of sodium silicate under controlled conditions.

Silica can be divided into two categories: conventional and highly dispersible silica. Highly dispersible silica has a similar morphology and surface area to carbon black but a different surface chemistry. The surface features polar hydroxyl (silanol) groups and a moisture "shell" surrounds the surface by hydrogen bonding from the production process. As a consequence of

this more polar surface, it is less compatible with non-polar diene rubbers. This is generally overcome by using coupling agents to modify the surface.

Silica is often used in applications such as tire manufacturing, and sometimes in conjunction with carbon black.

2.7.3 PLASTICISERS

Plasticisers are process aids that lower viscosity and enable the compound to be mixed better and manufactured with less energy. Plasticisers reduce physical entanglements and decrease friction internally, acting as a polymer chain lubricant. They may also improve flexibility in the elastomer at low temperatures [Gent. A. N, 2001]. Plasticisers commonly come in oils, fatty acids, esters, pine tar, liquid polymers and rosin.

Plasticisers greatly influence the properties of elastomers with regards to their processing and chain mobility contributions [Kim, D. Y, Kim, G. H, Nam, G. M, Kang, D. G and Seo, K. H, 2019]. However, they are especially sensitive ingredients in elastomer formulations. Previous research [O'Rourke, 2008] has shown that ester plasticisers are rapidly lost from rubber compounds at temperatures above 150°C. This is within the target temperature range for many oil and gas applications. Therefore, the potential loss of plasticiser in service is an important consideration when understanding elastomer ageing for oil and gas applications.

2.7.4 ANTI-DEGRADANTS

Anti-degradants mostly focus on protecting elastomers from oxygen and ozone attack. This attack alters the network structure of the elastomer by causing chain scission or crosslinking.

Chemical protectants either react with the degradant particle or interfere with the reaction process itself. Common types are aromatic amines, phenolics and phosphates. Physical protectants on the other hand act as physical barriers that migrate through the elastomer and bloom to the surface. These often take the form of waxes [Gent. A. N, 2001].

3. LITERATURE REVIEW

The purpose of this chapter is to build off the basic knowledge covered in the previous chapter and focus on the research necessary for this thesis. This will mainly cover crack propagation from static and dynamic origins and how elastomers suffer to degradational effects.

3.1 CRACK GROWTH IN ELASTOMERS

Crack growth phenomena of rubber is a process that usually begins at imperfections or voids either within or on the surface of the elastomer. These voids, usually on the micron scale, act as localised regions of high stress when load is applied. They grow under applied loads until they become cracks that propagate through the specimen potentially causing failure. Fracture mechanics is an approach used for understanding crack propagation and strength in rubber.

3.1.1 FRACTURE MECHANICS

The fracture mechanics approach used in rubber focuses on how much energy is required to propagate a crack. The research is based on work by [Griffith. A. A, 1920] who suggested that a crack in glass would grow if the elastic energy released by the growth was greater than the surface free energy of the surfaces created by it. This was later confirmed experimentally.

However, this is not the case for rubber. Irreversible processes occur in the area surrounding the crack tip that lead to energy losses. These local losses may be large even for elastomers where energy losses in the bulk are negligible. The magnitude of these losses is dependent on the viscoelastic properties of the elastomer, the strain in the crack region and the rate of crack growth. Therefore, the energy responsible to progress a crack further at a particular rate is likely to be a material characteristic of the rubber, even if it exceeds the thermodynamic surface free energy.

[Rivlin. R. S and Thomas. A. G, 1953] modified Griffith's approach to account for this irreversible energy loss effect at the crack tip and found an expression for the energy required to drive a crack at a particular rate, also known as tearing energy T or strain energy release rate:

$$T = -\left(\frac{\partial U}{\partial A_c}\right)_l \qquad (3.1)$$

where A_c is the area of one side of the fracture surface. The partial derivative indicates the sample is held at constant length, l, so that the applied forces do no work.

3.1.2 GEOMETRIES

As mentioned, Rivlin and Thomas hypothesised that the energy required to propagate a crack is a material characteristic and is therefore not influenced much by the way it is released. If this is the case, geometric changes to the elastomer sample should not influence the outcome. Experiments were carried out by [Rivlin. R. S and Thomas. A. G, 1953], [Greensmith, H.W. and Thomas, A.G, 1955], [Thomas, A.G, 1960] and [Lake, G.J. et al, 1969] to investigate this with various testing geometries to establish relationships for tearing energy. From these experiments, common geometries now used, and seen in figure 12, are:

1. Trouser test crack growth specimen:

Shaped similarly to a pair of trousers, the test piece is clamped at the end of both legs and extended in tension.

$$T = \frac{2F\lambda}{t} - bW \qquad (3.2)$$

F is the applied force, λ is the extension ratio in the legs, t is the thickness of the unstrained specimen, b is the total width of the specimen and W is the elastically stored energy density in the legs.

2. Pure shear crack growth specimen:

The pure shear specimen is rectangular to enable a region of pure shear to form in the centre of the sample.

$$T = Wl_0 \qquad (3.3)$$

W is the elastically stored energy density in the pure shear region and l_0 is the unstrained distance between the two parallel clamps. This test is often preferred for crack growth studies as complications due to crack tip and edge effects are removed and given an applied strain, the crack grows at a constant rate.

3. Angle crack growth specimen:

$$T = \frac{2F}{t}\sin\left(\frac{\theta}{2}\right) \tag{3.4}$$

In this sample, F is the applied force, t is the specimen thickness and θ is the angle between the separating legs.

4. Split crack growth specimen:

$$T = \left(\frac{F_A\lambda_A \sin\theta + F_B(\lambda_A \cos\theta - \lambda_B)}{t}\right) - w_0(W_A - W_B) \tag{3.5}$$

In this sample, F_A and F_B are the applied forces to the corresponding legs, λ_A and λ_B and W_A and W_B are the extension ratios and stored energy densities in the corresponding legs, 2θ corresponds to the angle of the opening crack where $\tan\theta = F_A/F_B$, w_0 is the width of the specimen and t is the thickness.

5. Edge crack specimen in tensile crack growth:

$$T = 2kW_c \tag{3.6}$$

where $k \approx \frac{\pi}{\sqrt{\lambda}}$

In this case, W is the elastically stored energy density in the bulk of the material at large strains, c is the crack length, k is a strain dependent term where λ is the extension ratio [Lake, G.J, 1970].
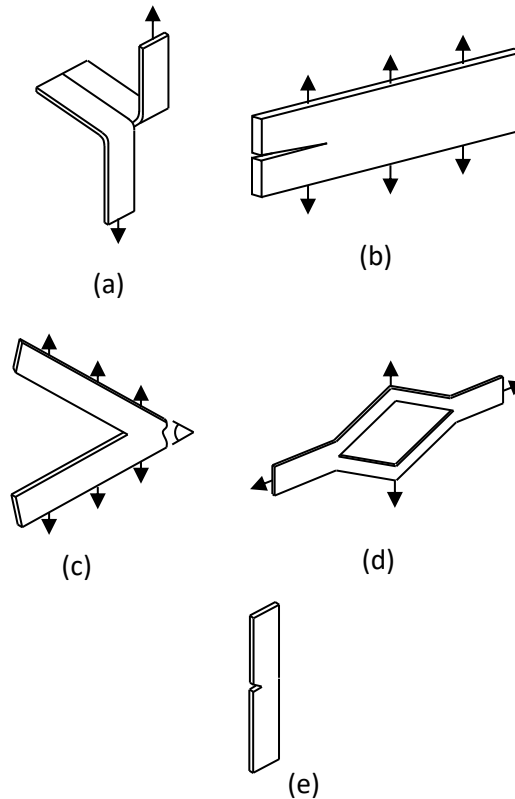
Figure 12: Different geometries used for fatigue testing. (a) trouser tear specimen, (b) pure shear specimen, (c) angle crack growth specimen, (d) split crack growth specimen and (e) edge crack specimen [Busfield. J. J. C, 2000]

3.1.3 FLAWS

As mentioned before, flaws and voids in the elastomer bulk or on the surface initiate cracks in elastomer products. However, the understanding the origin of these flaws and voids is still debated. Tsunoda [Tsunoda, K, 2001] notes that some causes could be due to physical defects such as scratches or manufacturing defects such as mould lines. Work by Gent and Tompkins [Gent, A.N. and Tompkins, D.A, 1969] also noted that even if the surface flaws were minimised by moulding against polished glass, the breaking strength is not increased dramatically. Leading to the idea that other sources of flaws such as dirt and dust particles must also be present.

Due to the inherent way elastomers are made, it is highly likely that local inhomogeneities will be present within the elastomer. The process of vulcanisation is not controlled on a molecular scale; therefore, crosslinks will not form uniformly and be distributed evenly throughout the

elastomer. Reinforcement particles, process aids or protectants can also act as nucleation sites due to chemical or physical bonding failure.

A common question in the rubber industry therefore discusses when a flaw or void becomes a crack. Other than crack tip size and shape, there is little distinction between crack initiation points and the propagation sites. As shown in the test geometries above, when these tests are done in laboratories a crack is placed in the samples usually using a blade. This is how the work will be done in this work. According to [Gent. A. N, 2001], the presence of a known initial crack leads to more reproducible tests and the sensitivity to defects, not inherent to the material properties, are eliminated. Presumably, as the energy required to propagate a crack is a material characteristic and is therefore not influenced much by the way it is released, whether it is a flaw or a crack has little influence. Results therefore can be better controlled and reproduced if cracks are purposefully introduced.

3.1.4 CRACK TIP

In response to crack growth behaviour being a material characteristic, this cannot be said of crack tip shape. [Lake. G. J, and Yeoh. O. H, 1987] found that for sharp crack tips tearing occurred, on a small scale, at very low energies not far above the threshold required for the onset of mechanical crack growth.

Thomas [Thomas. A. G, 1955] extended this original tearing energy work [Rivlin. R. S and Thomas. A. G, 1953] by investigating crack tip behaviour. He showed that by modelling a crack as a slit with parallel sides and a semi-circular tip, the tearing energy is closely related to the effective crack tip diameter.
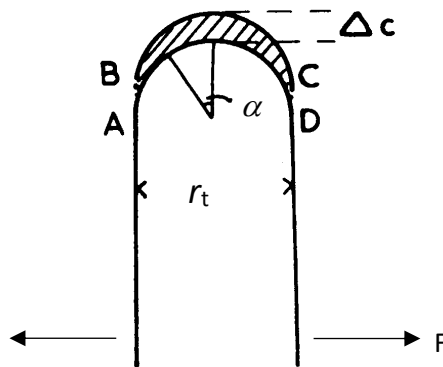
Figure 13: A diagram of the shape of a crack tip [Thomas. A. G, 1955]

From Figure 13, it is demonstrated that the material loses elastic stored energy per unit volume shown by the shaded area when the crack length is extended by length Δc as a result of force F. The amount lost, ΔU, is given by:

$$-\Delta U = \int_{-\frac{\pi}{2}}^{\frac{\pi}{2}} W_a \, \Delta c h r_t \cos\alpha \, d\alpha \tag{3.7}$$

where W_a is the elastically stored energy per unit volume of the rubber at the crack tip at an angular distance α from the pole, h is the thickness of the specimen and r_t is the radius of the semi-circle. Therefore, tearing energy can be given:

$$T = -\frac{1}{h}\left(\frac{dU}{dc}\right)_l = r_t \int_{-\frac{\pi}{2}}^{\frac{\pi}{2}} W_a \cos\alpha \, d\alpha = W_t 2 r_t = W_t d \tag{3.8}$$

where W_t is a suitable average of W_a and d is the diameter of the crack tip. Thomas then verified this by comparing the magnitudes of T calculated using the Eq. (3.8) and equation (3.2) from the trouser tear specimen as this specimen test focuses on the force required to propagate a crack tip further. This showed a good agreement, shown in figure 14.

49
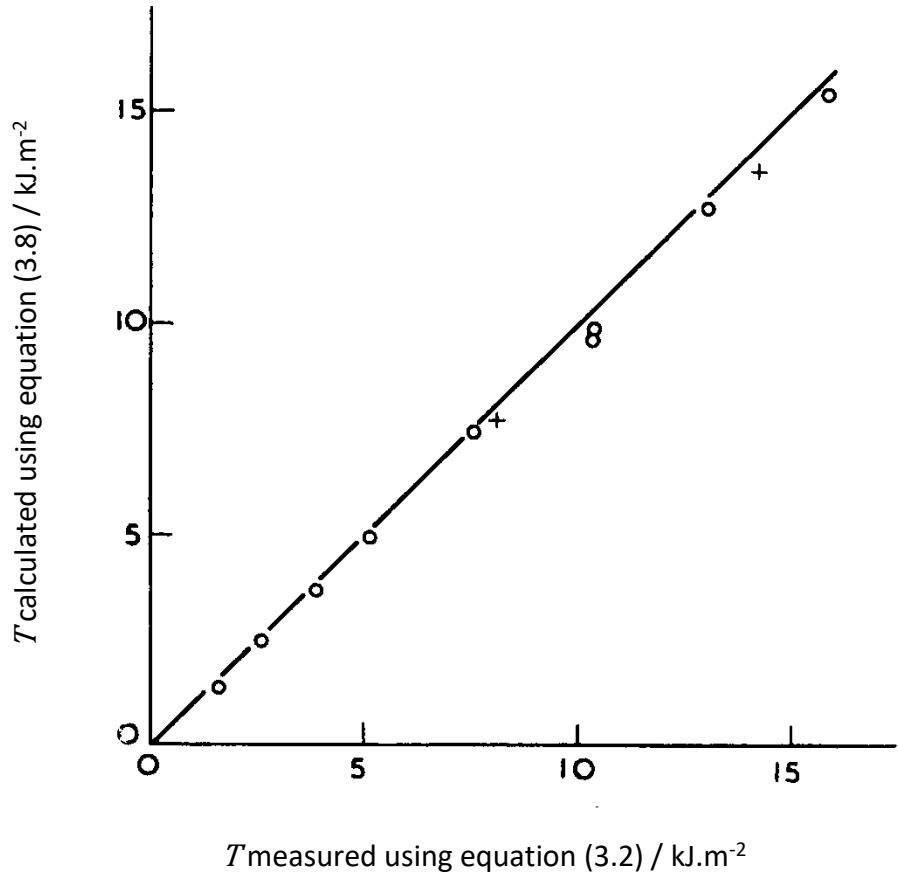
Figure 14: A comparison of tearing energy magnitudes from equations (3.2) and (3.8) [Thomas. A. G, 1955]

If the test piece was extended until tensile rupture occurred, W_t in Eq. (3.8) then represents the work to break per unit volume of rubber, W_b, and the equation is amended to:

$$T = W_b d_b \tag{3.9}$$

where d_b is the diameter of the strained crack tip that results in rupture. Thomas then verified this experimentally by measuring the tearing energy of the test pieces with model crack tip diameters ranging from 1mm to 3mm. He found that the relationship T with d_b was fairly constant and approximately equalled the work to break W_b in tensile tests.

Following this [Greensmith. H.W, 1960] investigated tearing energy for a range of crack growth rates with values of W_b measured on test pieces in tension at different testing rates. He plotted

50

T/d and W_b against the reciprocal of time or frequency, t^{-1}, by extending the test pieces till breaking point for unfilled and filled SBR.

(b)

(a)
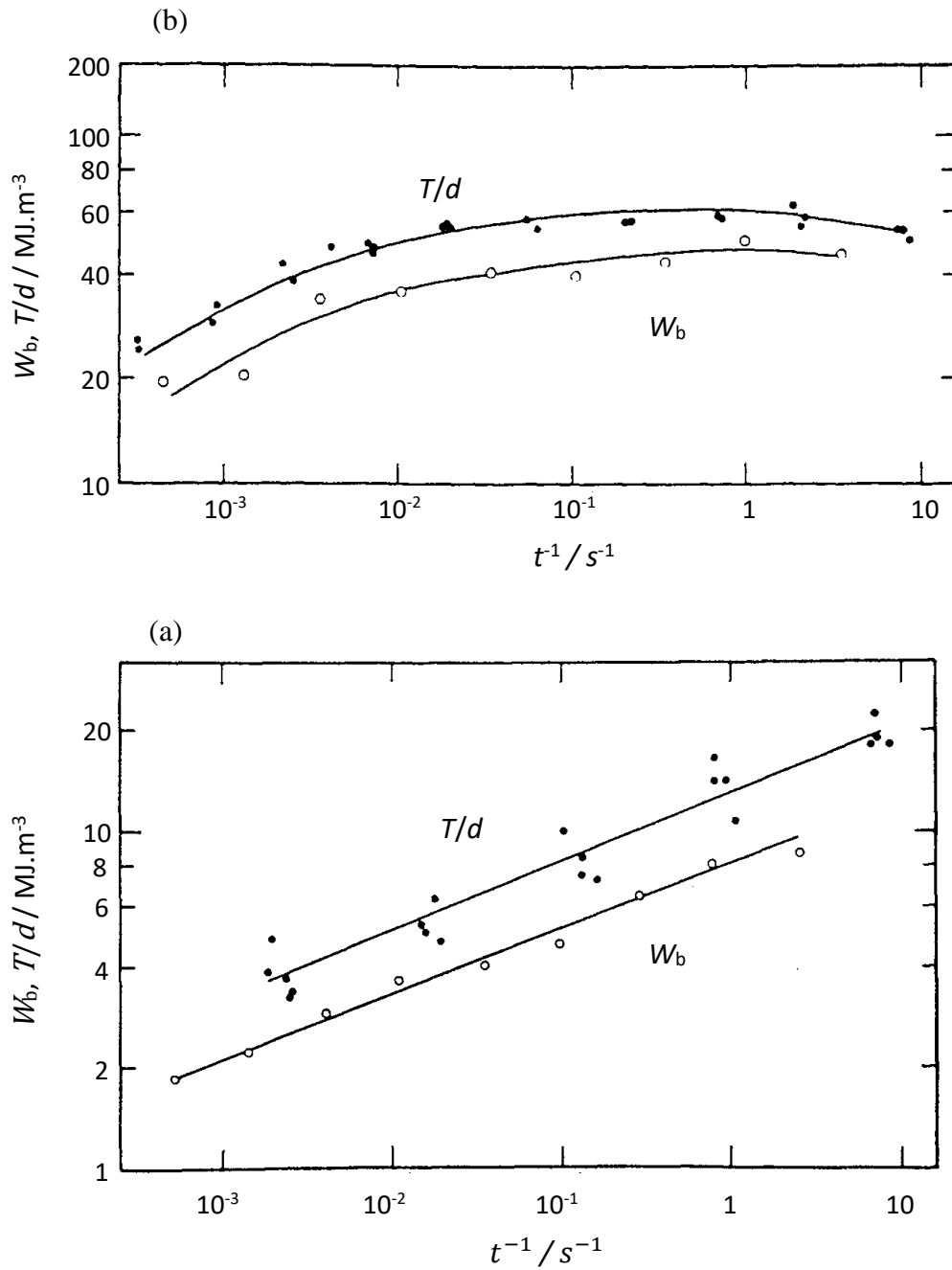
Figure 15: Comparison of the work to break per unit volume, W_b, and the tearing energy, T, to initiate crack growth at an incision at 25°C (a) for an unfilled SBR (b) for a SRF carbon black filled SBR [Greensmith, H.W, 1960]

In both cases it was clear that there was a similar dependence on time; however, values for T/d were higher. To account for this, the flaw theory of tensile strength was employed [Thomas. A. G, 1955]. As the volume of the test piece increases, tensile strength decreases as a result of there being more and larger flaws present in a larger sample than a small one due to probability [Higuchi. T, Leeper. H.M and Davies. D.S, 1948]. Adding to this point, the volume at the crack tip is much smaller than a tensile test piece. Therefore, there may be an apparent increased tensile strength and, as a result, higher energy absorption per unit volume than anticipated here, even when tested at the same extension rate.

[Gent, A.N and Henry, A.W, 1967] employed a new crack growth specimen to measure crack growth behaviour whilst restricting possible crack deviation paths from the planar path intended by adding metal strips. This created an upper limit to the magnitude of the tip diameter, *d*.
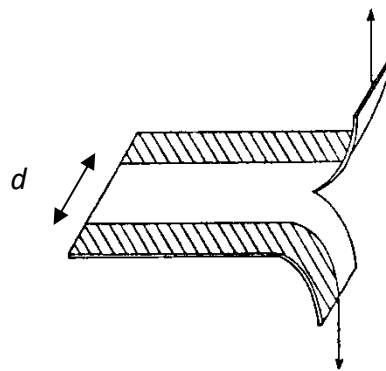
Figure 16: Diagram of a modified trouser tear test with metal strips [Gent, A.N and Henry, A.W, 1967]

These samples were created and worked by sticking metal strips parallel to the elastomer sample edges at various spacings in the range between 0.01cm and 3cm and testing the specimens over a range of crack growth rates and temperatures. The results are shown in figure 17 showing only results from gap width 0.01cm and 3cm.
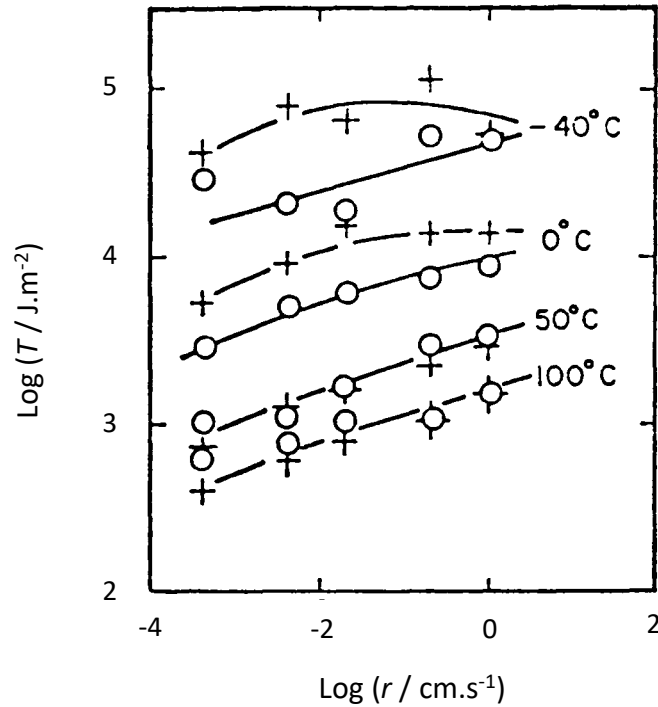
Figure 17: Experimental relationship for the measured tearing energy of an unfilled SBR vulcanizate as a function of crack growth rate at various temperatures. +: wide gap test piece (0.3cm), O: narrow-gap test piece (0.01cm) [Gent, A.N and Henry, A.W, 1967]

The results showed a similar response to those found by [Greensmith. H.W. and Thomas, A.G, 1955] who used non-restrictive test pieces. Results for narrow gap test pieces were very close at high temperatures. However at lower temperatures, the wide gap test pieces showed much higher tearing energy values. This was attributed to a significant increase in crack tip diameter, where values exceeded 0.01cm.

Thomas [Thomas, A.G, 1958] observed that during dynamic measurements on pure shear specimens with an initial sharp blade cut, the cut became very rough and so effectively increased its radius of curvature during loading. This increase in radius caused a reduction in stress concentration. He then suggested that if the roughened tip is assumed to consist of a number of small sharp tips, the value of strain energy release rate for one will be less than for

the whole tip. This model helped to describe the reduction in crack growth rate with increasing roughness. Greensmith [Greensmith, H.W. 1956] also reported that the presence of carbon black as a reinforcing filler significantly increases the phenomenon of crack deviation and therefore an increased strength of the material.

Further to this point, [Papadopoulos, I. C et al, 2008] investigated the rate transition in fatigue crack growth via the influence of the crack tip. He found as a general trend that when crack tips were initially cut with a sharp blade, crack propagation rate was much faster until slowing down to a steady-state rate. He concluded that this was a characteristic of the material and strain energy release rate. For all cases tested of filled and unfilled NR and SBR, there was a reliable comparison to this equation representing the rate of transitioning region:

$$c = RN + c_0 \left(1 - e^{\left(-\frac{N}{N_0} \right)} \right) \tag{3.10}$$

where R is the steady-state fatigue crack growth rate per cycle, N is the number of cycles, c_0 is the additional amount of crack growth comparatively to steady-state crack growth if that would have occurred and N_0 is a characteristic of the specific transition being measured and is related to the number of cycles that are required for steady state to be achieved. Final comments state that the crack tip splitting under strain was as a result of strain-induced anisotropy and that the extent of splitting, on average, determines the crack tip radius in steady state and the final roughness of the fractured surface.

3.1.5 THRESHOLD STRAIN ENERGY RELEASE RATE

It has been shown [Rivlin. R. S and Thomas. A. G, 1953] that at the crack tip and the highly strained regions around the tip, irreversible energy dissipation processes occur. When these energy dissipation processes are minimised under certain conditions, a minimum tearing energy can be determined called the threshold tearing energy, T_0. Generally, the conditions to find T_0 experimentally feature lowering the crack growth rate, increasing testing temperature and highly swelling the material with a low viscosity liquid.

Lake and Thomas [Lake, G.J. and Thomas, A.G, 1967] first tested for the threshold tearing limit in cyclic crack growth tests, defining T_0 as the minimum tearing energy at which cyclic crack growth could take place. Testing at tearing energies less than T_0 would result in crack growth

attributed only to chemical attack. A more detailed description of cyclic crack growth is given later.

Lake and Thomas found that regardless of a rubber's ability to crystallise or not and whether it featured high or low properties of tensile and tearing strengths, T_0 was more or less very similar with a magnitude being approximately 50 Jm^{-2}. This suggested that this value was purely as a result of the strength of the chemical bonds in the polymer backbone. They assumed the tip diameter of the advancing crack, d, had a minimum possible value, d_0, when the elastic stored energy, W, had a minimum value, W_0, determined by bond strength. Therefore equation (3.8) for a crack tip, on a molecular scale becomes:

$$T_0 = W_0 d_0 \qquad\qquad (3.11)$$

where W_0 is the minimum possible strain energy density at the tip and d_0 is the minimum possible crack tip diameter. The crack tip diameter is assumed to have its smallest possible value, d_o if:

$$d_0 = \xi\sqrt{\mu} \qquad\qquad (3.12)$$

where ξ is the length of a monomer unit and μ is the number of monomer units between crosslinks. This minimum distance possible is defined as the distance between adjacent crosslinks in the unstrained state. Combining the above equation (3.12) with (3.11) gives an estimate for the minimum energy required to drive a crack can be found:

$$T_0 \equiv b J_b \xi \sqrt{\mu} \qquad\qquad (3.13)$$

where b is the number of active bonds per unit volume, J_b is the bond rupture energy and these combined make up the elastic stored energy density at the crack tip. The threshold strain energy release rate using this principle is approximately 25 Jm^{-2} and is approximately a factor of 2 lower than experimental results. Considering the approximations used and the uncertainty of some assumptions used to derive the theory, the agreement can be regarded as very good.

3.1.6 TYPES OF CRACK GROWTH

Crack growth can occur in different ways. The two general types of crack growth are defined as steady and stick-slip [Greensmith, H.W. and Thomas, A.G, 1955]. They are simple to identify in

trouser tear tests by observing the specimen and force vs time graphs after a simple constant rate and constant grip test.

Graph   Crack growth pattern

Direction of crack growth ⟶

(a) steady crack growth

(b) stick-slip crack growth

(c) knotty crack growth
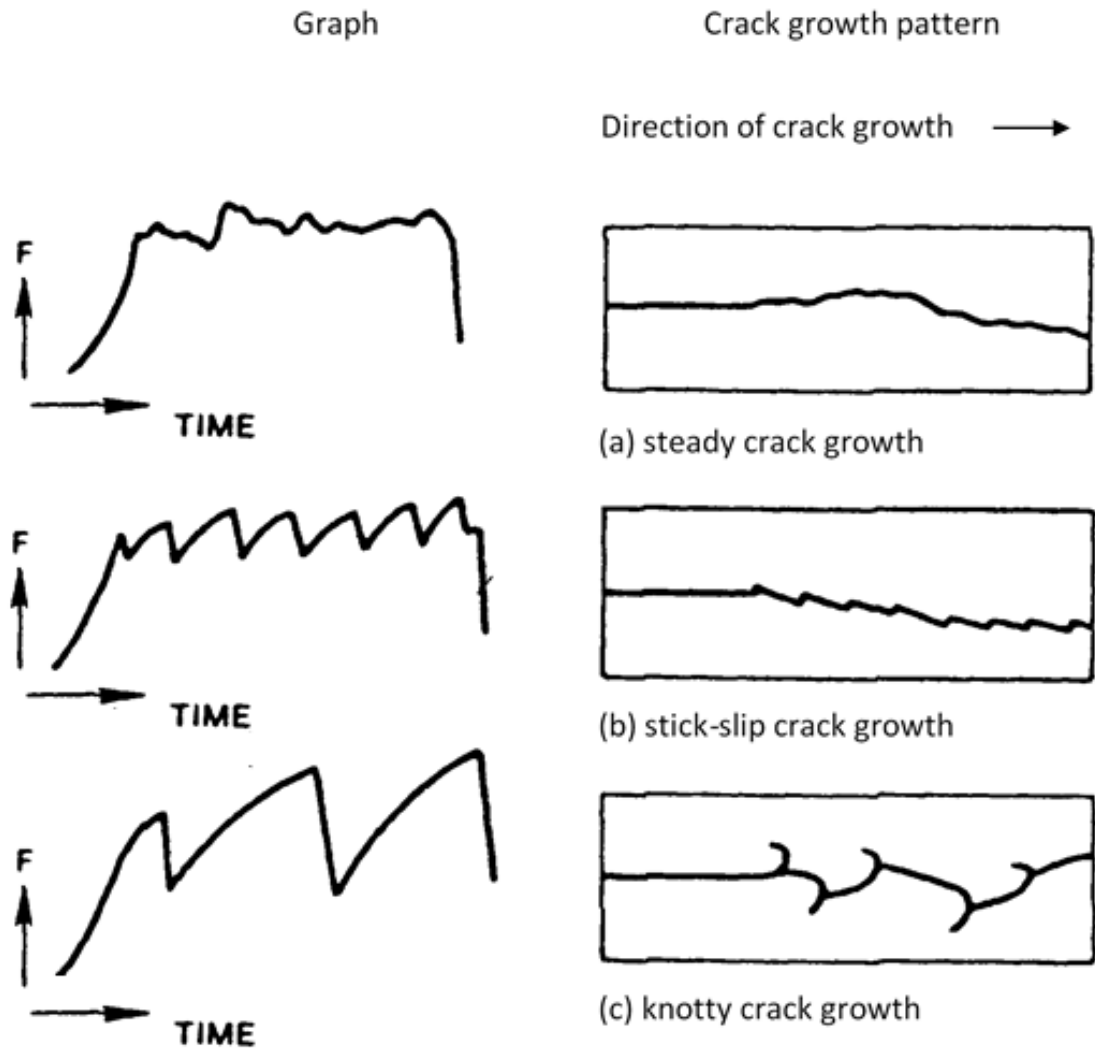
Figure 18: Diagram of typical crack growth patterns with their associated force vs time relationships. Adapted from [Papadopoulos, I. C, 2006]

As can be seen in figure 18, the steady crack growth (a) test, the force vs time plot generally features very little change in force with time once crack propagation starts. The specimen itself also sees very little deviation from the intended tearing path. The stick-slip crack growth (b) test however, features a force vs time plot with repeating and regular saw wave pattern. This occurs from a combination of smooth and rough tearing as a result of hysteresis and the fracture surfaces often reflect this with an irregular and rough surface for the stick region, and

a smoother tear surface for the slip region. The upturn in the force vs time plot indicates a stick region, and the downturn indicates the slip. The specimen also shows a tear path where small deviations were made for the crack to find the path of least resistance. An area of deviation indicates where each stick region was located. Finally, a knotty crack growth (c) test is an extreme example of a stick-slip test. In this test, the regions of stick are extreme enough to stop the crack entirely and turn the crack 90° or more to the intended tearing path. The reason for this extreme tearing is often due to an anisotropic region, forming a barrier to crack growth.

The understanding of a relationship between tearing energy and crack propagation rate was investigated by Greensmith [Greensmith, H.W. 1956] [Greensmith, H.W, 1960] for a range of filled NR and SBR materials. This was then continued by Kadir and Thomas [Kadir, A, and Thomas, A. G, 1981] for NR, SBR, NBR and butadiene rubber (BR) using a pure shear test geometry. By studying this, they found that a relationship was evident when tearing energy and crack propagation rate were plotted on a log vs log graph.
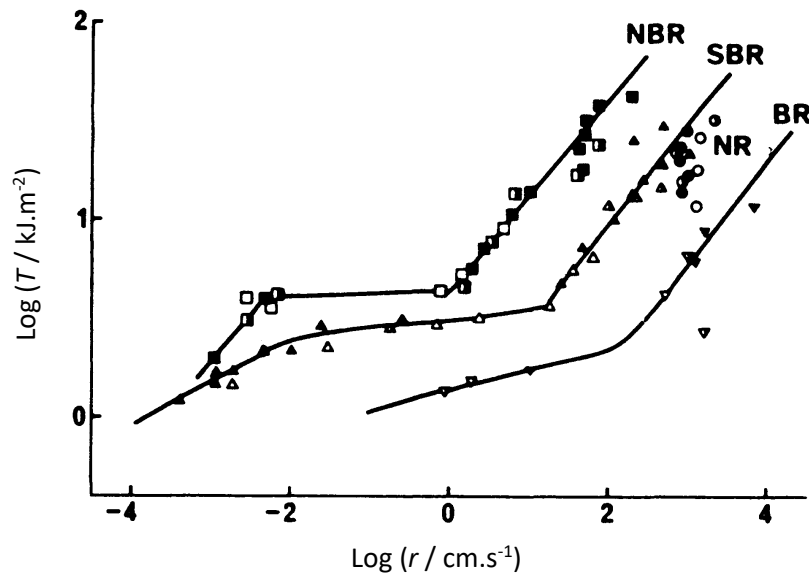
Figure 19: Tearing energy against rate relationship for four different rubbers determined using a pure shear test specimen in static, constant T, crack growth measurements

This work showed that tearing energy increased with crack propagation rate and also showed three distinct regions of tearing. Each region featured specific tearing regimes. The first region, found at low tearing energies and crack propagation rates, found cracks to propagate in a

steady manner with a rough surface. The next region, found in an intermediate tearing energy and crack propagation rate, tore in a stick-slip manner and was more sensitive to changes in tearing energy. The final region, at higher levels of tearing energies and crack propagation rates, featured cracks that tore smoothly and was least sensitive to changes in tearing energy.

For materials like NR, strain crystallisation plays a major role in crack propagation. Cracks can be stopped by crystalline structures that form at the crack tip due to strain effects. As seen in figure 19, this heavily affects cracks at lower tearing energies. Figure 20 shows the polymer chain movement at the crack tip to cause strain induced crystallisation at the crack tip.
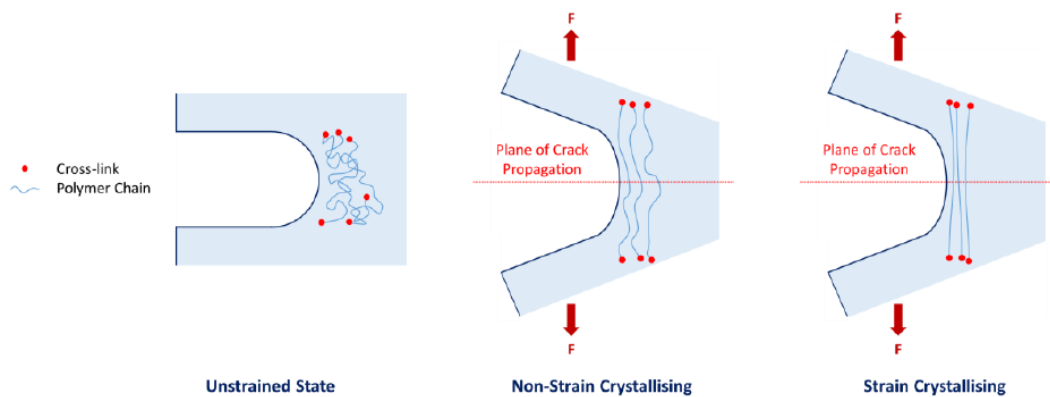
Figure 20: Morphology of polymer chains ahead of the crack tip for non-strain crystallising elastomers and strain crystallising elastomers. Adapted from [Windslow. R. J, 2018]

Researchers like Gent, Razzaghi-Kashani and Hamed [Gent, A. N, Razzaghi-Kashani, M, and Hamed, G. R, 2003] [Hamed, G. R, 2005] have researched into how crystallisation effects can cause directional changes in crack growth. Cracks attempt to move around crystalline regions until either new crystalline regions had formed stopping the newly deviated path or the local energy in the crack tip area had been released. Hamed has researched into blunting and longitudinal cracking of elastomers in trouser tearing specimens, again suggested that anisotropic regions cause crack deviation in NR as a result of strain induced crystallisation.

Another important influence of crack growth is temperature. The effects of temperature and crack propagation rate on tearing energy of SBR and NR can be seen in figure 21. The results by [Greensmith, H.W, 1960] show that for unfilled SBR, tearing energy decreases for increasing temperature and decreasing crack propagation rates. This reflects the viscoelastic energy dissipation behaviour of elastomers. For strain crystallising NR, a similar effect occurs at much

58

lower rates, attributed to the strain crystallising nature of NR. For carbon black filled SBR, the influence of reinforcement filler causes a much more complicated response. At lower crack rates, low temperature shows to increase tearing energy before reducing it. This is due to the combination of viscoelastic effects of the elastomer working with the strength anisotropy effects of the carbon black.
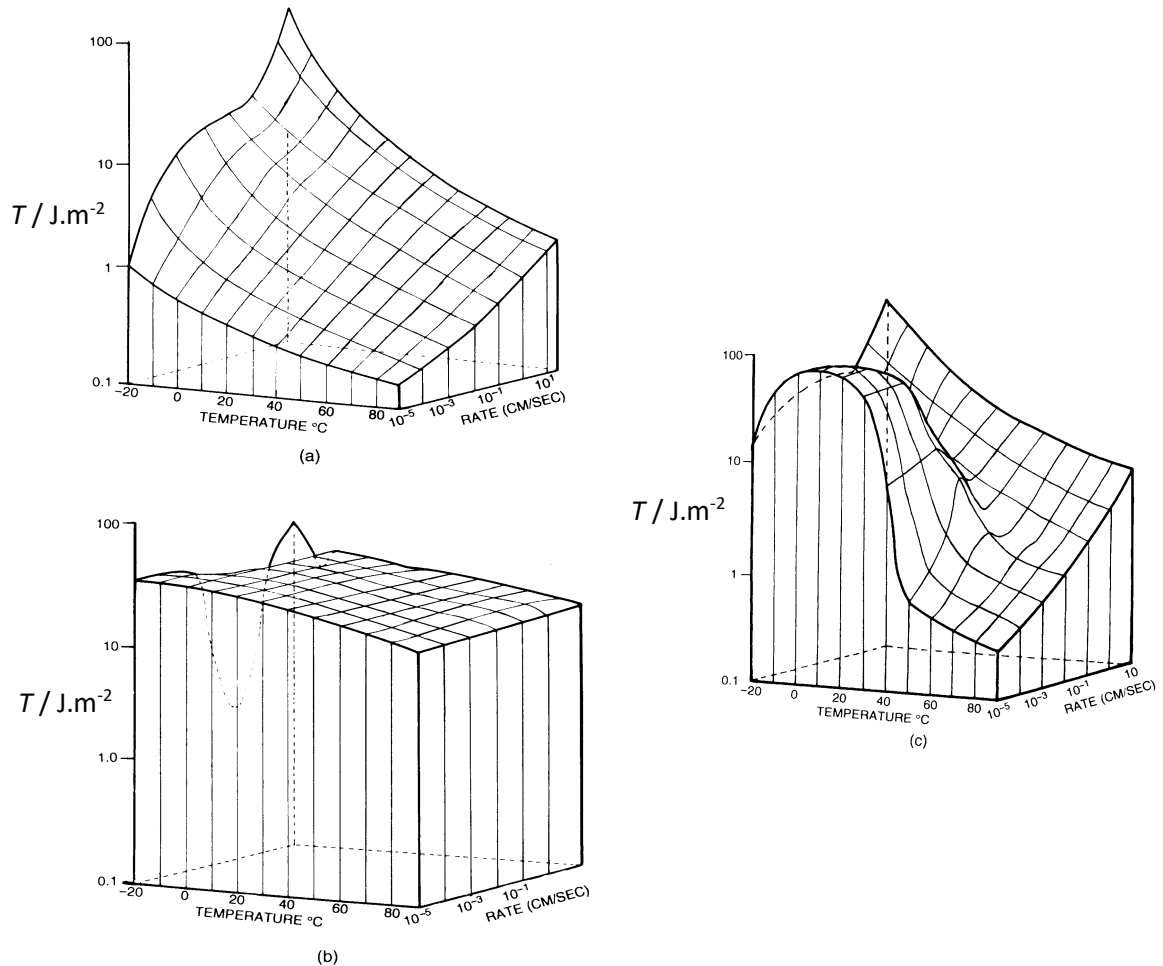
Figure 21: The effect of crack growth rate and temperature on tearing energy for (a) unfilled SBR, (b) unfilled NR and (c) FT black filled SBR [Greensmith, H.W, 1960]

What can be seen from this review is that the vast majority of research done in the field of static crack growth is focused on materials NR and SBR. These are common favourites in the field of elastomeric research as they are not only widely used in many applications, but they cover a large area of research including materials that crystallise and not. This has meant that materials like HNBR have been under researched until more recently when elastomers have

59

been needed for more demanding applications. Despite the fact the HNBR is commonly used for high demanding applications, the understanding behind why it is to successful in these applications is therefore widely under researched.

3.1.7 CYCLIC FATIGUE

The fracture mechanics approach explained so far primarily considers static conditions. However, a significant application for elastomeric parts also considers dynamically loaded parts.

For cyclically loaded parts, the initial Rivlin and Thomas [Gent, A.N, Lindley, P.B and Thomas, A.G, 1964] characteristic of crack rate can be applied. However, it is adapted to find that the extent of crack growth during each loading cycle is determined by the maximum strain energy release rate during the cycle and not influenced by the way it is reached, even for viscous materials [Gent et al. 1964]. The crack growth per cycle can be represented as:

$$\frac{dc}{dN} = f(T) \tag{3.14}$$

where c is crack length, N is the number of cycles and T is the maximum strain energy release rate during a cycle.

Figure 22 from [Lake, G.J, 1983] shows the cyclic crack growth rate results for an unfilled NR and SBR over a very wide range of tearing energies. This is plotted on logarithmic scales of tearing energy and crack propagation rate. The results can be divided into three distinct regions of fatigue, all resulting from different origins.
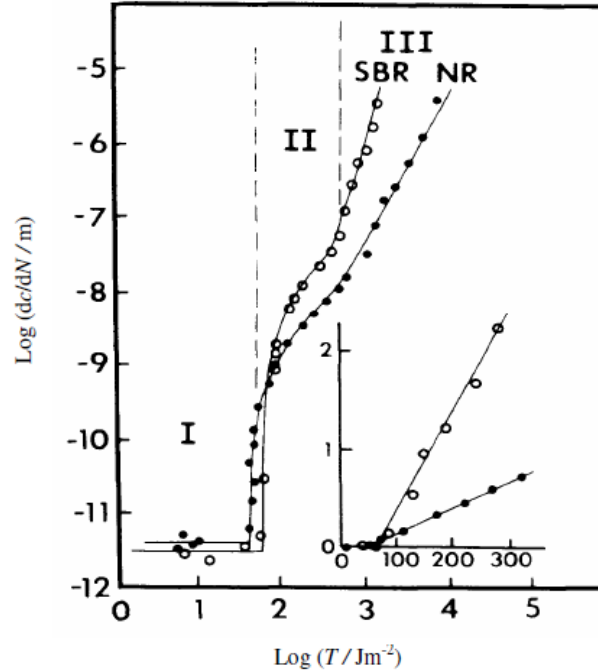
Figure 22: A graph of log of tearing energy against log crack growth rate per cycle, showing three tearing regions for NR and SBR [Lake, G. J, 1983]

Region 1 is shown at the lowest levels of tearing energies. Here the elastomers are subjected to tearing energies lower than the threshold strain energy release rate T_0. As a result, no crack propagation occurs as a result of mechanical work; it is all caused by chemical degradation due to ozone. The rate equation takes the form of:

$$\frac{dc}{dN} = k_z[O_3] = R_z \tag{3.15}$$

where k_z is the rate constant due to ozone, $[O_3]$ is the ozone concentration and R_z is the crack growth rate, which is independent of strain energy release rate. Here crack propagation occurs as a result of chain scission due to a chemical reaction between ozone and carbon-carbon double bonds. Ozone will attack rubbers above a critical tensile stress which corresponds to a strain energy of approximately 0.1 Jm^{-2} for unprotected NR and SBR compounds.

In region 2, cracks propagate as a result of both ozone attack and mechanical methods in an approximately additive and linear way. Therefore, the rate equation takes the form of:

$$\frac{dc}{dN} = R_z + A_t(T - T_o) \tag{3.16}$$

where A_t is a crack growth constant for region 2.

61

Region 3 features crack propagation predominantly as a result of mechanical work and features a power law dependency between crack growth rate and tearing energy for elastomer and some non-elastomers as well:

$$\frac{dc}{dN} = B\left(\frac{T}{T_u}\right)^{\beta}$$

(3.17)

where T_u=1 Jm^{-2} and is included only to make T/T_u dimensionless, B and β are material constants, characteristic of region 3. β is known to indicate elastomer properties that focus around hysteresis, ranging from values between 2 and 6 for most elastomers. Typical examples of this are: for NR, $\beta\sim2$ predominantly known to be a result of strain induce crystallisation effects, and SBR, $\beta\sim4$ due to not featuring SIC effects.

For tearing energy levels that exceed region 3, dc/dN approaches the velocity of the elastic waves in rubber which is approximately 50 ms^{-1}. Therefore, strain energy release rate reaches a critical rate where catastrophic tearing takes place. There tearing energy here is defined as:

$$T = T_c$$

(3.18)

where T_c is the critical strain energy release rate.

3.1.8 CYCLIC VS TIME DEPENDENT TEARING

Work by Busfield [Busfield. J. J. C et al, 2002] aims to understand and separate two independent components within crack propagation which both sum to the total crack propagation. A time component that is dependent on the length of time of each cycle and the tearing energy at each time interval within a single cycle, and a cyclic component that is independent of the length of time of each cycle and is genuine crack growth.

$$\frac{dc}{dn} = \left(\frac{dc}{dn}\right)_{time} + \left(\frac{dc}{dn}\right)_{cycle}$$

(3.19)

The time component can be found by utilising static crack growth measurements and the cyclic component is found by subtracting the time component away from the total. A pure shear geometry was used to measure the cyclic crack growth behaviour and trouser test geometries were used to measure the static crack growth behaviour.

The time dependent component can be found from the static crack growth using the following approach. Starting with a force-time relationship for one loading cycle, the tearing energy is represented as:

$$T = f(t) \tag{3.20}$$
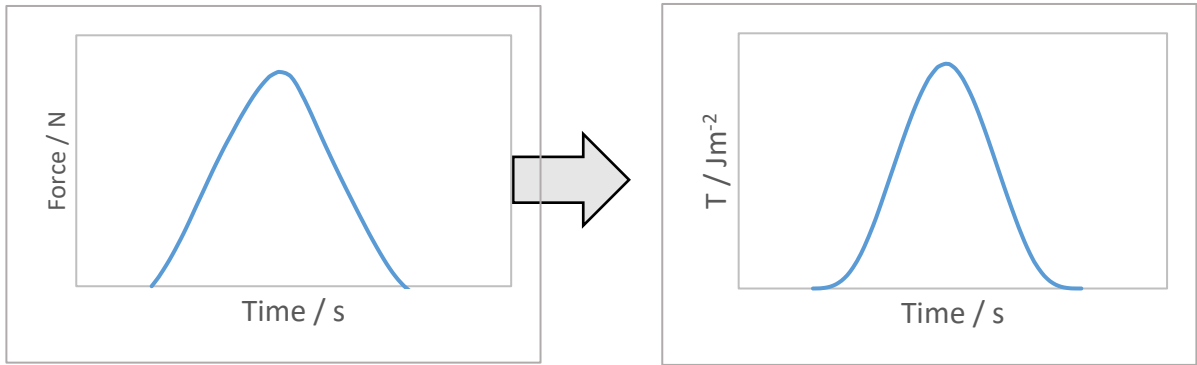
Figure 23: Graphs showing the processing of a force vs time plot to a tearing energy vs time plot.

The static crack growth measurements as a function of crack growth rate and tearing energy is represented as:

$$\frac{dc}{dt} = B_s \left(\frac{T}{T_u}\right)^{\beta_s} \tag{3.21}$$

By substituting equation (3.20) into (3.21), the relationship becomes:

$$\frac{dc}{dt} = B_s \big(f(t)\big)^{\beta_s} \tag{3.22}$$

This then leads to the increment of crack growth per cycle, Δc, which is the time component of the crack growth behaviour. This can be represented as:

$$\Delta c = \int_0^{t_s} B_s \big(f(t)\big)^{\beta_s} dt = \left(\frac{dc}{dn}\right)_{time} \tag{3.23}$$
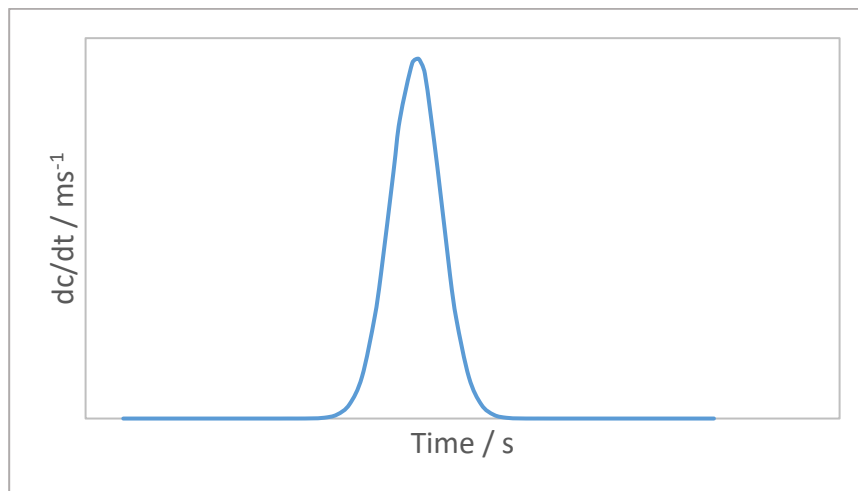
Figure 24: A graphical representation of the time component of crack growth

By integrating this curve, the area is approximately equal to the amount the crack grows during a single cycle.

3.1.9 FATIGUE LIFE PREDICTION

Industrially, the ability to understand an elastomeric material's relationship between tearing energy and crack propagation rate is very significant. Using information like this, predictions of fatigue life can be generated, especially as the energy required to propagate a crack is a material characteristic and not a geometric one.

One method of estimating fatigue life when a material is subject to a tensile or compressive cyclic stress with a non-zero mean stress is to use Goodman's Rule.

$$\Delta\sigma_{\sigma_m} = \Delta\sigma_0 \left(1 - \frac{|\sigma_m|}{\sigma_{TS}}\right) \tag{3.24}$$

In this equation, σ_{TS} is the tensile strength, σ_0 is the number of cycles till failure in N_f cycles under zero mean stress and $\Delta\sigma_\sigma$ is the number of cycles to failure for a mean stress of σ_m. Using this, a relationship can be found between a mean stress between 0 and σ_{TS} and the cyclic stress range. As the mean stress increases, the stress range to cause fatigue failure in the same number of cycles decreases. This is an empirical technique that is known to not be reliable for elastomers.

In addition to this, Miner's rule of cumulative damage has also been used which is seen to work well with elastomers.

$$\sum_i \frac{N_i}{N_{fi}} = 1 \tag{3.25}$$

Here N_{fi} is the number of cycles to fracture in region i, and $\frac{N_i}{N_{fi}}$ represents the fraction of the lifetime used up after N_i cycles in that region. Failure occurs when the summation is equal to 1. The summation of these different regions enables an analysis to be done on samples with varying cyclic stress ranges during a single test. This approach has been shown to be valid when predicting real life service conditions. A general engineering approach used in [Callister, W.D, 1994] has adopted an approach to determine fatigue life by plotting stress vs number of cycles to failure.

3.2 DEGRADATION OF ELASTOMERS

3.2.1 INTRODUCTION

Elastomers suffer many degradation effects that can generally be split into mechanical and chemical effects. Some of the mechanical effects have been explained previously from subjects including relaxation, creep and crack growth. The chemical effects that need to be considered in this study are mostly environmental based. Some of these effects include elevated temperatures, oxidation, ozone and contact with aqueous and hydrocarbon liquids. While some degradation effects like oxidation have been studied for some time, effects such as those caused by contact with hydrocarbons is a relatively new study area.

Specific oil and gas industry related papers are limited. Papers like [Campion. R, 2003] give inciteful overviews on aspects such as durability of elastomers subjected to severe fluid duties, however it is clear that much more focussed research is needed.

3.2.2 EFFECT OF OXYGEN

Oxidation can occur in almost all organic compounds. In polymers, such as elastomers, oxidation causes deterioration in elastomer properties and can also discolour, often making samples darker. This deterioration causes changes in molecular weight via crosslinking or via chain scission, with or without the influence of oxygen. With the addition or reduction of crosslinks, mechanical properties such as tensile strength, modulus, creep and relaxation are all affected. This process is considered degenerative and must be suppressed using antioxidants.

The reaction with oxygen is spontaneous and can be quite simple to understand in low molecular weight compounds, but fairly complex in other compounds. An understanding of it was developed in the early 1940s using free radical chain reaction theory based on experiments on low molecular weight hydrocarbons [Bateman, L, 1954]. This system is split into three sections: initiation, propagation and termination.

Initiation is the first reaction to the free radical chain. It is caused by thermal exposure, photo chemical exposure, mechanical exposure to metal ions or irradiation from high-energy sources. In elastomers, the rate of initiation is also affected by the composition and impurities can slow this reaction down. It has been suggested that mechanochemical chain scission during processing that yields macro alkyl radicals is the primary initiating process. This forms

hydroperoxides (ROOH) causing oxidation by decomposition. Another suggestion [Al-Malaika, S, 1995] is associated with heating or irradiating hydroperoxides. When hydroperoxides build up, their decomposition predominates as the initiating reaction in oxidation. The first suggestion shows a higher activation energy and so is generally favoured at elevated temperatures, whereas the second suggestion is thought to predominate only after hydroperoxides have accumulated.

Propagation is a degenerative reaction cycle characterized by the formation of hydroperoxides and the regeneration of new alkyl radicals. The hydro peroxides formed are mostly unstable and so may decompose forming additional radical intermediates. The number of propagation cycles before chain termination is referred to as the kinetic chain length. For polymers with long kinetic chain lengths, the hydroperoxides formed will dominate the initiation of new chains during prolonged oxidation.

Termination refers to the process where propagation chains are stopped by recombination of radicals. At low contents of oxygen, radicals either react with or without oxygen resulting in crosslinking. With added levels of oxygen, termination can occur through bimolecular termination.

Oxidation in polymers often experience a fast oxidation process that is caused by an induction period [Stenberg, B., Peterson, L.O., Flink, P. and Bjork, F, 1986]. This is an autocatalytic process as reactions are catalysed through heat, light and other radicals. This process is caused by various oxygenated groups being introduced to the polymer chain or at its ends by oxidation, potentially also forming other low molecular weight products.

Little research has been done on the fatigue properties of HNBR after ageing in air. However, some surprising results have originated based on the research done so far. An example of this is [Beranger, A.S. et al, 2018] where NBR, HNBR and HNBR ZSC compounds were aged in air for either 7 week or 21 days at 80°C and then tested in cyclic pure shear fatigue. While most samples got weaker as the ageing environments got more extreme as expected, some tests clearly showed an increase in toughness after ageing, especially in NBR. No explanation is given to justify this remarkable behaviour in the paper; however it clearly shows that the understanding of fatigue in post-aged nitrile elastomers is still an area that needs further investigation.

3.2.3 DIFFUSION

Oxidation is a process that occurs significantly more on the surface as environmental effects play a key role in catalysing the reaction process. However, penetration from the surface to the bulk material does occur.

Depth of penetration of oxidation decreases as temperature is increased. At high temperatures the consumption rate is increased beyond the rate of diffusion below the surface. Therefore, the increase in rate of oxygen consumption means that less oxygen is available for reactions below the surface. The permeability of oxygen is lower through oxidized material [Van Amerongen, G. J, 1964] [Mattson, B. and Stenberg, B, 1992] so that the bulk material might be completely deprived of oxygen even when an oxidized layer is formed on the surface [Mattson, B., Stenberg, B, Persson, S. and Ostman, E, 1990]. This can lead to an anaerobic ageing of the bulk material and a resistance to degradation governed by the thermal stability of the material. This can lead to an interesting problem when including antioxidants within the elastomer. For elastomers free of antioxidants, the outer layer rapidly oxidises, in comparison, and generates this oxidised layer on the surface. Whereas elastomer rich with antioxidants that bloom to the surface and provide a protective layer, the initial oxidised layer is not formed as fast and enables oxygen to diffuse more readily into the bulk material, potentially causing a thicker oxidised layer.

3.2.4 OZONE

Ozone degradation is a result of ozone reacting with carbon-carbon double bonds. This causes cracks to form on the surface as well as time-dependent crack growth. As mentioned previously, in cyclic loading cases where mechanical loading is below the threshold strain energy release rate T_0, ozone can be the dominant mechanism in crack growth.

Small concentrations of ozone in the atmosphere can cause surface cracking on an unprotected elastomer in a few weeks. This requires a minimum surface tensile strain, where the crack grows perpendicular to the strain. This is where crazing as a result of sunlight differs to ozone cracking.

3.2.5 ELASTOMERS AT ELEVATED TEMPERATURES

Elastomers are used in a wide range of temperatures, ranging from those just above T_g which can be as low as -70°C for example for NR, and higher operating temperatures like those found in the oil and gas industry of 180°C.

In ambient temperatures, the main degradation effects come as a result of poor elastomer processing and curing. For example, an incomplete cure can result in a slow continued crosslinking process even at ambient temperatures, causing hardening throughout the specimen. These conditions are then greatly catalysed by higher temperatures, causing an incomplete cure to crosslink faster and at a higher quantity [Gent. A. N, 2001].

3.2.6 ELASTOMERS IN FLUIDS

A large amount of the bulk elastomer, approximately 10%, is free volume. This is space between the molecules and polymer chains [Gent. A. N, 2001]. Whereas this aids with many elastomer characteristics such as elasticity and flexibility, this also offers space for material that is not intended.

Different elastomers react differently to various fluids; however, no elastomers can completely withstand the physical or chemical effects that arise from this contact. Mostly, if an elastomer absorbs a large volume of any liquid, its properties generally become weak and non-functional and progressively worsen due to chemical attack. Papers such as [Jerrams, S, Hanley, J, Murphy, N, Ali, H, 2008] show that fundamental properties of elastomers such as EPDM become severely altered after contact with oil and elevated temperatures within only 1 hour of interaction.

Two physical processes occur in the uptake of fluids by elastomers. Liquids and gases dissolve in through the surface via adsorption and penetrate further through the bulk via diffusion. The rate of swelling is a diffusion-controlled mechanism and for the fluid, and the initial surface concentration is determined by adsorption.

The rate of diffusion through the elastomer is independent of pressure at normal atmospheric pressures; however, at higher atmospheric pressures there is a considerable effect of pressure illustrated by gas permeation. This describes the movement of gas straight through an elastomer sample involving adsorption, diffusion and evaporation as the opposing process of the other side of the sample.

Free energy change:

$$\Delta G = \Delta H - T\Delta S \qquad\qquad (3.24)$$

where ΔH is enthalpy, T is temperature and ΔS is change of entropy

Another very important topic when understanding the problem of elastomer fluid interaction is leaching. Leaching is the process of removing material from the elastomer, either bound or loose, within the bulk via a liquid medium.

As fluids interact with the elastomer, they react with elastomer reinforcement fillers, process aids, protectants and compounding ingredients left over from an incomplete cure. The movement of ingredients to the outside of an elastomer can be advantageous. For example, certain protectants like wax antioxidants bloom to the surface to provide a protective layer. The process of leaching is mostly seen as a disadvantage though as the influence of the fluid mostly weakens elastomers and leaching usually does the same by removing material that helps to enhance the elastomer. The understanding of these interactions must be taken on a case by case basis; however certain factors influence how susceptible ingredients are at being leached out of the elastomer. These include whether an ingredient is physically or chemically bonded, the elastomer fluid solubility parameter, the fluid diffusion rate and temperature.

Measuring swelling and leaching is not an easy task experimentally. Both processes occur at the same time, interact with each other and are generally not very repeatable as mixing, curing and the elastomer life history are not only difficult to repeat and reproduce exactly, but also influence these tests significantly. Most understanding in this field is dealt by approximating both these values with respect to each other [Gent. A. N, 2001].

Small amounts of research into HNBR products aged in oil have been published, most of them more recently. Papers such as [Weitao, L., Weifang, Z., Xuerong, L., Wei, D. and Dan, X, 2017], [Alcock, B and Jorgensen, J. J, 2015] and [Alcock, B, Peters, T. A, Gaarder, R. H, Jorgensen, J. K, 2015] have done studies on the combinations of oil and elevated temperatures. However, a lot of these studies are primarily quantitative and struggle to grasp all the mechanisms behind the behaviour. This is not an easy task as many ageing and elastomeric mechanisms are active at the same time. Therefore, more research is needed to isolate mechanisms and understand the intricacies more.

69

3.2.7 AQUEOUS LIQUIDS

Almost all elastomers encounter a small amount of water after long time periods due to the presence of water vapour in the atmosphere. Both solubility parameters are often far from each other, especially when considering natural rubber; therefore water generally does not build up in these circumstances. However, certain applications require elastomer products to be permanently in contact with water, such as sealing.

Generally, swelling and diffusion of water into elastomers is to be restricted and minimised. Not only because it is required in applications like sealing, but also the addition of water diminishes elastomer properties and also leaches out material. It is difficult to predict the response of elastomers after interaction with water as the response can vary significantly depending on different factors. However, properties like tensile strength, hardness and toughness usually decrease.

Protection against adsorption and diffusion of water often comes in the form of hydrophobic fillers or metal oxides in the cure system. A polychloroprene cured with litharge restricts the amount of water absorbed much more effectively than one cured with magnesium oxide. The removal of impurities can also restrict water swelling as some impurities are hydrophilic.

Ingress of water into the bulk elastomer is a diffusion-controlled mechanism. Considering water and natural rubber interaction, even though the solubility parameters are far away from each other, natural rubber can feature hydrophilic impurities that water collects around. This can raise the swelling content of water higher than expected.

Natural rubber blended with SBR has been used to line water purification vessels used in power generators for many years. In this application, the long exposure to the water deteriorates the lining of the elastomer; however, regardless of this deterioration, vessels are largely corrosion free [Gent. A. N, 2001].

3.2.8 HYDROCARBON LIQUIDS

Elastomer interactions with hydrocarbon fluids often occurs in oil and gas and automotive applications. Solubility parameters between these two entities are often quite close leading to high swelling ratios. Hence, elastomers with specific oil resistance characteristics are often used. These generally include NBR, HNBR and fluoroelastomers.

Hydrocarbon liquids can include hostile materials like hydrogen sulfide which can target unsaturated elastomers such as NBR. Therefore, HNBR, the saturated version of NBR, is often a preferred choice in these applications.

For hydrocarbons, diffusion dominates movement of liquids into bulk just like water. Molecules move by "jumping" to adjacent free volume holes in the matrix during different mechanisms such as mechanical movement and thermal motion from kinetic energy. The thermodynamic drive behind this motion is then to equalise the concentration of the liquid throughout the elastomer [Gent. A. N, 2001].

The rate of diffusive migration is governed by Fick's first law of diffusion:

$$\left(\frac{1}{A}\right)\left(\frac{dm}{dt}\right) = -D\left(\frac{dc}{dx}\right) \tag{3.25}$$

where dm is the amount of liquid diffusing across area A in time dt to give a concentration gradient of dc/dx and D is the diffusion coefficient in m²/s.

Fick's second law considers incremental increases in concentration along the path of migrating:

$$\frac{dc}{dt} = D\left(\frac{d^2c}{dx^2}\right) \tag{3.26}$$

3.3 CONCLUSIONS

To summarise, the work shown in this chapter aims to highlight the understanding of the areas focussed in this body of work, from crack growth to elastomer degradational effects. What can mainly be concluded from this is that the vast majority of the work based around understanding these effects are focussed around common elastomers such as NR and SBR. These are elastomers that have not only been researched for the longest but are still essential in current engineering applications today. However, for applications that require more specialised materials, these elastomers cannot function to the same level. As the oil and gas industry ventures into environments that feature more extreme conditions, elastomers that are specialised in dealing with these conditions are vital. However, the understanding behind how they perform so successfully in these roles is vastly under researched. Therefore, this body of work aims to add to that understanding.

4. MATERIALS AND CHARACTERISATION

In this chapter, the focus of how the materials need to be tested and within what ranges will be addressed. This will begin by understanding how a positive displacement motor, or in this case a mud motor, works and what its environmental conditions are. This will shortly be followed by a description of the materials used for this work including basic characterisation work of the formulations. Finally, testing methods that will be used in the subsequent chapters will also be described.

4.1 INTRODUCTION

There are a broad range of applications, environments and functions for elastomers in the oil and gas industry. In practice there is a significant requirement to make elastomer products last longer in service. Depending on the particular application, this can be essential especially in safety critical applications such as a blow-out preventer (BOP) which ensures the safety of the entire oil platform as well as the entire crew working on the platform. Even for the product that is under examination in this work, the mud motor stator, which does not put the safety of oil platform workers at risk when this elastomer part reaches its end of life but does bring oil production to a standstill when it fails. An oil well that is out of action can cost in excess of $1M per day from lost production, so to extend the product life and reduce downtime is a high priority for the industry. So, it is desirable to be able to both predict and extend an elastomer product's lifetime.

4.2 MUD MOTOR APPLICATION (POWER SECTION OF MUD MOTOR)

The main application under examination in this work, is an elastomeric lining of the stator used in the power section of the mud motor. As shown in figure 25, the power section of the mud motor is composed of a rotor (connected to the shaft) and a stator. The stator is made of a steel tube with a helicoidal elastomer lining. This assembly uses the reverse principal of the cavity positive displacement Moineau pump. It allows to transform hydraulic power (flow and pressure) (pressurised fluid pumped from the surface) into mechanical power (speed and torque) to rotate the drilling bit.

Figure 25: A diagram of a mud motor including the metal rotor and cross section of the elastomer stator

The elastomeric stator has x number of lobes and the metallic rotor has x-1 lobes. This difference opens cavities allowing the pressurised drilling fluid to pass through. The stator and rotor both feature a profile that complement each other, and which allows the lobes to turn around the rotor or stator as shown in figure 26.
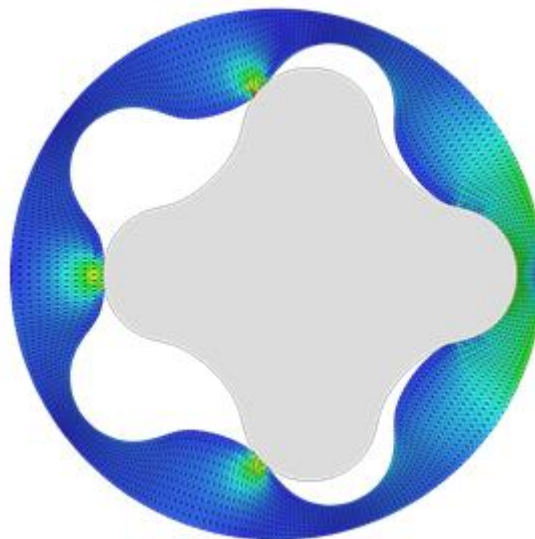
Figure 26: FEA (Finite element analysis) cross section of a mud motor rotor and stator

This means that as hydraulic pressure is applied at one end of the drill, which causes the drilling mud to progress through the motor, it transfers mechanical power to the rotor that spins it within the elastomer stator, therefore providing mechanical force to the drill bit. Different

designs have been developed (including metal to metal configuration between where both rotor and stator are metallic) however it is necessary for the stator to have an elastomer lining for several different reasons. To generate the necessary power a sealing is required between the cavities. At the sealing line the elastomer lining is compressed. This is called interference. The different degrees of interference are used considering the level of power and endurance required to perform the drilling job. In addition, the elastomer lining offers a good resistance to wear due to abrasion and erosion during the run. Large (several millimetres) solid particles, such as baryte, often circulate in the drilling fluids and can cause irreversible damage due to the highly pressurised flow.

The fluids used are called drilling fluids and are complex formulation to respond to the specific job to perform in term of formation to drill, temperature and pressure. They can be water or oil based (main phase). Most of the applications use an oil based fluid which is generally, an emulsion of oil and water. These fluids are used to power the mud motor, cool and lubricate the bearing and drilling bit and thanks to their high density carry the cuttings to the surface.

The stators are manufactured using an injection process in which the elastomer is injected between the stator tube and a former mandrel with the stator profile. Prior to injection process an adhesive is applied inside the tube allowing the bonding of the elastomer lining to the internal surface during the vulcanisation process.

Every mud motor design is tested using a dynamometer and the performance specifications sheets are available from the Dyna-Drill website.

During service, there are 3 main sources of failure of the rubber lining.

1. Fatigue: Crack initiation and propagation results in a chunking process whereby large amounts of a lobe section are torn off [Schlumberger, 2004]. This is the most common form of failure as there are many sources of crack initiation in the elastomer and the crack propagation is also dependent upon a wide range of the operating conditions. Therefore, it is difficult to identify which are the key factors, especially when they are all acting at the same time and potentially having a combined effect. However, the main influences are:

- Mechanical – Repeated cyclical loading of the rubber in the stator lobes causing a fatigue failure.

- Thermal – Increasing the temperature causes the rubber to thermally expand significantly more than the metal parts to which it is bonded which results in geometric changes in both size and shape. The operating temperature, in some cases, may already be high, but this is then increased further in service due to additional internal hysteretic heating from the elastomer.

- Chemical – The drilling fluids used can be absorbed by the elastomer materials which can cause swelling, leaching, geometric changes and also significant changes to the elastomer's mechanical properties by methods including chain scission.

2. Wear: As the rotor turns and spins within the stator, it comes into contact and compresses the elastomer. The fluid often contains particulates of barite to increase the specific gravity of the fluid and it also carries back to the surface the debris from the drilling process. These rigid particles could have a significant effect on the wear of the elastomer.

3. Debonding: the diffusion of drilling fluid and the crack appearance in the elastomer lining can allow drilling fluids to reach the stator-casing interface enhancing the chemical degradation of the bonding agent and initiate debonding between the rubber lining and the steel tube.

4.3 TESTING MATERIALS

The most common elastomers used for this application are NBR and HNBR with the respective temperature limit of 125 and 160° C [Dyna-Drill, 2013]. The nitrile-based elastomers are typically used because of their enhanced resistance to swell in hydrocarbons. NBR can also be hydrogenated to remove double bonds that react easily, making the polymer more chemically stable. The amount of acrylonitrile content in these elastomers offers an increased resistance to temperature and chemicals. A typical ACN (acrylonitrile content content) of the elastomers used in oil and gas application varies between 32 and 43% depending on the application and the environment.

Carbon black is commonly used as a reinforcement filler. The amount and the type of carbon black filler are adjusted to consider the viscosity of the unvulcanised materials and the hardness of the final product (from 65 to 90 shore A).

The curing system is either sulphur for lower temperature application and the peroxide based for higher temperature application. The peroxide curing systems are usually accompanied by co-agents to optimise the performance after the vulcanisation.

The choice of materials for this study focuses on extreme and high temperatures application. The base elastomer is HNBR with 43% ACN content (approximately 5.5% ±1 residual double bonds) using a peroxide curing system. The carbon black filler N550 has a surface area of 45m^2/g and an average particle size of 39-55 nm. The rest of the formulation uses very common plasticisers and antidegradants for the applications. The four compound formulations used are presented below. They are simplified and model materials.

(Unit: PHR)		HNBR 0	HNBR 60	HNBR 75	HNBR 75 NP
Elastomer	Therban 4364	100	100	100	100
Filler	N550		60	75	75
Antidegradants		1.5	1.5	1.5	1.5
Plasticisers		10	10	10	
Crosslink	Peroxide	8	8	8	8
Co -Agent 1		10	10	10	10
Co-agent 2	ZDA				

Table 1: The elastomer formulations used for all tests (PHR: Per Hundred Rubber)

All four formulations are very similar to each other:

- HNBR 0 is base formulation without any reinforcement filler. The number 0 refers to the compound's filler content.
- HNBR 60 is the same formulation as HNBR 0, with the addition of 60 phr of N550 carbon black.
- HNBR 75 has an even higher carbon black content, at 75 phr of N550.
- HNBR 75 NP is based on the HNBR 75 formulation, but on this occasion, it has had all of the processing plasticiser content reduced to 0 phr.

Throughout this study four different batches of each compound were produced in 1.2kg batches. This was done on purpose to ensure that a fresh compound was being used throughout the programme. This limited potential ageing mechanisms from occurring whilst a batch is left either uncured or untested over a long period of up to four years. The difference

between different mixing batches of the nominally similar compounds were measured on the cured sheets that were produced from each batch.

4.3.1 MIXING AND MOULDING

The mixing was undertaken at Tun Abdul Razak Research Centre (TARRC) based in Hertfordshire. Products were mixed in an internal mixer and finished on a two-roll mill. All testing specimen have been prepared at QMUL.

Before samples were cured, each of the samples from all batches were tested for their cure characteristics using a standard oscillating disk rubber cure rheometer. A small sample was placed in the rheometer and the resulting changes to the torque were tested at the intended curing temperature for an extended period. Testing temperature was curing temperature, 170°C. The resulting figures for these plots are shown here:
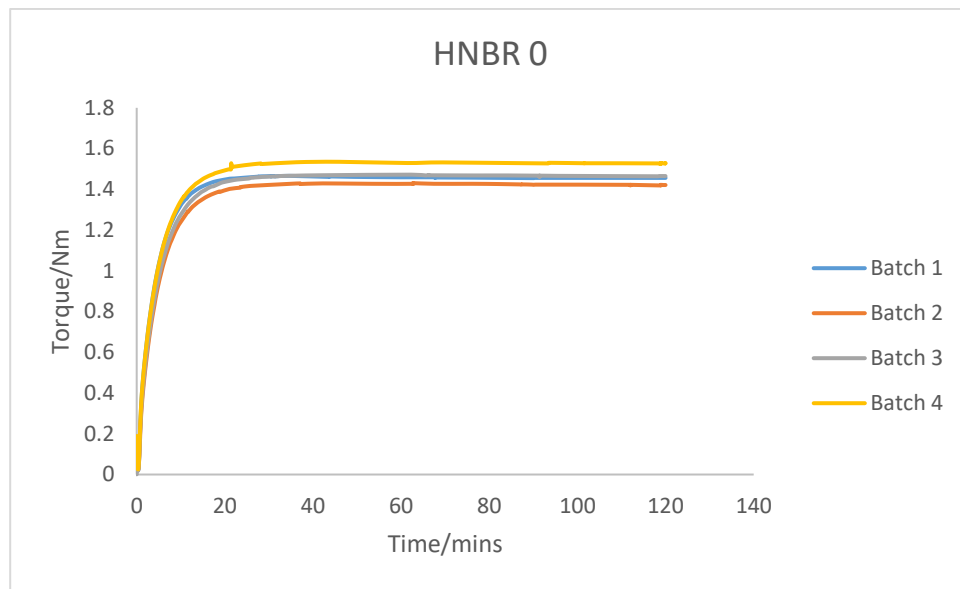
Figure 27: Rheometer curves for all four HNBR 0 batches
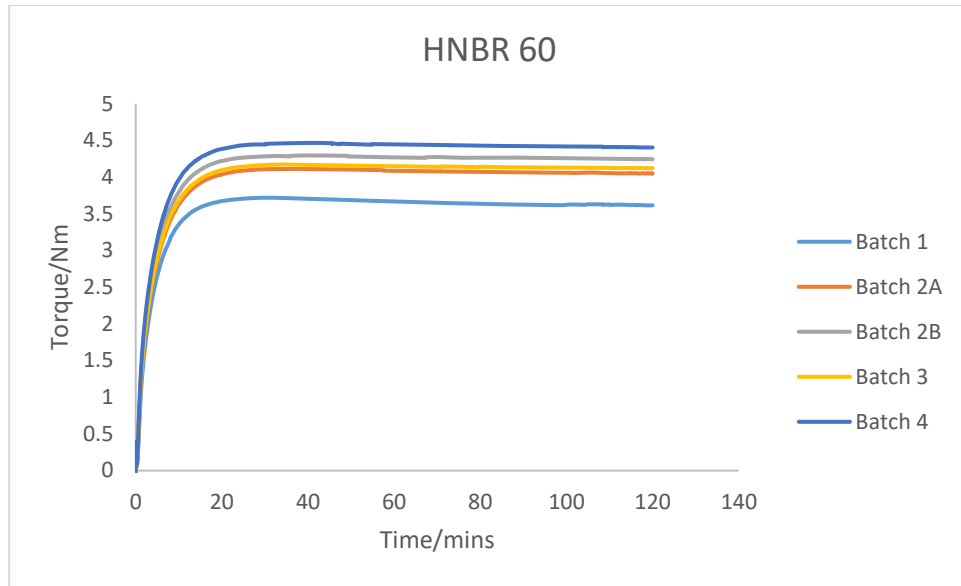
Figure 28: Rheometer curves for all five HNBR 60 batches
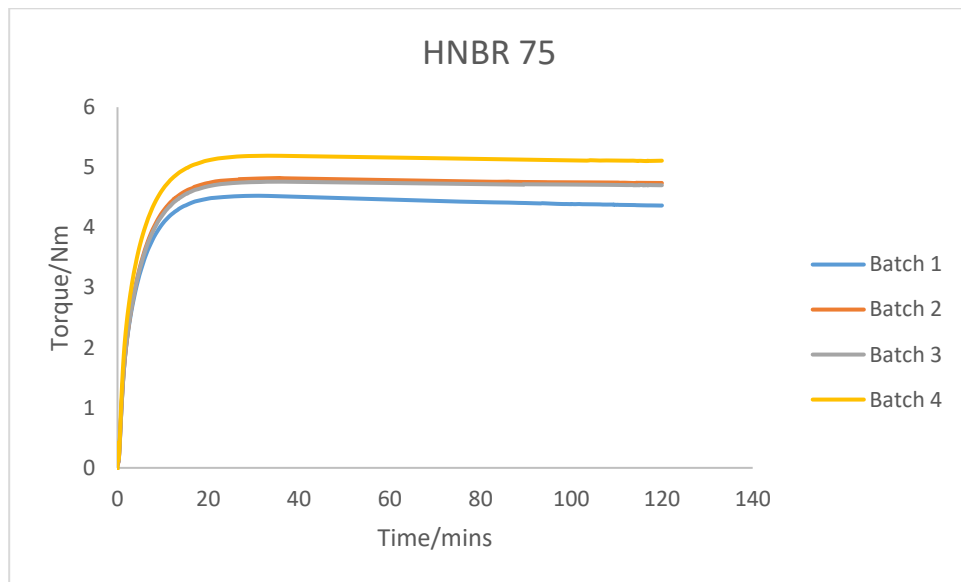
Figure 29: Rheometer curves for all four HNBR 75 batches
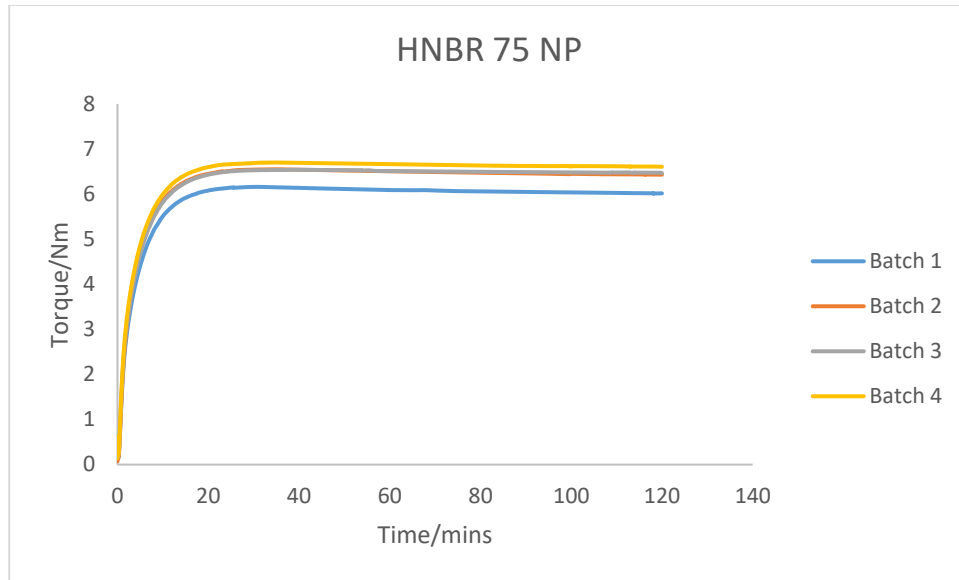
Figure 30: Rheometer curves for all four HNBR 75 NP batches

All curves feature the desired plateau cure. Plateau cures such as the ones shown hear are very stable and can produce reliable cured test samples so long as they are left in the mould to a full cure time. There is little possibility of over curing the compound unless the temperature control breaks down. The small differences that can be seen between batches is not enough to indicate any major rate changes in the curing chemistry over the duration of the project. The final plateau torque value reflects the filler reinforcement and the number of crosslinks found in the cured compound.

As it is unclear to see from figures 27-30, a focus of one of the samples in the first 20 mins is seen below to identify the 2 point rise.
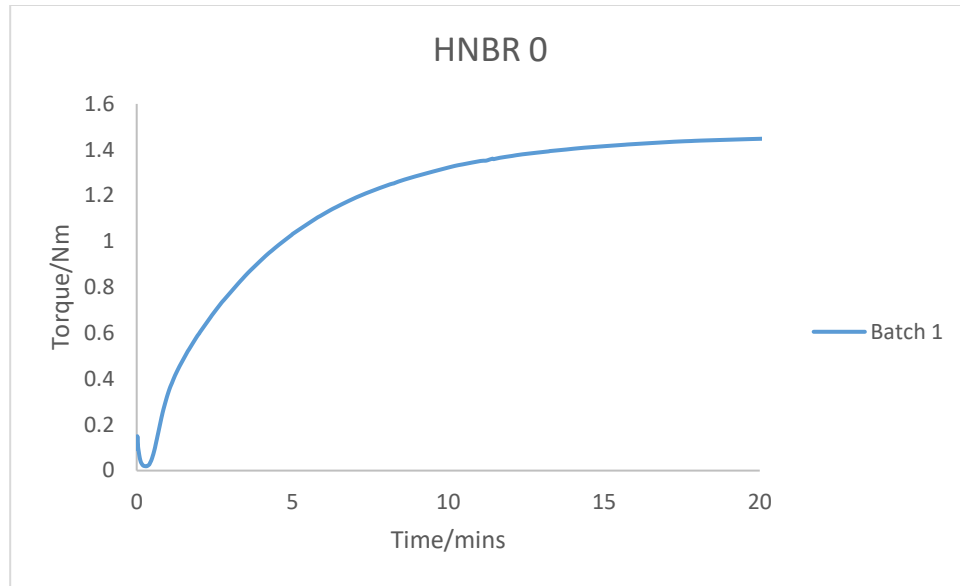
Figure 31: A focus on one rheometer test to identify the 2-point rise

Vulcanisation and moulding were performed using a hot press. This machine provides heat and mechanical pressure during the vulcanization process. The curing conditions were:

- Curing temperature: 170°C
- Curing time: 30mins
- Pressure: 12.3 MPa

Samples were placed in a metal mould that had previously been heated to the curing temperature and then placed in the press which was closed and the pressure applied. During the initial stage of curing several "bump" pressure cycles were quickly applied and released to encourage any trapped air bubbles to be released from the sample. Moulds were also sprayed with a silicon lubricant so that the moulded samples would not stick to the mould. This was necessary for the sample to be released without damage.

The preparation of the testing specimen involved moulding 2mm thick sheets and the use of standard cutters.

Across the study, four different batches of four materials have been prepared and as shown in the rheometric vulcanisation curves, similar level of quality has been achieved with time. Tensile tests have been performed to compare the batches with time, and a very low variability in the ultimate properties has been achieved of a maximum percentage difference of 11.8%.

These results demonstrate the consistency in the materials across the study allowing to compare the results at any time.

4.4 TESTING AND AGEING CONDITIONS

For mud motor applications, extreme environments and operational parameters consider:

- Temperatures up to 150°C (with peaks at 180°C)

- Pressures up to 150 MPa

- Constant contact with drilling fluids.

- Dynamic deformations (frequency up to 30Hz)

  - Strains up to 50%

  - Strain rates up to $100s^{-1}$

When the elastomer behaviour is essentially elastic in nature, these materials are described as exhibiting large strain hyper-elastic behaviour. The test temperature and the chemical environment, whilst being immersed in drilling fluids, has a large effect on this behaviour. As well as this, elastomers exhibit rate dependent behaviour. This rate dependence is known as the viscoelastic behaviour. In this case, the strain rate and pressure both change the physical behaviour of the elastomer. All of these effects also have coupling effects where they are affected by each other and the environment in different ways. Understanding all these coupling effects is very difficult as there are a lot of variables and the dependencies between them are very complex. To gain clarity of the extent of this problem, at an early stage of the project it was attempted to create a flow chart to capture all these environmental effects, rubber mechanics models and all the couplings and co-dependencies between them all. This enabled the project to be split up into constitutive parts that could be tackled independently.
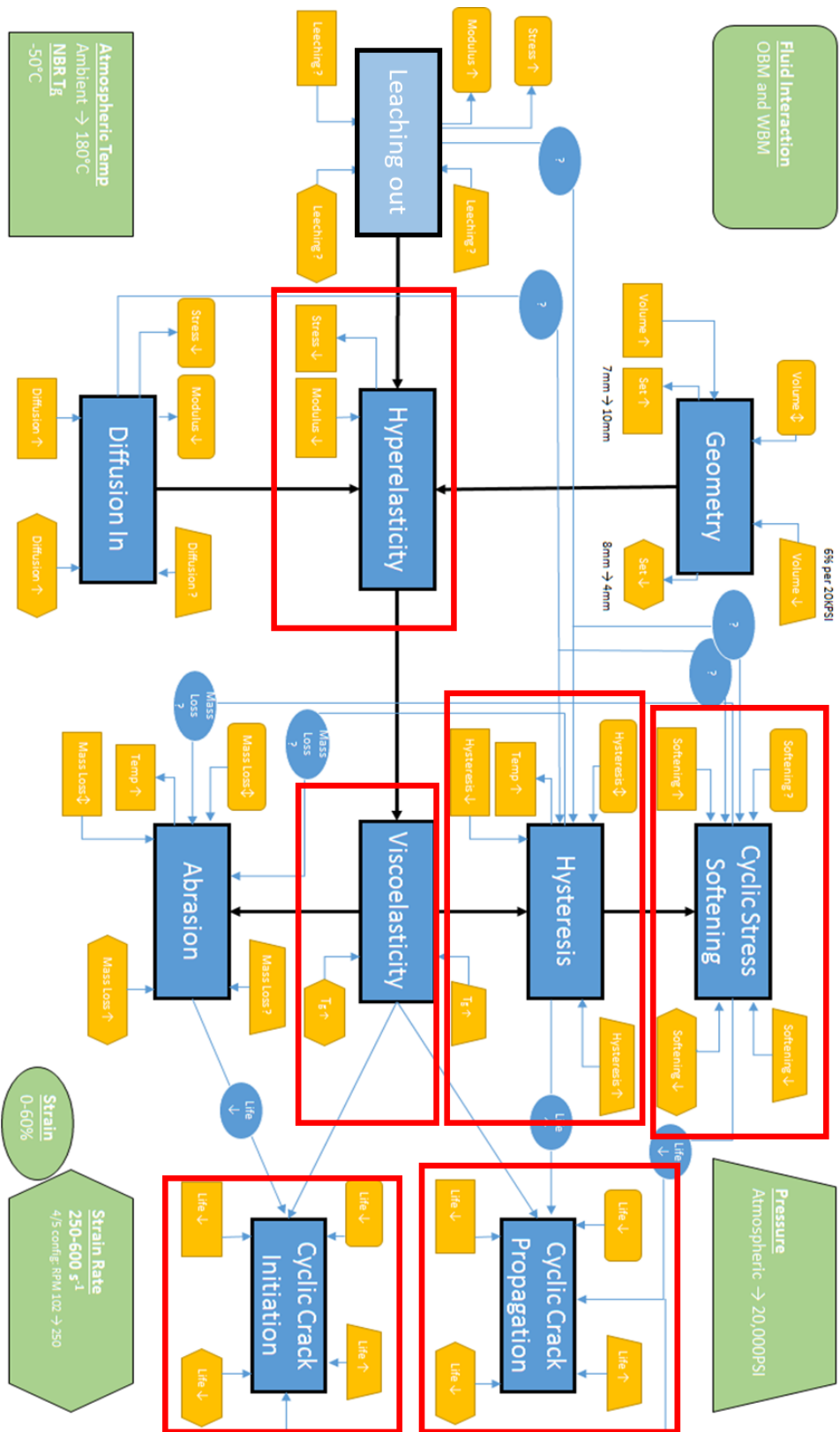
Figure 32: Elastomer Flow Chart Illustrating Models and their Interdependencies

Each blue box represents a rubber mechanics model or fatigue study model. The green boxes in the corners represent the environmental and mud motor conditions. These indicate the areas where the study was to focus. The yellow boxes to the corners of the models describe the impact the environmental effects have on each model. They are appropriately positioned in the same corners as the green boxes and with boxes that are the same shape. Finally, there are additional arrows linking the models to describe their impact on each other. The effects that they all have on each other is not fully known and there are some whose behaviour would vary depending upon the detailed combination of factors.

The scope of this PhD was to focus on the areas within red rectangles. The main areas of interest were identified as being the effect of the operating environment on the properties of the mud motor compounds. As the strain rate in service is very fast, this effect of rate was a priority. As well as this, the temperatures can reach the upper limits for NBR/HNBR elastomers and the fluid interaction also has a big impact on the behaviour. From previous testing [Tunnicliffe. L and Busfield. J. J. C, 2015], it was shown that the cyclic stress softening behaviour of these compounds plays a large role in the behaviour of these elastomers in service. This effect requires more understanding to ensure that suitable models of the elastomer in service reflect the true stress state rather than the stress state encountered only in the very first loading cycle in service. Also, it was known that primary failure mode in service resulted from cyclic crack growth, therefore a fatigue study is also important.

It was therefore decided that an initial material characterisation approach followed by an in depth fatigue and static tear study would be a very relevant and broad method of study for this application. By varying the mechanical and environmental conditions individually, the effects of each of these parameters can be modelled and understood separately with the future intention to combine their responses and analyse the mud motor application as a whole. This has the added benefit of being able to approximate the fatigue response if any of these individual parameters change in a mud motor application. An initial material characterisation analysis studying hyperelasticity, viscoelasticity and their effects with temperature, as well as differential scanning calorimetry (DSC), thermogravimetric analysis (TGA) and Fourier transform infrared spectroscopy (FTIR) would also provide a firm understanding on the basic nature of these materials. An alternative approach could have been done to undertake a single test where fatigue response could be measured whilst satisfying all the estimated environmental and

mechanical conditions. In this case, that would require testing these materials at strains of approximately 50%, strain rates in the order of 100/s, operating temperature of 150°C, within a fluid medium of oil and water mixtures at high pressures. However, the required technological development and cost to do such a test would be far beyond the scope of the project. Therefore, it was decided to analyse these effects individually first to then begin to combine them later on and in future projects.

The ageing conditions across the study are as follow:

- Aged in an air oven at 100°C for 168 hours (1 week)
- Aged in an air oven at 150°C for 168 hours
- Aged in an IRM903 oil at room temperature for 168 hours
- Aged in an IRM903 oil at 150°C for 168 hours

168 hours is realistic and representative duration of operation. IRM903 is a reference testing oil with an ASTM testing method (ASTM D471) commonly used in materials development for drilling application.

4.5 TESTING APPARATUS

All ageing and experimental tests were undertaken either at Queen Mary University of London or at Schlumberger Cambridge Research Centre.

All mechanical tests were done on Instron testing machines ranging from Electropulse E10000, Instron 8801 Servo-Hydraulic Testing Machine, Instron 5900R84 Screw Driven Testing Machine and Instron 5967 Testing Machine equipped with a video-extensometer. A range of static and dynamic load cells were available ranging from 1kN to 50kN as well as mechanical grips and attachments.

Additional ageing and characterisations have been performed by the industrial partner and include:

- Ageing in IRM903 oil at 150°C.
- The thermogravimetric analysis (TGA).
- The Fourier transform infra-red spectroscopy (FTIR).
- Equilibrium Swelling Tests.

4.6 CHARACTERISATION

4.6.1 TENSILE TESTS

Tensile tests using a dumbbell specimen geometry were undertaken to measure each material's performance in uniaxial tension. These test pieces were used to characterise each material's hyper-elastic, viscoelastic and cyclic stress softening behaviour.

The dumbbell specimen features two gripping ends with a larger cross section area and a working section at the centre of approximately 30 mm length, 6 mm width and approximately 2 mm thickness.
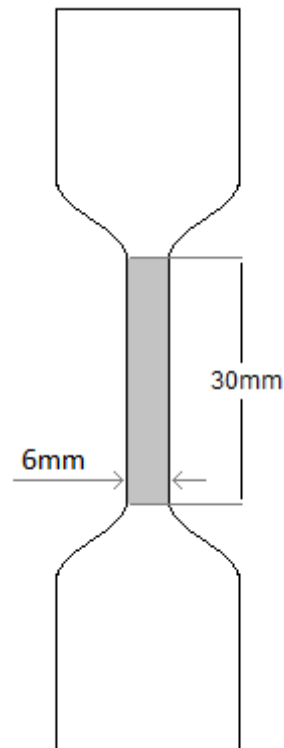
Figure 33: Typical dumbbell specimen with length and width dimensions.

For the initial stress versus strain characterisation, the testing parameters were:

- Maximum Strain: 50%
- Strain rate: 0.01/s (Quasistatic)

For tests that featured more than one cycle, at the end of the unloading process, samples were brought down to zero force before the next cycle began. This was to avoid the sample buckling during the tests. The results are as follows:

HNBR 0 - 0.01/s - Room Temperature
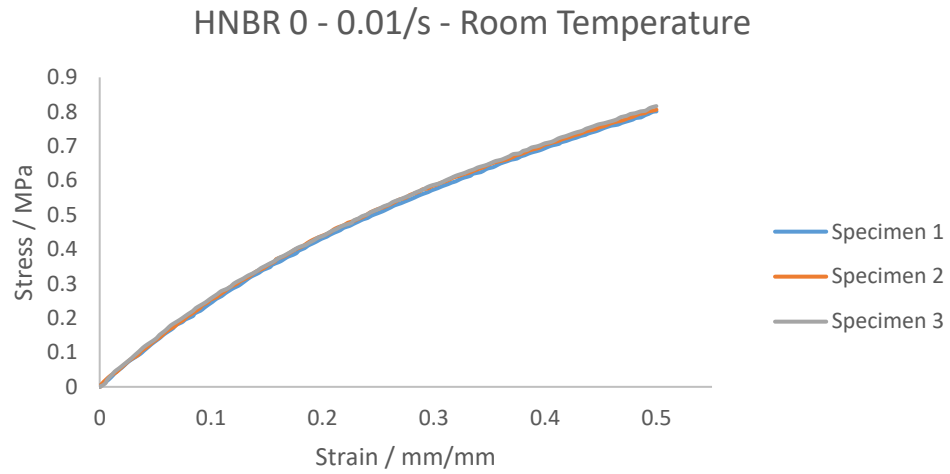
Figure 34: Tensile tests of HNBR 0 to 50%: Three Repeats

HNBR 60 - 0.01/s - Room Temperature
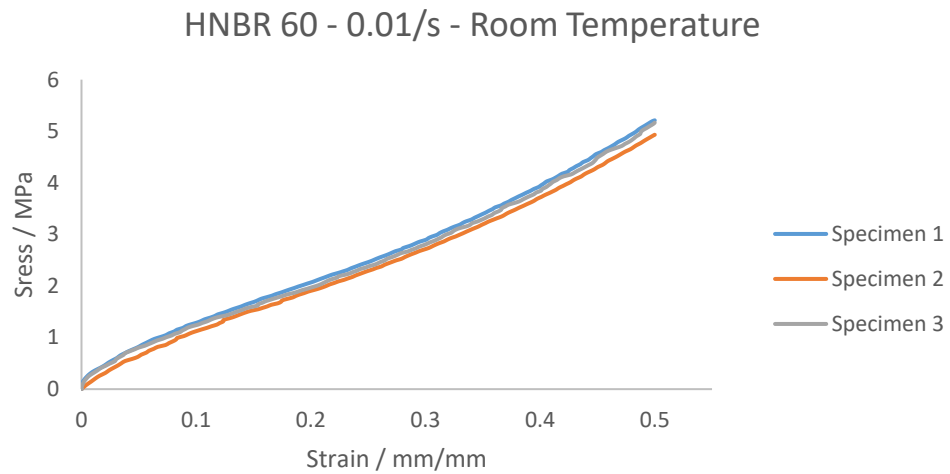
Figure 35: Tensile Tests of HNBR 60 to 50%: Three Repeats

HNBR 75 - 0.01/s - Room Temperature
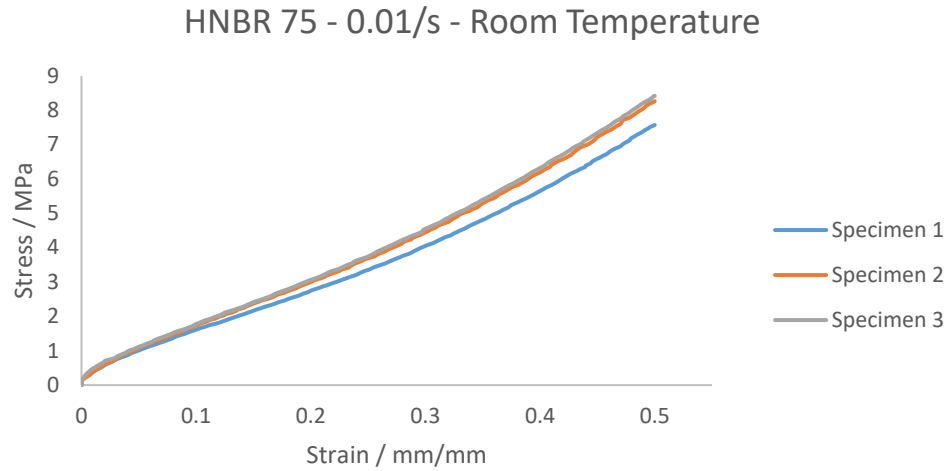
Figure 36: Tensile Tests of HNBR 75 to 50%: Three Repeats

HNBR 75 NP - 0.01/s - Room Temperature
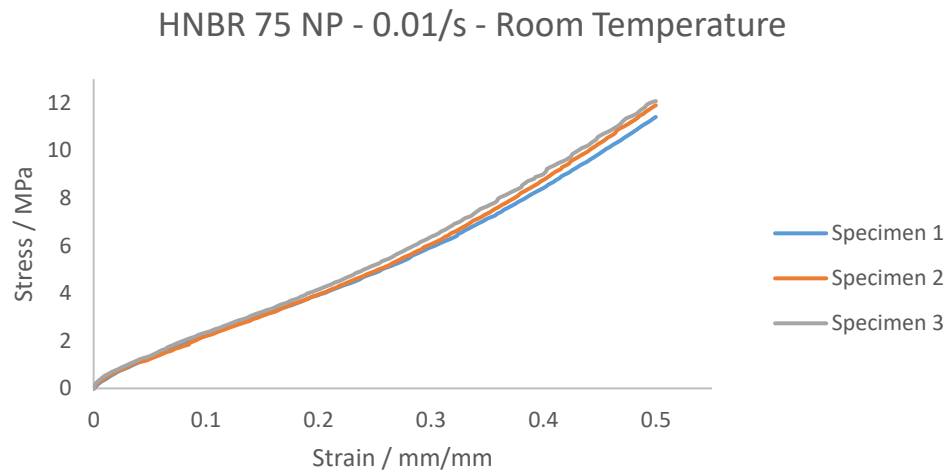
Figure 37: Tensile Tests of HNBR 75 NP to 50%: Three Repeats

The figures 34-37 show that the unfilled sample, HNBR 0, has the lowest modulus and stress at any point within the test, as a result of no reinforcing filler particles being present. As expected HNBR 60 and HNBR 75 both have a higher measured modulus as reinforcing filler volume fraction is increased. HNBR 75 NP, the compound without plasticiser, has the highest modulus of all the samples, indicating the significant role the plasticiser has on the measured behaviour.

4.6.2 MODEL

In order to undertake computational finite element modelling, an appropriate elastic stored energy function, also known as a hyperelastic model, needed to be identified for these high modulus and high strength elastomers. Within Abaqus there are features such as an evaluation tool that can be used for hyperelastic modelling. Test data is measured, and the tool calculates using a least squares fitting algorithm, the most appropriate model constants to fit to the data. This can be done for a wide range of different stored energy functions including polynomial expansions, reduced polynomials, Ogden [Ogden. R. W, 1986] and the Arruda Boyce model [Arruda. E. M and M. C. Boyce, 1993]. The most widely available materials model for elastomers is the polynomial originally derived independently by Rivlin [Rivlin. R. S, 1948] and the most common reduced polynomial models are the Neo-Hookean, the Mooney-Rivlin and Yeoh [Yeoh. O. H, 1990] models

The most suitable model out of all of these various choices to model the initial behaviour was evaluated to be the Yeoh model:

$$W = \sum_{i=1}^{3} C_{i0}(I_1 - 3)^i \tag{4.1}$$

As well as a very high R^2 fit, the Yeoh model was chosen as most suitable as it takes a cubic form and is only a function of the invariant I_1 therefore only one set of experimental test data is needed to fit the materials behaviour, enabling it to be simple and feature a low computational processing speed. It takes its roots from the Mooney-Rivlin model however simplifies itself by firstly assuming the material is incompressible, therefore $I_3=0$ and by referencing work by [Kawabata. A and Kawai. H, 1977] explains that for a filled elastomer, $\frac{\Delta W}{\Delta I_2}$ is much smaller than $\frac{\Delta W}{\Delta I_1}$ and is very close to zero, therefore $\frac{\Delta W}{\Delta I_2}$ can then beapproximated to 0. If this is the case then a stored energy function that can be expressed in I_1 alone is needed. As this equation is also cubic with C_{10}, C_{20} and C_{30}, two points of inflection can be found to better describe the power law stress strain relationship. During these calibration tests, the Yeoh model produced the most accurate fit when compared to the Neo-Hookean or the Mooney-Rivlin models for all four samples. The Ogden model requires more measurement data in more than one deformation mode to fully calibrate the model.

Therefore, the Yeoh model fits are as follows:

Hyperelastic Model: HNBR 0
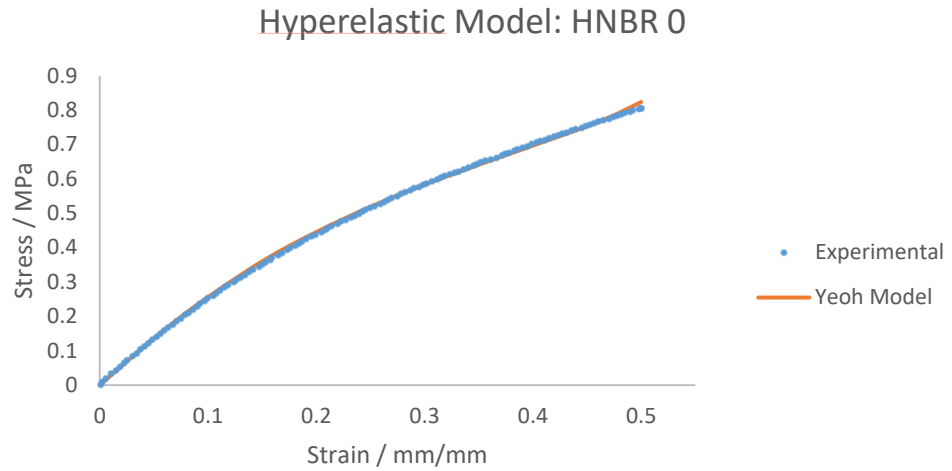
Figure 38: Experimental data of HNBR 0 fitted to a Yeoh model

Hyperelastic Model: HNBR 60
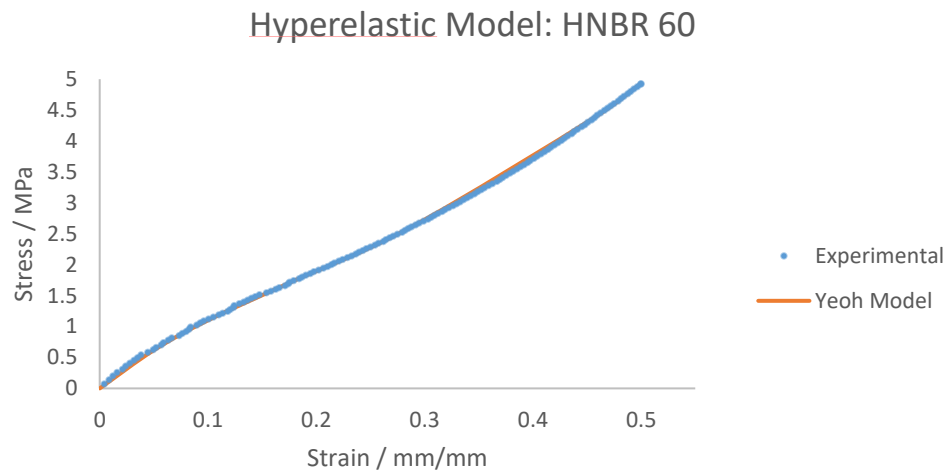
Figure 39: Experimental data of HNBR 60 fitted to a Yeoh model
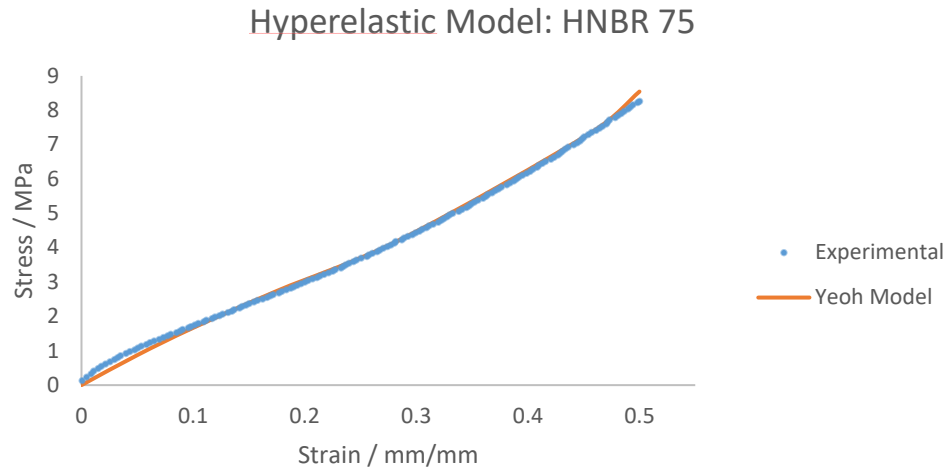
Figure 40: Experimental data of HNBR 75 fitted to a Yeoh model
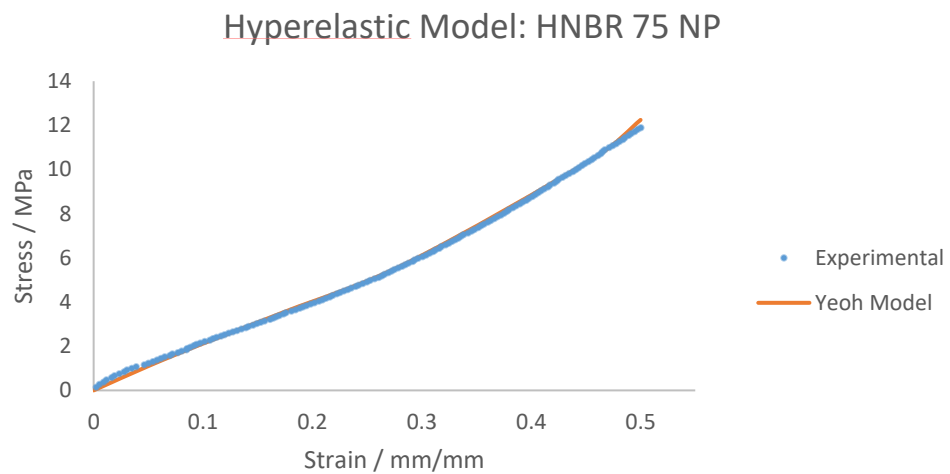
Figure 41: Experimental data of HNBR 75 NP fitted to a Yeoh model

As can be seen, the Yeoh model gives a very reliable fit for these samples especially considering that only one data set can be used to calibrate the model. As the stress strain behaviour varies between samples, model parameters are found for each sample. These model parameters can be seen below:

Sample at 50% Strain	C_{10}/MPa	C_{20}/MPa	C_{30}/MPa
HNBR 0	0.48	-0.19	0.13
HNBR 60	2.12	-0.42	0.87
HNBR 75	3.06	-0.26	1.27
HNBR 75 NP	3.98	-0.16	1.74

Table 2: Yeoh model parameters for all four material samples

4.6.3 TENSILE TESTS AT ELEVATED TEMPERATURES

First cycle tensile tests were also performed at elevated temperatures, 100°C and 150°C. In these tests it was possible to see directly how equation (2.8) derived using the entropy spring theory of rubber elasticity relates to a material with a higher modulus as the temperature increases. However, when the filler reinforcement particles are added another stronger mechanism masks this effect. As the filler particles interact with the polymer itself, this can have a significant effect on the fundamental characteristics of an elastomer. For example, in figure 43-45 it shows that for an elastomer highly filled with carbon black, the reverse effect can occur where an increase in temperature produces a reduction in the Young's modulus rather than an increase. This reduction is as a result of the breakdown of the filler network interaction with strain and, as such, the elastomer loses some of the mechanical benefits associated with the reinforcement filler.

The most obvious observation from these tests is that the reliability of the data starts to reduce at more extreme conditions. By elevating the temperature, the elastomers become very weak and pose a problematic balance between clamping the specimen too strongly and causing fracture at the grips or clamping too weakly and incurring slippage out of the tensile grips. As tensile tests progress the force exerted on the specimen increases, which increases the likelihood of slippage. Therefore, in these circumstances where a reliable test cannot be engineered, data is plotted up to the point where slippage can be identified, which is mostly clear to see.
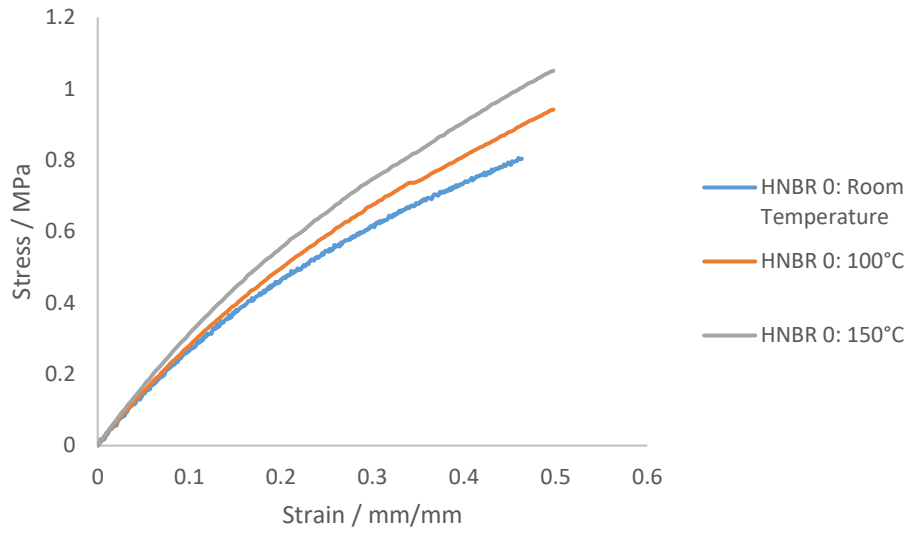
Figure 42: Experimental data of HNBR 0 at elevated temperatures
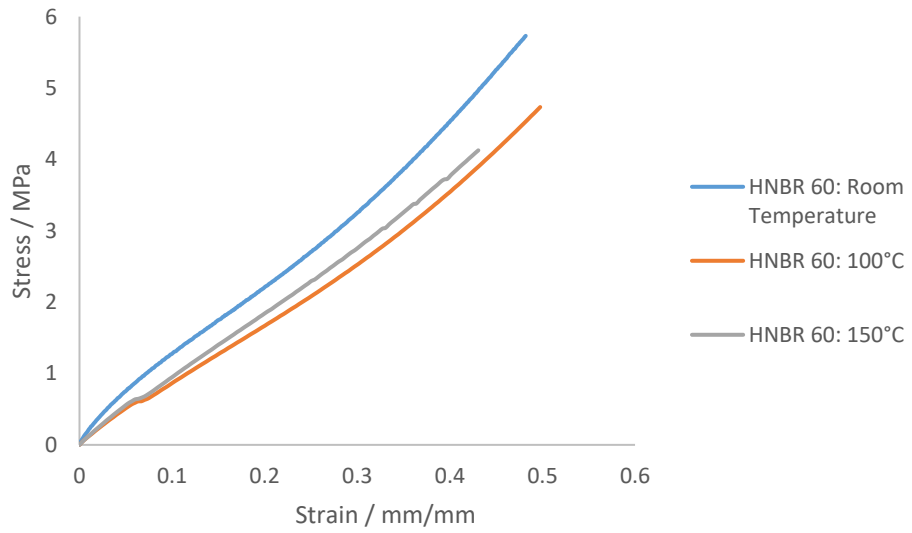
Figure 43: Experimental data of HNBR 60 at elevated temperatures
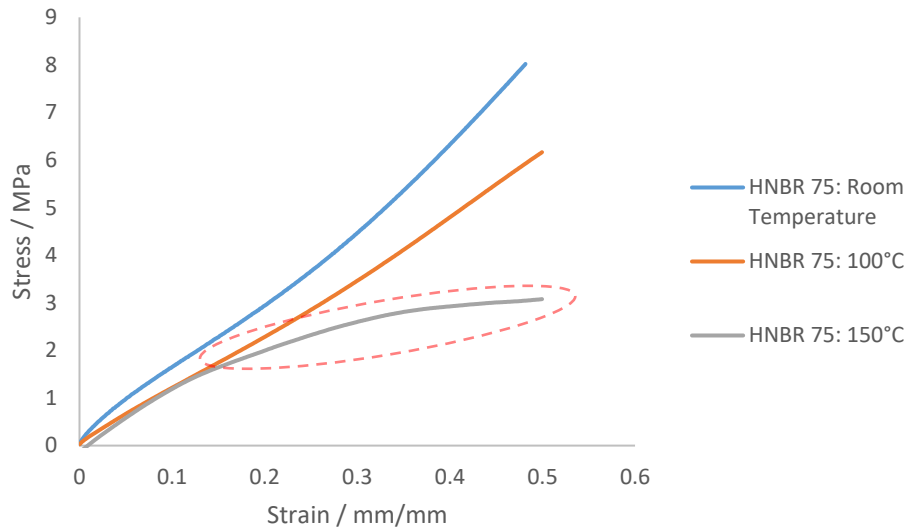
Figure 44: Experimental data of HNBR 75 at elevated temperatures. Dotted red circle indicating region of test slippage in 150°C test.
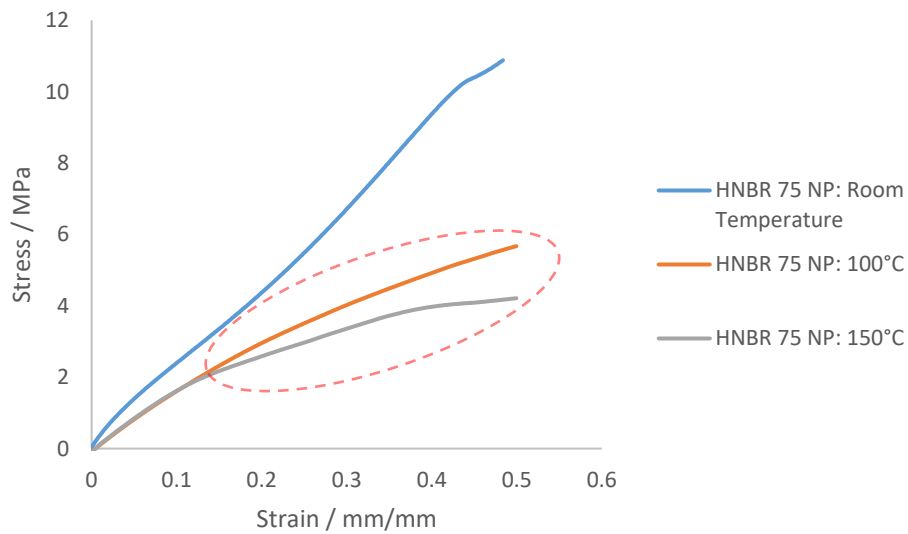
Figure 45: Experimental data of HNBR 75 NP at elevated temperatures. Dotted red circle indicating region of test slippage in 100°C and 150°C tests.

It is evident that in these tensile tests, the elevated temperature tests feature severe slippage especially in the highly filled materials HNBR 75 and HNBR 75 NP and small areas of slippage in HNBR 0 and HNBR 60.

However, it is still easy to grasp the idea from these figures that for unfilled materials, an increase in testing temperature causes an increase in modulus. Then as reinforcement filler is added, the opposing effect occurs, where elevated temperature testing reduces the modulus as the filler interaction becomes less effective.

4.6.4 HYSTERESIS TEST

Tensile tests were also carried out to understand the elastomers unloading curve characteristics. As explained before in chapter 2, elastomers feature an energy dissipation behaviour between loading and unloading curves. This behaviour is known as hysteresis. All four samples were characterised in this way up with the following conditions:

- Strain: 50%
- Strain rate: 0.01/s quasi-static
- Temperature: Room Temperature

Three repeats were done for each sample on virgin specimen using a dumbbell specimen geometry. Tests began at 0N, were stretched to 50% strain and then brought down to 0N. The results can be seen below:
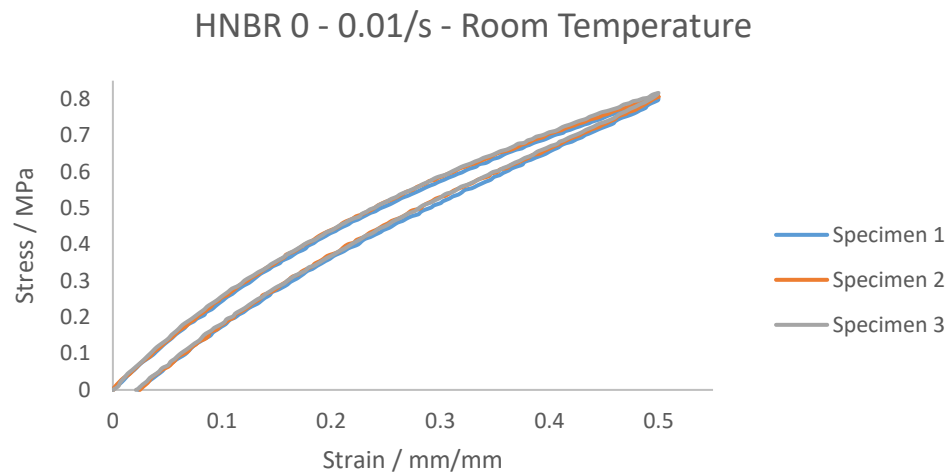
Figure 46: HNBR 0 characterised in tension with loading and unloading curve
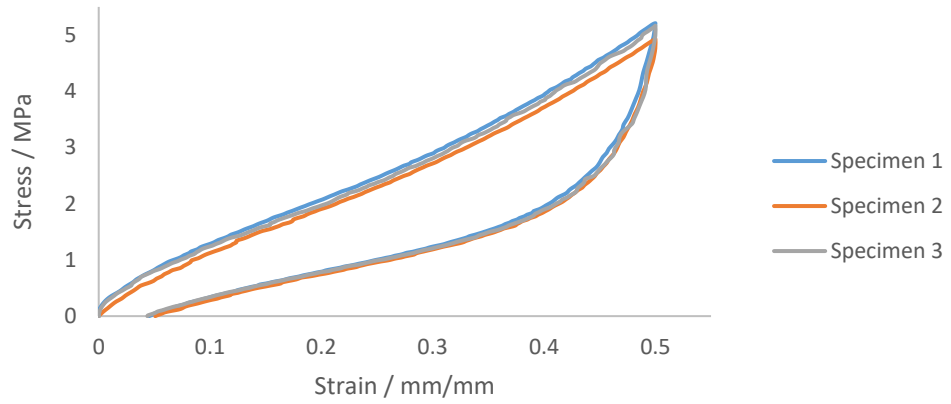
Figure 47: HNBR 60 characterised in tension with loading and unloading curve
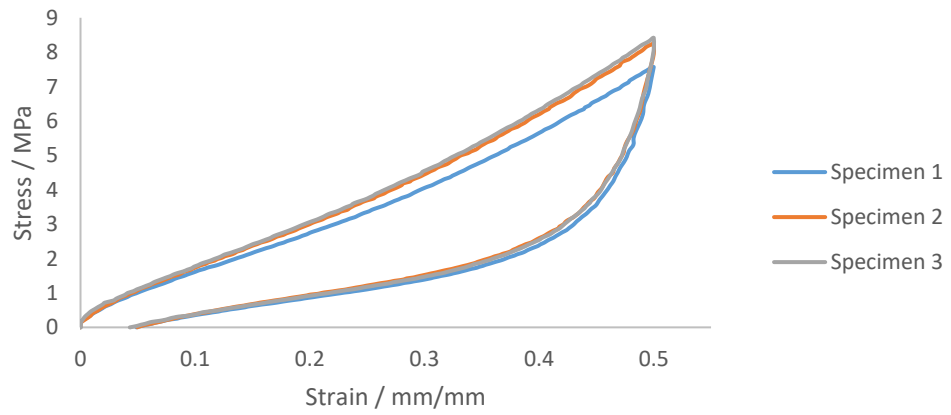
Figure 48: HNBR 75 characterised in tension with loading and unloading curve
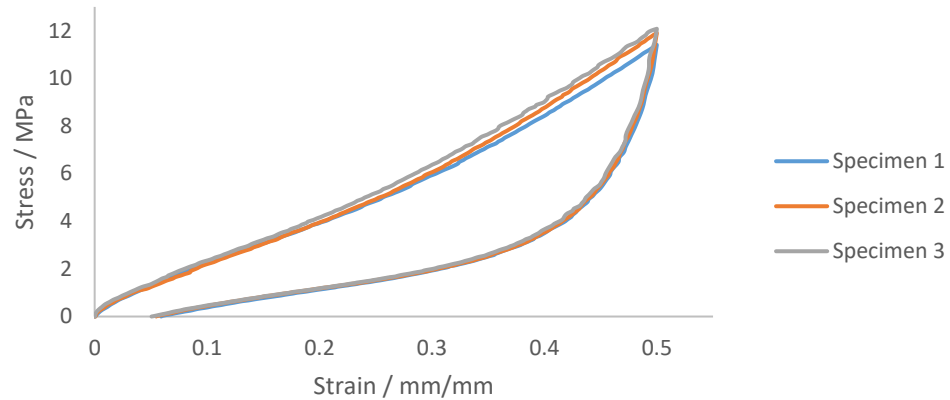
Figure 49: HNBR 75 NP characterised in tension with loading and unloading curve

The most obvious differences between these tests can be seen as a result of carbon black filler and plasticiser content. HNBR 0 obviously features the least amount of energy dissipation between loading and unloading curves. As filler content is added, the amount of hysteresis between curves increases, the largest increase seen between HNBR 0 and HNBR 60. The removal of plasticiser also encourages an increase in hysteresis seen in sample HNBR 75 NP. As well as this, it can also be seen that the increase in filler content and removal of plasticiser increases the amount of permanent set as the sample fails to return to its original position. Permanent set is a lasting damage that in some cases does not recover, and in other can recover in the time span of months.

Abaqus has one model for analysing the unloading curve in rubbers, this is based on the Ogden Roxburgh model [Ogden. R. W and Roxburgh. D. G, 1999]. The phenomenological model works in a way to introduce a damage variable to the model:

$$\eta = 1 - \frac{1}{r}\operatorname{erf}\left(\frac{U_{dev}^m - U_{dev}}{m + \beta U_{dev}^m}\right) \tag{4.2}$$

Where η is the damage variable, erf(x) is the function error, U_{dev} is the current deviatoric strain energy density and U_{dev}^m is the maximum deviatoric strain energy density. r, m and β are all material constants.

It is applied to a hyperelastic model, in this case the Yeoh model, and assigns a damage parameter to capture the unloading behaviour:

Yeoh Model wth Ogden Roxburgh: HNBR 0
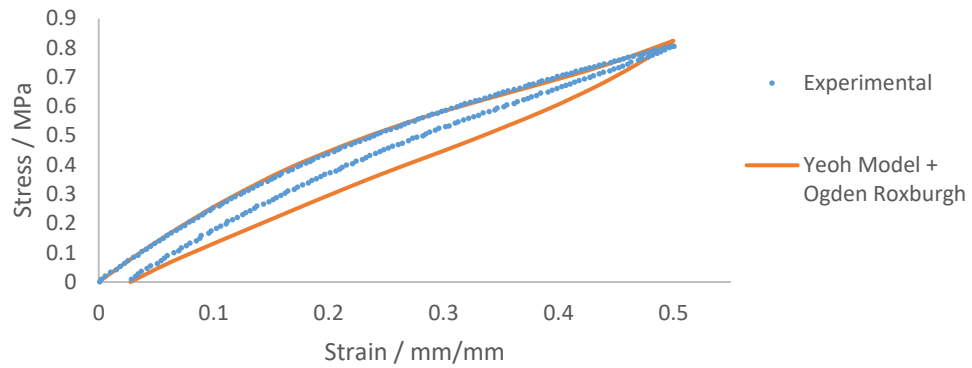
Figure 50: HNBR 0 data fitted with a Yeoh hyperelastic model and the Ogden Roxburgh model

Yeoh Model wth Ogden Roxburgh: HNBR 60
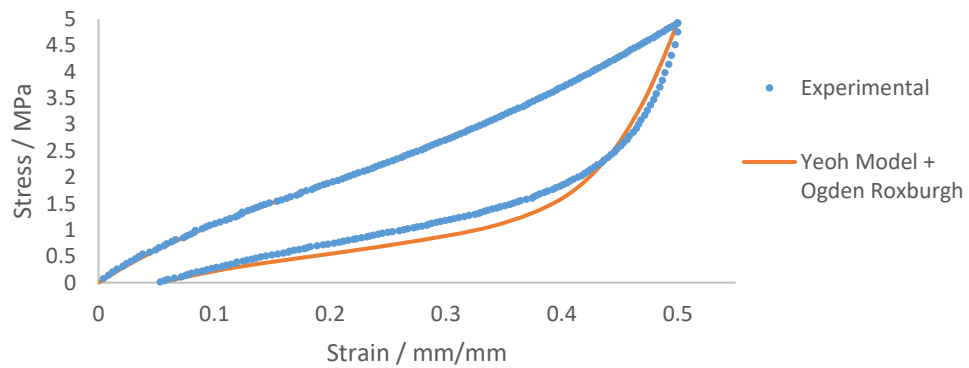
Figure 51: HNBR 60 data fitted with a Yeoh hyperelastic model and the Ogden Roxburgh model

Yeoh Model wth Ogden Roxburgh: HNBR 75
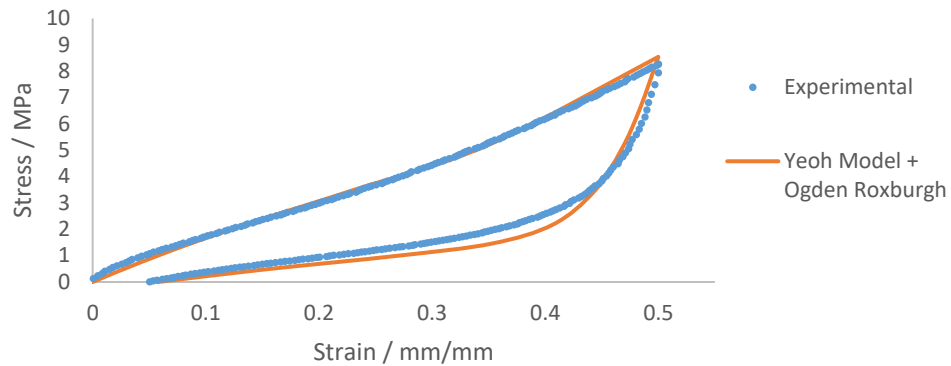
Figure 52: HNBR 75 data fitted with a Yeoh hyperelastic model and the Ogden Roxburgh model

Yeoh Model wth Ogden Roxburgh: HNBR 75 NP
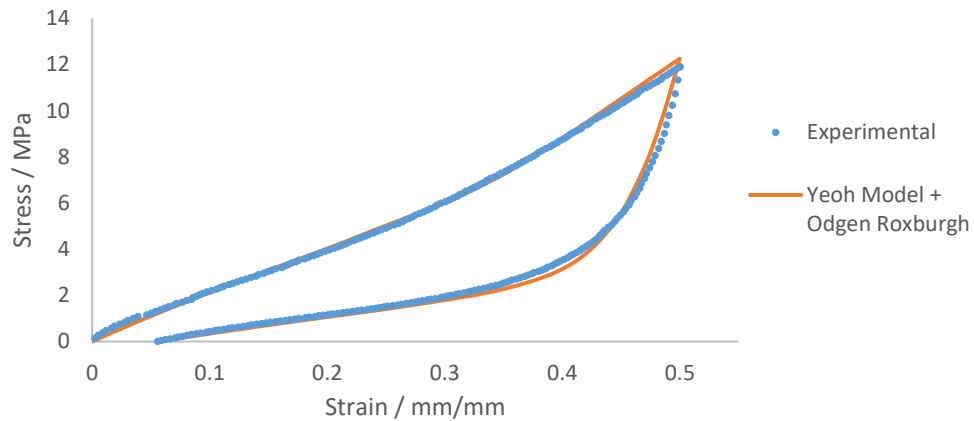
Figure 53: HNBR 75 NP data fitted with a Yeoh hyperelastic model and the Ogden Roxburgh model

As can be seen, the Ogden Roxburgh model captures the behaviour of the filled materials more successfully than the unfilled. However, this model is also just limited to first unloading cycle and does not capture behaviour beyond the first unloading cycle.

4.6.5 TENSILE TESTS AT HIGHER STRAIN RATES

Tensile tests were also undertaken at elevated strain rates. As elastomeric materials are viscoelastic, they feature a material response that is rate dependent. These tests were done to

help capture this response from these samples. Whereas strain rates experienced in the mud motors are in the order of 100/s, these tests help to understand the response of these materials approaching these strain rates. The test parameters were:

- Strain: 50%
- Strain rates: 0.01/s, 0.1/s and 1/s
- Temperature: Room Temperature
- 1 cycle

These tests were carried out on the Electropulse E10000 which is fitted with a 25kN load cell. This load cell captured the behaviour of the filled the samples well, however featured a small amount of noise in the unfilled tests. Nevertheless, results can still be analysed easily whist taking this into account.
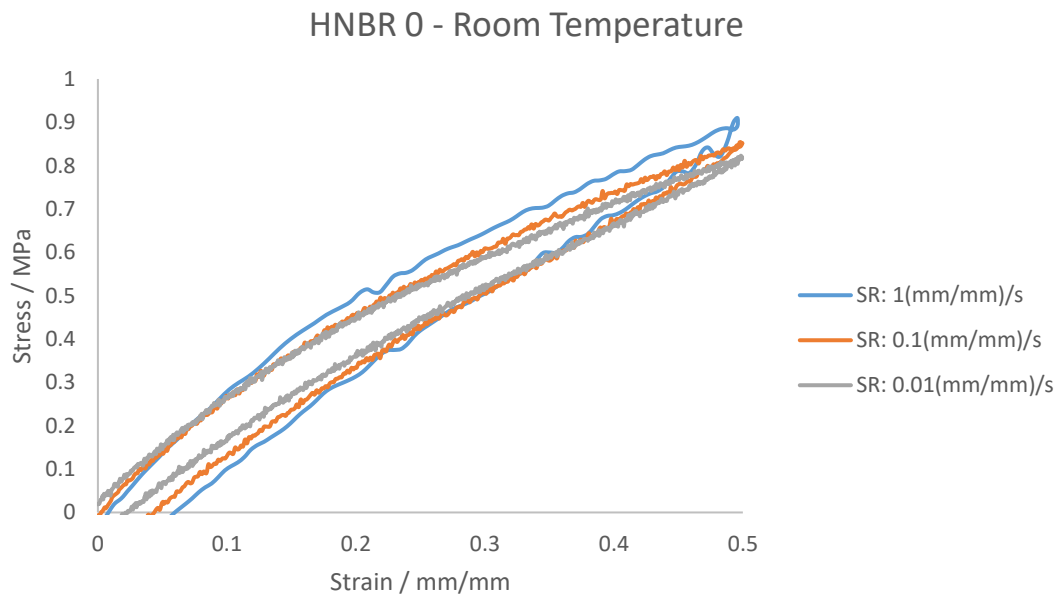
Figure 54: HNBR 0 loading and unloading curves at various strain rates

HNBR 60 - Room Temperature
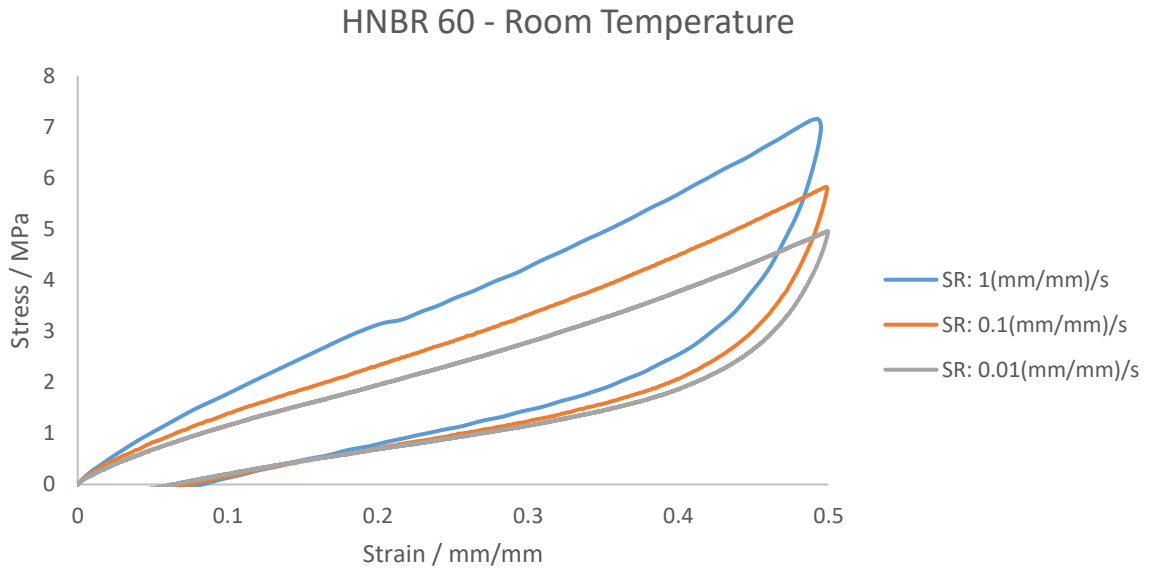
Figure 55: HNBR 60 loading and unloading curves at various strain rates

HNBR 75 - Room Temperature
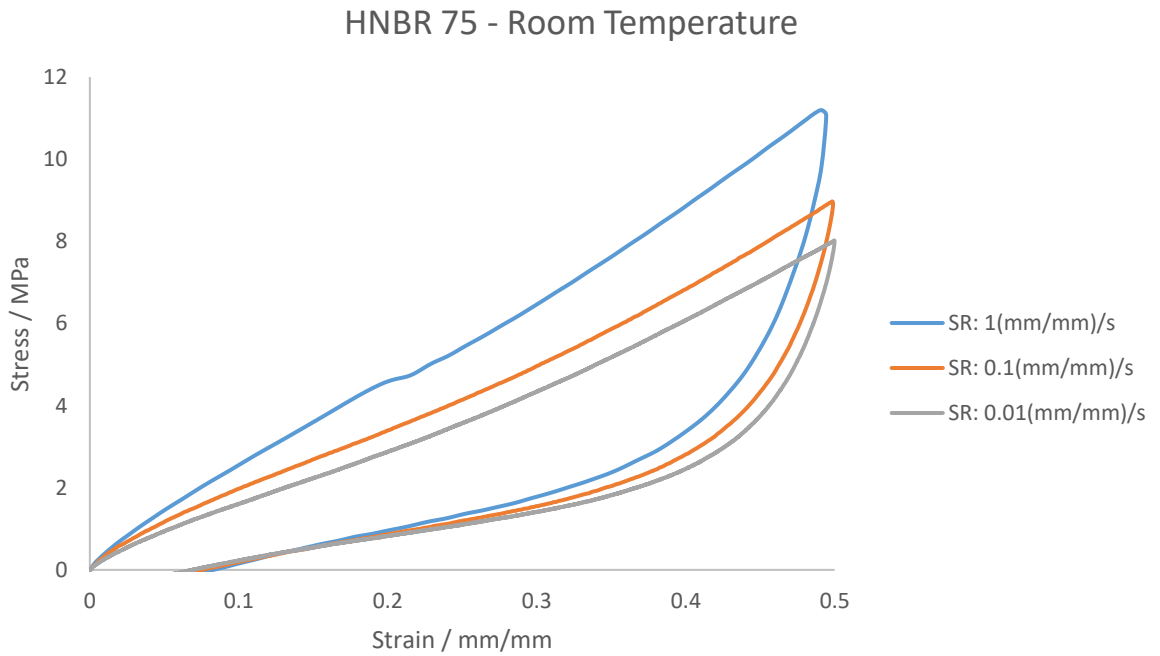
Figure 56: HNBR 75 loading and unloading curves at various strain rates
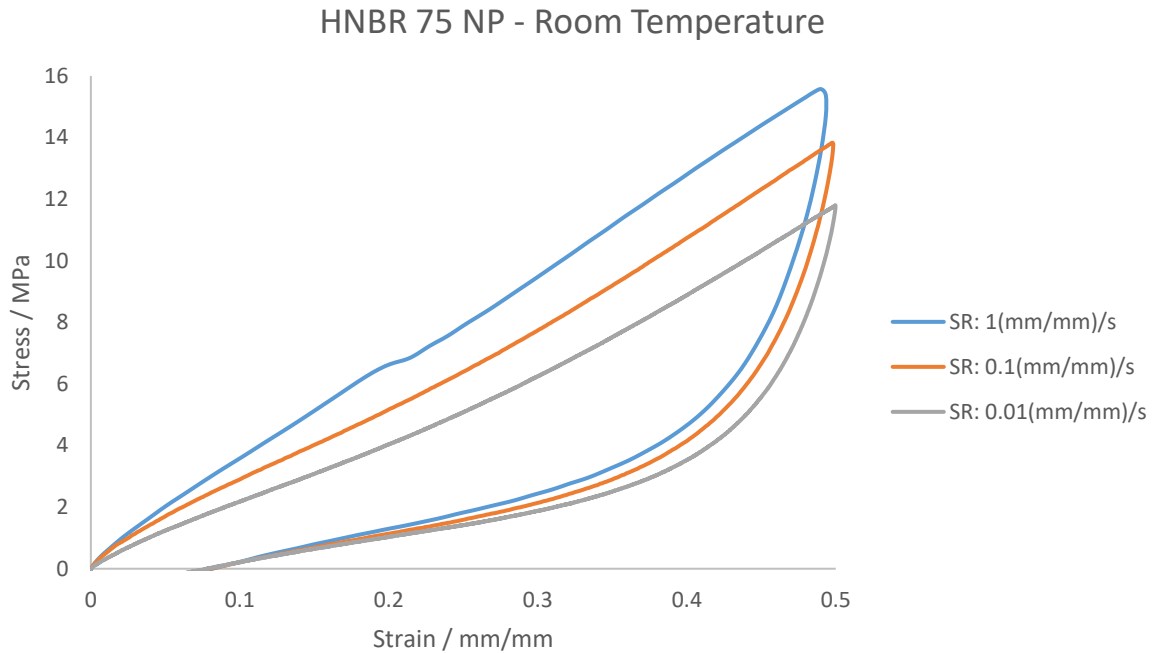
Figure 57: HNBR 75 NP loading and unloading curves at various strain rates

It should be noted that at a strain of 0.2 for all specimen strained at a strain rate of 1/s, a small kink in the loading curve is observed which might relate to a small amount of slipping of the rubber in the grips. However, these tests all still behave broadly as expected.

When the samples are tested at elevated strain rates, the modulus, hysteresis and permanent set are all increased as a result of the shifting T_g. As filler content is increased, viscoelastic properties increase as well causing higher modulus responses at higher rates and larger amounts of hysteresis. The understanding of how hysteresis is affected by strain rate can be better observed by the following figure, plotting hysteresis vs strain rate for all four samples.

Hysteresis vs Strain Rate
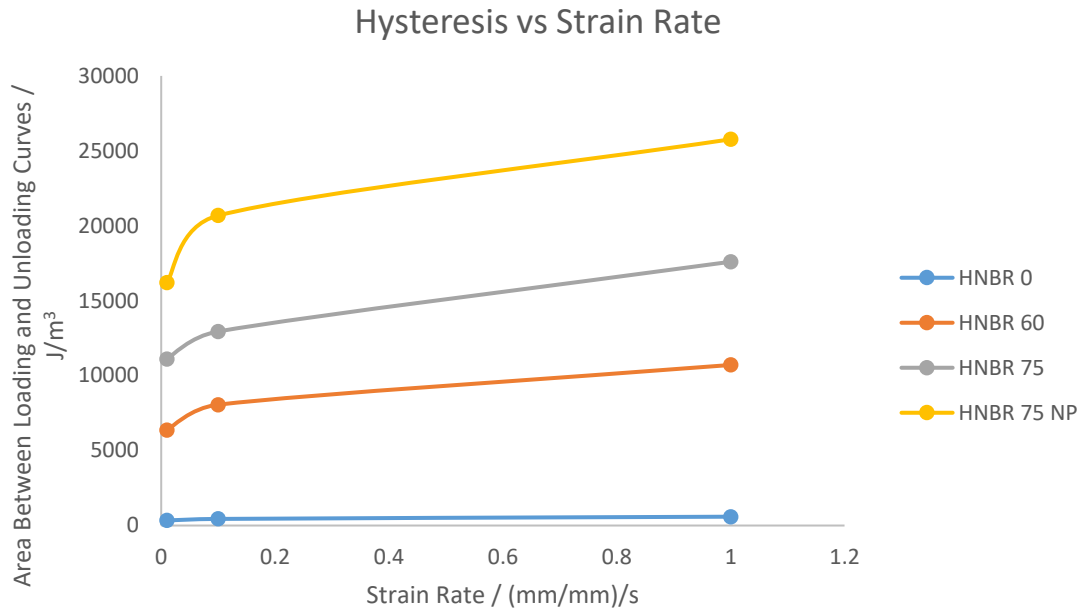
Figure 58: Hysteresis vs strain rate for all four samples

Evidently as filler content and strain rate are increased, so does the amount of hysteresis between loading and unloading cycles. It is also clear to see that the lack of plasticiser here increases hysteresis as well.

4.6.6 CYCLIC STRESS SOFTENING TEST

Samples were also stretched beyond the first loading and unloading curves in tension to understand the initial cyclic stress softening behaviour. It was identified by Tunnicliffe [Tunnicliffe. L and Busfield. J. J. C, 2015] that the materials used in these applications featured large amounts of softening behaviour.

Test parameters were:

- Strain: 50%
- Strain rate: 0.01/s
- Room Temperature
- 10 Cycles

Tests began at 0N, were strained to 50% and unloaded to 0N before beginning the next cycle. This avoided any buckling as a result of permanent set.
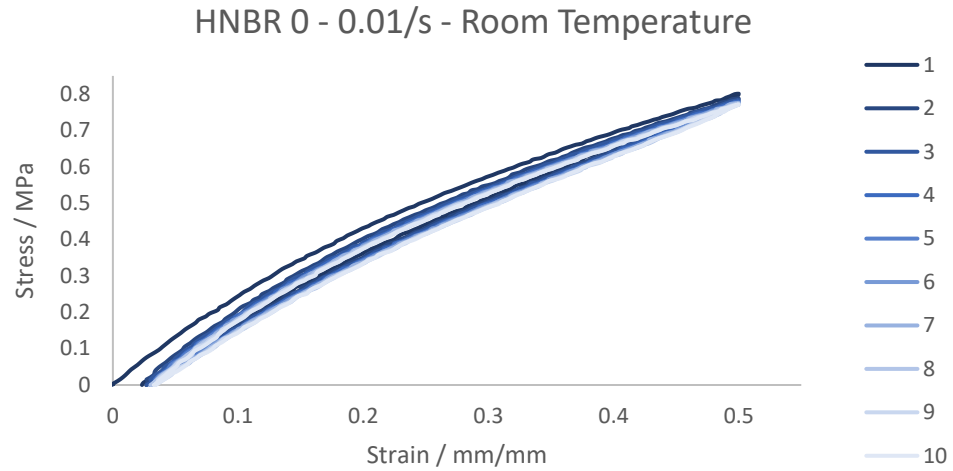
Figure 59: Cyclic stress softening behaviour of HNBR 0
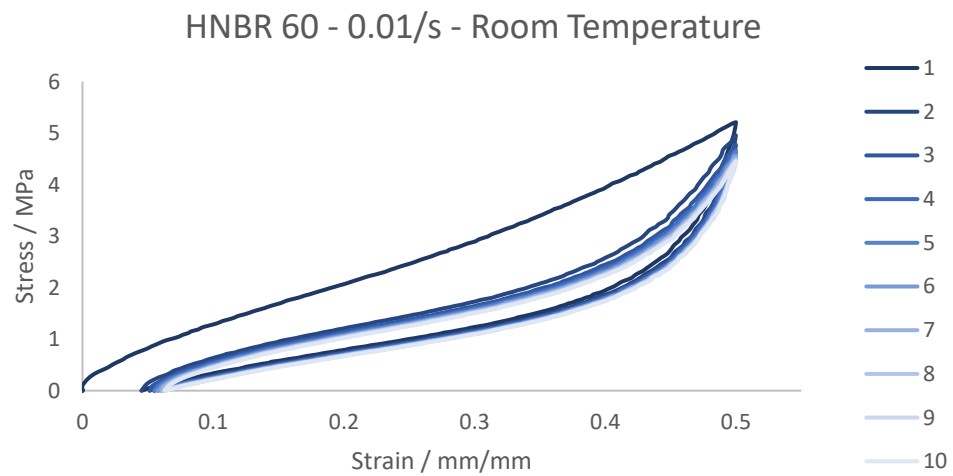
Figure 60: Cyclic stress softening behaviour of HNBR 60
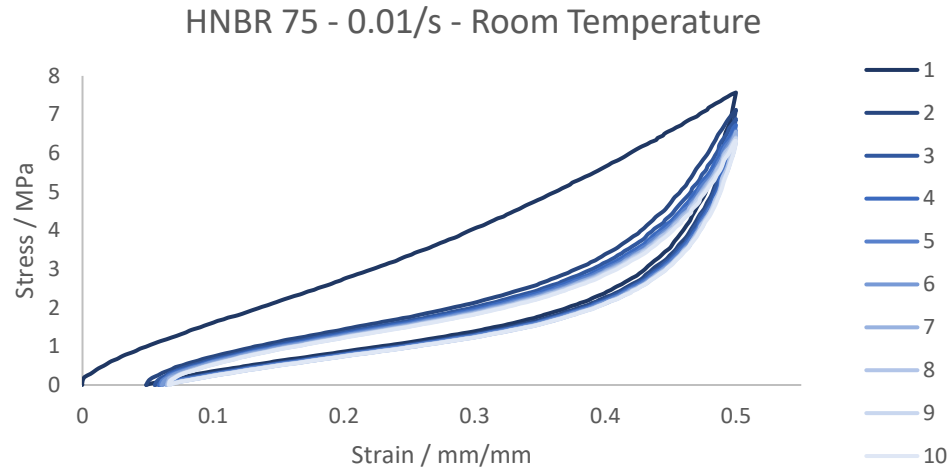
Figure 61: Cyclic stress softening behaviour of HNBR 75
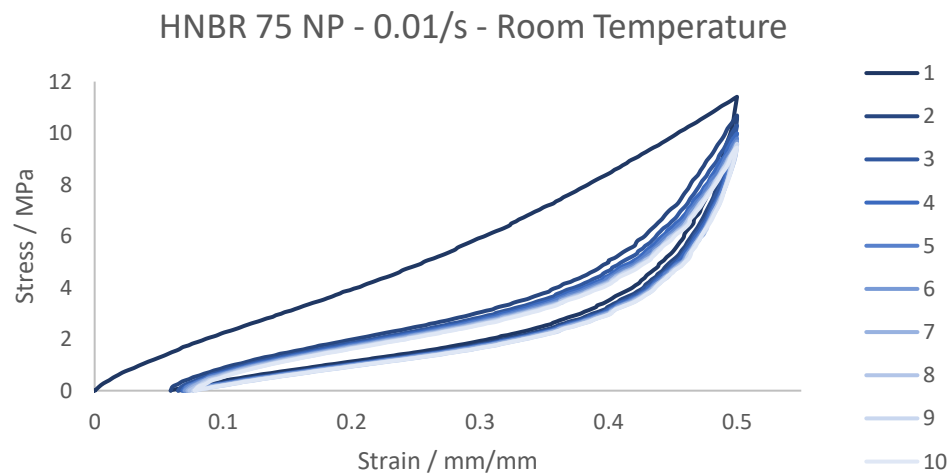
Figure 62: Cyclic stress softening behaviour of HNBR 75 NP

As expected, when filler content is increased, the amount of cyclic stress softening is increased. This is also the case for the removal of plasticiser. The initial loss of modulus between cycles one and two is the greatest and this starts to approach an equilibrium value. This can be better observed in the following figures that plot the maximum stress per cycle (at 50% strain) again the cycle number. These results can be seen for not just a quasistatic strain rate but also for 0.1/s and 1/s.
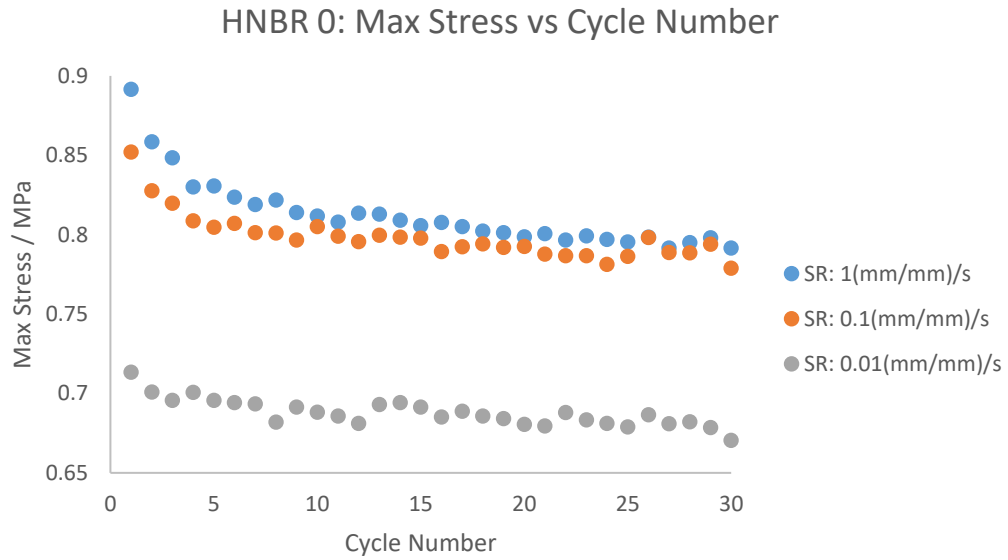
Figure 63: Maximum stress vs cycle number for cyclic tension tests of HNBR 0
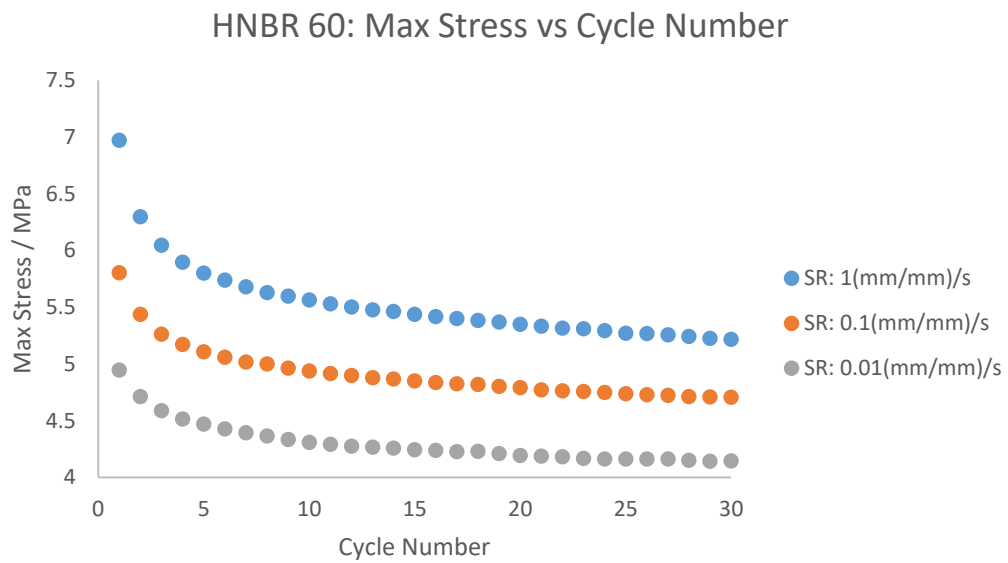
Figure 64: Maximum stress vs cycle number for cyclic tension tests of HNBR 60
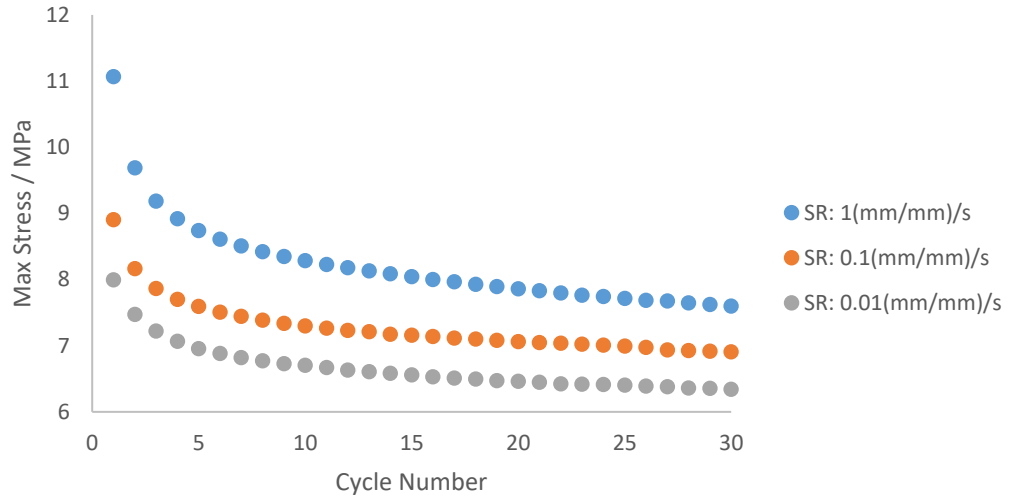
Figure 65: Maximum stress vs cycle number for cyclic tension tests of HNBR 75
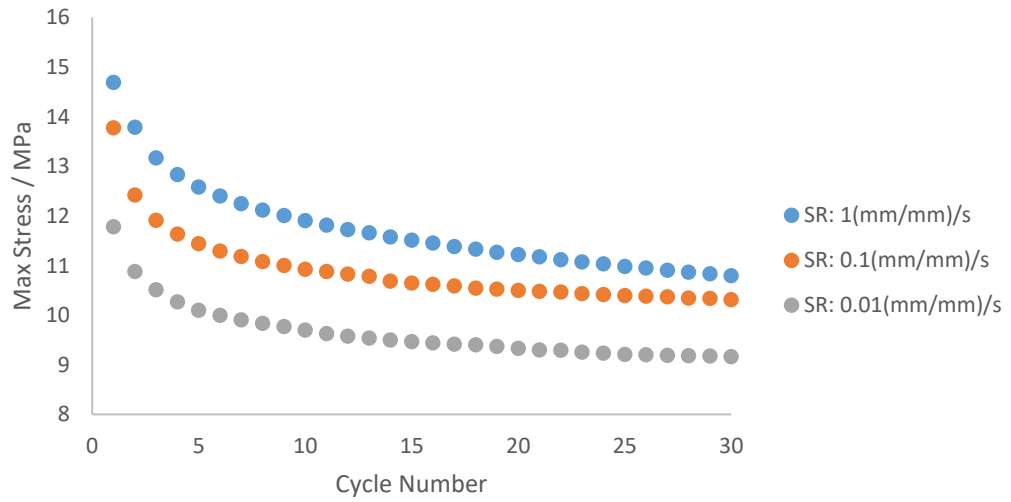
Figure 66: Maximum stress vs cycle number for cyclic tension tests of HNBR 75 NP

Strain Rate / s⁻¹	Hysteresis / J/m³			
	HNBR 0	HNBR 60	HNBR 75	HNBR 75 NP
1	589	10712	17598	25771
0.1	441	8062	12948	20683
0.01	337	6359	11107	16200

Table 3: Hysteresis values at cycle 1 for all four samples at different strain rates

In figures 63 to 66, the rate at which the initial softening behaviour slows down to an equilibrium value is easily seen, however this value is obviously not captured on these graphs. This value is estimated at approximately 1000 cycles according to [Papadopoulos, I. C et al, 2008]. The degree of softening also generally increases as strain rate increases. This can be easier to observe in the following figure plotting percentage softening from cycles 1-10 against strain rate.
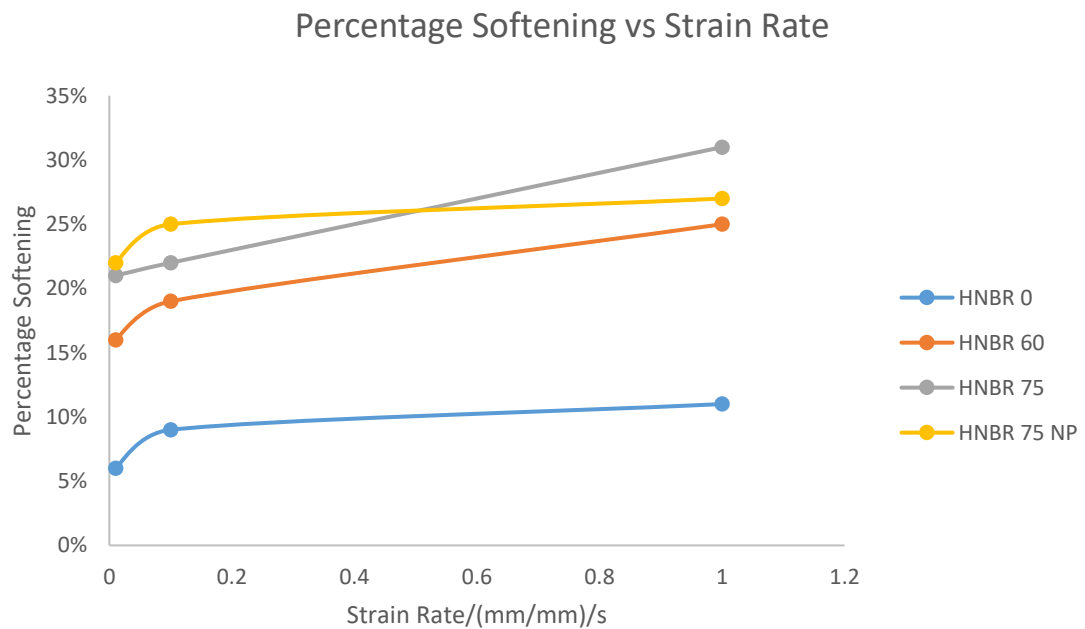
Figure 67: Percentage softening vs strain rate for all four samples

Understandably as filler content increases, percentage softening increases and as strain rate increases so does percentage softening. As the filler content increases, the rate change of percentage softening decreases as strain rate is increased. The influence of the plasticiser has little effect at quasistatic rate, however, softening start to decrease significantly as the strain rate is increased from there.

107

4.6.7 CYCLIC STRAIN SOFTENING

Another interesting analysis is understanding strain history of elastomeric samples. In the application of mud motors, the rotor stator interaction is not one that instantly transitions from no power to full power. There is a steady increase of power meaning that the strain experienced by the elastomer sample is gradually increased as the power of the motor increases. Therefore, having an understanding of how elastomers react when initially loaded at a lower strain and then increased to a larger strain can be helpful for this application.

The tests performed here feature samples loaded in three stages. These stages differ only in the amount of strain the elastomer experiences. The parameters of the test are as follows:

- Cycles 1-10: Strained to 25%
- Cycles 11-20: Strained to 50%
- Cycles 21-30: Strained to 100%
- Strain Rate: Quasistatic 0.01/s
- Temperature: Room Temperature

The results shown are data from cycles 1, 11 and 21 which feature the most dramatic effects from these types of tests.

Three repeats were done for each sample. Data is not given for HNBR 75 NP as this sample could not reach 100% strain without fracturing.
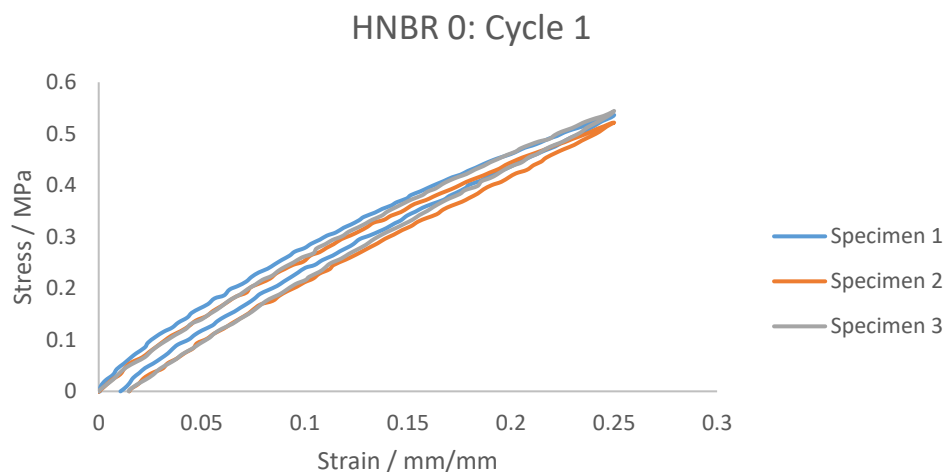
Figure 68: Cycle 1 of a stage changing cyclic stress softening test for HNBR 0
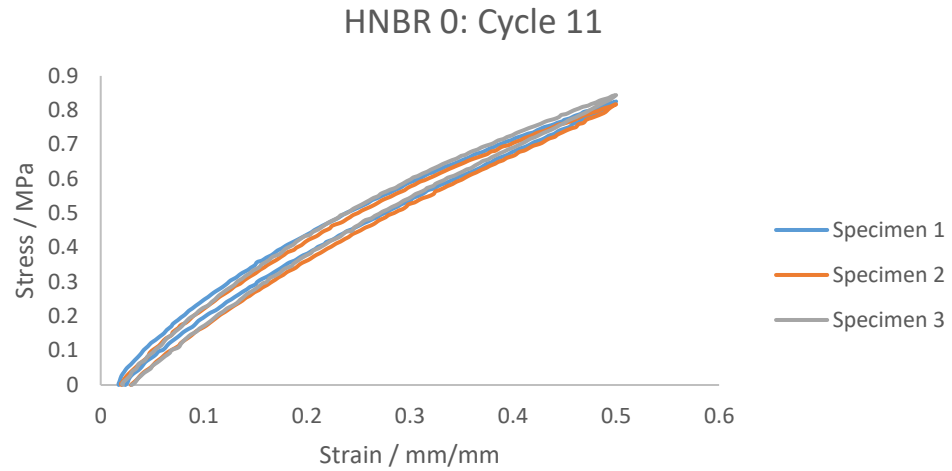
HNBR 0: Cycle 11

Figure 69: Cycle 11 of a stage changing cyclic stress softening test for HNBR 0
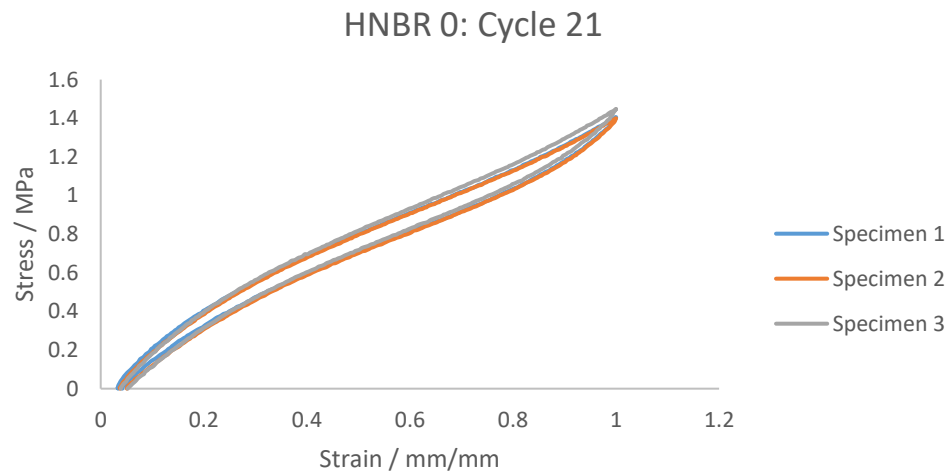
HNBR 0: Cycle 21

Figure 70: Cycle 21 of a stage changing cyclic stress softening test for HNBR 0
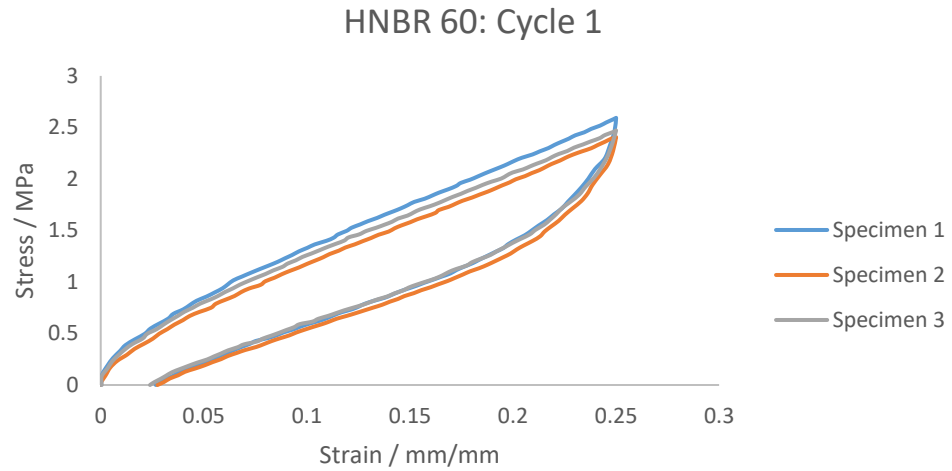
Figure 71: Cycle 1 of a stage changing cyclic stress softening test for HNBR 60
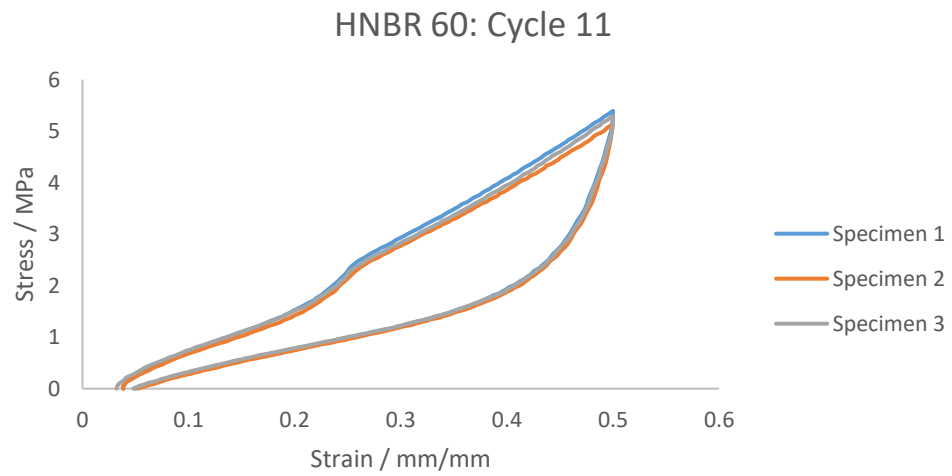
Figure 72: Cycle 11 of a stage changing cyclic stress softening test for HNBR 60
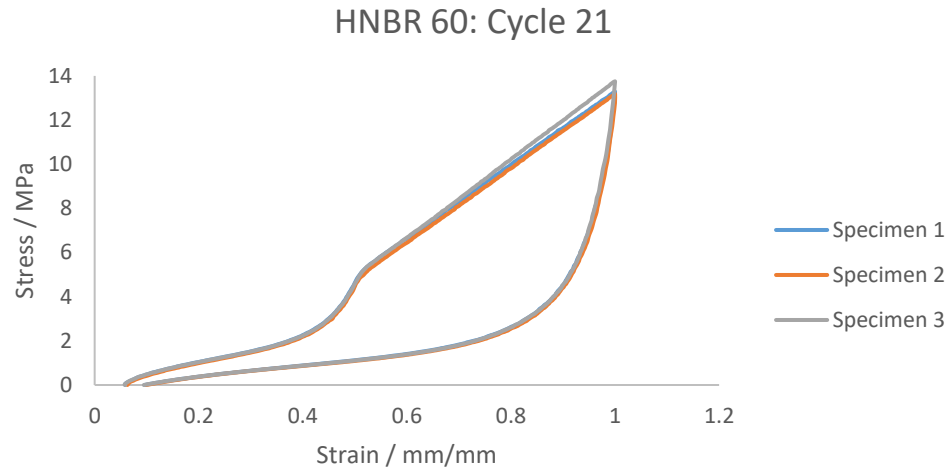
HNBR 60: Cycle 21

Figure 73: Cycle 21 of a stage changing cyclic stress softening test for HNBR 60
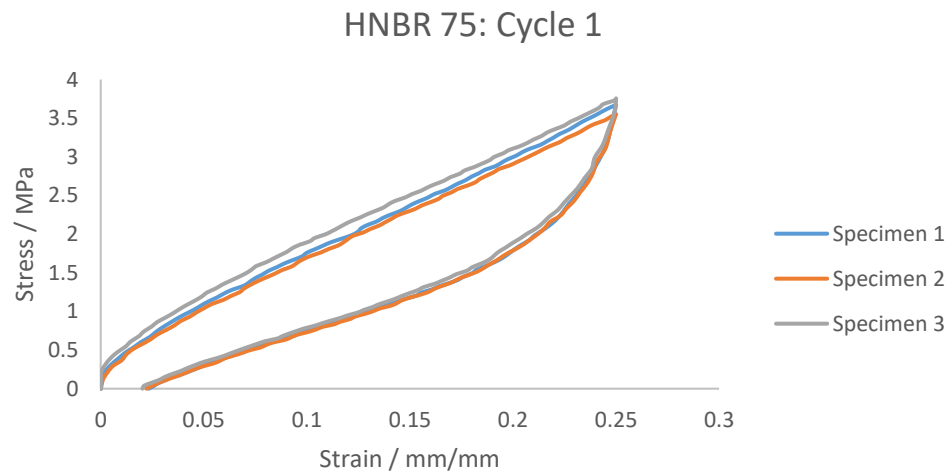
HNBR 75: Cycle 1

Figure 74: Cycle 1 of a stage changing cyclic stress softening test for HNBR 75
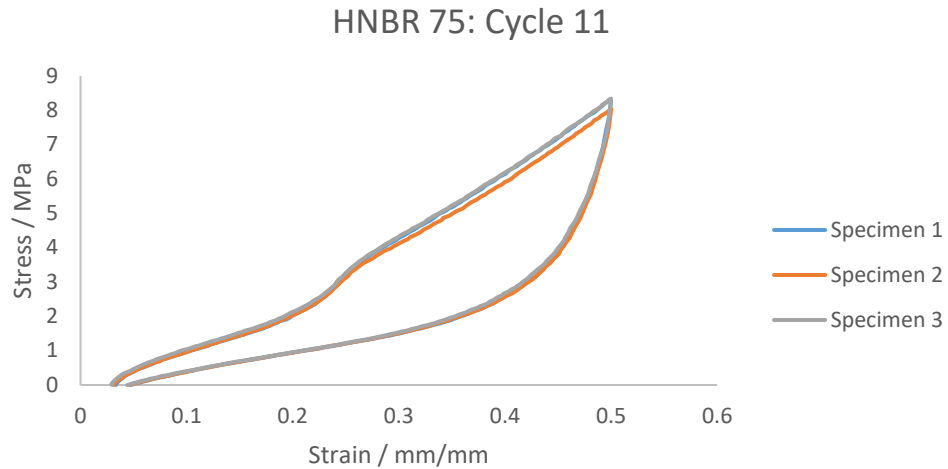
Figure 75: Cycle 11 of a stage changing cyclic stress softening test for HNBR 75
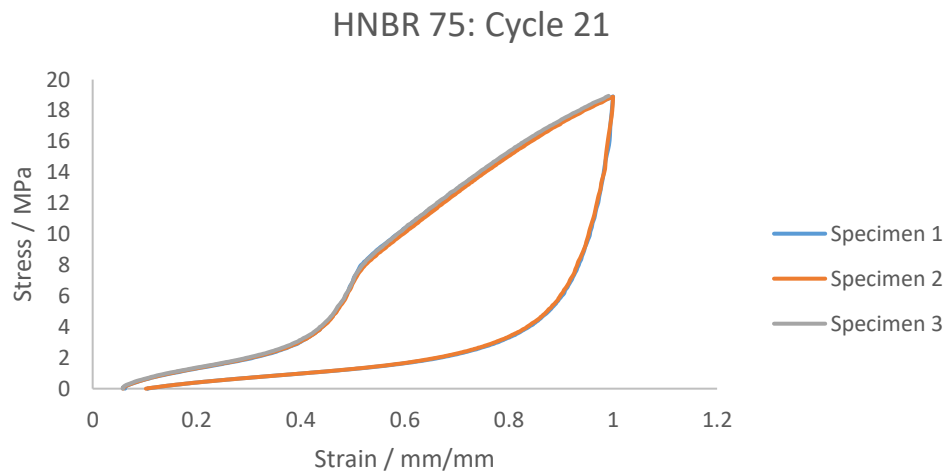
Figure 76: Cycle 21 of a stage changing cyclic stress softening test for HNBR 75

As sample tests increase in strain stages, it is evident to see the softening behaviour from previous stages effecting the stress vs strain behaviour. The stress vs strain results for the samples beyond the previous strain stage is unaffected and responded similarly to a virgin unstrained test. The results for unfilled HNBR 0 are very small in comparison of HNBR 60 and HNBR 75 as the viscoelastic properties of filled materials are much greater. As can be seen between these specimen, the data is very reproduceable. This data is very helpful when understanding elastomer behaviour during the start-up sequence for the mud motor.

4.6.8 DIFFERENTIAL SCANNING CALORIMETRY (DSC)

Differential Scanning Calorimetry (DSC) tests were performed on all samples. DSC is a technique that can be used to find material properties such as:

- Glass transition temperature, T_g
- Melting and recrystallisation temperature and heat determinations
- Curing measurements

It does this by measuring heat flux to a sample with respect to time or temperature. This is done by placing a testing sample in a pan and monitoring the heat flux in response to a programmed temperature input, with respect to a separate empty reference pan. The temperature difference between them gives insight into exothermic or endothermic processes occurring within the sample. A differential power signal is recorded with respect to the sample temperature [Groenewoud, W. M, 2001].

DSC tests were performed on all four formulations to measure T_g differences. Sample temperatures were lowered to -90°C and left to equilibrate for 10mins. A standard temperature ramp was then performed with samples starting at -90°C and then raised to 100°C at a rate of 10°C/min. Samples were again left to equilibrate for 10mins before returning back to room temperature.

All formulations were tested four times for an average reading of T_g in an unstrained state. Results for these DSC tests can be seen below.
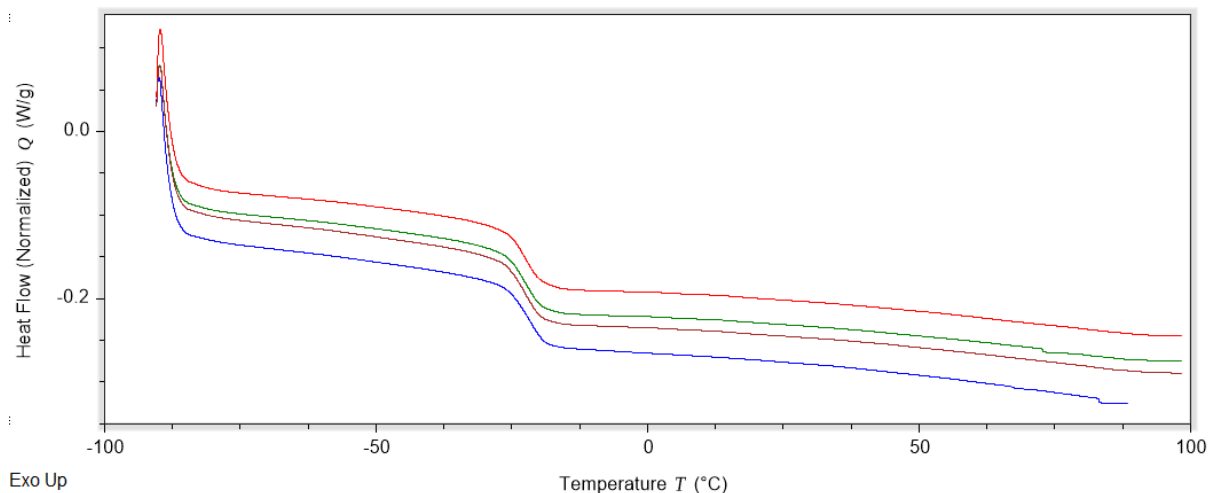
Figure 77: Four DSC tests performed on unstrained and unaged HNBR 0
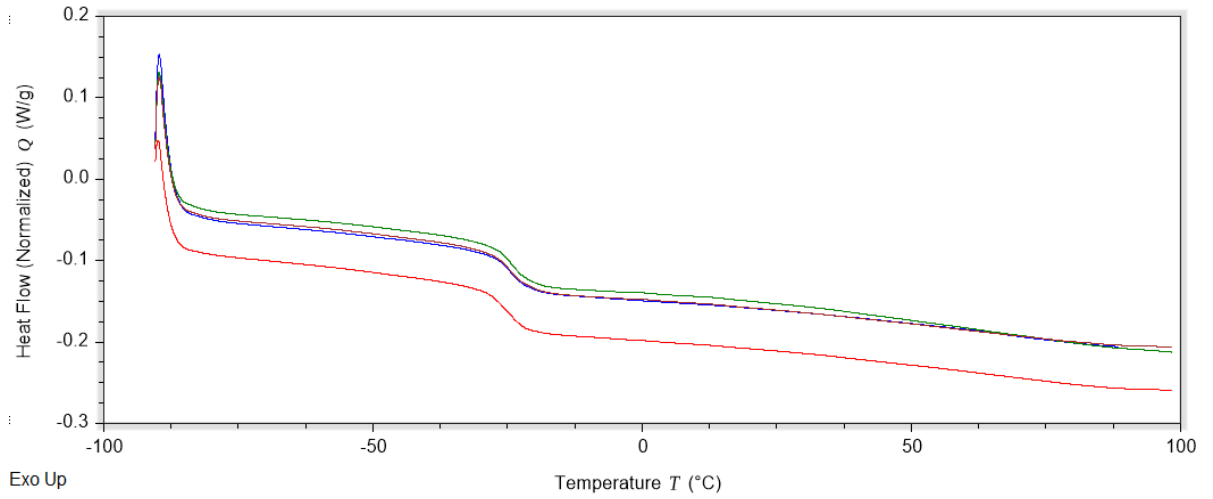
Figure 78: Four DSC tests performed on unstrained and unaged HNBR 60
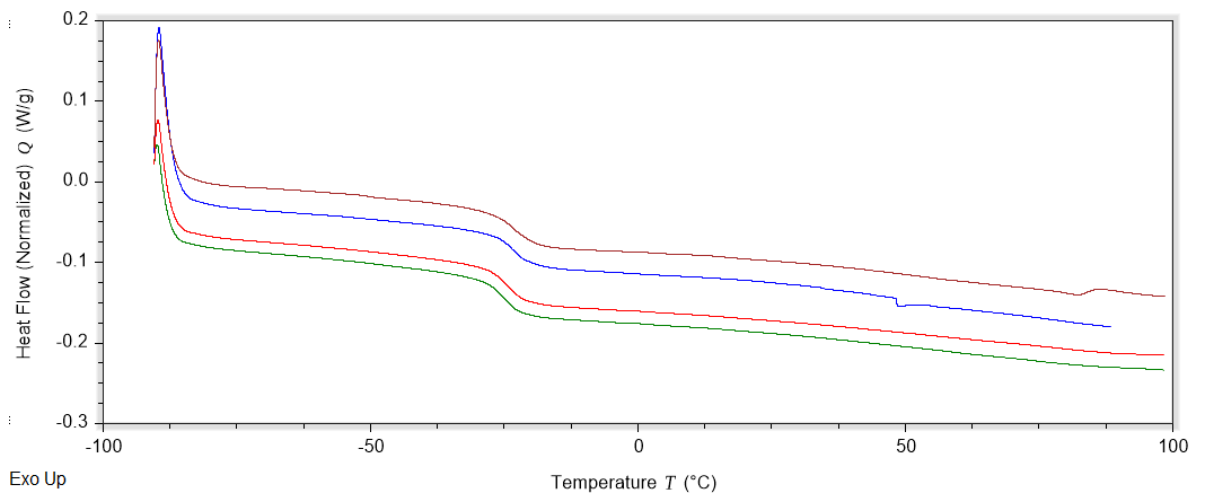
Figure 79: Four DSC tests performed on unstrained and unaged HNBR 75
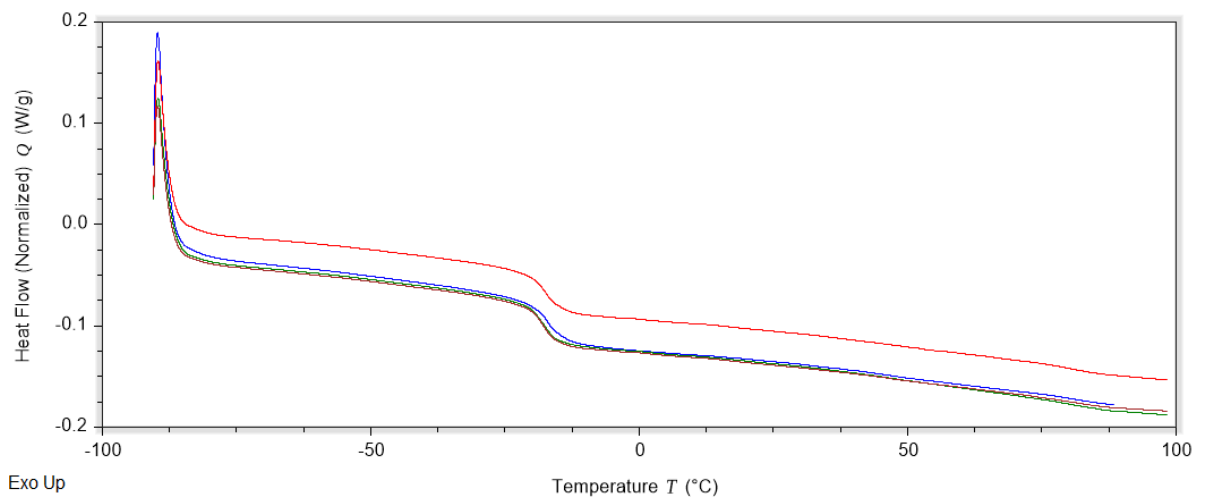
Figure 80: Four DSC tests performed on unstrained and unaged HNBR 75 NP

HNBR 0	T_g / °C		HNBR 60	T_g / °C		HNBR 75	T_g / °C		HNBR 75 NP	T_g / °C
Test 1	-22.52		Test 1	-24.00		Test 1	-23.52		Test 1	-17.88
Test 2	-22.72		Test 2	-24.26		Test 2	-23.51		Test 2	-17.14
Test 3	-22.81		Test 3	-24.37		Test 3	-24.61		Test 3	-18.24
Test 4	-22.32		Test 4	-25.07		Test 4	-25.42		Test 4	-18.29
Average	**-22.59**		**Average**	**-24.43**		**Average**	**-24.27**		**Average**	**-17.89**

Table 4: Resulting T_g measurements from DSC tests

T_g is measured as the midpoint of the dramatic heat flow drop found at approximately -22°C. As can be seen from the results, by adding carbon black reinforcement to the samples, T_g is lowered a by approximately 1.7°C – 1.8°C, overall a small decrease. The lack of plasticiser has much more effect on the T_g of these materials as is causes an average increase of 6.4°C. Changes in T_g can cause changes in hysteresis which must be monitored closely with respect to crack growth tests.

4.7 PURE SHEAR FATIGUE CRACK GROWTH TESTING

Pure shear fatigue crack growth test pieces were used to characterise cyclic fatigue crack growth behaviour. This enables a material model to be developed that relates the rate of crack growth in an elastomer to the strain energy release rate. A pure shear specimen is cut with a horizontal length that is significantly larger than the vertical height between the long sample grips. The thickness is then significantly shorter than the other two dimensions. The specimen is gripped along the longest horizontal sides and it is strained perpendicularly to an extension ratio λ_1. Due to the specific shape of the specimen, during this deformation the other extension ratios are constrained λ_2 = 1 or defined as $\lambda_3 = 1/\lambda_1$. If a test piece features a horizontal length that is ten times longer than its vertical height length, as is the case with a pure shear test specimen, then a pure shear region can be found anywhere away from the vicinity of the free edge. These are regions that are in uniform homogeneous pure shear.

This test piece, developed by [Rivlin. R. S and Thomas. A. G, 1953], features a tearing energy that is dependent on elastic strain energy density, *W*, in the pure shear region and the height of the sample, l_0.

115

$$T = Wl_0 \tag{4.3}$$

The approach used by [Rivlin. R. S and Thomas. A. G, 1953] focuses on identifying four distinctive regions within a strained pure shear test piece, seen in figure 81.
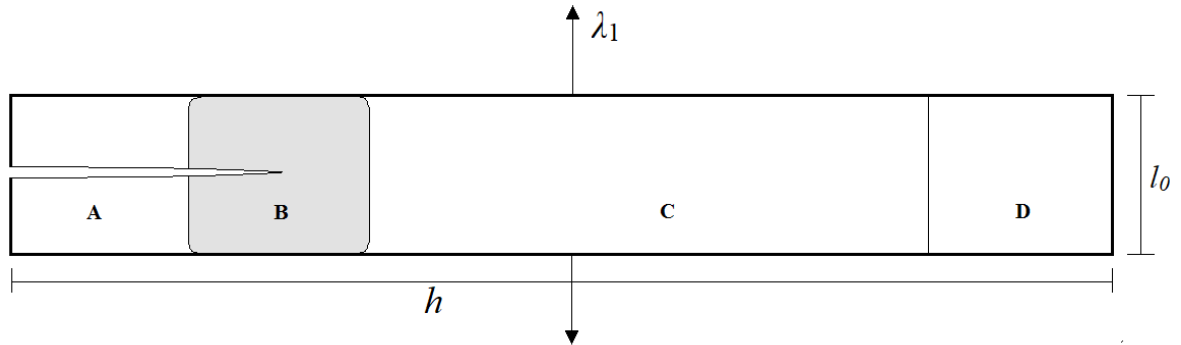
Figure 81: Diagram of the tearing regions on a pure shear test piece

Region A is featured as the fully relaxed region to the left of the crack tip that experiences no strains when the cracked sample is stretched. In this region the elastic strain energy U_A is equal to 0. Region B is featured at and around the crack tip. The stress field in this region is complex and the value of U_B, the elastic strain energy in region B, is unknown. Region D is similar to region B. As this region is close to the free edge, it is not in pure shear and the value of U_D is also unknown. Region C is deformed in uniform homogeneous pure shear. The value of elastic strain energy $U_C=WV_C$ where W is the strain energy density in region C and V_C is the volume of material that is found in region C.

As the crack propagates through the sample, these regions move and change size. As the crack progresses, region B moves into region C. As the size and location of region D is only dependent on the opposing free edge, this region is unaffected by the crack development and the result is that region C decreases in size and region A increases in size. The total volume of materials that is lost in region C when a crack extends an additional distance dc can be seen to be:

$$\Delta V = l_0 t dc \tag{4.4}$$

where t is the sample thickness. Therefore, the total loss of strain energy as a result of the crack extending is:

$$\Delta U = -Wl_0 t dc \tag{4.5}$$

116

As the area of one side of the fracture surface is equal to:

$$\Delta A = t\mathrm{d}c \tag{4.6}$$

the tearing energy equation can be seen to be given by:

$$T = \frac{-\Delta U}{\Delta A} = Wl_0 \tag{4.7}$$

It is worth noting that the tearing energy is independent of crack length when using this fatigue crack test piece geometry. This enables the crack growth rate to be monitored over any time interval and strain level. As well as this, as the tearing energy depends only on the changes in the volume of the materials present in Region C, any complications due to the detailed crack tip geometry can be ignored.

Busfield et al [Busfield, J. J. C. Ratsimba, C. H. H. and Thomas, A.G, 1997] suggested an alternative way to calculate the tearing energy using the direct measurement of the force and displacement data during the crack growth test. This allows for the effects of cyclic stress softening to be accounted for directly. To calculate the elastic strain energy, U, it is simply a job of integrating the loading curve of the force vs deflection graph at a particular point during the test, seen in figure 82.
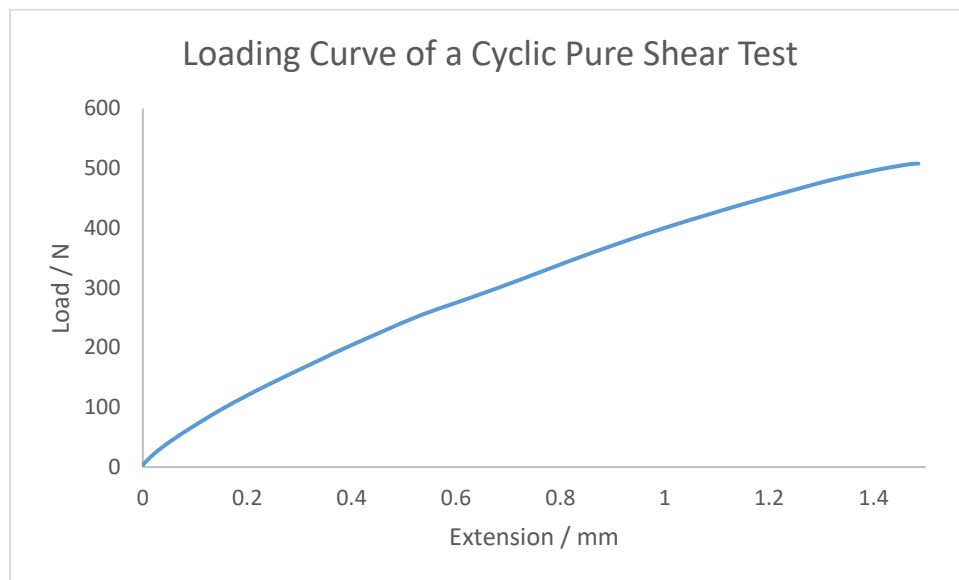
Figure 82: Typical stress strain loading curve of sample HNBR 60, used to find the elastic strain
energy.

Equation (4.7) can be adapted to:

$$W = \frac{U}{V} \tag{4.8}$$

The equation for volume, *V*, here can be expressed as:

$$V = l_0 t(h - c) \tag{4.9}$$

where *t* is the thickness of the sample, *h* is the longitudinal length of the sample and *c* is the length of the crack. Only the uncracked length is considered here. However, in practice, [De, D. K, 1994] found that there was an extra length *x* which was not energy free. Measuring this experimentally he found that this length was approximately equal to 28% of the unstrained sample height l_0 and was also independent of crack length. This then adapts the volume of material in the pure shear region to be:

$$V = l_0 t(h - c + x) \tag{4.10}$$

This can then be incorporated as the effective volume into equation (4.7) to derive a more robust tearing energy expression measured throughout the test of:

$$T = \frac{U}{t(h-c+x)} \tag{4.11}$$

Objectively, this experiment can determine a relationship between tearing energy and crack growth rate which is the parameter of interest when trying to quantify the fatigue resistance of a material. As mentioned before, using equation (4.11), tearing energy can be found by measuring and monitoring the dimensions of the specimen as well as determining the elastic strain energy which can be found by integrating the loading curve of the force vs deformation graph. This graph is obtained as an output from the testing machines used and measured using an appropriate load cell. The crack growth rate is measured by periodically taking photos of the sample during the test. The photos monitor the length of the crack at different time periods that can then be processed using computer software, such as 'Image J'. This software scales pixels on a photograph to physical lengths. By taking a photo of a length scale before the test begins, this scale can be determined and the length of the crack can be calculated between each photo. The time scale can be linked to cycle number which then gives us the crack growth rate per cycle $\mathrm{d}C/\mathrm{d}N$.

All the values for the crack propagation rates and tearing energies were taken from beyond the 1000th cycle. In fixed deformation dynamic tests, cycle 1000 is often used to determine the point where cyclic stress softening effects reach an equilibrium. In the early stages of a fatigue test, this effect adds an extra non-linear effect that causes higher elastically stored energy values and crack growth rate values when active that reduce non-linearly after each cycle. Therefore, to reduce complexities in the test, the first 1000 cycles are always neglected [Papadopoulos, I. C et al, 2008].

Pure shear test specimen used in this body of work were cut into rectangular shapes measuring 175 x 45 x ~2 mm. The precise thickness depended on the thickness of the mould. As it is a very important value, several different measurements were made at a range of different location on each test piece which were then averaged before every test. All the samples were cut by hand. The crack of 30 mm was inserted via a blade and then propagated a small amount by hand to roughen the crack tip to a more typical steady state crack tip. The top and bottom grips both gripped the sample along the full longitudinal length leaving a sample height between the grips of approximately 15 mm. Therefore the working section of the pure shear test piece was reduced from the cut shape dimension of 45 mm to just 15 mm between the grips. This ensured a working section length to height ratio of approximately 10 times, which is the amount that is satisfy the requirement for the central region of the test piece to be in pure shear.

Samples were all tested on the Instron 8801 Servo-Hydraulic Testing Machine. Testing parameters range accordingly:

- Strain values: 10 – 50%
- Strain rate values: 20 – 100%/s
- Testing frequency: 1Hz
- Number of cycles: 1000-5000

To enable samples to be compared, crack growth rate was kept within a certain range for all tests. This enabled the tests to be managed easier as tests needed to satisfy at least 1000 cycles to be used as a successful test and neglect cyclic strain softening effects. It also enabled unfilled materials to be compared to filled materials which in practice can typically take higher

loads. With this in mind, strains were done over different ranges for each elastomer to ensure a comparable crack propagation rate.

The test procedure consisted of accurately measuring the specimen's dimensions, including an average thickness over the sample. The sample was placed in the grips and tightened. As the specimen was gripped tighter it would start to buckle as volume was forced out between the grips. The grips were then moved to adjust for this so that the test would start at zero load. A line is drawn onto the sample along the grip edge. This helps to identify any slippage that might occur in the grips as this needs to be avoided. The camera was set up to periodically take pictures of the crack as it propagates. As the testing frequency was set at 1Hz, cycles were taken every 60 seconds, meaning that every picture was taken at every 60th cycle. A length scale was caught in the frame of reference for each image. In the first cycle of every test, the camera was initially triggered to begin taking pictures at the maximum displacement of every cycle.

After this, data was collected and processed to determine the tearing energy and crack growth rate for each test after the 1000th cycle.

4.8 TROUSER TESTS

Trouser test specimens were used to characterise static crack growth behaviour. A trouser test specimen is a rectangular specimen featuring a large crack that is often approximately half the length of the specimen. Also developed by [Rivlin. R. S and Thomas. A. G, 1953], this test piece is also a geometry used for determining static fracture behaviour in elastomers due to the simple nature of the test.

It functions by separately gripping both legs from the cut end of the sample. The test is the performed in a simple uniaxial tension regime where the crack then propagates down the centre of the sample.
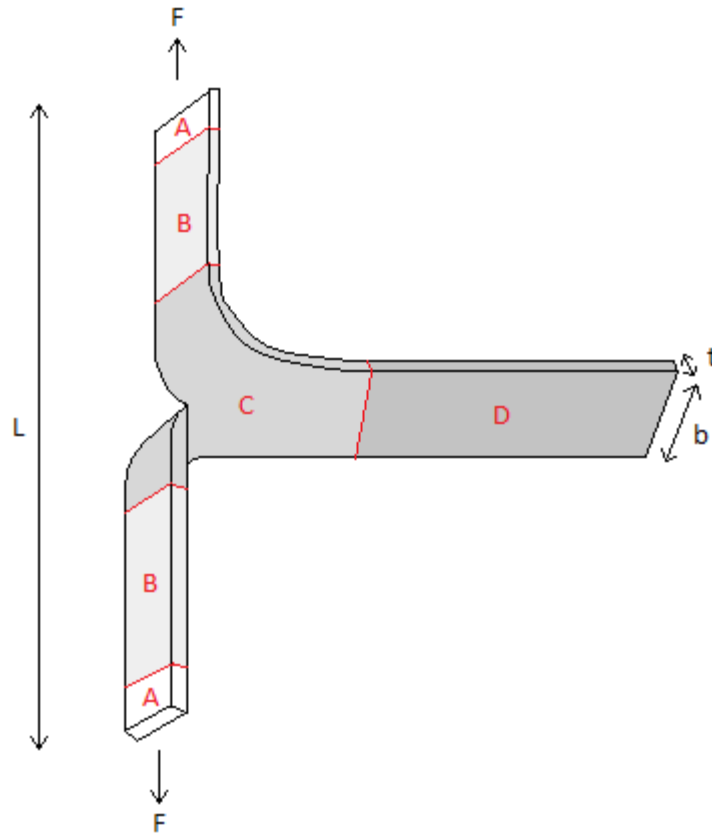
Figure 83: Diagram of the tearing regions on a trouser tear test piece

The sample, similarly to the pure shear specimen can be separated into different regimes. Dimensions on this test piece in this work feature a length of 60mm, width of 25mm and thickness of 2mm. Regions (A) is where the sample is gripped by tensile grips, regions (B) is found in the legs between the gripped region and the crack tip region. This region is predominantly in uniaxial tension. Region (C) is the area containing the crack tip. Both regions (A) and (C) feature a complex stress field due to crack tip and edge effects. Region (D), provided it is of a sufficient length, remains unstrained.

For the crack to propagate through the sample, a threshold tearing energy must be reached at the crack tip. This is often one of the main objectives of the test, to identify this value. Assuming the crack tip geometry does not change significantly to alter the stress field, as the crack propagates through the sample, regions (A) stays the same size and keeps to the same location, regions (B) gets progressively larger as the test continues, region (C) stays the same size but moves with the crack tip and region (D) progressively gets smaller as regions (B) gets larger.

The volume lost in region (D) is approximately equal to:

$$dV = tb\mathrm{d}c \tag{4.12}$$

where t is the sample thickness, b is the sample width and $\mathrm{d}c$ is how much the sample has progressed by. As the crack grows by $\mathrm{d}c$ the distance between the clamped regions, L, increases by $\mathrm{d}l$, which is equivalent to:

$$\mathrm{d}l = 2\lambda\mathrm{d}c \tag{4.13}$$

The strain energy stored in the crack piece, U, varies as a result of the crack length and the strain in the legs, regions (B). This strain in the legs can be approximated by using the force measured before the crack is .

$$dU = \left(\frac{\partial U}{\partial c}\right)_l dc + \left(\frac{\partial U}{\partial l}\right)_c dl \tag{4.14}$$

As the force due to the change in extension is related to the stored energy in the following way:

$$F = \left(\frac{\partial U}{\partial l}\right)_c \tag{4.15}$$

Combining equations (4.13), (4.14) and (4.15) gives:

$$\left(\frac{\partial U}{\partial c}\right)_l = \left(\frac{\partial U}{\partial c}\right)_F - 2F\lambda \tag{4.16}$$

As the change in stored energy is as a result of regions (B) getting bigger and region (D) getting smaller, this is the equivalent strain energy density in regions (B), w_0, combined with (4.12) gives:

$$dU = btw_0\mathrm{d}c \tag{4.17}$$

This can be rearranged and combined with (4.16) to give:

$$\left(\frac{\partial U}{\partial c}\right)_l = btw_0 - 2F\lambda \tag{4.18}$$

Assuming a uniform thickness, t, the change in area of one side of the crack is given as the thickness multiplied by $\mathrm{d}c$.

$$T = -\frac{1}{t}\left(\frac{\partial U}{\partial c}\right)_l \tag{4.19}$$

Inserting (4.18) into (4.19) gives the tearing energy for a trouser test configuration:

$$T = \frac{2F\lambda}{t} - bW \qquad (4.20)$$

Where *F* is the force at the point where the crack begins to propagate further and *b* is the thickness of the sample. For elastomer samples that are highly filled, the force required to extend samples in tension can sometimes be much higher than the forces experienced in trouser tear tests. This can render the final term negligible. Where, λ, the extension ratio of the legs, becomes equal to 1 and W, the elastic energy stored in the legs, becomes equal to 0.

The difficulty that occurs is which point to take the measurement of F. Research by [Windslow. R. J and Busfield, J. J. C, 2017] suggests that a good estimate of this point is the point of inflection in the stress strain plot. This can be confirmed by placing a contrasting colour on the crack tip and monitoring the colour change. This was also carried out for this body of work. For example, for the test done at 50 °C at 0.01cm/s, the stress strain plot was as follows in figures 84 and 85:
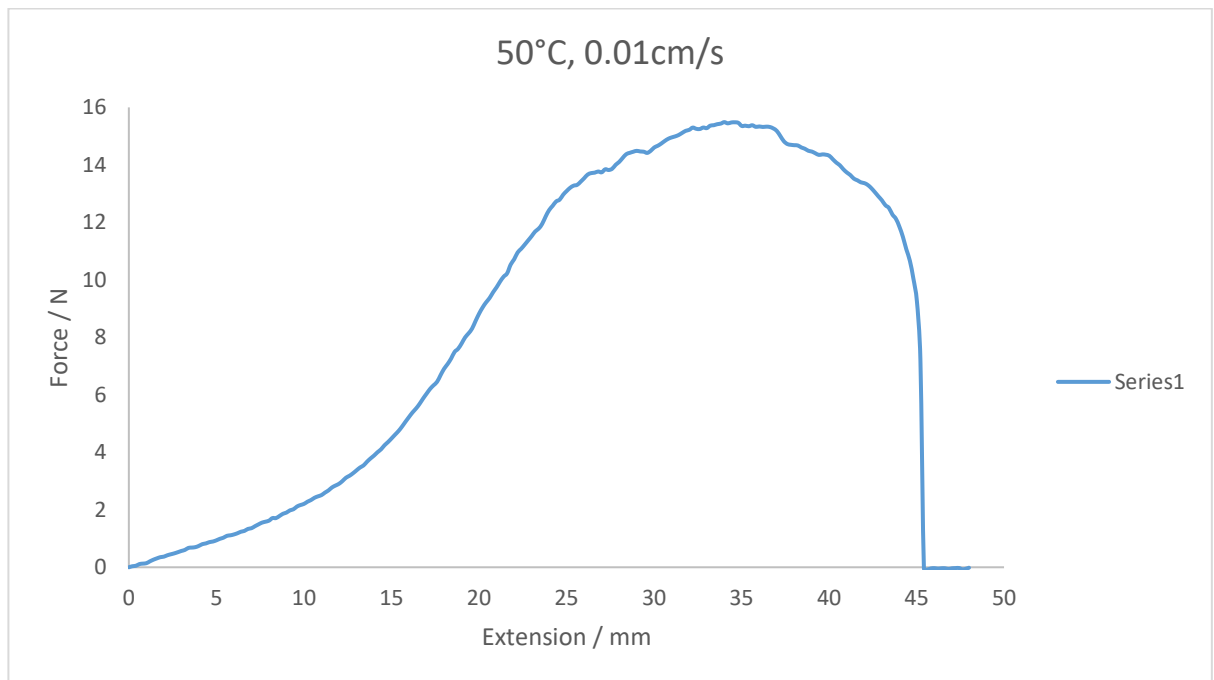
Figure 84: Force vs extension plot for an example trouser tear test

By taking a central differencing scheme, the point of inflection was able to be identified:
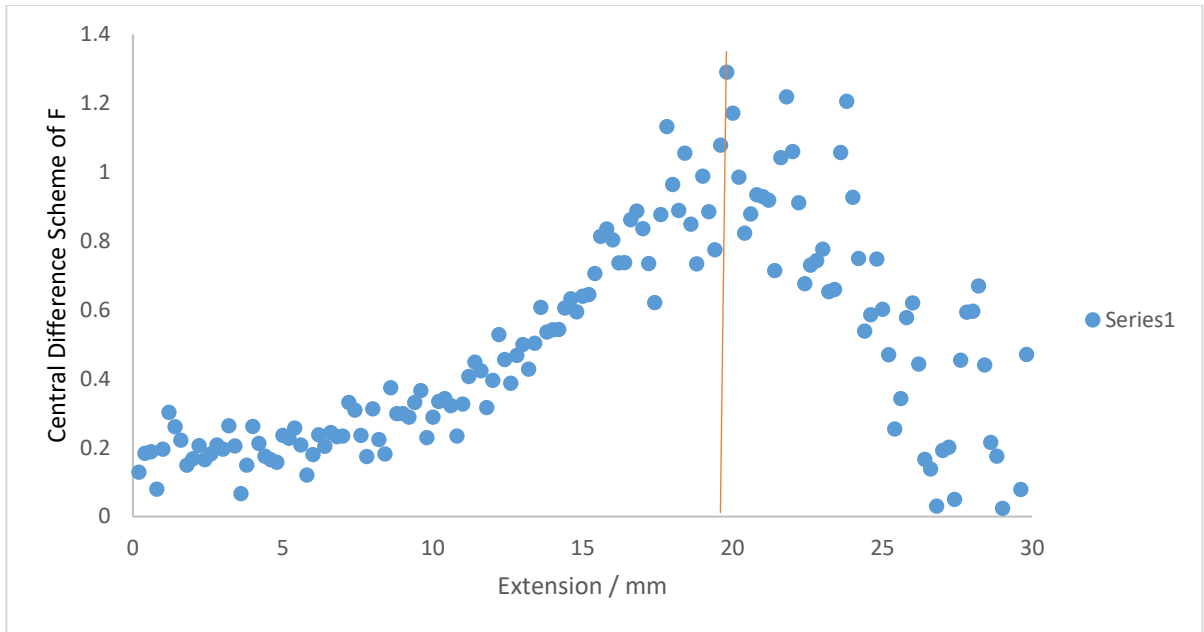
Figure 85: Central difference scheme of force vs extension plot of an example trouser tear test

It was then evaluated from this that the inflection point was at approximately 19.8mm which then lead to the tearing energy being evaluated as:

Extension at Peak	Force at Peak	Sample Thickness	Tearing Energy
/mm	/N	/mm	/Jm^{-2}
19.81	8.57	2.20	7791

Table 5: Example tearing energy result for an example trouser tear test

This method was later confirmed by placing a white coloured mark on the crack trip of the trouser test piece and filming the test run. It was identified that the point where the colour mark was split and elastomer could be seen, indicating crack growth, was at this inflection point. It was therefore used for the rest of the testing procedure.

4.9 FOURIER TRANSFORM INFRARED SPECTROSCOPY (FTIR)

Later in this body of work, samples unaged and aged are characterised using Fourier Transform Infrared Spectroscopy (FTIR). FTIR is a fast, effective and non-destructive method of analysing materials by focusing infrared (IR) radiation into a sample and monitoring the spectrum out. FTIR functions by using an IR source of specific frequency range 300 – 4000 cm^{-1} to direct an IR beam into the sample. The IR beam interacts with the sample by either being absorbed or

124

transmitted and a detector then receives the spectrum once interacted with the sample. The IR beam interacts with the samples by causing localised vibrations of individual bonds or functional groups. These vibrations manifest in the form of stretching, bending, rocking, twisting and wagging as a result of absorbing energy and causing a change of energy state from lower to higher. As a result, specific bonds and functional groups can be identified within samples enabling sample constituents and components to be identified.

The use of FTIR on elastomer samples in common and has been used for comparing elastomer formulations before and after ageing [Lou, W, Zhang, W, Liu, X, Dai, W. and Xu, D, 2017] [Fernandez-Berridi, M, Gonzalez, N, Mugica, A. and Bernicot, C, 2006].

In the case of this work, samples were tested before and after ageing, on the surface and within a cross-section of the sample. This provided a wide analysis with which spectrum could be analysed before and after ageing. Different techniques can be used to analyse FTIR data. However, in this case, FTIR spectrum of all individual ingredients from all samples were provided and used to match the formulations used in this work. This enabled a direct correlation from individual ingredients to full formulations. By comparing, loss of ingredients could be identified.

4.10 CONCLUSIONS

From this chapter, the mechanical and environmental range under which a mud motor operates and the mechanisms behind how the elastomeric stator reach the end of their service life have been analysed. From this, a conclusion about the testing ranges for the remaining chapters has been reached. Basic characterisation tests have shown how these elastomers behave at a fundamental level and how differ from each other. Finally, using the techniques described at the end of this chapter, the analysis of how these materials operate under these extreme environments can be investigated.

5. CYCLIC FATIGUE AND AGEING OF HNBR FOR OIL AND GAS

5.1 INTRODUCTION

This chapter discusses a study to characterise and understand the fatigue response of model oil and gas HNBR elastomer compounds under typical conditions encountered in service. As the energy required to propagate a crack is a material characteristic, using a test-piece geometry with known tearing energy relationship enables a fatigue understanding that can be directly correlated to a service life prediction when designing an elastomeric part.

The test used here is a cyclic pure shear fatigue crack growth test as described in both chapters 3 and 4. This geometry is very useful for cyclic fatigue tests as the crack typically grow at a constant rate for a given strain energy release rate and complications about the details of the crack tip geometry can be avoided. Materials are cyclically loaded with an initial crack cut into the specimen using a razor blade and the crack propagation rate is measured with respect to the strain energy release rate or tearing energy. This is then presented on a logarithmic scale of crack propagation rate vs tearing energy to allow the parameters in the power law region to be measured. The testing parameters are also focussed on the range of use of the mud motor, where the strains are 50% or lower and consequently, the crack growth process will be almost entirely mechanically driven. The range of testing parameters are as follows:

- Strain values: 10 – 50%
- Strain rate values: 20 – 100%/s
- Testing frequency: 1Hz
- Number of cycles: 1000-5000

All four compounds were initially characterised in a virgin, unaged state at room temperature to establish a baseline for their cyclic pure shear fatigue response. Samples were then tested under a similar range of conditions after an ageing period. The four different ageing processes that occurred were as follows:

- Aged in an air oven at 100°C for 1 week
- Aged in an air oven at 150°C for 1 week
- Aged in IRM903 oil at room temperature for 1 week
- Aged in IRM903 oil at 150°C for 1 week

Materials were then tested at elevated temperatures in an unaged state. These testing temperatures were:

- 100°C
- 150°C

Finally, one of the compounds was tested after a post-curing process. The post-curing process involved placing the sheet back in the mould at a curing temperature of 170°C for 2 hours.

To investigate further how the compounds responded to the ageing conditions, samples were put through a series of different characterisation tests in both unaged and aged states. Tests that were conducted included:

- Thermogravimetric Analysis (TGA)
- Fourier-Transform Infrared Spectroscopy (FTIR)

5.2 MECHANICAL FATIGUE TESTS

5.2.1 CYCLIC PURE SHEAR FATIGUE FOR UNAGED SAMPLES

Cyclic pure shear fatigue tests follow a tearing energy relationship as demonstrated by Rivlin and Thomas [Rivlin. R. S and Thomas. A. G, 1953]:

$$T = W l_0 \tag{5.1}$$

where W is the elastically stored energy density in the pure shear region and l_0 is the unstrained distance between the two parallel clamps. In conjunction with Lake [Lake G.J., 1983], a tearing energy and crack propagation rate relationship is observed in the range of strains that we are working that exhibits a power law dependency:

$$\frac{dc}{dN} = B \left(\frac{T}{T_u}\right)^{\beta} \tag{5.2}$$

where T_u=1Jm^{-2} and is included only to make T/T_u dimensionless, B and β are material constants. β is the slope of the following graphs as they are plotted on logarithmic scales and is known to reflect [Papadopoulos, I. C, 2006] elastomer properties that relate to the amount of hysteresis. Figure 86 shows these plots for the four unaged materials, and table 6 summarises the calculated B and β parameters.
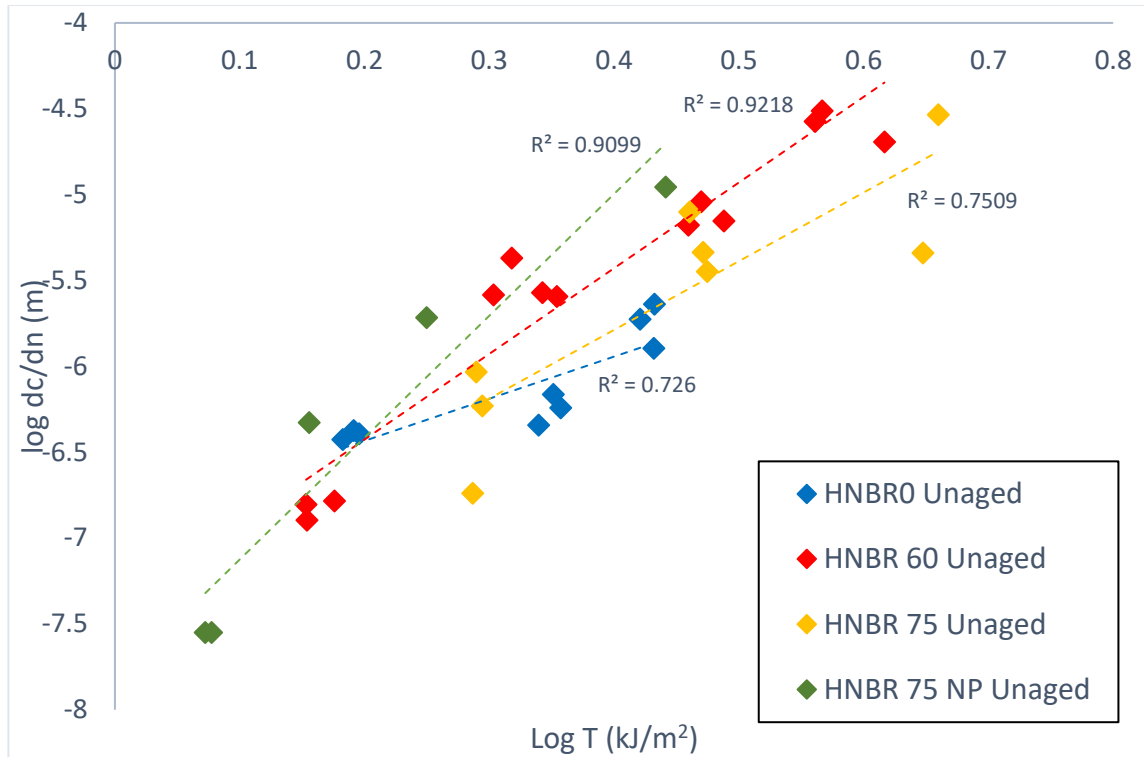
Figure 86: Cyclic pure shear fatigue of all four compounds unaged at room temperature, in air and at 1Hz.

	B / m	β
HNBR 0	9.83×10^{-4}	2.5
HNBR 60	5.97×10^{-4}	5.0
HNBR 75	6.19×10^{-4}	4.0
HNBR 75 NP	3.96×10^{-4}	7.1

Table 6: Material constants found for unaged compounds tested in cyclic pure shear fatigue at room temperature

When plotted in this way, the tougher materials are the ones with the slower crack growth rate per cycle at a given strain energy release rate. In this case the toughest materials are the ones that are furthest to the bottom right on the graph. The cyclic pure shear fatigue testing of virgin unaged samples shows results that were to be expected and some that were not anticipated.

Understandably, as carbon black content was increased between HNBR 60 and HNBR 75, an increase in toughness was seen alongside a decrease in material constant β. Both of these

128

properties correspond to an increase in hysteresis, mirrored in the tensile tests shown in chapter 4.

Surprisingly, the sample with no carbon black filler, HNBR 0, was tougher than the filled samples for tests above a tearing energy of 0.2 kJ/m^2. Despite this outcome not being anticipated, it can be attributed to a number of factors. The β value of the unfilled sample is much lower than the filled samples. As explained before, this indicates a high level of hysteresis at the crack tip and so, for some elastomers like NR that can exhibit strain induced crystallisation, values are often seen in the range of 2 – 2.5. This is also reflected in the crack tip shape as shown in figure 88.

Figure 88: Crack tip shapes for HNBR 0 (left) and HNBR 75 (right) during cyclic pure shear tests at the same strain

In this figure, the difference between the crack tip profile of the HNBR 0 (on the left) and HNBR 75 (on the right) is significant, as the unfilled sample has a much blunter and wider crack tip, again indicating that a high amount of hysteresis is occurring. What also is apparent, is the higher level of scatter in the filled results when compared to the unfilled. This is easily attributed to the variation in the crack propagation rate during tests. What can often be seen in these cyclic pure shear fatigue tests of filled samples is a transitional tearing event, where tearing moves between sections of smooth tearing and knotty tearing. Examples are seen in figures 88, 89 and 90. These figures show the relationship between crack length and cycle number for three separate tests on a filled compound, along with a picture of the crack profile after each test. Each figure shows the marked difference between a smooth tear, a test with mildly knotty tearing regions and a test with a severely knotty tearing region.
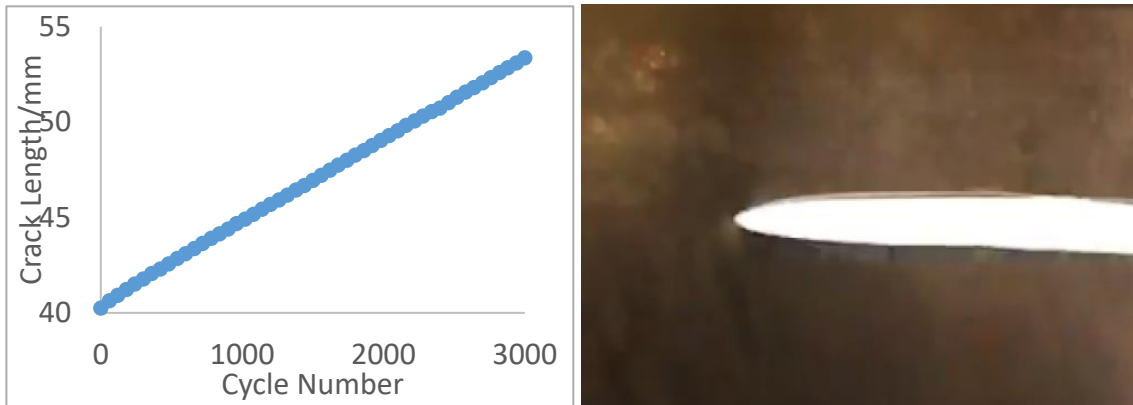
Figure 88: A typical graph of crack growth rate vs cycle number with a picture of the crack for a smooth tearing relationship
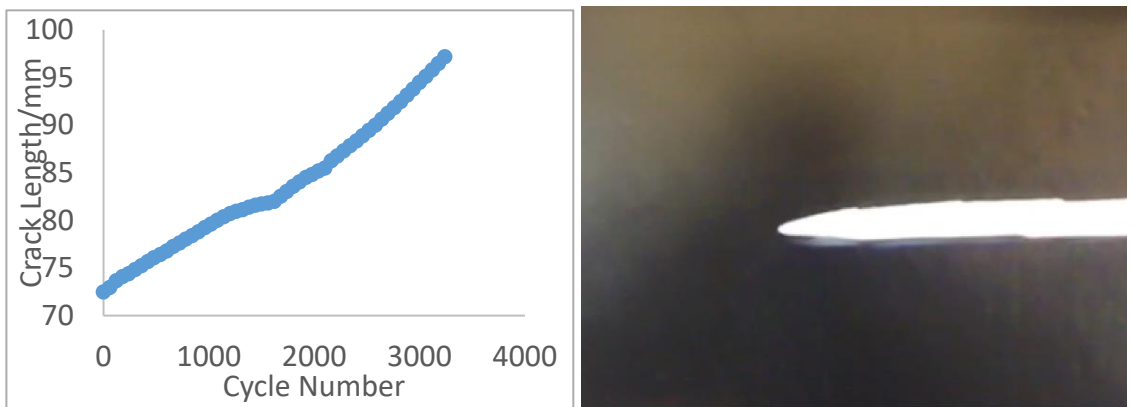
Figure 89: A typical graph of crack growth rate vs cycle number with a picture of the crack for a mildly knotty tearing relationship
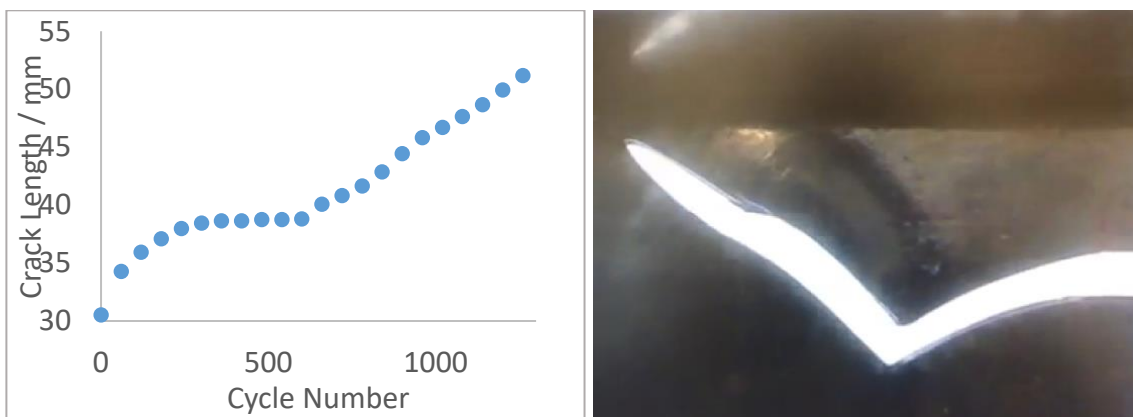
Figure 90: A typical graph of crack growth rate vs cycle number with a picture of the crack for a severely knotty tearing relationship

Tests showing this transitioning type of behaviour were common and the position of the knotty behaviour was unpredictable. This unpredictable behaviour opens up an issue with how to measure the crack propagation rate. When taking into account regions of mildly knotty crack propagation behaviour, tearing energy vs crack propagation rate results become mildly scattered. However, when results consider regions exhibiting severe knotty behaviour, tearing energy vs. crack propagation rate results become quite significantly scattered. As these regions are transitional within tests, areas containing these regions can be isolated and either focussed on or omitted for an individual data point. So as to have understandable tearing energy vs. crack propagation rate results, a decision was made to omit regions of severe knotty behaviour from crack propagation rate calculations for these results specifically. This enabled the regions of severely knotty behaviour to be isolated and analysed separately, whilst featuring results with a more reproducible tearing energy vs crack propagation rate relationship.

These regions of knotty tearing behaviour not only make sample results much more scattered, but when omitted, they specifically show that the results scatter only to lower crack propagation rates. Knotty tearing never accelerated the crack growth behaviour to faster rates. It can therefore be assumed that the knotty tearing behaviour, whilst being unpredictable, results in a material with a tougher fatigue response. It is also apparent that the, scatter range increases as tearing energy increases, showing that this toughness response does not simply translate the tearing energy vs. crack propagation rate relationship higher or lower, it affects the gradient of this relationship and more specifically the β material constant, which represents the hysteresis response of the material.

Another noticeable difference is crack tip shape between regions of knotty tearing and smooth tearing in all the samples. In regions of knotty tearing, crack tips become much blunter and rounder whereas smooth tearing regions are much sharper.

The sample with no plasticiser, HNBR 75 NP had a significantly lower fatigue resistance than its counterpart HNBR 75 that incorporated a plasticiser. In fact, results for this sample could only be tested between the range of $6 - 8\%$ strain before catastrophic tearing took place. A very clear change in β value was observed here as well. The plasticiser has a significant effect on chain mobility which in turn influences the hysteresis. The effect here on hysteresis is to lower the glass transition temperature T_g, of the compound. By removing plasticiser, hysteresis effects should increase and the T_g should be higher. In chapter 4, tensile tests showed this to

be the case which in combination with DSC tests showed that the plasticiser lowered the T_g by approximately 6.4°C. It therefore gives evidence that the plasticiser's influence of reducing chain mobility has a significantly greater effect on the fatigue response than that of increasing the hysteresis response. It could be deduced that the reduction of chain mobility within the elastomer causes physical polymer chain entanglements to have a greater effect, causing a larger stress field to occur within the sample, which produces larger tearing energies at lower strains.

5.2.2 CYCLIC PURE SHEAR FATIGUE FOR PRE-AGED SAMPLES

Samples HNBR 0, HNBR 60 and HNBR 75 were then tested under similar conditions after having been aged in four different conditions as described on page 124.

HNBR 75 NP was aged and characterised under these conditions however, the ageing process reduced the fatigue properties of the sample to such a low level that it was not possible to perform a functional test. Test strains of 8% resulted in catastrophic tearing. Below this value of strain, characterising crack propagation rate becomes significantly more difficult as gripping the test pieces without cutting through the samples was difficult and capturing photographs of the crack became very narrow. It was decided to abandon these tests as reliable crack propagation readings could not be made.

For all the tests, sheets of the compounds were cured, cooled to room temperature and then cut into pure shear specimen shapes without a crack. These samples were then aged in an air oven at 100°C or 150°C for 1 week. The oven temperature was measured continuously with a thermocouple to ensure the correct temperature was maintained. After ageing, the samples were left to cool and equilibrate to room temperature conditions before an initial cut for the cracked region was inserted into the sample. Samples aged in IRM 903 at room temperature were placed in a plastic container half full of IRM 903 oil. The test samples were completely submerged. The container was sealed with an airtight lid and covered completely so that no light could penetrate to the samples. Samples were left for 1 week undisturbed, then removed by hand and cleaned with tissue paper.

Samples aged in IRM 903 at 150°C for 1 week were aged at Schlumberger Cambridge Research Centre. Samples were placed in cylindrical pressure vessels which fully submerged the samples in IRM903. The vessels were then pressurised with N_2 to 690kPa to associate with oil well

conditions and then placed in an oven at 150°C that slowly rotated the vessels throughout the ageing process. After 1 week, vessels were removed from the oven and the samples were cleaned with tissue paper before introducing the crack in the samples prior to testing.

Samples were all tested at room temperature using the same testing parameters as the unaged samples (see page 124 for details). The results are shown in figure 91, and B and β parameters are summarised in table 7.
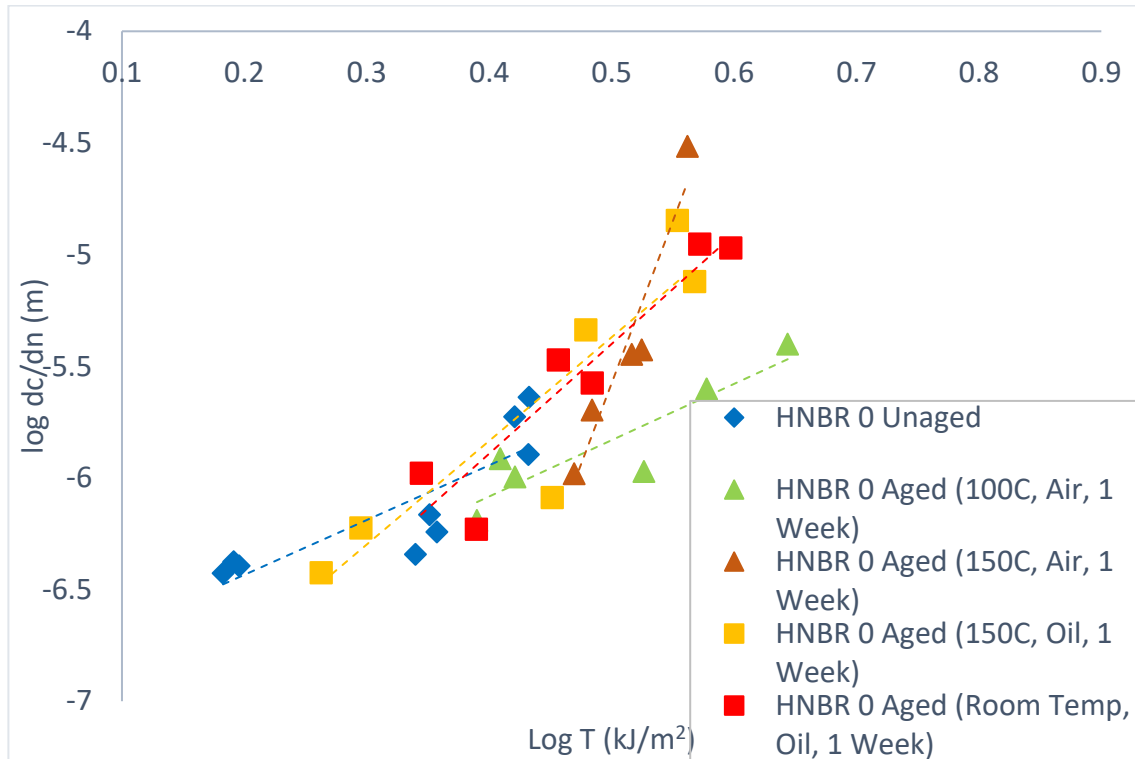
Figure 91: Cyclic pure shear fatigue for HNBR 0 after different ageing conditions, tested at room temperature

	B / m	β
HNBR 0 Unaged	9.83 x10^{-4}	2.5
HNBR 0 Aged (100°C, Air, 1 Week)	8.32 x10^{-4}	2.5
HNBR 0 Aged (150°C, Air, 1 Week)	2.66 x10^{-6}	14.5
HNBR 0 Aged (150°C, Oil, 1 Week)	4.57 x10^{-4}	4.6
HNBR 0 Aged (Room Temp, Oil, 1 Week)	3.87 x10^{-4}	4.9

Table 7: Material constants found for HNBR 0 after different ageing conditions in cyclic pure shear fatigue, tested at room temperature

The aged results for unfilled HNBR 0 are shown in figure 91 with a comparison to the unaged room temperature test. Similarly to the results for all four sample unaged tests, some of the results were as anticipated, however some of the results were more surprising.

HNBR 0 aged at 100°C in air was the most surprising result. The results had a similar gradient to unaged HNBR 0. However, the results were shifted showing slower crack propagation (higher toughness) than the unaged material. The β value was largely unchanged signifying no obvious change in hysteresis. However, this β value was still very low with a similar value to that found in a strain induced crystallising elastomer such as NR. This does not confirm SIC but is an indication of such effects,

HNBR 0 aged at 150°C in air features possibly the most drastic ageing response. Most noticeable is the change in gradient indicating a major change in hysteresis. It also meant that the transition between a slow steady crack propagation to fast catastrophic crack propagation was much quicker than for the unaged sample. This change in β value could be as a result of many influences, some of which might include polymer backbone break down or main chain scission, or the break down or reformation of crosslinks, or the loss of elastomer ingredients by mechanisms like evaporation. All of which are investigated further in this chapter.

HNBR 0 aged at 150°C in oil feature an increased gradient but mostly a lower fatigue resistance compared with the unaged test. Interestingly, the sample aged at 150°C in oil was much tougher than the sample aged at 150°C in air. This highlights potential mechanisms that might occur in each specific test. Firstly, the influence of oxidation on the fatigue properties of the samples aged in air might be much more severe than the influence of the IRM903 oil. This is an understandable assumption to make as HNBR is an elastomer that is tailored to resist hydrocarbon fluids partly as a result of its ACN content. Secondly, ageing in hot air or IRM903 will result in very different balances between absorption of material by diffusion resulting in swelling and loss of components by evaporation or leaching. It is much more likely material is lost in the test aged in air, signifying that evaporation is the dominating process here. For the samples aged in oil, the combination of swelling and leaching will be very complicated and needs to be investigated further. This has been done later in the chapter using additional materials characterisations tests. However, it is safe to assume at this time that as the influence of hysteresis after ageing in IRM903 is significantly reduced compared to the sample aged in air, that the oil is either restricting the leaching out of elastomer ingredients such as

134

the plasticiser, or it is potentially displacing some of these ingredients and acting in a similar role.

HNBR 0 aged at room temperature in oil features a similar result to the sample aged at 150°C in oil, however, it shows a slightly tougher response. The similarity between these two tests suggests that the influence of temperature has on the ageing process is more significant when it is in combination with ageing mechanisms such as oxidation.
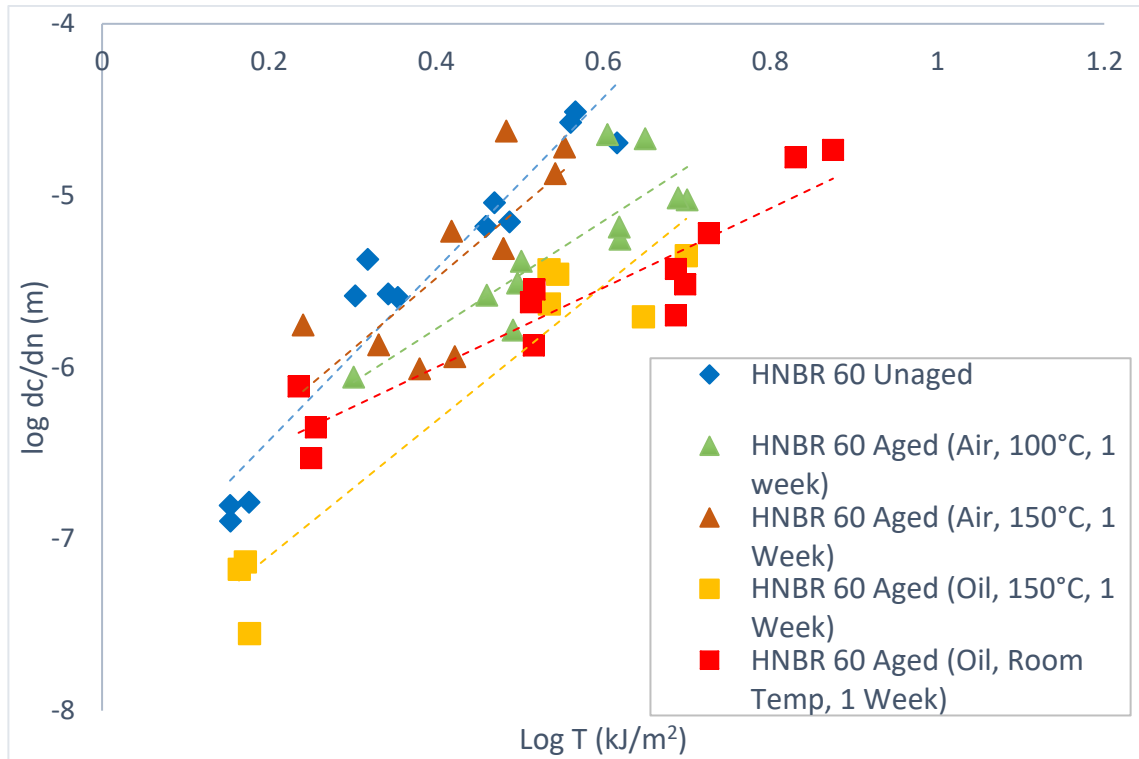
Figure 92: Cyclic pure shear fatigue for HNBR 60 after different pre-aging conditions, tested at room temperature

	B / m	β
HNBR 60 Unaged	5.97 x10^{-4}	5.0
HNBR 60 Aged (100°C, Air, 1 Week)	8.84 x10^{-4}	3.1
HNBR 60 Aged (150°C, Air, 1 Week)	8.00 x10^{-4}	4.1
HNBR 60 Aged (150°C, Oil, 1 Week)	3.76 x10^{-4}	3.9
HNBR 60 Aged (Room Temp, Oil, 1 Week)	9.82 x10^{-4}	2.3

Table 8: Material constants found for HNBR 60 after different pre-aging conditions in cyclic pure shear fatigue, tested at room temperature

The results for ageing HNBR 60, shown in figure 92, samples show increased fatigue resistance post-ageing.

HNBR 60 aged at 100°C in air not only shows an increase in toughness but also features a lower β value. There is also reasonable level of scatter in the results, especially at higher tearing energies. This indicates an increase in knotty behaviour producing increased scatter at higher tearing energies, resulting in a lower value of β (rather than a true change in hysteresis). It can, therefore, be argued that ageing in air at 100°C increases the incidence of knotty behaviour which introduces an additional toughening mechanism that as yet still has to be identified. Another question this raises is whether the toughening behaviour is evident over the entire tested tearing energy range. At higher tearing energies the toughening mechanism could still be occurring but is overcome by the high levels of strain rate. At lower tearing energies the toughening behaviour is still present, but the low levels of strain rate are not large enough compensate for this behaviour, causing a translation in results to lower values without scattering.

HNBR 60 aged at 150°C in air understandably shows further reduction in fatigue resistance compared to materials that were aged at 100°C in air. However, the gradient of the plot (value of β) is similar to the unaged material. There was however an increase in the measured experimental scatter resulting from an increase in knotty tearing. Scatter is present both above and below the unaged results, indicating that the general behaviour of the elastomer after ageing at 150°C in air is weaker than the unaged results, but that the frequency at which knotty tearing occurs increases much like the other tests.

HNBR 60 aged at 150°C in oil shows the most significant increase in fatigue properties and a slight lowering of β value. Whilst this is a surprising result, it also mirrors the response for the unfilled HNBR 0 sample where ageing at 150°C in oil offers significantly better fatigue properties compared to ageing at 150°C in air.

HNBR 60 aged at room temperature in oil also shows an increased fatigue performance however the most significant change compared to the other aged samples is the reduction of the β value. This indicates that, in this case, the oil is having significant effect on the hysteresis properties of the samples potentially as a result of oil diffusing into the compound during ageing and some of the elastomer ingredients leaching out.
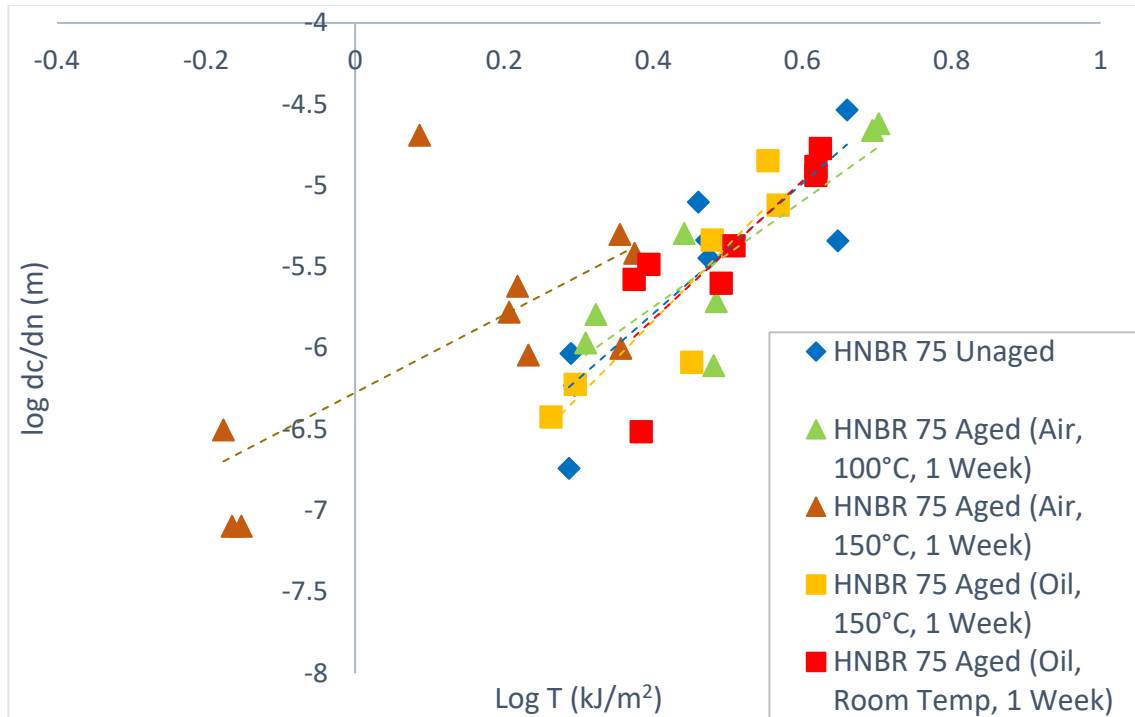
Figure 93: Cyclic pure shear fatigue for HNBR 75 after different ageing conditions, tested at room temperature

	B / m	β
HNBR 75 Unaged	6.19 x10^{-4}	4.0
HNBR 75 Aged (100°C, Air, 1 Week)	8.67 x10^{-4}	3.3
HNBR 75 Aged (150°C, Air, 1 Week)	1.88 x10^{-3}	2.4
HNBR 75 Aged (150°C, Oil, 1 Week)	4.57 x10^{-4}	4.6
HNBR 75 Aged (Room Temp, Oil, 1 Week)	5.41 x10^{-4}	4.3

Table 9: Material constants found for HNBR 75 after different ageing conditions in cyclic pure shear fatigue, tested at room temperature

Figure 93 shows the results for HNBR 75 before and after ageing. In general there was little change in fatigue resistance after ageing. HNBR 75 aged at 100°C in air featured fatigue crack growth results similar to that of the unaged material, except with a broader scatter in the measured behaviour. Any lowering of β value here should be understood with that in mind, similarly to the aged results seen in HNBR 60. Minor changes in the fatigue properties of this elastomer after ageing might be expected as HNBR with larger amounts of carbon black filler is known to withstand higher temperatures.

137

HNBR 75 aged at 150°C in air showed a significant reduction of the fatigue resistance, together with a major increase in the experimental scatter. It might be expected that once a certain threshold temperature had been exceeded during ageing, that the fatigue properties would inevitably decrease. In this case, 150°C was clearly above this threshold when compared to the tests aged at 100°C. In this case, oxidation was obviously having a significant effect on the elastomer as a result of this increase in temperature.

HNBR 75 aged at 150°C in oil interestingly showed a similar behaviour to the samples that were aged at 100°C in air. This further highlights the point that this material suffered a more significant reduction in fatigue behaviour when aged in air rather than in the IRM903 oil.

HNBR 75 aged at room temperature in oil showed similar behaviour to the unaged material, suggesting that IRM903 at room temperature had little effect on this elastomer compound. Small changes might be seen in β value, however, should be understood with respect to the level of scatter.

5.2.3 TENSILE TESTS OF AGED HNBR SAMPLES

In addition to cyclic pure shear fatigue tests done on unaged and aged samples, samples were also tested in tension to identify the effect of each of the ageing conditions on the modulus and hysteresis for two of the compounds.

Samples were tested with the following parameters:

- Strain: 50%
- Strain Rate: Quasistatic (0.01/s)
- Temperature: Room Temperature
- 1 Cycle

Tests were done on the unfilled sample (HNBR 0) and one filled sample (HNBR 60) and tested using standard dumbbell specimens. The results are shown in Figures 94 and 95 below.
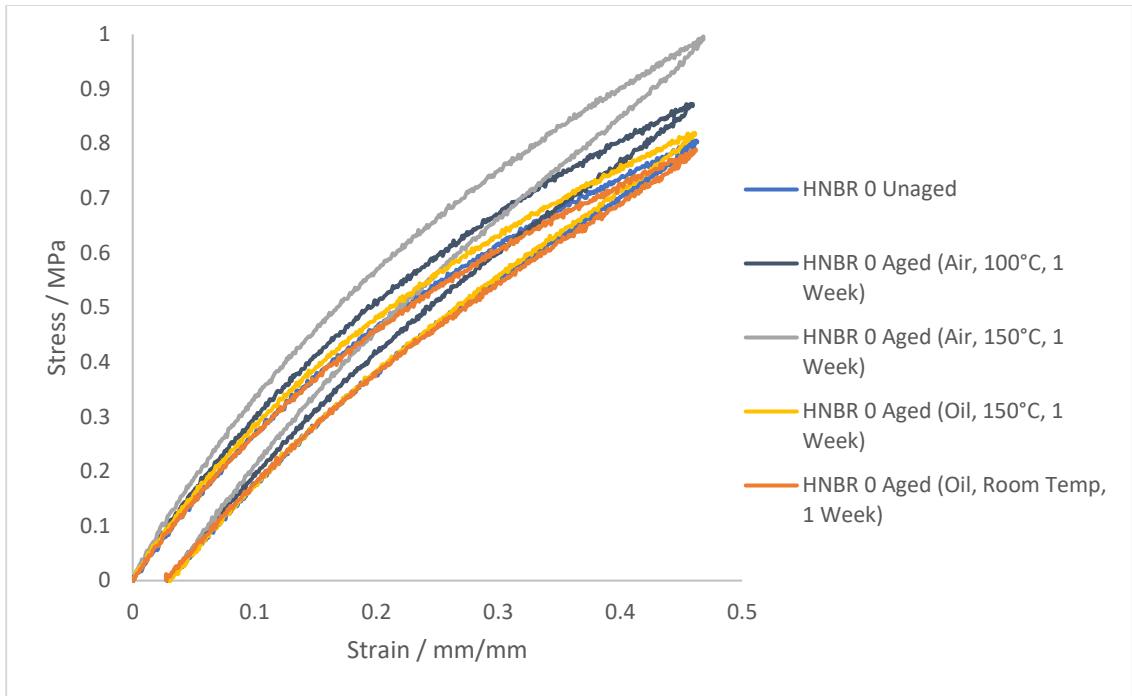
Figure 94: Tensile tests for HNBR 0 after different ageing conditions, tested at room temperature
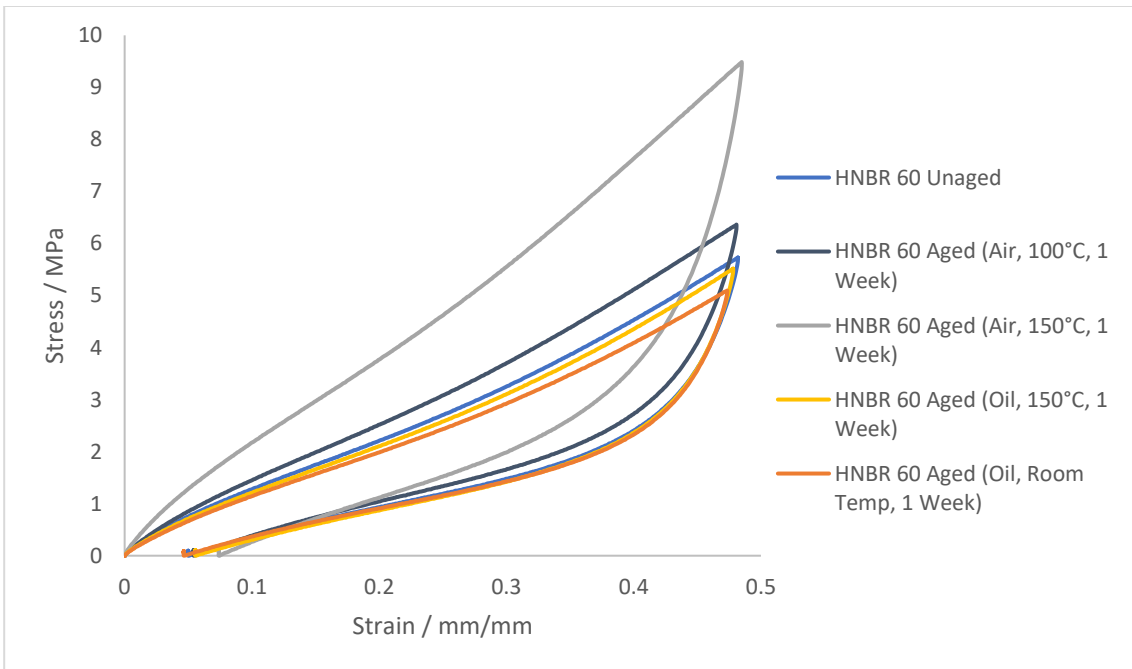
Figure 95: Tensile tests for HNBR 60 after different ageing conditions, tested at room temperature

It is evident that ageing introduced a significant change to the stress vs. strain behaviour in terms of both the modulus and the hysteresis. Both unfilled and filled samples showed the same general trends after ageing, differing in the extent of change.

Both samples when aged in air showed an increase in modulus, with a larger increase after ageing at 150°C. This led to the conclusion that oxidation effects that are activated more readily at higher temperatures were taking place. This also caused an increase in hysteresis, especially for the samples aged at 150°C. Oxidation effects are certainly apparent, however other effects could be occurring as well including a change in elastomer composition and crosslink density which are investigated later in the chapter.

Samples aged in IRM903 oil at room temperature both showed a decrease in modulus, potentially because the oil had diffused into the elastomer. Then it can act to increase chain mobility and perform similarly to a plasticiser. There are some chemical similarities between long-chain hydrocarbon molecules present in oils and plasticisers, so this was not altogether unexpected.

Samples aged in IRM903 oil at 150°C seem to show a very similar response to the unaged material. Potentially several different mechanisms might be occurring simultaneously including the swelling of rubber with the oil, the thermal ageing of the elastomer, the leaching out of some of the elastomer ingredients and potential changes to the crosslink density. These factors are all investigated further in this chapter.

5.2.4 CYCLIC PURE SHEAR FATIGUE TESTING AT ELEVATED TEMPERATURES

Unaged samples of HNBR 60 and HNBR 75 also had their fatigue behaviour characterised at elevated temperatures of both 100°C and 150°C. It was also attempted to measure HNBR 0 under these conditions, however for similar reasons that are explained in chapter 4, at elevated temperatures the mechanical testing of elastomers becomes more difficult as the elastomers are known to become weaker and less tough. In this particular case, when testing HNBR 0 at elevated temperatures without the additional reinforcement from the carbon black, it became difficult to optimise the gripping pressure. If it was too low then the samples slipped out of the grips but if it was too high then it was easy to fracture the elastomer in the grips. Reliable results could not be obtained, and so these tests were not included in this report.

The process for testing elastomers at elevated temperatures was as follows. Pure shear specimens were prepared as described earlier. The oven was placed around the testing area of the Instron machine with two holes on the top and bottom of the oven to connect the arms that held the grips and the specimen to the test machine frame. The load cell was placed outside the oven and the camera was placed at the front window of the oven. The oven was heated up to the designated temperature with the pure shear grips installed inside. Once the oven temperature reached equilibrium, the sample whose dimensions had been accurately measured, was placed in the grips as quickly as possible. This ensured that heat loss from the oven was minimised. The grips were not tightened at this stage but were loosely placed over the sample. This allowed the sample to heat back up to the designated test temperature and expand in size without the introduction of any additional mechanical stress being placed on it. Following advice from the Schlumberger Cambridge Research Centre team, and confirmed on tests done using a thermocouple, the test pieces heated up to the designated testing temperature within 30mins. After this, the oven was opened and the grips were tightened sufficiently. The specimen were left a further 15mins to restore the sample to the required test temperature again. The grips were moved to account for any buckling in the sample so that the force at the start of the test was zero. Once the temperature had reached equilibrium, the fatigue crack growth test was started. The results for these tests were as shown in figures 96 and 97.
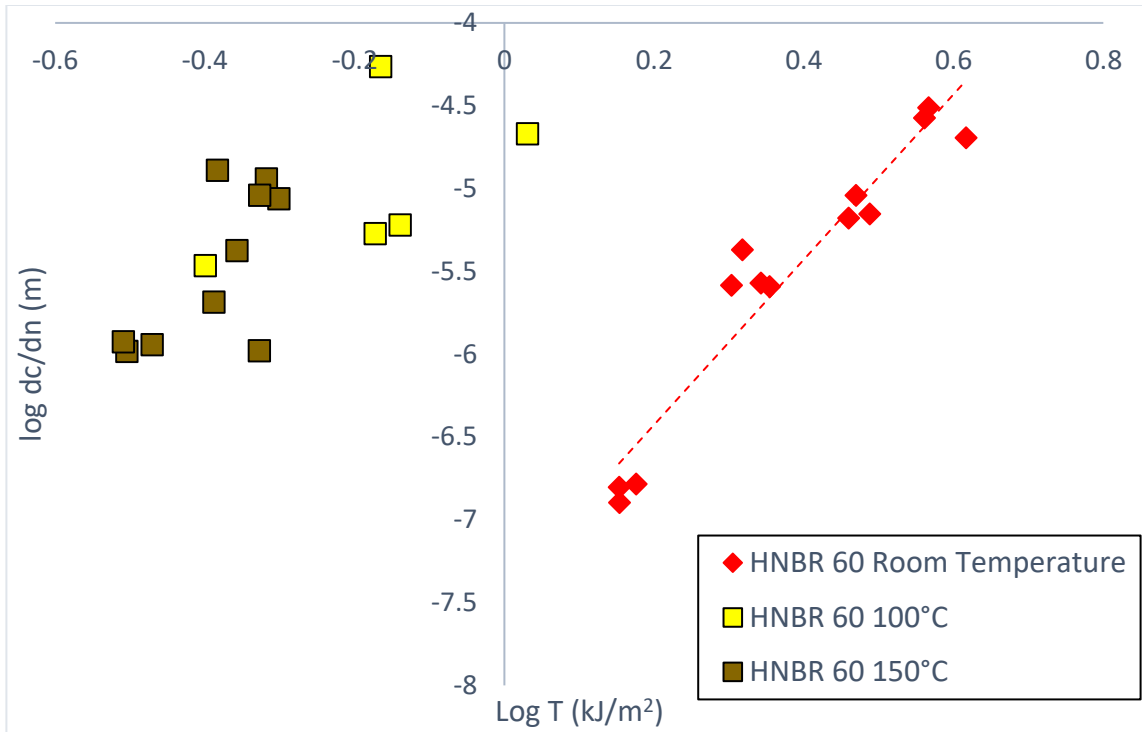
Figure 96: Cyclic pure shear fatigue for unaged HNBR 60 tested at different temperatures
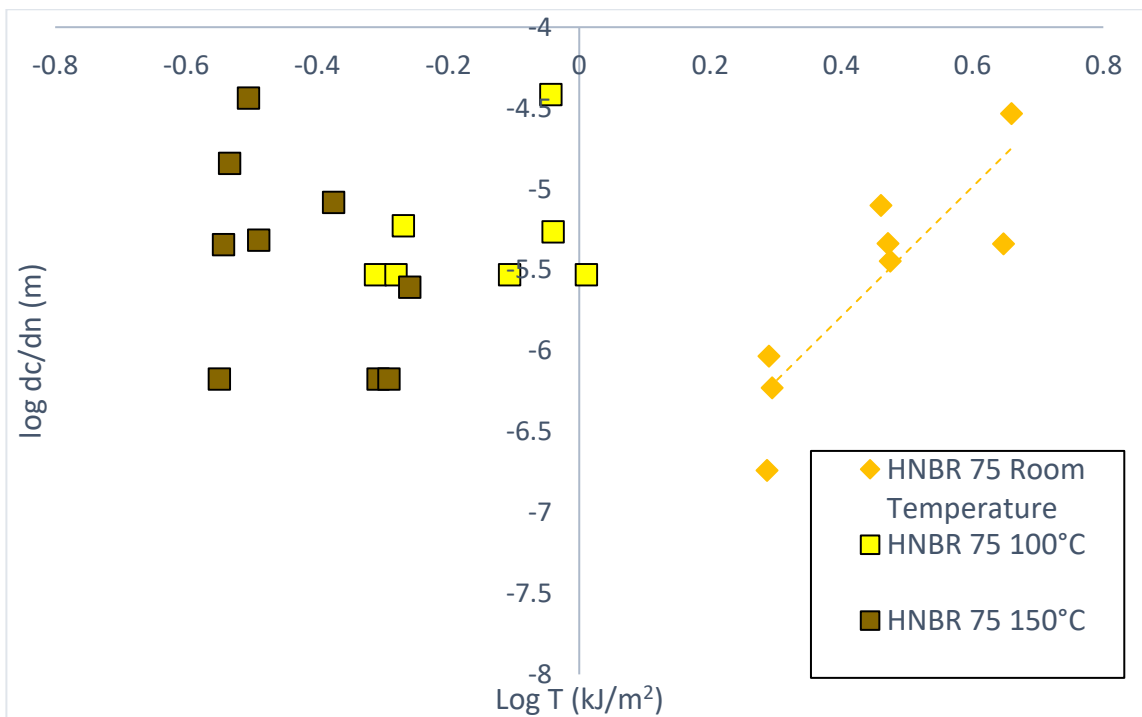
Figure 97: Cyclic pure shear fatigue for unaged HNBR 75 tested at different temperatures

For both compounds, the results show that as the testing temperature was increased, the fatigue resistance of each material was significantly reduced. This is supported by Gent et al., who found that testing at elevated temperatures can reduce fatigue properties of an elastomer by as much as a factor of 10^4 [Gent. A. N, 2001]. The results measured at 150°C show a weaker fatigue resistance, as expected.

Additionally, the scatter for these tests was much greater, to the point where it was difficult to see any particular trend between the tearing energy and the crack propagation rate. These graphs are a representation of what cyclic pure shear fatigue results can look like when severely knotty behaviour is observed and the data is filtered to remove the knotty behaviour from the measured data. In order to process this data more easily, it was decided to try to isolate the tests that feature significant knotty tearing by combining both an observation of test the specimens after fatigue fracture has taken place, and then examining the crack length vs. cycle number graph for each value of tearing energy. An example of this approach is shown in figure 98.
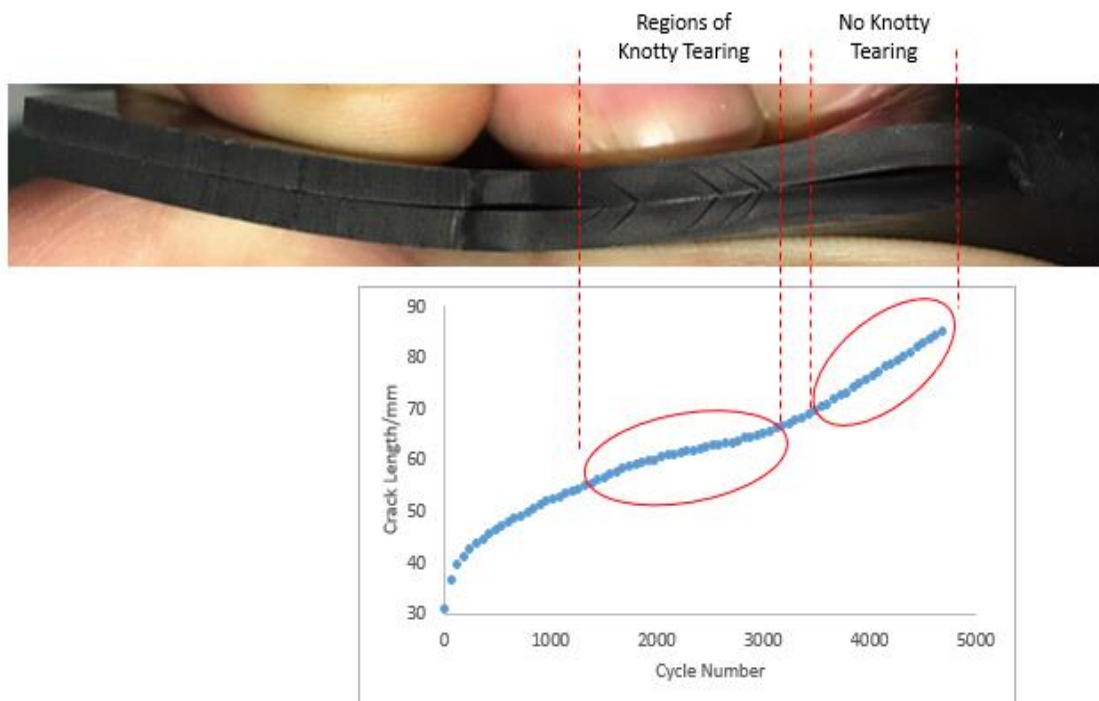
Figure 98: HNBR 60 sample crack surface with corresponding crack length versus cycle number graph to identify regions of knotty tearing

143

Figure 99 shows that regions of knotty tearing are easily observable as raised sharp surface lines along the cracked surface profile, reflecting where the crack had deviated from the original path. These regions also feature an obvious and significant reduction in gradient on the corresponding crack length vs. cycle number graph.

In all of the previous tests, crack propagation rates were measured by avoiding any areas of severe knotty tearing. In this section, the significant knotty tearing observed at elevated temperature is not avoided but it is identified and highlighted. This allows the cyclic pure shear fatigue crack growth results to be identified by two separate categories, namely: smooth tearing and knotty tearing.

This isolation of results can be seen in figures 99 and 100.
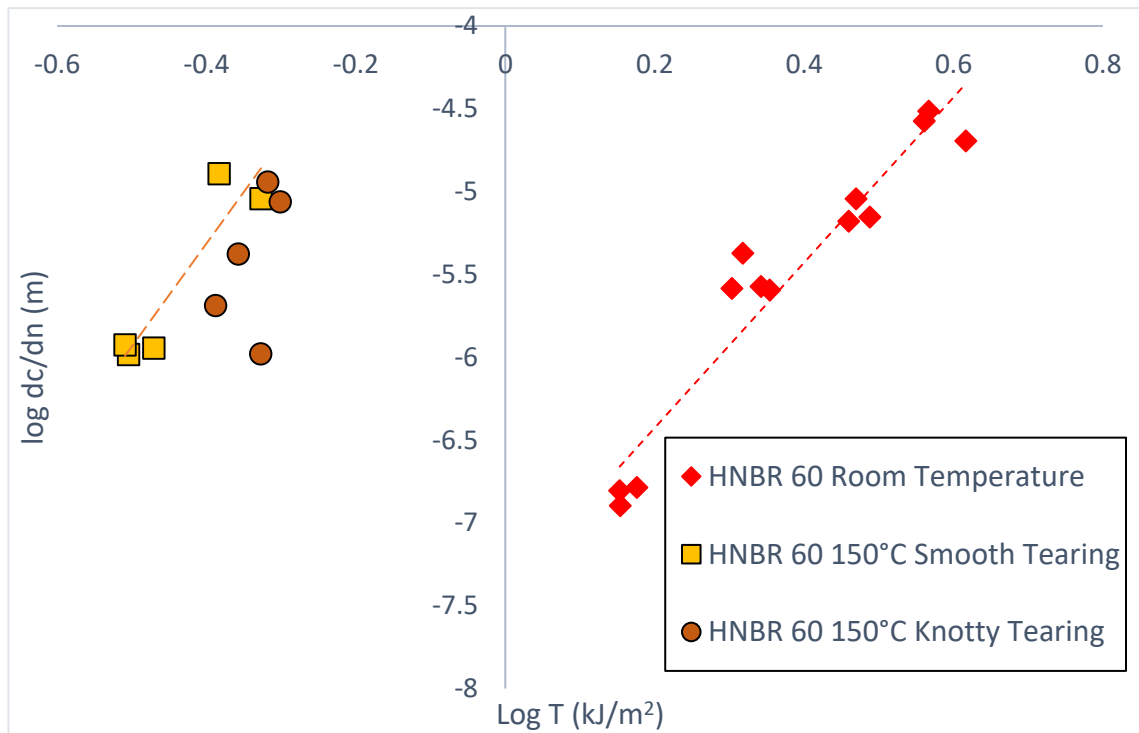
Figure 99: Cyclic pure shear fatigue tests for unaged HNBR 60 measured at room temperature and 150°C where data showing knotty and smooth tearing have been isolated from each other
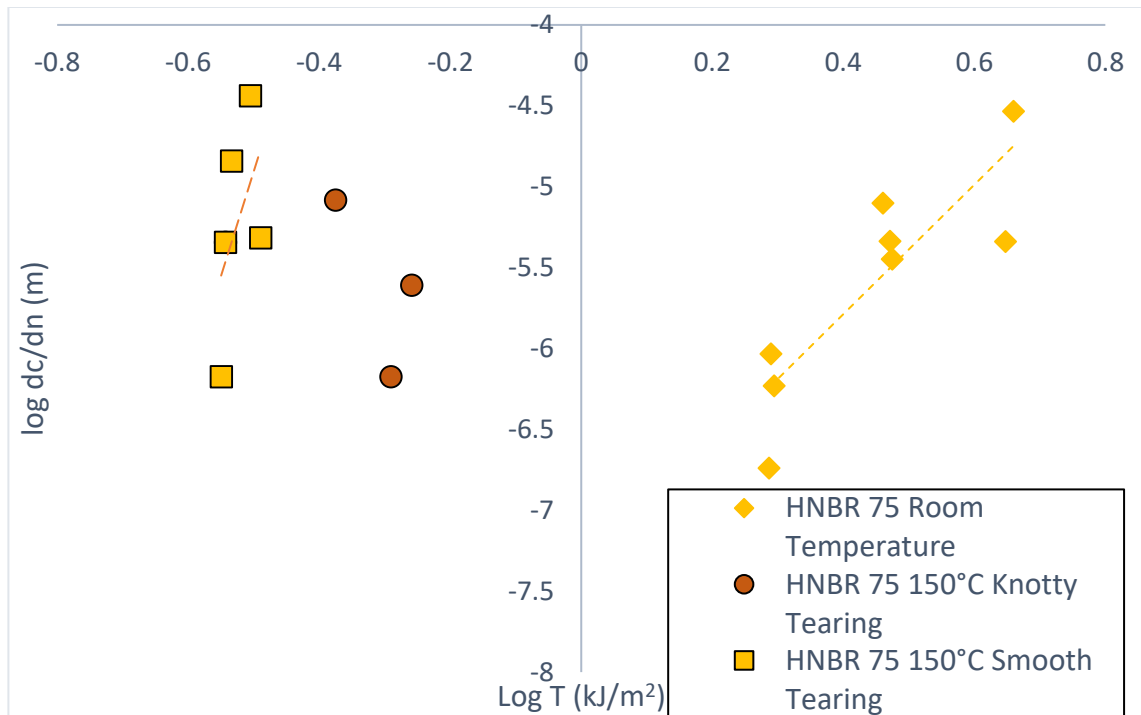
Figure 100: Cyclic pure shear fatigue tests for unaged HNBR 75 measured at room temperature and 150°C where data showing knotty and smooth tearing have been isolated from each other

This method enables scattered results with no obvious trend between tearing energy and crack propagation rate as a result of knotty tearing to be split into these two categories. One category featuring knotty tearing, which is the cause of scatter in these results, and another category featuring smooth tearing behaviour which identifies the relationship during smooth tearing between the tearing energy and the crack propagation rate as defined by [Lake, G. J, 1983]

This method also clearly shows that the knotty tearing behaviour improves the tear resistance of the material, however at this stage, not in a predictable way.

5.2.6 CYCLIC PURE SHEAR FATIGUE TESTING OF POST CURED SAMPLES

Following discussion with Schlumberger Cambridge Research Centre and also in response to comments from other researchers who saw this work presented at international conferences, it was decided to check that the compounds had been fully cured prior to fatigue crack growth testing. To do this some fully cured test pieces of HNBR60 were post-cured to make sure that the test samples were not being further cured during the ageing processes.

Therefore, the following post-curing process was used. First, the sample was cured for the same time and temperature as all of the previous samples. It was then cooled down to room temperature after which it was placed back in the hot press mould at a curing temperature 170°C for an extended cure time of four hours. No pressure was applied during this post-curing heat cycle. The hot press was only used so that the two metal plates of 170°C were applied to the top and bottom surfaces of the sample sheet. The sample was then removed and cooled to room temperature before the pure shear test specimens were cut out.

Tensile tests were also performed on this post-cured sample which were compared to the single cured measured behaviour. In addition to this, samples were tested: one that had the initial cure time doubled from 30mins to 60mins and another with a 60mins initial cure but also with a post-cure. This meant in total that four different samples of HNBR 60 were characterised in tension:

- HNBR 60: Normal cure time (30mins) with no post-cure
- HNBR 60: Normal cure time with a 4hr post-cure
- HNBR 60: Double cure time (60mins) with no post-cure
- HNBR 60: Double cure time with a 4hr post-cure

The testing parameters were the same as those used for the unaged specimen. The results are shown in figures 101 and 102.
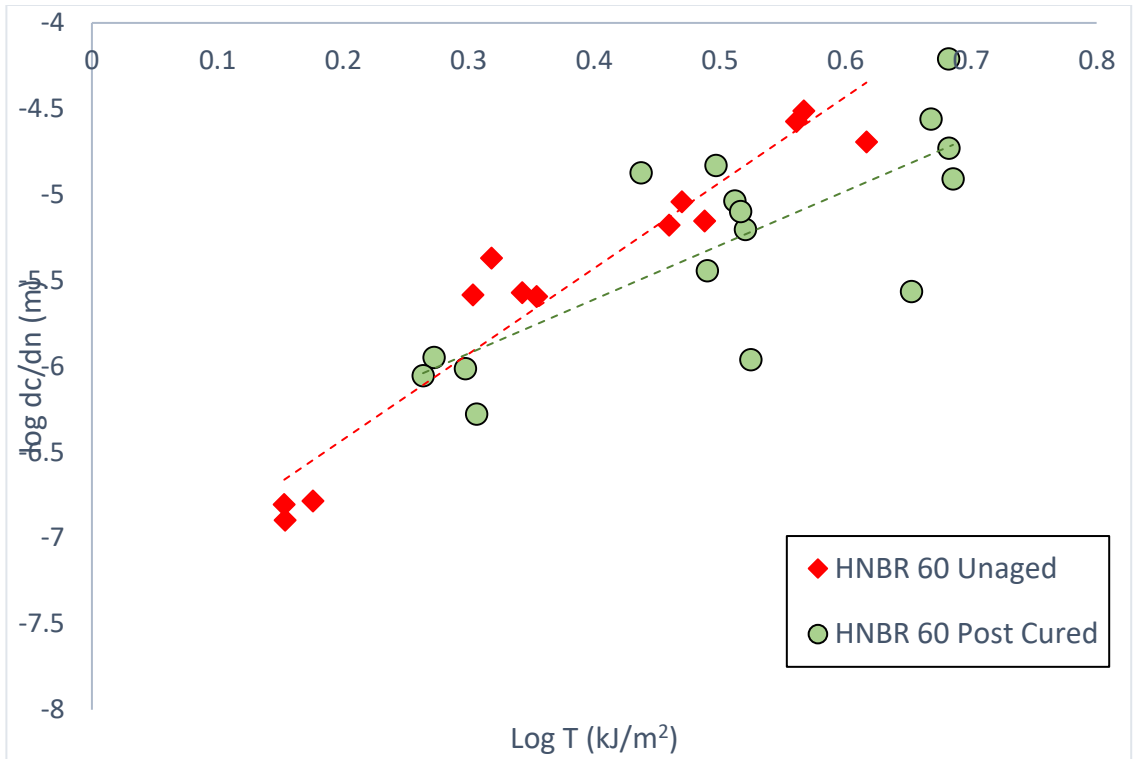
Figure 101: Cyclic pure shear fatigue tests performed on unaged HNBR 60 samples, one with a standard cure, one with an additional post-cure
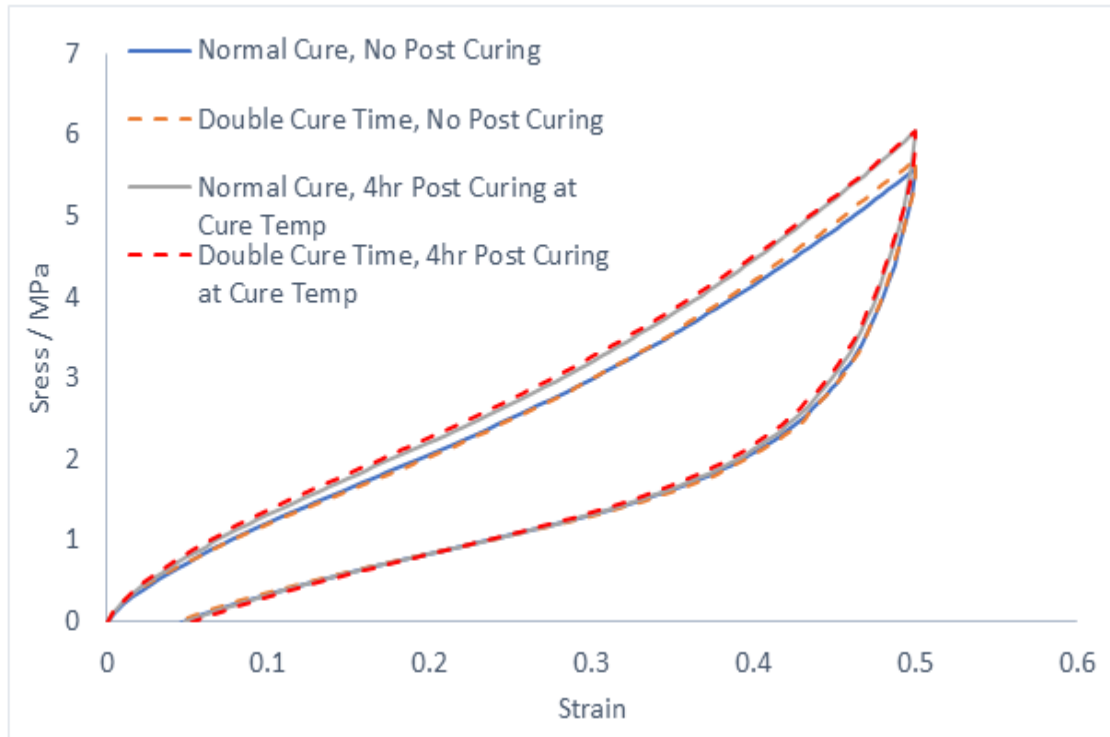
Figure 102: Tensile tests performed on unaged HNBR 60 samples with different curing characteristics

The results show that the post-curing process causes an increase in the experimental scatter during the fatigue crack growth testing due to a significant increase in the knotty tearing behaviour. This process caused no noticeable decrease in fatigue properties, however the increase in scatter due to knotty tearing produced slower crack growth rates depending on the level of knottiness. Any decrease in β value results from knotty tearing which increased as tearing energy increased.

Tensile tests show that doubling the initial cure time from 30mins to 60mins in both samples with and without post-curing had negligible difference in the stress versus strain behaviour. A small increase in the modulus was seen when a post-cure was used. If the samples were not fully cured, it be predicted that a double cure or a post-cure should have a significant effect on the stiffness of the compound. As the changes are very modest it can be deduced that the reason for the improvement in fatigue properties after certain types of ageing was not as a consequence of the test samples being under-cured prior to ageing. It is also clear that the changes in the fatigue properties during ageing that introduce more knotty tearing must be more complex than a simple change in the crosslinking network.

148

As a result of these tests it was decided that post-curing process was unnecessary and would not be used in any subsequent testing.

5.3 MATERIAL CHARACTERISATION TESTS

5.3.1 INTRODUCTION

In order to understand the effect of ageing on the fatigue resistance of these elastomers clearer, different material characterisation techniques were used. These included:

- Thermogravimetric Analysis (TGA)
- Fourier-Transform Infrared Spectroscopy (FTIR)

These tests were done on virgin samples that had not been through any previous mechanical testing. Samples were cured and then either aged in the same way as has already been described or left unaged.

Samples were cured at Queen Mary University of London for this work (as previously). However, all the characterisation tests and ageing procedures done in this section were carried out by the author at Schlumberger Cambridge Research Centre. All ageing procedures remained the same, though the air aged samples for this test were aged in a different oven.

Specimens were made from the same elastomeric sheet mould used for all previous tests and then cut into rectangular shapes. Each sample had five specimens cut for each ageing condition.

5.3.2 PERCENTAGE MASS CHANGES AFTER AGEING

All specimens were weighed before and after ageing shown in table 10. All mass measurements were average measurements of five samples. Results are presented as percentage differences between pre-aged and post-aged conditions. Negative percentages indicate a loss of mass, positive indicate a gain in mass.

	Percentage Difference			
Sample	**Aged at 100°C in Air**	**Aged at 150°C in Air**	**Aged at Room Temp in Oil**	**Aged at 150°C in Oil**
HNBR 0	-2.64%	-10.08%	0.22%	0.27%
HNBR 60	-1.85%	-6.88%	0.38%	-1.14%
HNBR 75	-1.72%	-5.53%	0.06%	-0.93%
HNBR 75 NP	-1.76%	-2.39%	0.25%	3.63%

Table 10: Percentage mass differences between aged and unaged samples.

As expected, all of the test samples aged in air showed a loss of mass. A more dramatic material loss was observed in the samples aged at 150°C compared to those aged at 100°C. The unfilled HNBR 0 had the greatest proportional amount of mass loss under both air ageing conditions. As carbon black filler content is increased, the percentage loss after ageing was reduced. Finally, samples without plasticiser showed the lowest amount of mass loss.

All of the samples aged in IRM903 oil at room temperature showed a small increase in mass. Interestingly HNBR 60 featured the greatest mass gain and HNBR 75 featured the smallest. It is clear though that the percentage changes were all much smaller than the values measured for ageing in air. It is worth noting, that all four samples gained mass which indicates a certain level of swelling for all the materials. It cannot be determined from this test if this is solely due to absorption of oil by the rubber, or if other components of the compound have also been leached out. FTIR was used to characterise the IRM903 used to age the samples, but possible changes due to the extraction of ingredients of the elastomer were not detectable due to the strong IR spectrum of the oil, and the low concentration of any leached substances.

HNBR 0 and HNBR 75 NP gained mass after ageing in IRM903 oil at 150°C and HNBR 60 and HNBR 75 lost mass. HNBR 0 featured an almost identical increase in mass as was experienced at room temperature and HNBR 75 NP featured a higher mass increase at this elevated ageing temperature. Whereas the influence of temperature caused a greater loss of mass in HNBR 60 compared to HNBR 75.

This experiment suggests that the rate of swelling and leaching have different thermal dependencies and the detailed response is dependent not only on the initial compound composition but also on the temperature of the ageing test.

5.3.4 TGA

TGA tests were undertaken to attempt to understand more about the composition of each sample before and after ageing. This involves measuring the mass loss as a sample is heated up to a high temperature in an inert atmosphere. The thermal decomposition of the material is measured as the percentage mass loss. Samples were cut with a sharp blade into pieces that were approximately 10 mg, which were placed in a crucible and tested in an inert N_2 atmosphere. Tests began at room temperature and the temperature was raised by 10°C/min up to 800°C. Results were plotted as the percentage mass loss with temperature. Changes in mass could be highlighted by plotting the differential of the mass loss. This highlighted the gradient changes observed in the results so that specific regions where the mass loss rate was greatest could be identified and analysed individually.

The results are shown in the following figures 103 - 105
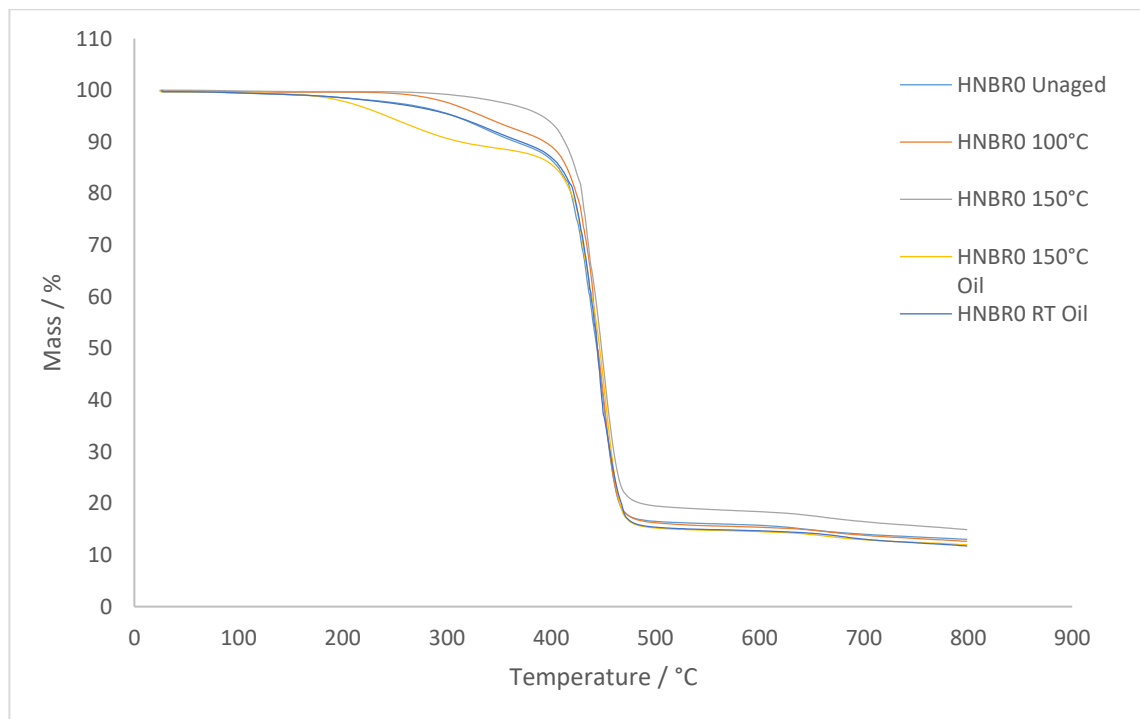
Figure 103: TGA results for HNBR 0 after different ageing conditions
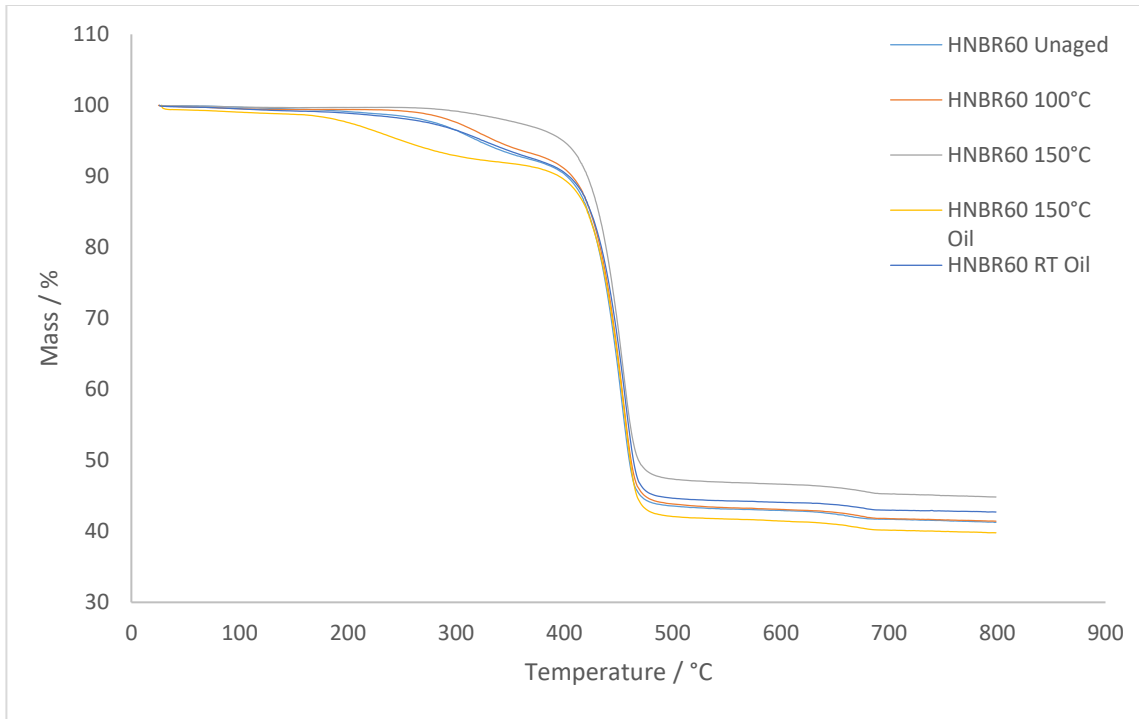
Figure 104: TGA results for HNBR 60 after different ageing conditions
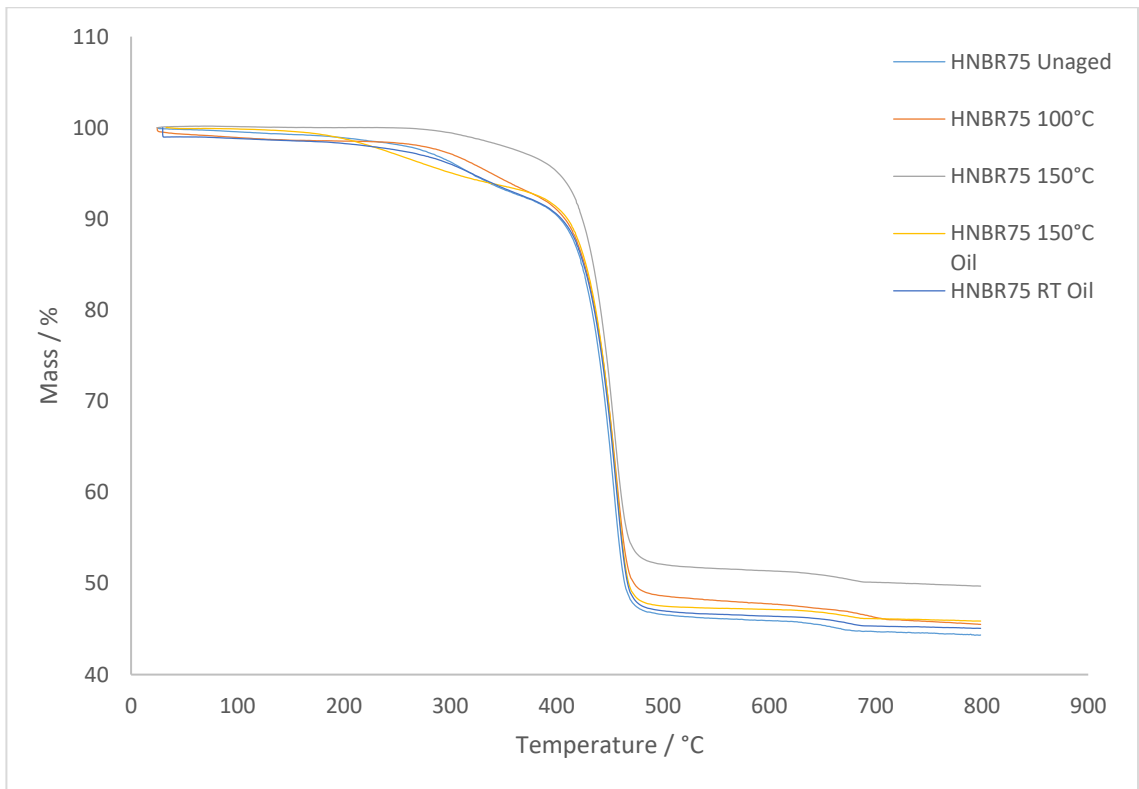
Figure 105: TGA results for HNBR 75 after different ageing conditions
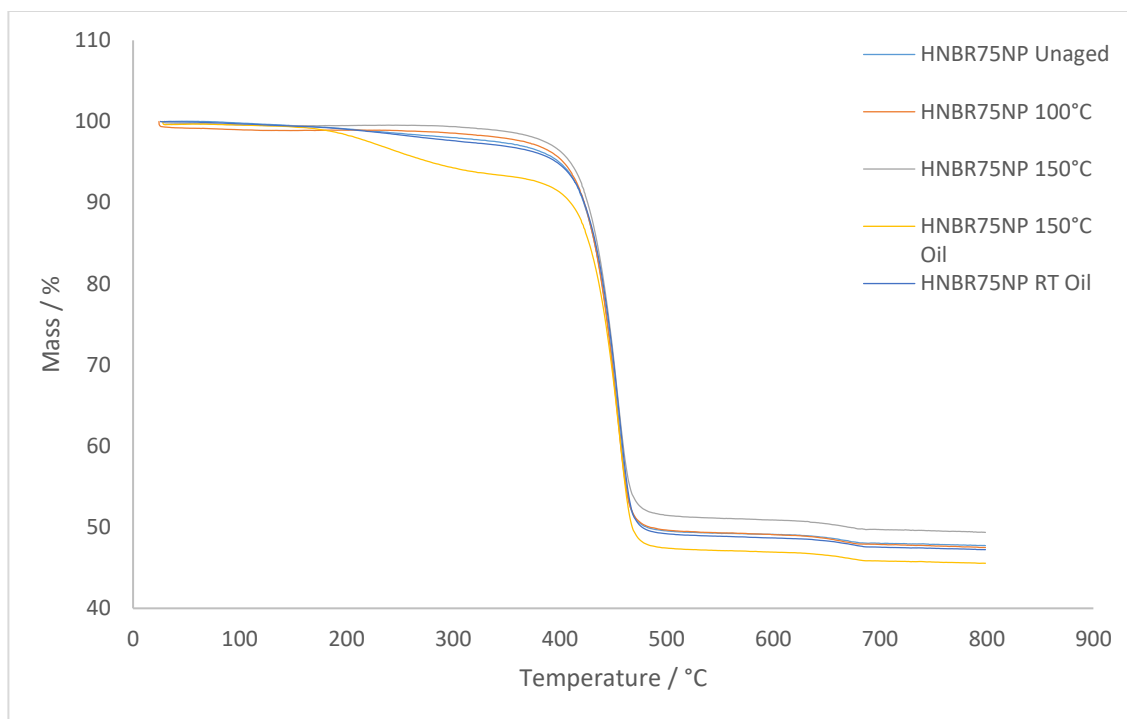
Figure 106: TGA results for HNBR 75 NP after different ageing conditions

It is important to note that the TGA results are normalised so that the initial test mass is 100%. It is clear from the previous experiment that the masses of the samples have already been altered by the ageing process. So after ageing, different samples even from the same initial compound, can finish at different percentage masses depending on the ageing process as can be seen particularly clearly in figures 103 - 106. There were larger differences in behaviour between the elastomer materials. For example, the unaged sample of HNBR 0 finishes at an approximate percentage mass of 13% and the unaged sample of HNBR 60 has a residual mass of 41% at 800°C. This is mainly explained by the difference in filler content between each compound. In this example, the residue of the unaged HNBR 0 sample is in part due to the inorganic compounds that were incorporated into the compound, and carbon-based degradation products of the base polymer, with most of the oil and the polymer having completely broken down. In contrast, the unaged sample of HNBR 60 has a large mass fraction of carbon black in the sample as a reinforcement filler, the residual mass is therefore mainly thermally resistant carbon black filler remaining after the test. Therefore, samples with different initial carbon black content, samples with or without plasticiser incorporated or samples containing swollen in oil, will each have a variation of final percentage mass.

The general behaviour is similar for all the samples: there is a small mass loss of up to ~ 10% below approximately 360°C, followed by the main mass loss from 360 – 480°C due to the backbone polymer breakdown. In the unfilled sample, this is 70 – 78% of the initial mass. There is then a very small additional mass loss up to 800°C.

The largest variation in the TGA results for different samples occurred between 25°C and 360°C. In this temperature range the losses are likely a result of losing low molecular weight materials, such as plasticisers and substances that have been absorbed into the material during ageing.

Focussing on the temperature range 25°C - 360°C, all samples see a steady mass loss between 25°C and approximately 180°C. This loss is very small, ranging from values of 0.30% - 1.50%. Different low molecular weight molecules will be lost in this range and it would be difficult to isolate ingredients purely on these results alone. However, it is common in this range to lose water due to evaporation. It is also likely that there is a small loss of any extra crosslinking agents and co-agents not yet vulcanised as well as small amounts of antidegradants and plasticiser. As the percentage mass loss in this region is very low, it is quite hard to analyse.

The results show a variety of responses between 180°C and 360°C. By using the unaged tests in each graph as a base, for HNBR 0, HNBR 60 and HNBR 75 it can be seen that samples aged in air at 100°C feature a slightly smaller mass loss in this region, samples aged in air at 150°C feature a significantly smaller mass loss in this region, samples aged in oil at room temperature feature a slight increase in mass loss and samples aged in oil at 150°C feature a significant increase in mass loss. It is therefore possible to conclude that after ageing in air, some of the elastomer compound is lost during the ageing process, much more so when aged at 150°C. As well as this, it is very likely that the increased mass loss in the oil-aged samples is a result of oil absorbed into the sample during ageing. This supports the mass changes after ageing seen above in table 10.

TGA results for samples HNBR 75 NP that had not been aged in oil, appeared to not feature any significant mass loss between 25°C and 360°C. This suggests that the material ingredients lost in this temperature range were not significant in the initial formulation. So in this case it would suggest that in the other compounds it is the lower molecular weight and more volatile plasticiser that is lost over this temperature range. It is however, hard to conclude anything

about the antidegradants which only take up 1.5 phr of the initial formulation, indicating that the loss of this material would be very hard to isolate in this particular test. Therefore, the main conclusion for these tests is that only water and potentially small amounts of other low molecular weight ingredients were lost in HNBR 75 NP tests in this region. The samples aged in oil did feature an extra mass loss stage in this region which is likely to be attributed to oil having diffused into the elastomer.

Using the unfilled elastomer as an example, the percentage mass loss within the approximate region of 180°C and 360°C for the samples aged in air is approximately:

- HNBR 0 Unaged: 8.7%
- HNBR 0 Aged at 100°C in air: 7.8%
- HNBR 0 Aged at 150°C in air: 2.4%

This suggests that some of the lower molecular weight elastomer ingredients have already been lost during the ageing in air. In this test alone it is difficult to isolate any specific mechanisms, however in this situation, the two most useful tests to compare are HNBR 75 and HNBR 75 NP. These two samples differ only by plasticiser content and so any differences seen between these two samples can mostly be attributed to this difference. A figure comparing the TGA results of the unaged samples of HNBR 75 and HNBR 75 NP is shown here in figure 107:
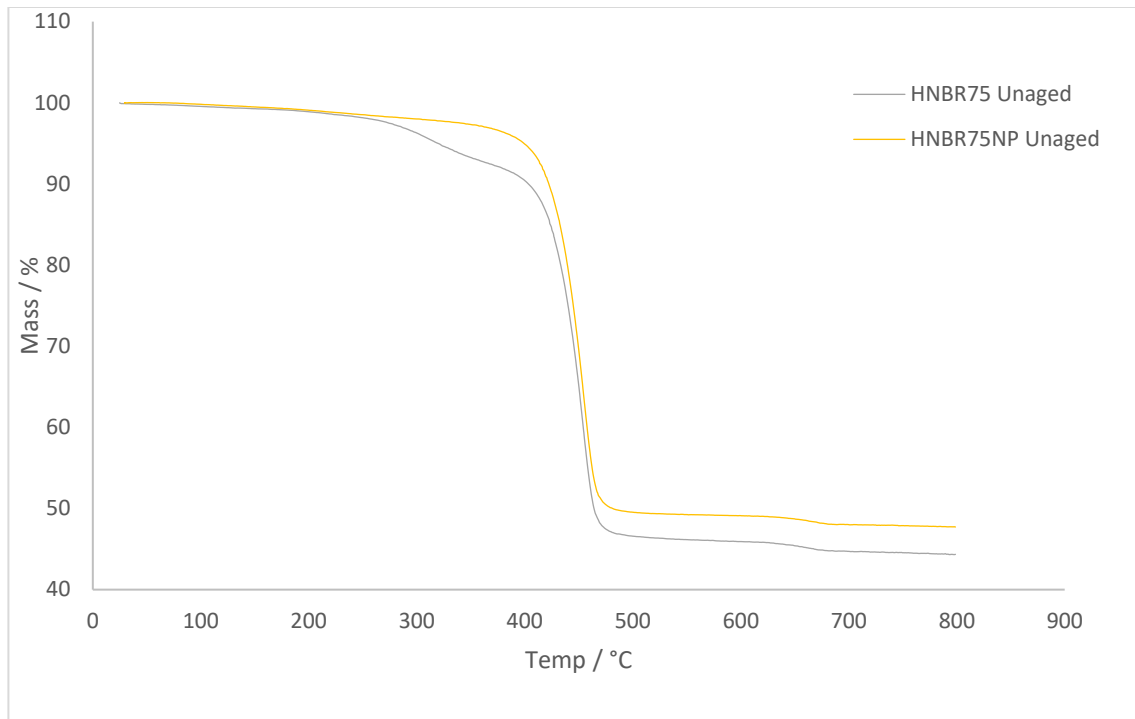
Figure 107: TGA results for unaged HNBR 75 compared to unaged HNBR 75 NP

The percentage mass loss within the approximate region of 25°C and 360°C for these two samples is approximately:

- HNBR 75 Unaged: 7.7%
- HNBR 75 NP Unaged: 2.9%

This percentage mass loss difference can be almost entirely be attributed to plasticiser content, this extra mass loss stage beginning at approximately 225°C.

The HNBR 75 NP TGA tests can also help identify any differences in plasticiser content before and after ageing for other samples. Firstly, for HNBR 75 NP samples aged in air, very small differences were seen in the region of 25°C and 360°C. These were approximately:

- HNBR 75 NP Unaged: 2.9%
- HNBR 75 NP Aged at 100°C in air: 1.4%
- HNBR 75 NP Aged at 150°C in air: 0.8%

Assuming the approximate water content is the same, these differences must come from very small losses of extra crosslinking ingredients not used during vulcanisation and ingredients with a low initial mass fraction such as the antidegradants.

Visually, HNBR 0, HNBR 60 and HNBR 75 samples aged in air at 150°C show a very similar TGA curve to HNBR 75 NP unaged or aged in air. By comparing the unaged sample test of HNBR 75 NP with the sample test of HNBR 75 aged at 150°C in air, we can identify the degree to which plasticiser was lost in the ageing process (see figure 108).
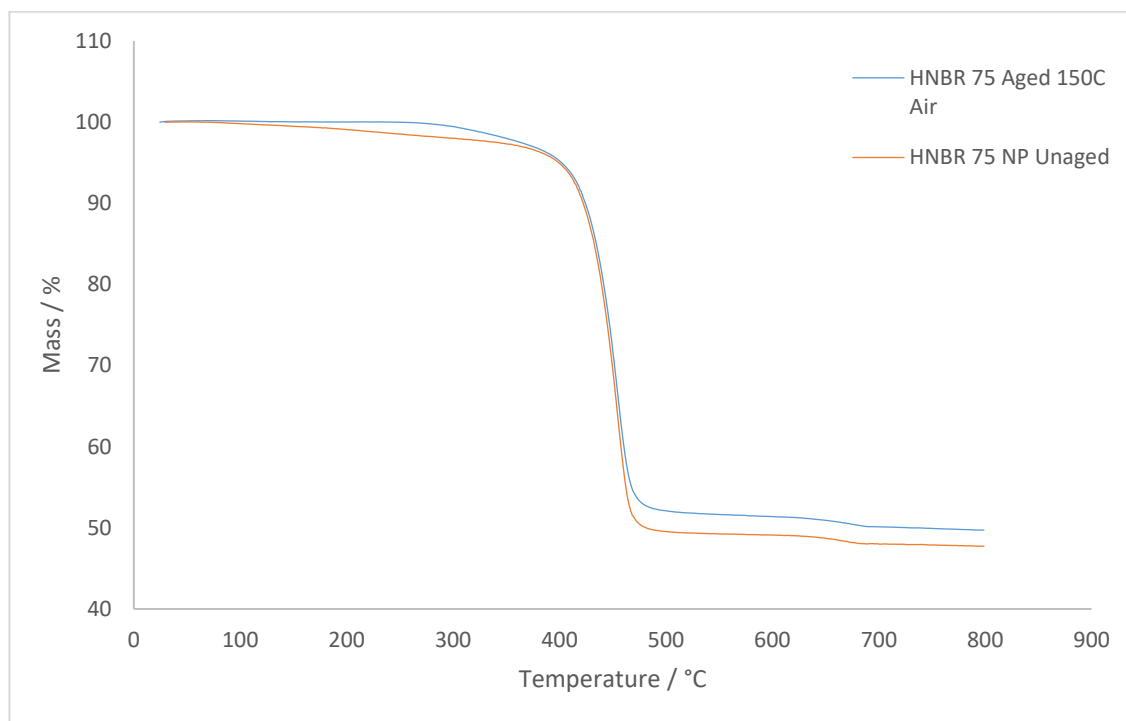
Figure 108: TGA results for aged HNBR 75 compared to unaged HNBR 75 NP

The similarity between these two tests is striking. Small differences can be seen between 25°C and 360°C with an increased mass loss for the unaged HNBR 75 NP sample. As previously discussed, this can be explained by the additional loss of low molecular weight components such as residues of crosslinkers and anti-degradants from HNBR 75 during hot air ageing.

By comparing HNBR 75 aged at 150°C in air with HNBR 75 NP aged at 150°C in air, these differences should be minimised further, as can be seen in figure 109.
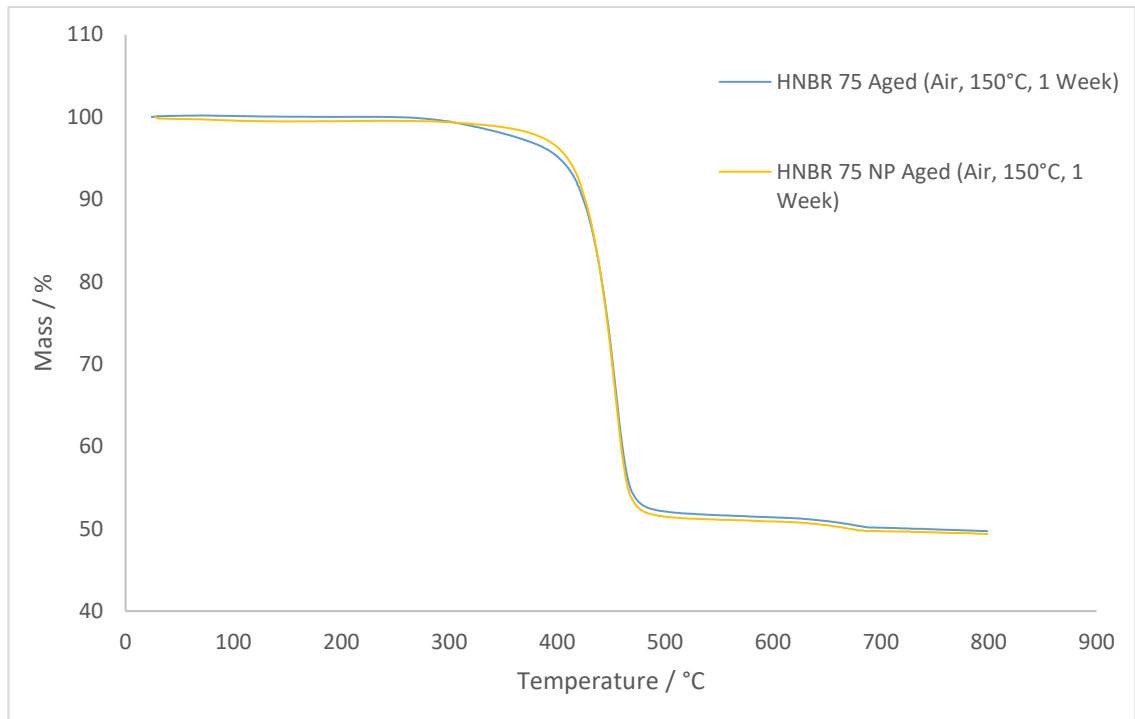
Figure 109: TGA results for aged HNBR 75 compared to aged HNBR 75 NP

The graph that compares how the HNBR 75 aged at 150°C in air compares with the HNBR 75 NP aged at 150°C in air shows negligible differences.

Considering all these analysis points, it is therefore highly likely that after ageing all samples in air at 150°C, the plasticiser content is mostly removed together with the other low molecular weight materials. Ageing in air at 100°C contributes to a proportional loss of this material, perhaps the substances with the highest volatility, which must also be taken into account. This conclusion offers much more understanding as to why ageing increased the modulus and hysteresis of these samples in the tensile tests as has been shown previously in figures 94 and 95. As these samples were peroxide-cured, oxidation and temperature effects are not enough to explain this behaviour on their own. It also helps to identify why ageing in air at 150°C resulted in the largest changes in cyclic pure shear fatigue. HNBR 75 aged in air at 150°C becomes a very similar material to HNBR 75 NP which had a low cyclic pure shear fatigue resistance. Therefore, it is understandable why this HNBR 75 aged in air at 150°C had a worse fatigue resistance. As samples aged in air at 100°C lost a proportion of the plasticiser, it is likely that the small increase in modulus and hysteresis seen on the tensile tests was partly a result of this, and the increase in hysteresis caused a minor increase in fatigue response. The HNBR

158

60 material that was aged in air at 150°C must feature a combination of these two mechanisms. The loss of plasticiser caused an increase in modulus and hysteresis, potentially improving the fatigue resistance, while also featuring less carbon black content, causing a smaller strain amplification at the crack tip compared to HNBR75.

Using the unfilled elastomer as an example, the percentage mass loss within the approximate region of 180°C and 360°C for the samples aged in oil is approximately:

- HNBR 0 Unaged: 8.7%

- HNBR 0 Aged at room temperate in oil: 9.0%

- HNBR 0 Aged at 150°C in oil: 10.7%

For all samples, including HNBR 75 NP, there was an extra loss of mass for samples that have been aged in oil. This must be attributed to the absorption of oil by the sample. The additional loss of mass that can be seen in the samples aged in oil at 150°C, in combination with the percentage mass difference before and after ageing shown in table 10, potentially shows that more oil is swollen into the sample at 150°C. The higher temperature increases the rate of diffusion and the free volume in the polymer both of which will encourage the swelling of the polymer by the oil. It is also possible that leaching could be occurring where material is lost which is then replaced by the oil.

To investigate this further, FTIR was used to characterise all the samples.

5.3.5 FTIR

FTIR tests were done on all samples, unaged and aged. This was done to attempt to identify significant changes in composition before and after ageing to answer and confirm the results from the fatigue experiments and the TGA.

Each sample, that were either unaged or aged, was tested at least three times so as to look for any potential changes within the samples and to use the results with the strongest signal. All samples were both tested on the exterior surface and in the cross-section of the specimen that had been cut using sharp scissors. This enabled a comparison of chemistry at both the sample surface and within the cross-section where external materials, such as dirt on surface can be eliminated. The results shown here are all from the freshly cut cross-sections of the samples.

All the materials were characterised, however results from filled materials HNBR 60, HNBR 75 and HNBR 75 NP, showed a rising base line with derivative-like peaks, which are more difficult to analyse. A comparison of typical signals from the FTIR for HNBR 0 and HNBR 60 are shown below in figure 110.
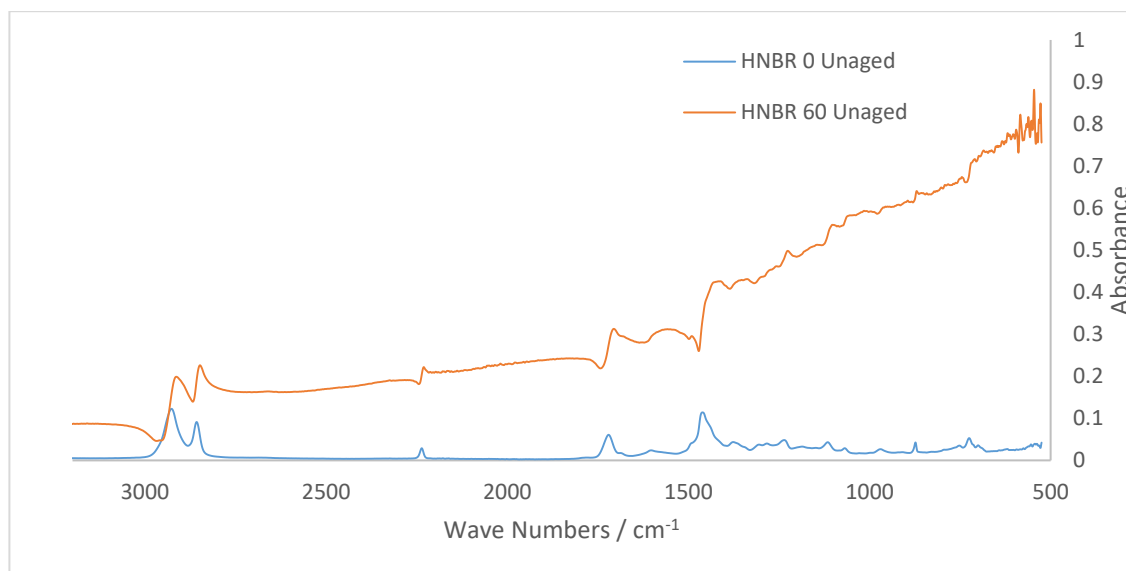
Figure 110: FTIR comparison of HNBR 0 and HNBR 60

These spectra are for HNBR 0 and HNBR 60, where the only difference between their compositions is in their carbon black filler content. The filler causes an effect where the base line rises and the peaks show a derivative-like nature. This is thought to be as a result of internal reflection from the carbon black particles, it causes peaks to become lost and harder to identify, especially at lower wave numbers. As the chemical composition of all the compounds is similar apart from the filler content, the changes due to ageing that can be detected by FTIR are likely to be similar, so the analysis in this section will focus on HNBR 0 as this materials can more readily be used to identify chemical differences before and after ageing.

A quantitative measurement between compounds can be made by comparing the area under certain peaks with respect each other and then between different spectra. This allows the amount of certain types of chemical group to be quantified and this is explained in more details in the discussion of the results.

Identifying peaks was done by using a combination of literature sources to identify bond types and using previously collected FTIR spectra for individual elastomer ingredients. Unfortunately, the exact elastomer formulation is confidential, so the FTIR spectra of the individual ingredients cannot be used in this document. However, the peaks in the FTIR spectra of the elastomers can be assigned to different compound components. The spectra for all HNBR 0 aged and unaged samples can be seen below in figure 111.
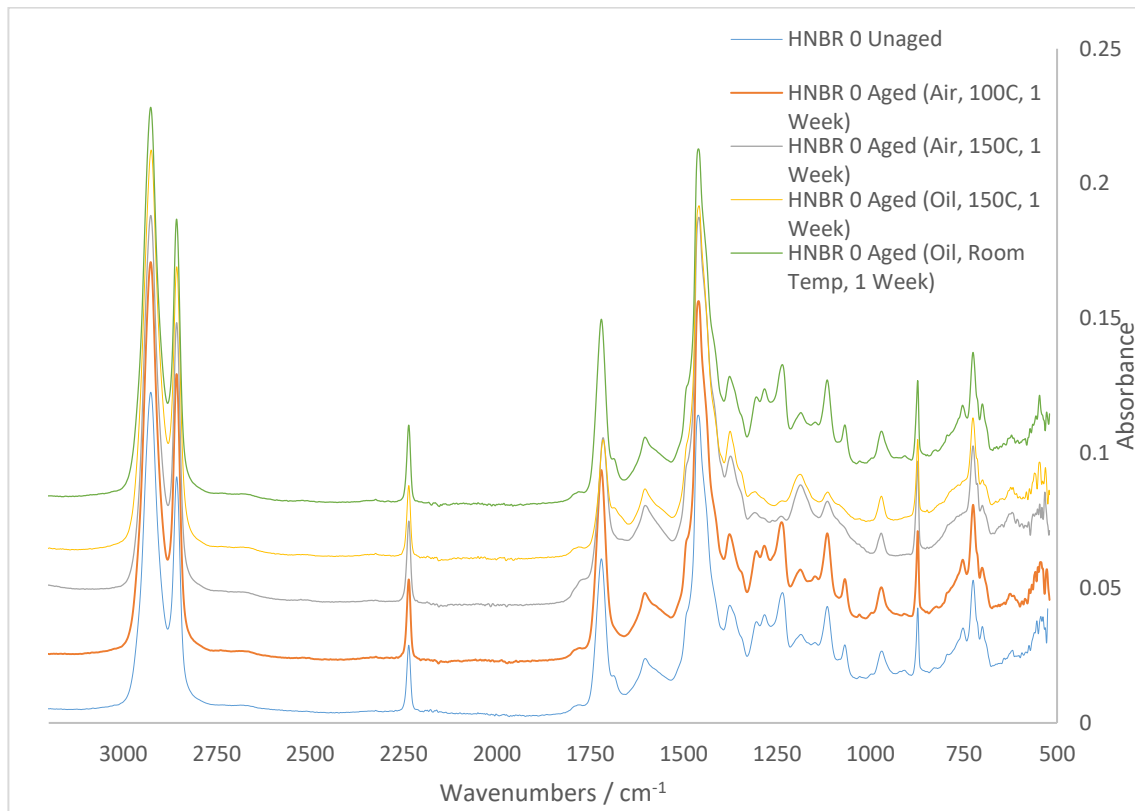
Figure 111: FTIR comparison of HNBR 0 after different ageing conditions, spectra offset for clarity

As the individual component FTIR spectra cannot be presented here, a list of all the peaks and their associated compound components has been given below. Peaks above 1500 cm^{-1} are easier to identify with respect to their bond types, therefore these will be described as clearly as possible. Below ~ 1500 cm^{-1}, some peaks will be as a result of a combination of bond types and elastomer ingredients. Therefore, this list should firstly be used only as a guideline for these components. Secondly, ingredients such as antidegradants are in such small mass fractions that they cannot be detected in an elastomer compound by FTIR. For wavenumbers

above 1500 cm^{-1}, a bond type and primary elastomer ingredient contributor will be described. For wavenumbers below 1500 cm^{-1}, only a primary elastomer ingredient contributor with be given:

- Wavenumbers: 3030 – 2775 cm^{-1}: C – H Stretch: mainly from HNBR base polymer
- Wavenumbers: 2260 – 2215 cm^{-1}: C ≡ N bond: HNBR base polymer
- Wavenumbers: 1765 – 1660 cm^{-1}: C=O bond: plasticiser
- Wavenumbers: 1660 – 1530 cm^{-1}: Co-Agent
- Wavenumbers: 1530 – 1400 cm^{-1}: C – H bend (CH$_2$): mainly from HNBR base polymer
- Wavenumbers: 1400 – 1330 cm^{-1}: C-H bend (CH$_3$): mainly from HNBR base polymer
- Wavenumbers: 1330 – 1220 cm^{-1}: Plasticiser
- Wavenumbers: 1150 – 1050 cm^{-1}: Plasticiser
- Wavenumbers: 900 – 840 cm^{-1}: Peroxide crosslink (this peak is present in both the peroxide and the reaction products after the peroxide groups have formed crosslinks, so does not directly indicate changes in crosslink density)
- Wavenumbers: 750 – 680 cm^{-1}: (CH$_2$)$_n$ rock (n > 4): mainly from HNBR base polymer

The focus of this test was to compare samples before and after ageing. Figure 112 below aims to highlight the particular peaks where there are clear differences.
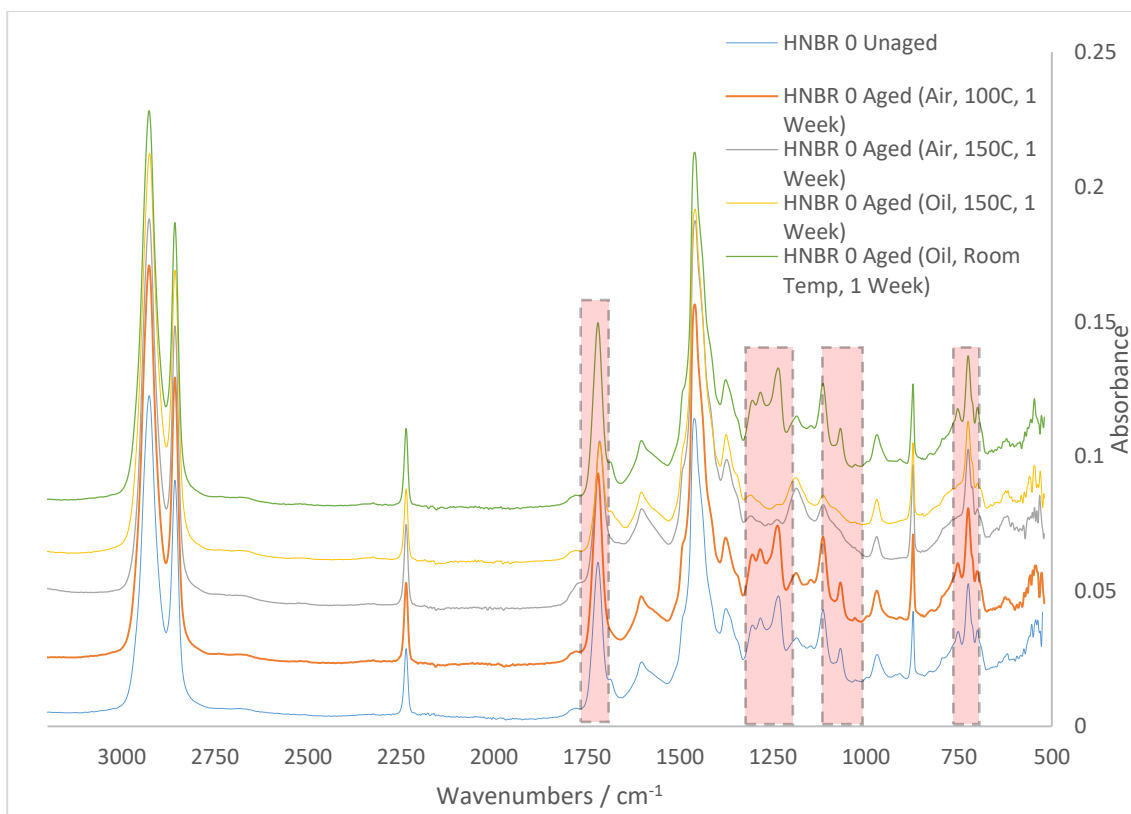
Figure 112: FTIR of different aged HNBR 0 samples (same spectra as in figure 111), highlighting peaks showing significant change after ageing, spectra offset for clarity

The FTIR peaks associated with these significant changes were 1765 – 1660 cm^{-1}, 1330 – 1220 cm^{-1}, 1150 – 1050 cm^{-1} and 820 – 750 cm^{-1}. These are all due to the plasticiser.

The FTIR results primarily show that the peaks most affected by ageing are associated with the plasticiser content. This confirms the results from the TGA tests that ageing in air is removing some of the plasticiser.

Another way of analysing these results is through ratios of areas under peaks. This allows semi-quantitative analysis that can be used to understand the mechanisms that are occurring during ageing. In this analysis, the peak at wavenumbers 2260 – 2215 cm^{-1}, indicating C ≡ N bond from the HNBR base elastomer, is used as a reference, and is assumed not to be affected by ageing under these conditions (this is supported by previous, unpublished work done at Schlumberger Cambridge Research).

Figure 113 shows the ratio of the area under the peak from 1765 – 1660 cm^{-1} indicating the C = O bond for the plasticiser, compared to the area under wavenumbers 2260 – 2215 cm^{-1} indicating the C ≡ N bond for the HNBR base polymer.
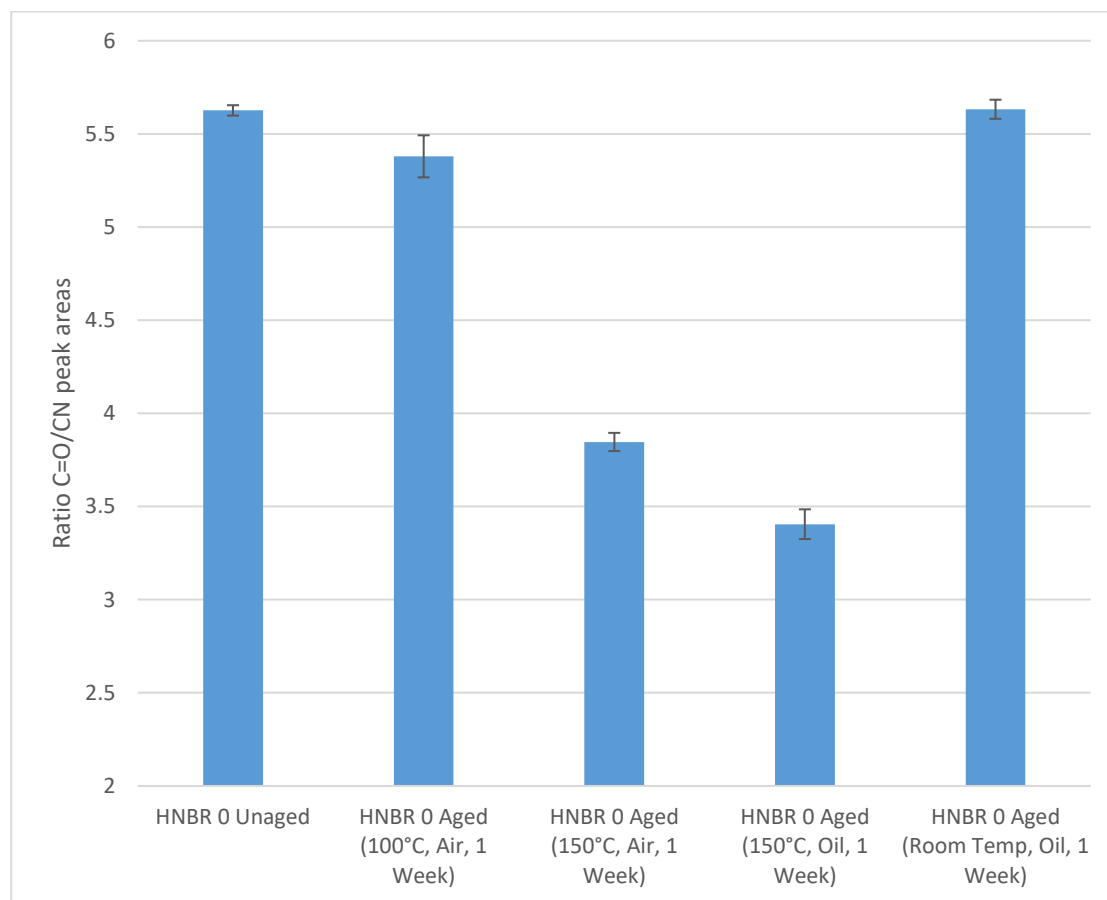
Figure 113: Semi-quantitative comparison of aged HNBR 0 FTIR plots using a ratio of C=O/C≡N peak areas

Using an analysis like this helps to quantify the effect each ageing condition has on the plasticiser content. Here it can be shown that the ageing effects to have the greatest effects on the plasticiser are ageing in oil or air at 150°C, showing that temperature is the most influential factor in removing the plasticiser. Ageing in oil at 150°C shows the largest loss of plasticiser (~ 40% decrease in C=O/C≡N) indicating that in this ageing regime, leaching also adds to the removal of this ingredient.

A small loss of plasticiser is seen in the samples aged in air at 100°C as expected. Interestingly, FTIR results indicate exposure to IRM903 at room temperature seems to have negligible effects

on the removal of plasticiser. This indicated that for samples aged at room temperature in oil, the elastomer matrix now includes a combination of plasticiser and new oil that has been absorbed.

When taking this into account with the other mechanical tests, we can start to understand that, for example, the HNBR 60 aged in oil at room temperature; the slight loss of modulus, hysteresis and the lowering of β material constant in the cyclic pure shear fatigue tests, could be due to the potentially small addition of oil to the samples, that has effectively simply displaced some of the plasticiser with a material that has a similar effect as the plasticiser. When samples were then aged at 150°C in oil, much more plasticiser was lost due to the elevated temperatures. However, this also encouraged absorption of oil, as can be seen in the percentage weight gain after ageing. As the oil provides a similar role to the elastomer as the plasticiser, only small differences were found in the tensile and cyclic pure shear fatigue tests.

5.3.6 CONCLUSIONS

The work in this chapter has examined cyclic pure shear fatigue tests done on a range of both unaged and aged samples of HNBR 0, HNBR 60, HNBR 75 and HNBR 75NP. These tests show that:

- Some of the materials have a fatigue response that varied from a smooth tearing process to a severely knotty tearing behaviour depending upon the detailed testing conditions or ageing conditions.
- Aged samples can become tougher or weaker depending on the ageing conditions. However, generally samples aged at 150°C in air had a reduced fatigue resistance, samples aged at 100°C in air became tougher, samples aged at 150°C in oil had very similar response to unaged material and samples aged at room temperature in oil mainly featured modest changes in the hysteresis.
- Tensile tests showed samples generally featured an increased modulus and hysteresis after ageing in air. Samples generally featured a lower modulus and hysteresis when aged in oil, more so when aged at room temperature.
- Samples aged in air lost mass, samples aged in oil at room temperature gained very small amounts of mass and samples HNBR 0 and HNBR 75 NP aged in oil at 150°C gained mass and the others aged in oil at 150°C lost mass.

- TGA results showed that samples aged in air featured losses that indicated changes in plasticiser content, especially in samples aged at 150°C. This explains further the increase in modulus and hysteresis in the corresponding tensile tests and can answer why some cyclic pure shear fatigue tests showed a toughening behaviour.
- FTIR results confirmed the significant loss of plasticiser after ageing in air and oil at 150°C, and showed that the loss of plasticiser was primarily a temperature driven process with additional leaching in oil. Samples aged at room temperature in oil featured negligible losses in plasticiser explaining why ageing in this regime only modestly affects the hysteresis properties.
- The oil used for the ageing, IRM903, appears to have similar properties to the plasticiser when absorbed into the elastomer. This indicated that samples aged in oil at 150°C, whilst they lost significant amounts of plasticiser, was substituted in with IRM903 oil, which could to some degree compensate for this.

The material characterisation tests helped answer many questions with regards to cyclic pure shear fatigue tests. However, still unanswered is the origin of knotty tearing and the toughening mechanism. The next chapters aim is to answer where this behaviour comes from.

6. STATIC TEAR AND TOUGHENING MECHANISMS IN HNBR COMPOUNDS

6.1 INTRODUCTION

This chapter describes an investigation into how the tear behaviour of four different HNBR elastomers changed with tear rate at both room temperature and at elevated temperatures. This investigation primarily used a test piece geometry where the tearing energy can be readily calculated so that the material characteristic of the tearing energy versus crack propagation rate can be measured over a wide range of tearing rates.

Based on the work by [Rivlin. R. S and Thomas. A. G, 1953], the geometry used in this work was a trouser tear test piece, that was described previously in chapters 3 and 4. The specimen was clamped at the end of both legs and pulled in tension causing the crack to propagate at approximately half the rate of the crosshead speed of the testing machine. A force versus time plot shows the force required to progress the crack which can then be used to calculate the corresponding tearing energy. The power law relationship between the crack propagation rate and the tearing energy can be found by plotting the relationship on logarithmic scales. The general testing parameters are as follows.

- Crosshead Speeds: 25cm/s – 0.001cm/s
- Approximate Crack Growth Rates: 12.5cm/s – 0.0005cm/s
- Temperatures: Room Temperature, 100°C, 150°C

In this chapter the four compounds were only characterised in the unaged state.

This work was then used to further analyse the cyclic pure shear fatigue crack growth work that has been characterised previously in chapter 5. By using both static tear and cyclic fatigue tests, an analysis developed by [Busfield. J. J. C et al, 2002] can be used to separate the cyclic and time dependent components of crack growth rate to further understand the crack growth behaviour measured in chapter 5. The time dependent component is only dependent on the time and tearing energy and the other cyclic component is independent of time but requires the crack tip to be unloaded and then reloaded. the methodology used is explained in more detail in chapter 3. The purpose of this is to further understand the mechanism behind the crack growth so it can be exploited in the material development phase and then engineered

into a product's design. In the previous chapter, it was seen that the crack growth varied from smooth crack propagation to severely knotty crack propagation depending on the tearing energy, compound formulation and ageing history. The mechanism behind this behaviour is potentially a toughening cyclic component dependent one. One example of this type of mechanism being strain induced crystallisation in a rubber such as natural rubber.

Further analysis on potential crystallisation phenomenon was undertaken using X-ray diffraction tests (XRD). Test pieces in an unstretched state were tested in XRD, building upon work done by [Bielinski, D. M, Slusarski, L, Wlochowicz, A and Slusarczyk, C, 1997] and [Severe, G and White, J. L, 2000] who both claimed that crystallisation can be identified in high ACN HNBR products.

6.2 MECHANICAL STATIC TEAR TESTS

6.2.1 STATIC TROUSER TEAR TESTS AT ROOM TEMPERATURE

As demonstrated by [Rivlin. R. S and Thomas. A. G, 1953], static trouser tear tests feature the following tearing energy relationship:

$$T = \frac{2F\lambda}{t} - bW \qquad (6.1)$$

where F is the applied force, λ is the extension ratio in the legs, t is the thickness of the unstrained specimen, b is the total width of the specimen and W is the elastic stored energy density in the legs.

As identified by Windslow [Windslow. R. J, 2018], the second term in this tearing energy relationship reflects the fact that in this test piece as the crack is extended an increased region of strained rubber is being created in the trouser legs. The energy required to stretch the legs of the trouser test requires additional energy which is therefore not available to drive the crack. In special cases where the strain generated in the tensile regions of the legs is relatively small as the cracks propagate, the value of this term is negligible in comparison to the first term. Therefore, equation (6.1) can be simplified to just:

$$T = \frac{2F}{t} \qquad (6.2)$$

As the four compounds used in this body of work all broadly satisfied this special case, equation (6.2) was used in all of the following analyses. The measured results over a wide range of different testing rates are all presented on a log vs log plot of tearing energy vs crack propagation rate for all four materials at three different temperatures.

The results for static trouser tear at room temperature were tested with the following parameters:

- Crosshead Speeds: 25cm/s – 0.001cm/s
- Crack Growth Rates: 12.5cm/s – 0.0005cm/s

Specimen were cut from a sheet and a crack was placed down the centre of the specimen. The crack is then progressed by hand by approximately 1mm to create a more typical representative crack tip profile to allow a more realistic test according to [Tsunoda, K, 2001].

The results are shown below.
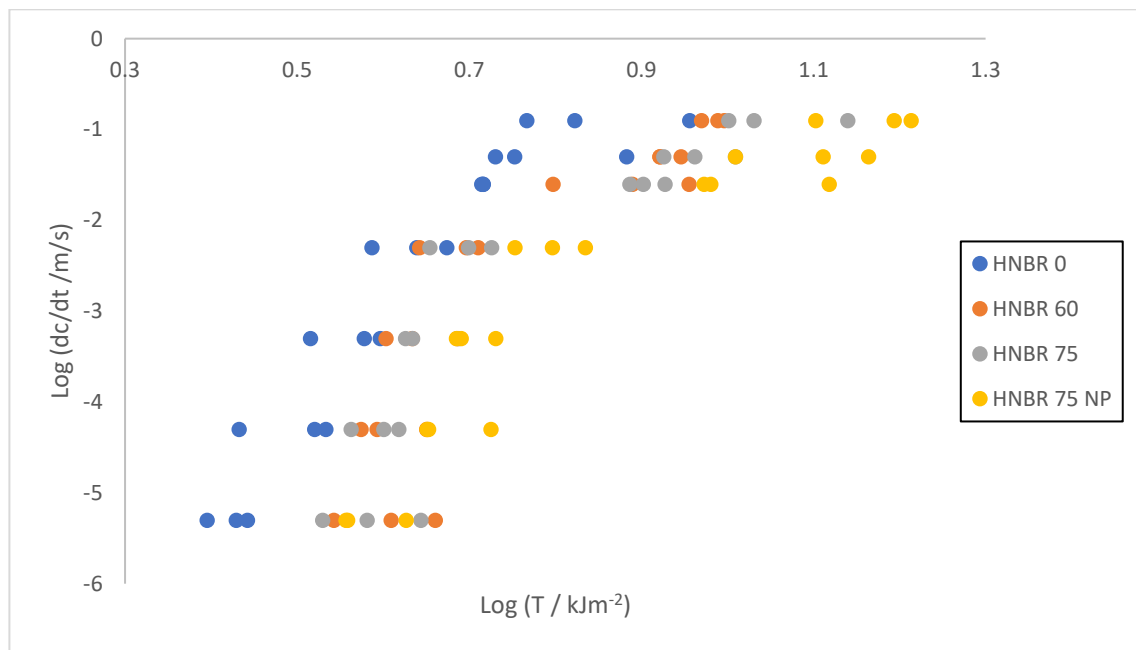
Figure 114: Trouser test results for all four materials at room temperature

	B / ms^{-1}	β
HNBR 0	4.15 x10^{-5}	11.90
HNBR 60	2.67 x10^{-6}	14.26
HNBR 75	1.08 x10^{-6}	15.77
HNBR 75 NP	4.56 x10^{-6}	12.34

Table 11: Material constants for room temperature trouser test results

The results shown here were as expected. They show that there is an increase in the static tearing resistance as the amount of carbon black reinforcement filler is increased. Interestingly, the static tear resistance also increased when the plasticiser was removed from the HNBR 75 sample. This is understandable as an increase in the carbon black filler volume fraction and the removal of the plasticiser all result in an increase in the hysteresis, which is the toughening mechanism in this work.

It can also be seen that the tearing energy value where the log of crack propagation rate is greater than -2.5cm/s shows a clear change the behaviour, shown in figure 114 as tearing energy values where crack growth rate is greater than a tearing energy of -2m/s. This can be expected as explained in chapter 3. The difference between these tearing regions is more defined as filler content is increased and plasticiser is removed.

6.2.2 STATIC TROUSER TEAR TESTS AT ELEVATED TEMPERATURES

All four compounds were also tested at elevated temperatures. The temperatures used were chosen to represent typical and the extreme mud motor operating conditions. The testing parameters can be seen below:

- Crosshead Speeds: 1cm/s – 0.001cm/s
- Crack Growth Rates: 0.5cm/s – 0.0005cm/s
- Temperatures: 100°C and 150°C

The method used for testing trouser specimen at elevated temperatures was similar to the method used for the cyclic pure shear fatigue testing at elevated temperatures. After specimen geometries had been cut from a large sheet and an initial crack that had been cut into them and hand propagated a small distance in excess of 1mm. The oven was then stabilised at the desired temperature. Each specimen was put in the oven and placed on a small rack,

effectively elevated above the floor. This phase of preheating the test sample was for 30 mins. The oven was then opened and the specimen were placed into the tensile grips which were then tightly clamped. Once clamped, the specimen was left a further 15 mins for the oven in order to recover any lost temperature from opening the oven and clamping the specimen. The test was then started after this stage.

The results for each sample at room temperature and elevated temperatures can be seen below.
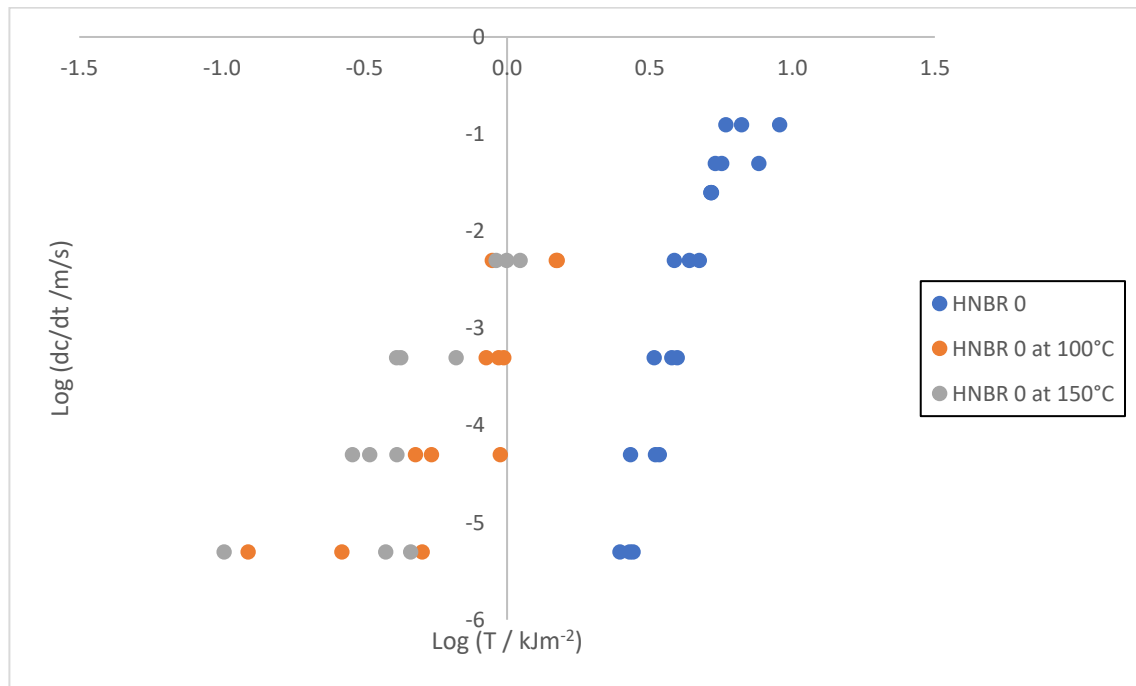
Figure 115: Trouser test results for HNBR 0 at room temperature and elevated temperatures

	B / ms^{-1}	β
HNBR 0: Room Temperature	4.15 x10^{-5}	11.90
HNBR 0: 100°C	3.96 x10^{-2}	3.11
HNBR 0: 150°C	6.84 x10^{-2}	3.27

Table 12: Material constants for HNBR 0 trouser test results at room temperature and elevated temperatures
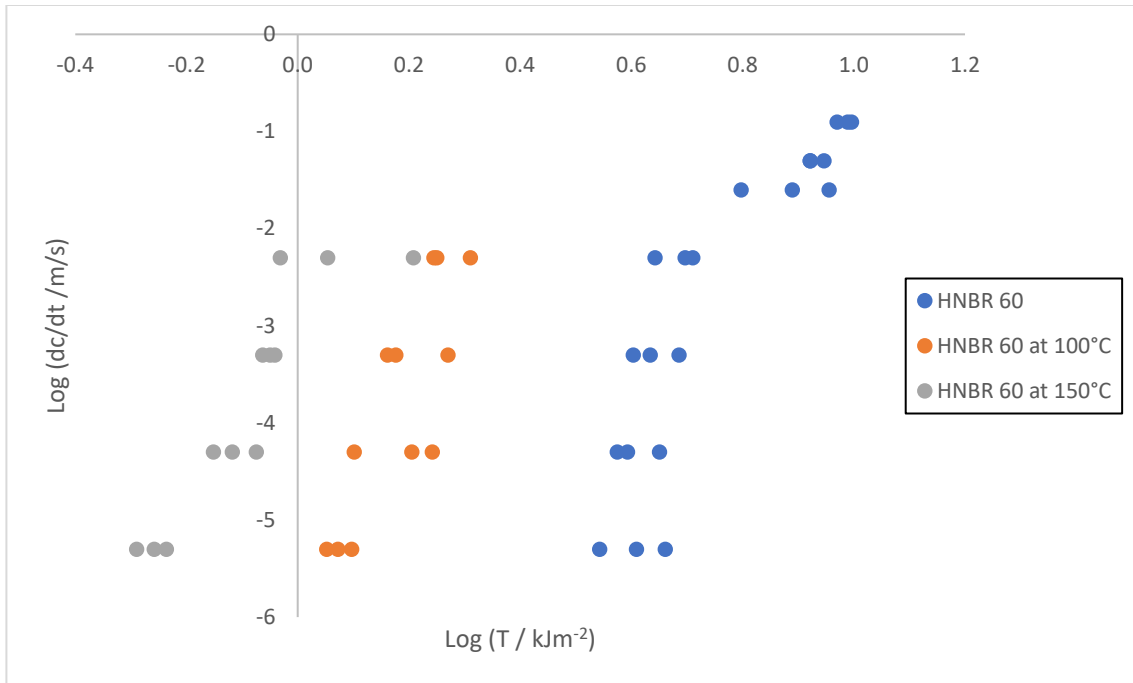
Figure 116: Trouser test results for HNBR 60 at room temperature and elevated temperatures

	B / ms^{-1}	β
HNBR 60: Room Temperature	2.67 x10^{-6}	14.26
HNBR 60: 100°C	2.85 x10^{-3}	11.31
HNBR 60: 150°C	4.36 x10^{-2}	7.63

Table 13: Material constants for HNBR 60 trouser test results at room temperature and elevated temperatures
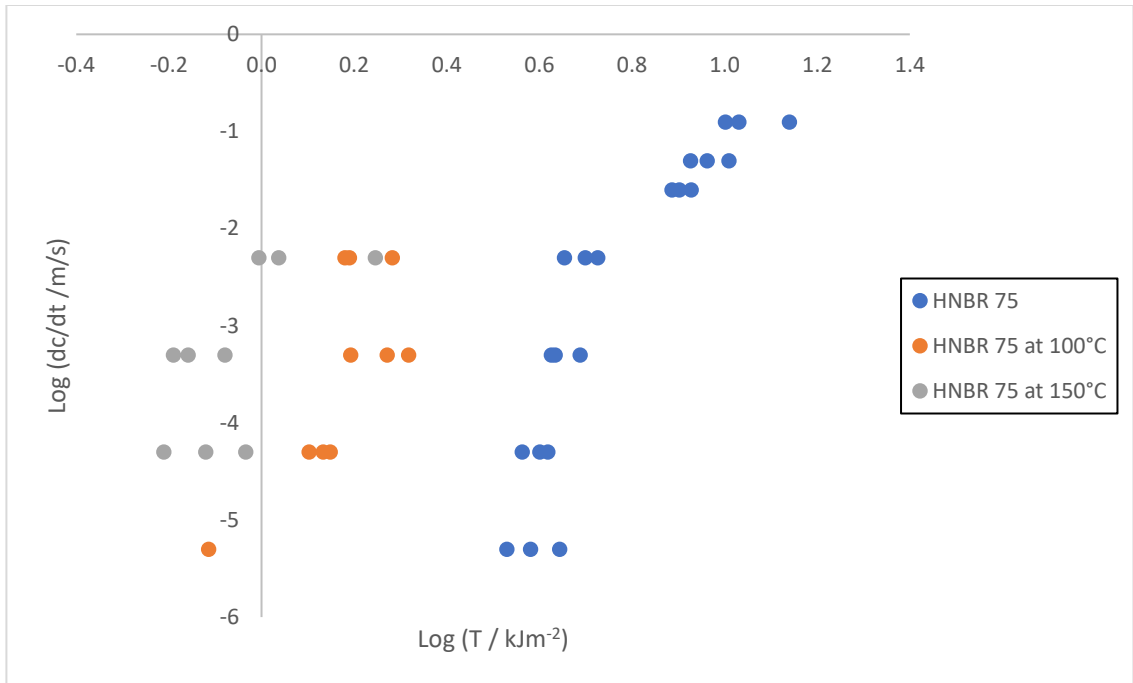
Figure 117: Trouser test results for HNBR 75 at room temperature and elevated temperatures

	B / ms^{-1}	β
HNBR 75: Room Temperature	1.08 x10^{-6}	15.77
HNBR 75: 100°c	1.03 x10^{-2}	6.30
HNBR 75: 150°C	4.64 x10^{-2}	4.02

Table 14: Material constants for HNBR 75 trouser test results at room temperature and

elevated temperatures
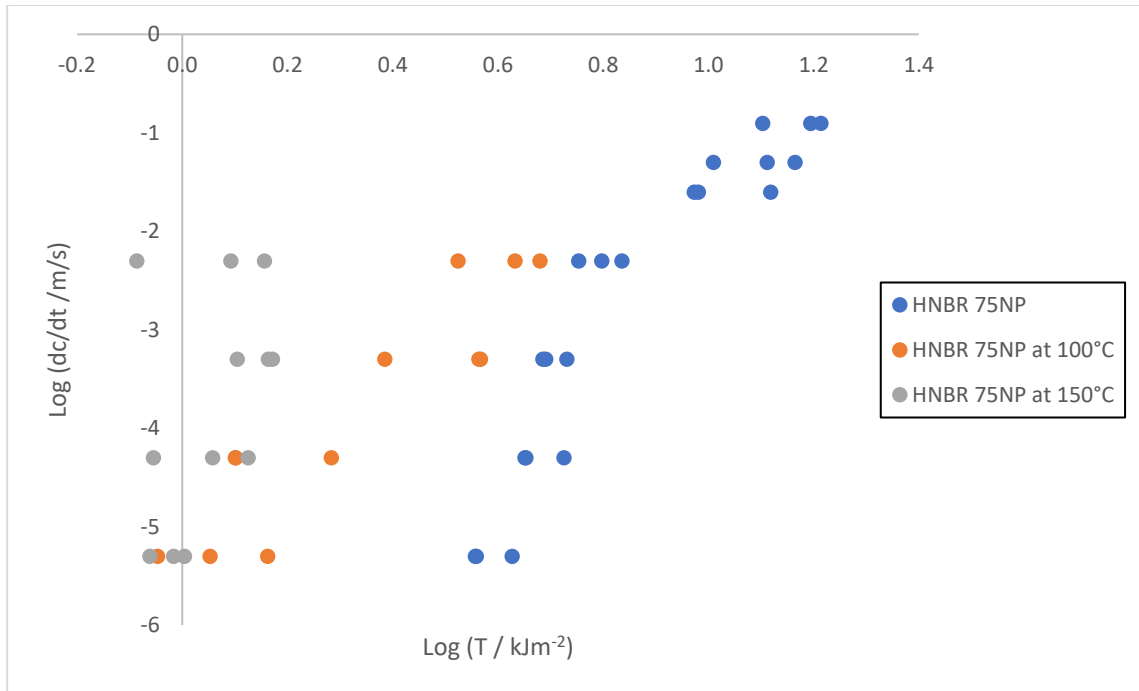
Figure 118: Trouser test results for HNBR 75 NP at room temperature and elevated temperatures

	B / ms^{-1}	β
HNBR 75 NP: Room Temperature	4.6 x10^{-6}	12.34
HNBR 75 NP: 100°C	5.5 x10^{-3}	4.20
HNBR 75 NP: 150°C	1.7 x10^{-2}	5.21

Table 15: Material constants for HNBR 75 NP trouser test results at room temperature and elevated temperatures

All results showed very similar responses at elevated temperatures. Similarly, to the cyclic pure shear fatigue results, as the testing temperature was raised, the static tear resistance of all four materials was reduced. This is to be expected as raising the temperature not only moves the operating temperature away from T_g and therefore reduces hysteresis but also reduces the effectiveness of the carbon black reinforcement fillers that have been incorporated into three of the elastomer compounds.

There is the change of rate, β, with respect to temperature. As temperature is increased, the β value is reduced indicating a change of hysteresis. This is surprising given the movement away from T_g.

174

Similar to the cyclic pure shear fatigue data, as the compounds were tested at elevated temperatures the scatter of the data also increased. It is more difficult to identify the cause of scatter in trouser tear data compared to cyclic pure shear fatigue data given the nature of the test, and it could arise because of many different reasons. However, an important finding was identified when observing the trouser tear test specimen after testing. All compounds showed that as the rate of testing was lowered and the operating temperature was raised, the nature of the crack growth changed dramatically from progressing through the specimen with steady or stick-slip crack growth, to turning 90° very rapidly and then completing the test though to the side of the specimen. The pictures of all specimen can be seen below.
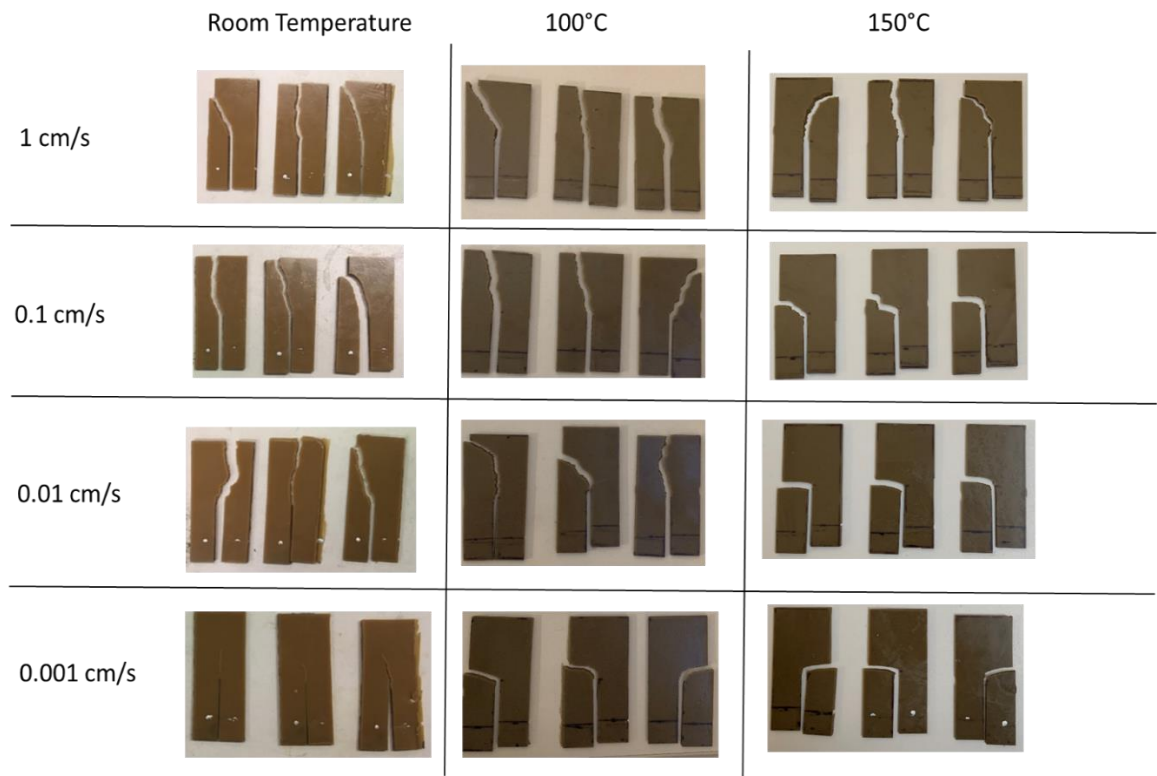
Figure 119: HNBR 0 trouser tear test pieces after testing
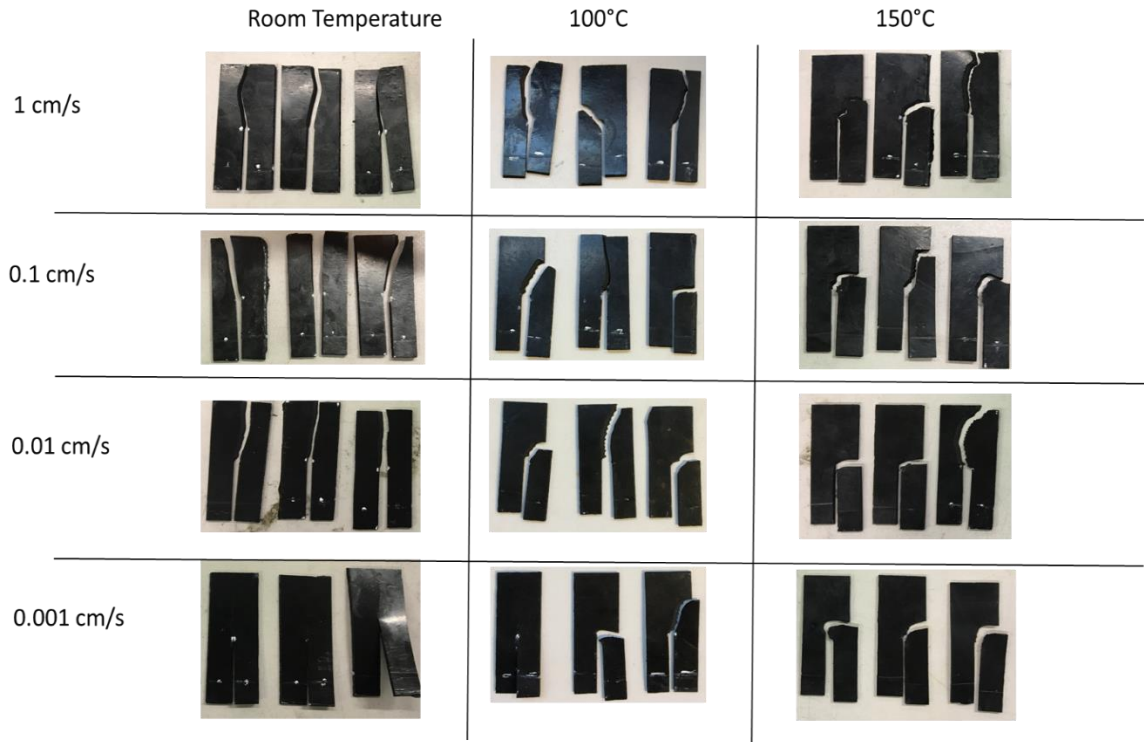
Figure 120: HNBR 60 trouser tear test pieces after testing
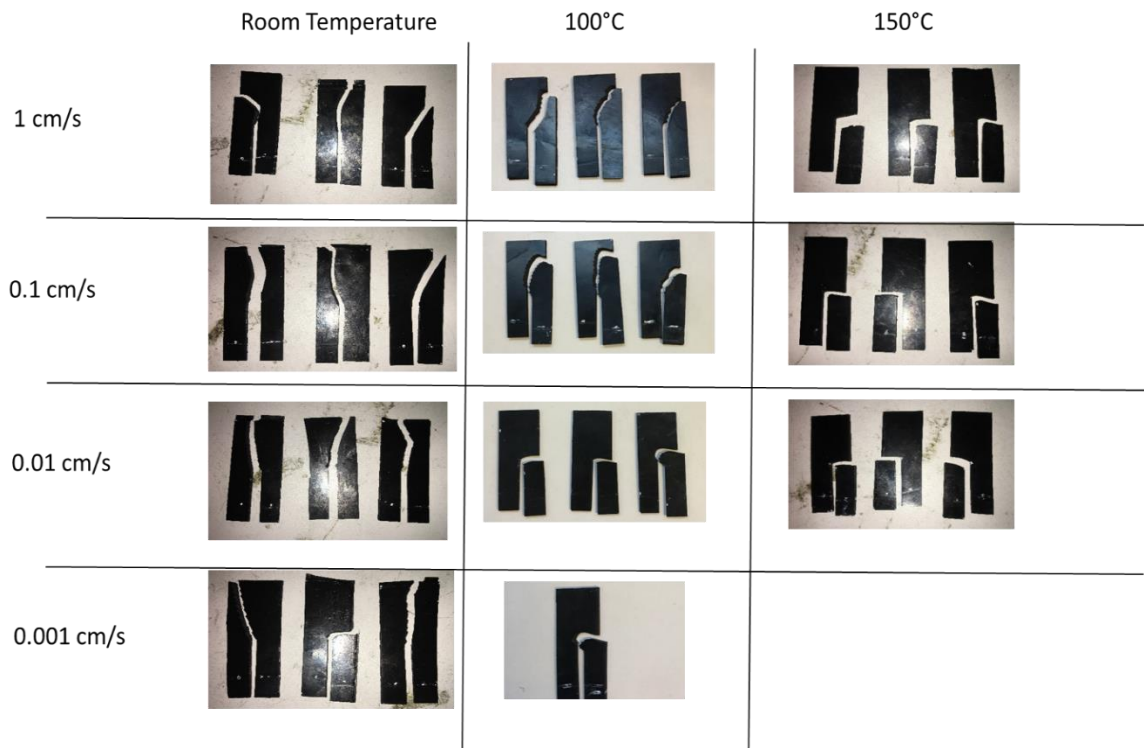
Figure 121: HNBR 75 trouser tear test pieces after testing
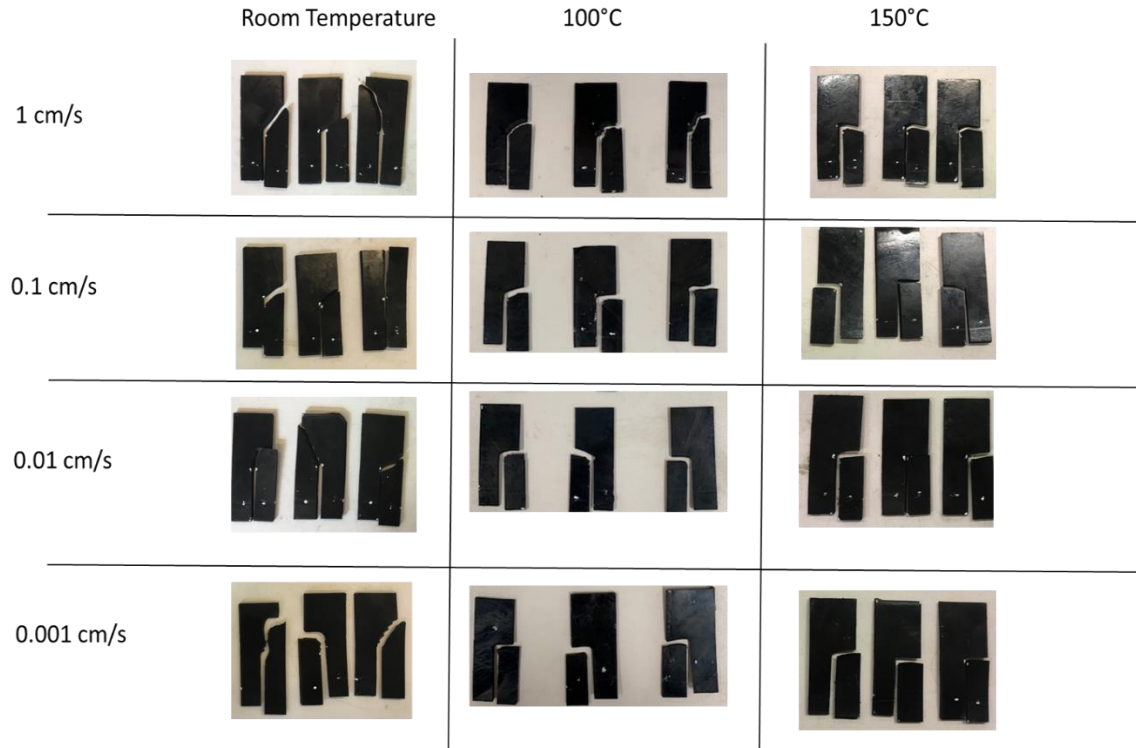
Figure 122: HNBR 75 NP trouser tear test pieces after testing

The figures 119 - 121 clearly show a transitional tearing behaviour from steady and stick-slip type tearing to completely knotty tearing behaviour as the temperature is increased. This behaviour is not new in trouser tear tests, however it is only documented in elastomers with a known toughening mechanism such as strain induced crystallising materials like NR. Hamed [Hamed, G. R, 2005] is one of the first to document this 90° crack turn in trouser tear tests in NR and attributes it to strain induced crystallisation. However, the results found in this body of work are not so simple to explain. What is surprising is that this toughening mechanism increases its effectiveness at lower tearing rates and at the higher range of the operating temperatures, which appears to oppose the generally known understanding of strain induced crystallisation.

It is evident that this behaviour occurs in unfilled HNBR, mostly at elevated temperatures, however the addition of carbon black and removal of plasticiser obviously increase its effect significantly. This could indicate a strain amplification effect in the matrix elastomer at the crack tip by adding carbon black and the removal of the plasticiser acts to increase the effect of strain at the crack tip. This belief is analysed further later in this chapter.

Research in the ability of HNBR elastomers to undergo strain induced crystallisation is limited. Some preliminary research documenting it has emerged recently [Narynbek, U. K, Dragicevic, M, Albouy, P, Huneau, B, Beranger, A. and Heuillet, P, 2017]. What papers like this struggle to explain is the detailed mechanism behind the crystallisation behaviour.

One paper in particular by Severe and White [Severe, G and White, J. L, 2000] looks at testing HNBR of varying ACN contents using different methods of material characterisation. These test focus on DSC and wide angle x-ray diffraction (WAXD). They concluded that there are potentially two mechanisms occurring for crystallisation. In low ACN content HNBR, the crystallisation can occur as a result of large quantity and length of hydrogenated butadiene, and high ACN content HNBR can crystallise as a result of alternating sequence of tetramethylene and acrylonitrile. As the HNBR products in this work are 43% ACN, they satisfy the bracket of high ACN content HNBR.

6.2.3 MECHANICAL TESTS: CYCLIC VS TIME DEPENDANT CRACKING

The fatigue crack growth data was further analysed by attempting to breakdown the fatigue fracture components into cyclic and time dependant components according to the approach proposed by Busfield et al [2002]. As is explained earlier in chapter 3, it is possible to explore the cyclic pure shear fatigue tests done in chapter 5 more carefully by examining the tearing relationship data measured using the static trouser tear test results. Then the cyclic pure shear fatigue results can be split into two separate components as follows:

$$\frac{dc}{dn} = \left(\frac{dc}{dn}\right)_{time} + \left(\frac{dc}{dn}\right)_{cycle} \hspace{2cm} (6.3)$$

The time component is dependent on the length of time a specific tearing energy value is achieved in each cycle and then by calculating how much steady tearing would have taken place within a single cycle, and the cyclic component is independent of the cycle frequency but is additional crack growth that results from the unloading and reloading of the test piece. The time dependent component can be found by utilising the coefficients, B and β, that were measured using the static trouser tear test and the cyclic component is found by subtracting the time component away from the total measured in the cyclic fatigue test.

Significant contributions from the cyclic contribution have been found for materials that feature strain induced crystallisation behaviour in the past.

6.2.4 CYCLIC VS TIME DEPENDANT CRACKING RESULTS AT ROOM TEMPERATURE

This method was initially used to analyse all four compounds at room temperature. The data points shown are of the total cyclic pure shear fatigue tests shown in chapter 5 and the dotted line shows the calculated time dependent component. Therefore, the difference between these two set of data are the cyclic component contribution.

Figure 123: Total cyclic pure shear fatigue plotted with the time dependent component for HNBR 0 at room temperature

Figure 124: Total cyclic pure shear fatigue plotted with the time dependent component for HNBR 60 at room temperature

Figure 125: Total cyclic pure shear fatigue plotted with the time dependent component for HNBR 75 at room temperature

Figure 126: Total cyclic pure shear fatigue plotted with the time dependent component for HNBR 75 NP at room temperature

The detailed contributions of the time dependent and cyclic components vary between compounds, however, the compounds HNBR 0, HNBR 60 and HNBR 75 all showed a similar response. HNBR 75 NP showed a different behaviour.

For the compounds HNBR 0, HNBR 60 and HNBR 75, it is clear that at higher tearing energies and faster crack propagation rates, the contribution of fracture is just time component dependent. As the tearing energy and crack propagation rate are lowered, the response becomes much less time component dependent and much more cyclic component dependent. This transition from time dependent to cyclic component is more severe for the filled compounds and is as a consequence of higher β values. However, it is best noted that these time dependent component results, based on the material constants from trouser tear test data, are very sensitive to small changes in the trouser tear data. Therefore, the best way to analyse these results is through observing general trends rather than very small details, especially as both cyclic pure shear fatigue and static trouser tear results suffer to knotty tearing behaviour that cause significant scatter in the data.

The results clearly follow a similar theme to the figures 119 - 122 where knottier tearing behaviour at lower tearing energies and lower crack propagation rates was observed. When the tearing energy was lowered, fracture became much more cyclic component dependent

indicating an extra toughening mechanism was at work in this region, causing a tougher response.

Results for HNBR 75 NP showed an almost entirely cyclic dependent response. This toughening is evidenced even at room temperature where the test specimen all exhibit a 90° turn.

6.2.5 CYCLIC VS TIME DEPENDANT CRACKING RESULTS AT ELEVATED TEMPERATURES

Results for elevated temperature tests were also processed using the same approach. However, as explained in chapter 5, cyclic pure shear fatigue results at elevated temperatures for HNBR 0 and HNBR 75 NP could not be completed as the materials became too difficult to test easily. Therefore, is the case, only HNBR 60 and HNBR 75 could have cyclic and time dependent contributions identified. The results are shown in the following figures.
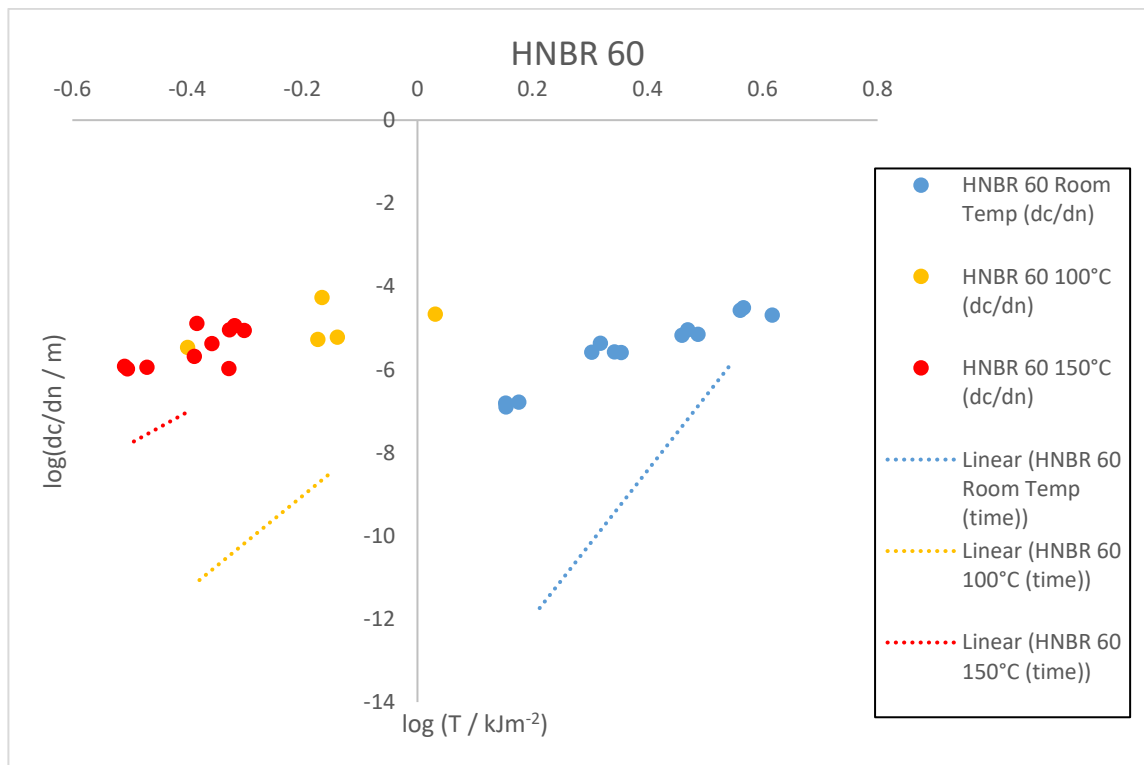
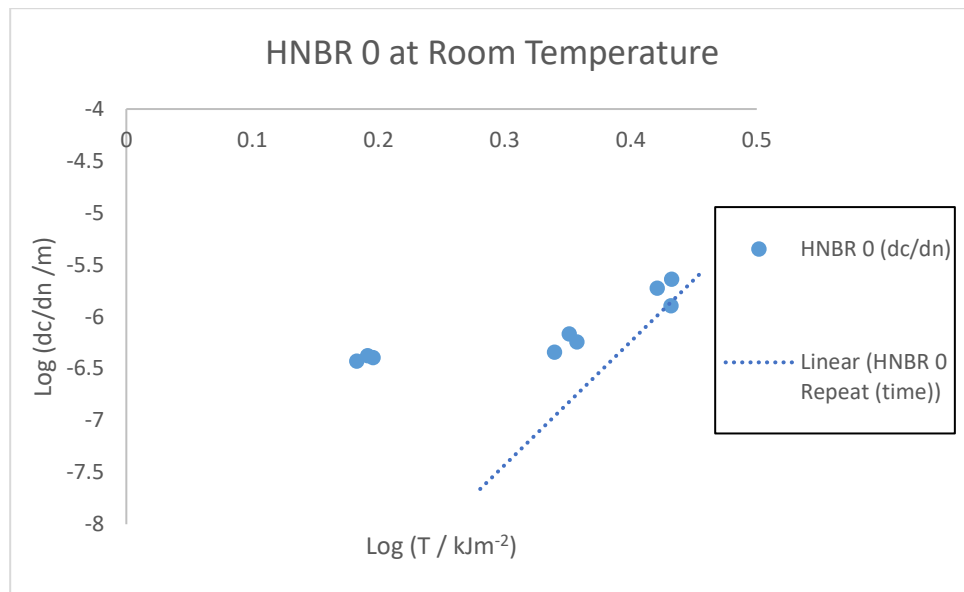*Figure 127: Total cyclic pure shear fatigue plotted with the time dependent component for HNBR 60 at room temperature and elevated temperatures*
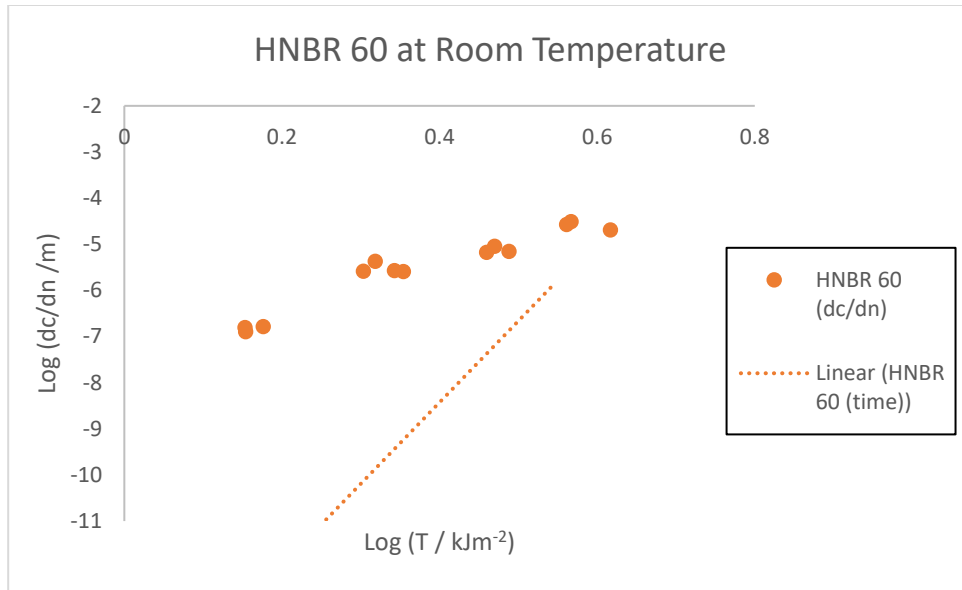
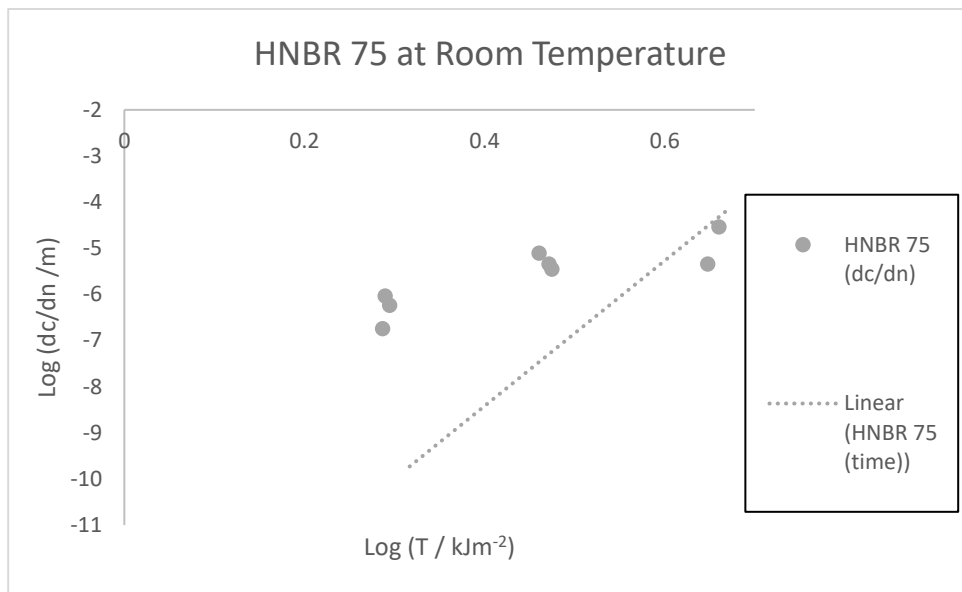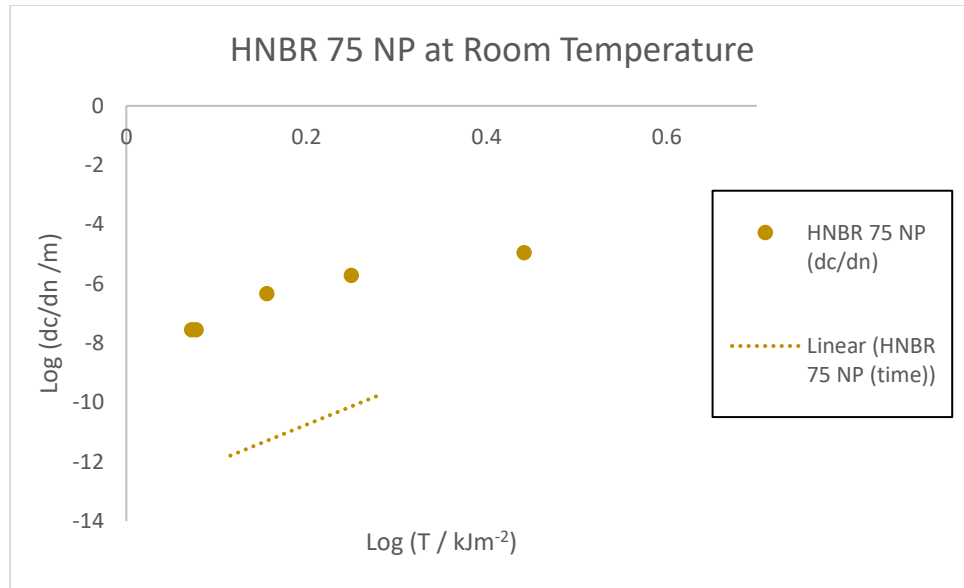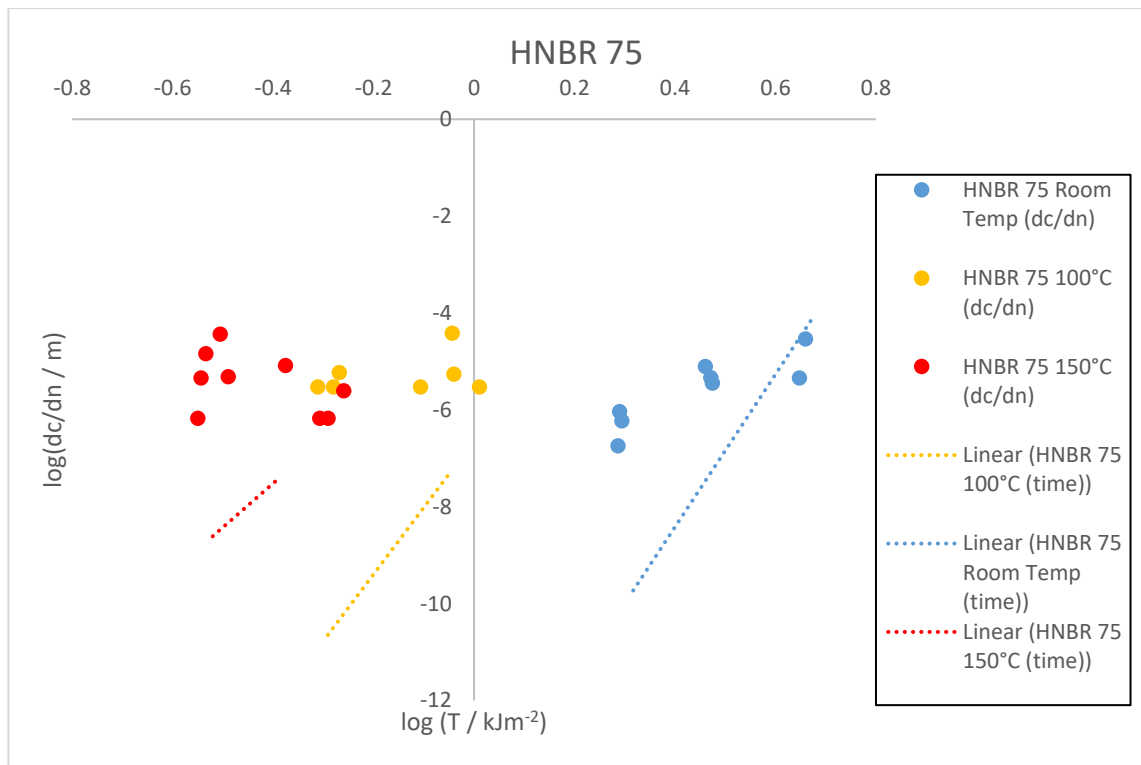*Figure 128: Total cyclic pure shear fatigue plotted with the time dependent component for HNBR 75 at room temperature and elevated temperatures*

The cyclic and time dependent components when separated at elevated temperatures for HNBR 60 and HNBR 75 show very similar results to each other. Evidently as the testing temperature is elevated, the relationship becomes less dependent on the time dependent component and more dependent on the cyclic component. This is partly due to the lowering of β values in tables 13 and 14 for trouser tearing results at elevated temperatures.

However, this confirms the same results as the trouser tear data and the resultant knotty tearing behaviour observed on many of the test specimen. Not only does the tearing behaviour become more cyclic component dependent at lower tearing energies and lower crack propagation rates, it also becomes much more cyclic component dependent at higher testing temperatures indicating an extra toughening mechanism being developed at higher temperatures.

This indicates that the toughening mechanism, characterised by the cyclic component of this analysis, can not only be identified but can potentially be engineered to enable HNBR products to permanently work within a range of increased toughness. This is an important detail for future designs of elastomer parts as this could enable HNBR parts to be developed that can last longer.

6.3 MATERIAL CHARACTERISATION: XRD TESTS

As explained previously, according to [Severe, G and White, J. L, 2000] there are potentially two crystallisation mechanisms occurring in HNBR materials. In low ACN content HNBR, crystallisation can occur as a result of large quantity and length of hydrogenated butadiene, and high ACN content HNBR can crystallise as a result of alternating sequence of tetramethylene and acrylonitrile. Throughout this thesis all the materials used were high ACN content materials.

Another paper that focuses on XRD tests on HNBR of varying ACN content is [Bielinski, D. M, Slusarski, L, Wlochowicz, A and Slusarczyk, C, 1997]. They concluded that during XRD tests, two differing ordered structures at $2\theta = 19°$ and $23°$ were found whose signal increased in intensity when the specimen were stretched. Compounds were even found to have small a small degree of ordering before stretching. The changes were more pronounced in HNBR compounds over NBR potentially as a result of the removal of unsaturated butadiene monomers that inhibit the alternating sequence.

With this research in mind, XRD tests were done on all four compounds to locate any crystalline peaks at $2\theta = 19°$ and $23°$. With the equipment based at Queen Mary University of London, it is not possible to prestretch the test pieces and test them. Therefore, all the compounds were only tested in an unstretched state. According to [Bielinski, D. M, Slusarski, L, Wlochowicz, A and Slusarczyk, C, 1997], a small amount of crystallinity should still be able to be seen. All the tests were only conducted at room temperature.

The results for all four compounds can be seen below.
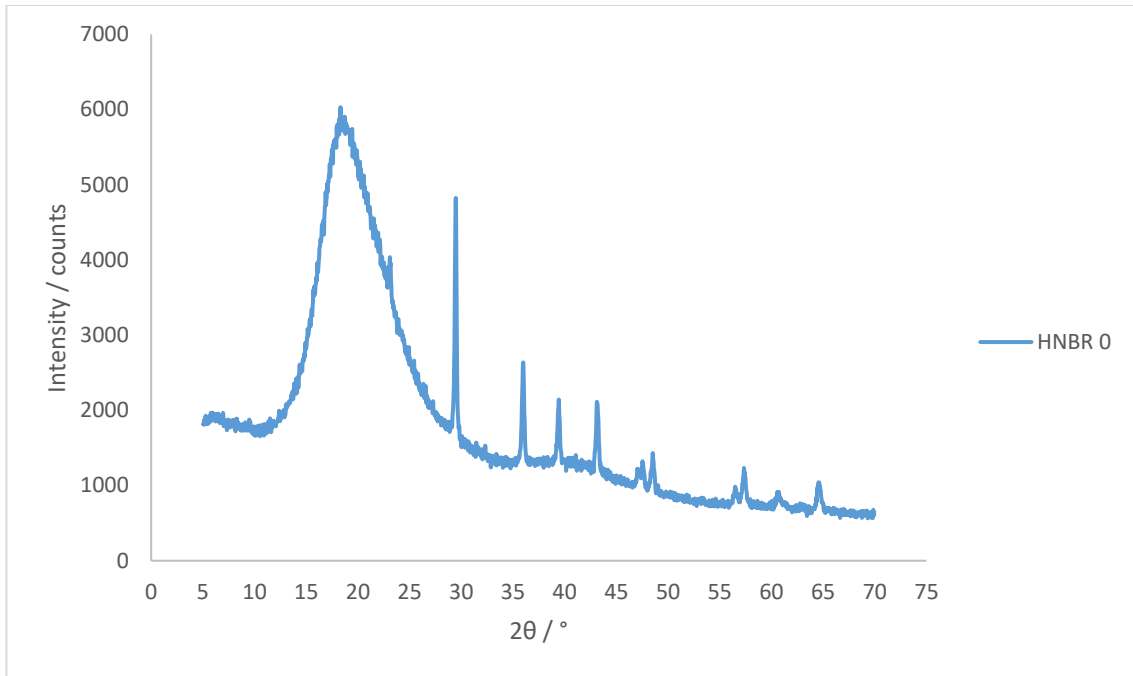
Figure 129: XRD plots for unaged and unstrained HNBR 0, tested at toom temperature
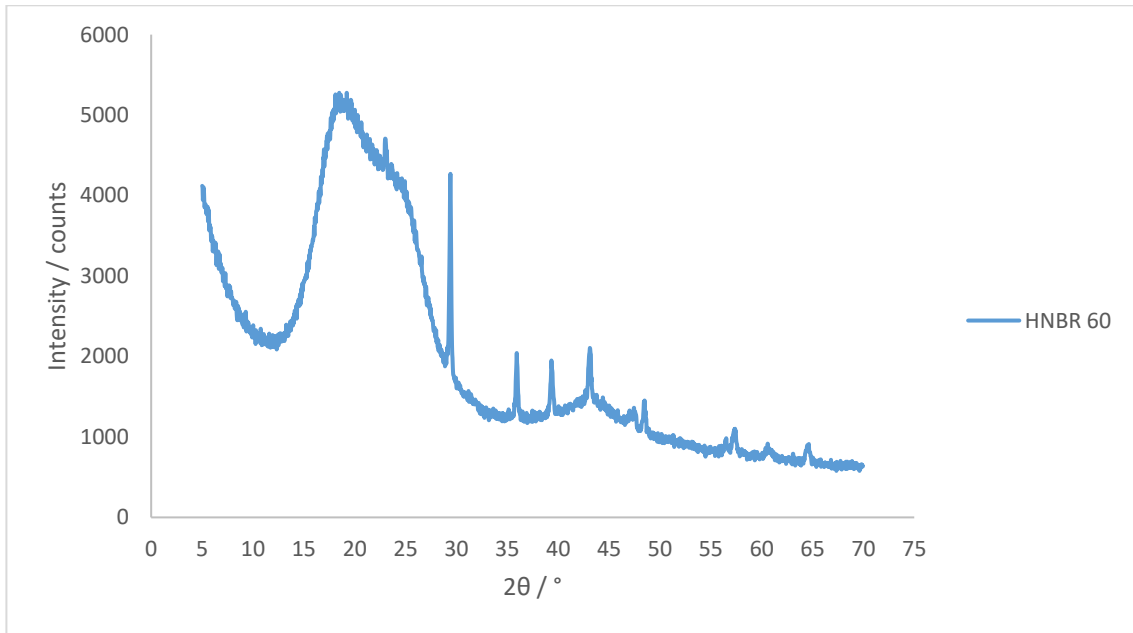
Figure 130: XRD plots for unaged and unstrained HNBR 60, tested at toom temperature
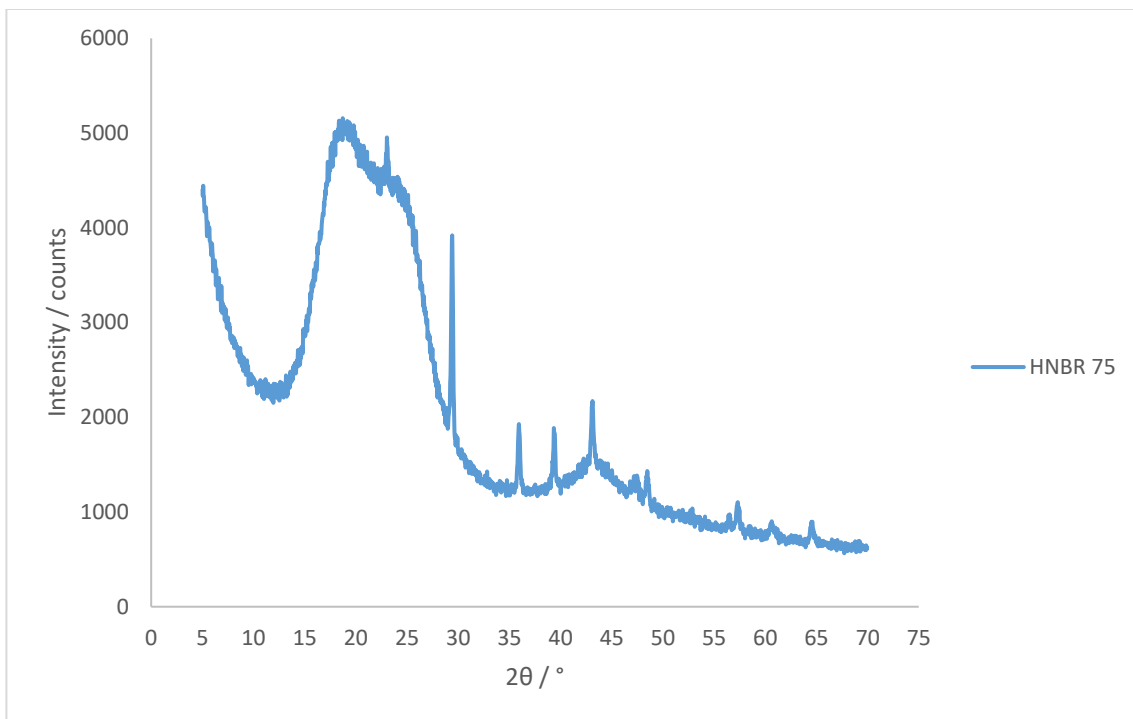
Figure 131: XRD plots for unaged and unstrained HNBR 75, tested at toom temperature
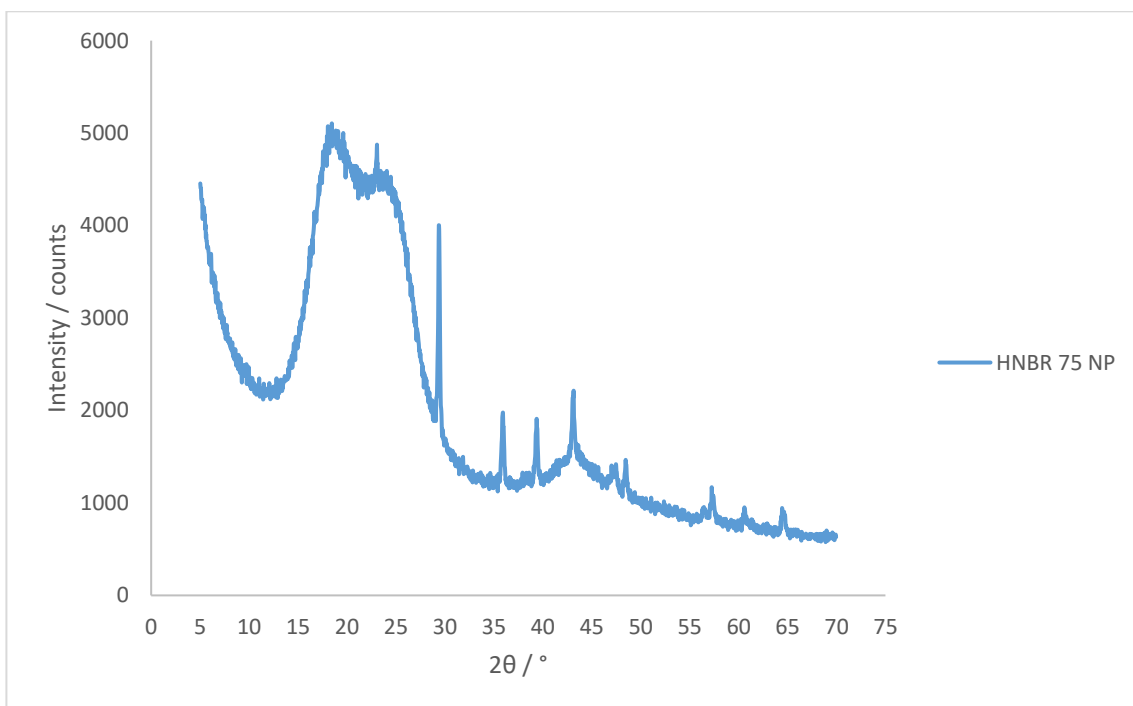
Figure 132: XRD plots for unaged and unstrained HNBR 75 NP, tested at toom temperature

The results from the XRD tests clearly show a lot of individual crystalline peaks and some amorphous peaks. Therefore, these need to be analysed individually.

A broad peak is found at approximately 17° for all four compounds. This is most likely the general amorphous nature of the elastomer itself and is therefore expected. According to [Tunnicliffe. L, 2015], a broad peak is expected at approximately 25° for compounds featuring carbon black reinforcement. This corresponds to an amorphous distribution of carbon black. It is likely that the second smaller broad peak at 43° is similarly as a result of carbon black. All the sharp peaks found from 28° and higher are as a result of elastomer compound ingredients. These can mostly be accounted for as:

- 29°: Calcite
- 36°: ZnO
- 39°: Calcite
- 43°: MgO
- 47°: ZnO

The areas of interest according to [Bielinski, D. M, Slusarski, L, Wlochowicz, A and Slusarczyk, C, 1997] are $2\theta = 19°$ and 23°. In all four compounds a small sharp crystalline peak can be seen at 23°. Interestingly the peak at 23° grows in intensity as carbon black filler is increased, indicating that the crystallinity found in the unstrained HNBR 0 material is increased by the addition of carbon black. Research by Tao [Tao, Y, 2018] shows evidence that testing stretched HNBR can increase the volume of the peak at $2\theta = 23°$, indicating that there is a potential for the crystalline peak to increase in volume after stretching in this work as well.

It was concluded earlier in the chapter that carbon black enabled the knotty tearing behaviour seen in the trouser tear specimen in figures 119 - 122 however it was assumed this was a strain amplification effect. Whereas this might still be the case, there is obviously another mechanism occurring here that is unrelated to strain as these compounds were tested in an unstrained state. This mechanism could be related to the explanation given by [Severe, G and White, J. L, 2000] that high ACN content HNBR can crystallise as a result of alternating sequence of tetramethylene and acrylonitrile. If this is the case, it is understandable that a small degree of crystallinity can be found in the unstrained state. It is also potentially the case that the carbon black surface might help to form these crystallisation structures more readily.

This crystallinity might help to understand some of the previous questions left unanswered from chapter 5. This type of behaviour might be the source of the knotty tearing found in the cyclic pure shear fatigue tests.

However, the materials typically grow progressively more knotty as the testing temperatures were increased when the fatigue crack growth behaviour becomes more cyclic component dependent. Normally it would be expected that crystallisation is reduced at elevated temperatures. So crystallisation alone is unlikely to be able to explain the observed effects. It is likely that there is still some source of significant strain induced anisotropy that has yet to be identified that is the reason for the additional toughening. What is also clear is that the ageing tests in chapter 5 were also seen to encourage the appearance of this toughening mechanism. It is possible that some sort of physical ageing of the filler network that can create a local anisotropy of the polymer network with time. This process is accelerated at higher temperatures. The understanding of crystallinity could be applied here as well. Whereas the common understanding states that high temperatures inhibit the formation of crystals, the addition of temperature could alternatively act to provide energy to the polymer chains and encourage them to form crystals. The combination cyclic strain, a high strain region at the crack tip and higher temperatures could therefore lead to the formation of crystals upon loading and then subsequent melting upon unloading. This therefore is an area that could be investigated in future projects. Any future investigation must focus on the physical ageing processes taking place in these materials and should consider if they are accelerated with temperature and can they be seen to toughen the materials even further after curing.

6.4 CONCLUSIONS

To conclude:

- Static trouser tear tests were done on all four elastomers for a range of crack propagation rates and a range of temperatures from room temperature up to 150°C
- A distinct knotty tearing behaviour defined by a sharp 90° crack turn in the trouser test compounds was seen for many of the tests. Whereas this is known to happen for strain crystallising elastomers, this behaviour was observed more often at lower tearing energies and lower crack propagation rates which is not the normal behaviour for SIC materials.

- The cyclic components and time dependant components were isolated at room and elevated temperatures for the fatigue crack growth test data for all four compounds and a similar mechanism was found to occur. A more cyclic dependent component behaviour was found at lower tearing energies and lower crack propagation rates, indicating a significant toughening mechanism is taking place. This also suggested a potential engineering design area where HNBR products could be designed to encourage this toughening behaviour.

- Following work from [Severe, G and White, J. L, 2000] and [Bielinski, D. M, Slusarski, L, Wlochowicz, A and Slusarczyk, C, 1997], XRD testing was done on unstrained test pieces at room temperature to investigate any crystallinity. A potentially crystalline region was found in all tests which grew in signal intensity as the carbon black was added to the compound.

- This indicated that potential crystallisation effects were occurring as a result of alternating sequence of tetramethylene and acrylonitrile which was then encouraged by the addition of carbon black.

- Unanswered questions remain as to what the reinforcement mechanism is that toughens these materials so well at higher temperatures and after ageing. Perhaps some sort of flocculation of the fillers is creating a tougher filler network structure or perhaps there is some sort physical ageing of the filler network. This should be the focus of any follow up investigation into this behaviour.

7. SUMMARY, CONLCUSIONS AND FUTURE WORK

This body of work focuses on understanding how typical HNBR formulations used in oil and gas applications perform in their very demanding applications. In this case, we have examined the materials specifically for use in the mud motor stator. HNBR is widely used in a wide range of extreme environments, however it is not completely understood why it performs so well in these applications due to a limited amount of specific research in this area. This thesis investigates two aspects of this behaviour. The first is to understand how HNBR elastomers respond to ageing and how they operate at high temperatures through a fatigue study on unaged and aged materials. This work is explored in detail in chapter 5. The second is to understand if HNBR elastomers feature an extra toughening mechanism to be able to operate at such high levels of performance, and if so to postulate the source of this toughening mechanism. This work is explored in detail in chapter 6.

7.1 SUMMARY OF CYCLIC FATIGUE AND AGEING OF HNBR

In chapter 5, a study combining a fatigue analysis with a combination of ageing mechanisms and high operating temperatures was undertaken to further understand how HNBR materials used in oil and gas applications respond when operating in extreme environments. The response of materials varied widely from materials that improved their toughness post ageing, to materials that featured large changes to their modulus and hysteresis with ageing and also materials that developed different crack propagation characteristics, ranging from smooth tearing to severely knotty tearing in what seemed at first to be an unpredictable manner. However general trends became clear where in general the samples that were aged at 150°C in air had a weaker fatigue response, samples aged at 100°C in air had a tougher response, samples aged at 150°C in oil had very similar response to unaged tests and samples aged at room temperature in oil mainly featured changes in their hysteresis. Samples were also tested at higher temperatures, where they exhibited a more significant knotty type of behaviour and the data was more scattered. This greater extent of knotty tearing could be clearly identified after ageing. It was apparent that the knotty tearing caused the results to scatter but only in the direction where the results became tougher, indicating that the knotty tearing was at the very least a manifestation of an additional toughening mechanism.

Further investigations were carried out with materials characterisation techniques such as TGA and FTIR to compare how samples post ageing had responded to their different ageing

conditions. Prior to this, samples were weighed pre and post ageing to measure any mass loss or gain during ageing. The TGA showed all samples featured a similar response at the start of the tests and in the polymer backbone breakdown temperature range. Between these temperatures though, the responses varied depending upon how samples had lost or gained ingredients during their ageing process. It was clear that for samples aged in air there was a significant loss of plasticiser, much more so at the highest ageing temperature. Relating this to tensile test results, this response had a significant effect on the modulus and hysteresis of the materials and produced an increase in toughness in certain circumstances. However, it was unclear how samples aged in oil responded after ageing using TGA tests as both the oil that might have swollen in and the plasticiser that might have evaporated were both lost in the test over a similar temperature range. FTIR tests then semi-quantifiably confirmed that all the samples aged in air indeed lost plasticiser. As well as that, samples aged in oil at high temperatures lost significant amount of plasticiser whereas the samples aged in oil at room temperature had not. This indicated that the loss of plasticiser was a temperature driven process and that swelling and leaching of oil helped with the process but in general it did not cause it. The swelling of the oil into the samples caused a hysteresis change in the samples that was similar in performance to that of the originally incorporated plasticiser. Therefore, samples aged in oil at elevated temperatures lost plasticiser but kept a similar hysteresis response due to the oil replacing the plasticiser in the sample.

The combination of these tests answered many questions regarding how toughness was increased after ageing in some circumstances and how the hysteresis of each material varied so widely after ageing. However, the understanding of the precise toughening mechanism that created the knotty tearing of the compounds remained unclear. Trying to understand this purpose was the reason to undertake the investigation in chapter 6.

7.2 SUMMARY OF STATIC TEAR AND TOUGHENING OF HNBR

In chapter 6, static trouser tear tests were performed over a wide range crack propagation rates and operating temperatures. The results were unsurprising; however, data did become more scattered at elevated temperatures similarly to the cyclic pure shear fatigue tests. An important finding was the observed crack paths developed during the trouser tear tests. It was shown that as samples were tested at lower tearing rates, higher operating temperatures and with larger amount of carbon black filler, the crack paths rapidly diverted sharply by 90°. This

indicated that a toughening mechanism at the crack tip was present that was encouraged under these specific conditions.

Using a method developed by Busfield [Busfield. J. J. C et al, 2002], cyclic and time dependent tear components were identified by using by cyclic pure shear fatigue data and static trouser tear data. It was shown that both contributions varied as a result of varying the crack propagation rate and changing the operating temperatures and carbon black filler volume fraction. The results became significantly more cyclic component dependent at lower tearing rates, higher operating temperatures and with samples featuring higher carbon black filler contents, confirming that a potential toughening mechanism occurred under these parameters.

Following on from the work of [Severe, G and White, J. L, 2000] and [Bielinski, D. M, Slusarski, L, Wlochowicz, A and Slusarczyk, C, 1997], XRD tests were done on unstretched samples at room temperature. It was understood from these papers that HNBR had the potential to crystallise under specific conditions. In this case, as the HNBR compounds featured a high ACN content, they had the potential to crystallise as a result of alternating sequence of tetramethylene and acrylonitrile. By examining the detailed XRD data, potential crystalline regions could be found at $2\theta = 19°$ and 23° even in the unstrained state. These tests were performed on all samples and a clear crystalline peak was found at 23° that increased in size as samples featured higher levels of carbon black. This therefore indicated that potential crystallisation effects were occurring as a result of alternating sequence of tetramethylene and acrylonitrile which was then encouraged by the addition of carbon black. This is therefore likely to be a primary source of the knotty tearing behaviour found in both cyclic pure shear fatigue test and static trouser tear tests.

7.3 SUGGESTIONS FOR FUTURE WORK

The work in this thesis provides a much clearer understanding for why typical oil and gas elastomers can function at such high operating levels and extreme environments due to changes in composition as a result of ageing and due to extra toughening mechanisms within the elastomer itself. However, further investigation and evaluation would help clarify more details within this area of study.

As demonstrated in chapter 4, elastomers used in mud motor applications and wider oil and gas applications suffer to many sources of failure. This thesis contains a study focussing mainly on the fatigue and crack initiation failure modes. However, still under researched are failures as a result of wear, debonding of the elastomer from the metal casing and as a result of a suboptimal curing process. A study that mud motor applications would specifically benefit from is the analysis of how injection moulding effects the resulting elastomer properties. In light of this body of work, if potential alternating sequences of tetramethylene and acrylonitrile are causing crystalline effects in an unstretched state, it is likely that the process of injection moulding might have a role in aligning some of the polymer chains due to boundary layer interactions at the mould injection points and within the elastomer part mould itself.

What remains unknown right now is how precisely does an increase in carbon black volume fraction, a rise in test temperature or the increased toughness resulting from ageing all develop from what appears to be an enhanced crystallisation behaviour in the crack tip region. It is possible that ageing introduces some sort of physical ageing of the filler network or that the constrained polymer molecules between filler particles might be more susceptible to strain induced crystallisation as a consequence of strain amplification or that the elevated temperatures allow the more mobile polymer molecules to orientate and form crystals more readily when a crack tip region is strained. These questions need to be addressed potentially by examining the crystallisation behaviour more carefully under strain using perhaps a synchrotron source to see how chain mobility alters the rate of crystal development.

Further investigation is needed into understanding the mechanism behind crystallinity within HNBR elastomers of varying ACN content. If understood further, crystallinity within HNBR could become a controlled feature enabling tougher HNBR compounds to be purposely developed.

In addition to practical experiments that could further understand these materials, developing FEA software to account for the effects demonstrated in this thesis would enable closer predictions of fatigue life and help determine when elastomer properties are going to change over the course of their lifetime. The work in this thesis is the beginning of understanding these mechanisms so that FEA software can then use to predict these factors. This process can then ultimately ensure that elastomer parts are developed to accurately perform their tasks and alter their behaviour predictably.

8. REFERENCES

[Abaqus, 2012] Abaqus User Manual

[Alcock, B and Jorgensen, J. J, 2015] The mechanical properties of a model hydrogenated nitrile butadiene rubber (HNBR) following simulated sweet oil exposure at elevated temperature and pressure, Polymer Testing, vol 46, pg 50

[Alcock, B, Peters, T. A, Gaarder, R. H, Jorgensen, J. K, 2015] The Effect of Hydrocarbon Ageing on the Mechanical Properties, Apparent Crosslink Density and CO_2 Diffusion of Hydrogenated Nitrile Butadiene Rubber (HNBR), Polymer Testing, vol 47, pg 22

[Allen. P, Jones. K, 1988] Natural Rubber Science and Technology, Oxford University Press, Oxford

[Al-Malaika, S, 1995] Atmospheric Oxidation and Antioxidants, ed. Scott, G., Elsevier Publishing Company, Amsterdam, vol 1

[Arruda. E.M and Boyce. M. C, 1993] A Three-Dimensional Constitutive Model for the Large Stretch Behaviour of Rubber Elastic Materials, Journal of the Mechanics and Physics of Solids, vol 41, no.2

[Asare. S, 2014] Failure of Rubber Components under Fatigue, PhD Thesis Queen Mary University of London

[Bateman, L, 1954] Olefin Oxidation, Quart. Reve. London, vol 8, pg 147

[Beranger. A.S. et al, 2018] Beranger, A.S. et al, 2018, Fatigue Crack Growth Behavior of NBR, HNBR, HNBR ZSC Compounds, Procedia Engineering, vol 213, pg 145

[Bergstrom. J. S and Boyce. M. C, 1998] Constitutive Modelling of the Large Strain Time-Dependent Behaviour of Elastomers, Journal of the Mechanics and Physics of Solids, vol. 46, pg 931

[Bergstrom. J. S, 2019] Bergstrom. J. S, 2019, https://polymerfem.com/content.php?77-bergstrom-boyce-model, accessed 20/10/19 17:00 GMT

[Bielinski, D. M, Slusarski, L, Wlochowicz, A and Slusarczyk, C, 1997] Structure and Mechanical Properties of Nitrile Rubbers Modified with Iodine, Journal of Applied Polymer Science, vol 67, pg 501

[Blanchard, A, Parkinson, D, 1952] Breakage of carbon-rubber networks by applied stress, Industrial & Engineering Chemistry, vol 44, pg 799

[Boyce. M. C and Arruda E. M, 2000] Constitutive Models of Rubber Elasticity: A Review, Rubber Chemistry and Technology, vol. 73, no. 3, pg 504

[Busfield, J. J. C, Ratsimba, C. H. H. and Thomas, A.G, 1997] Crack growth and strain induced anisotropy in carbon black filled natural rubber, Journal of Natural Rubber Research, vol. 12, pg 131.

[Busfield. J. J. C, 2000] The Prediction of the Mechanical Performance of Elastomeric Components using Finite Element Analysis, PhD Thesis Queen Mary University of London

[Busfield. J. J. C et al, 2002] Contributions of Time Dependent and Cyclic Crack Growth to the Crack Growth Behavior of Non Strain-Crystallizing Elastomers, Rubber Chemistry and Technology, vol 75, Issue 4, pg 643

[Callister, W.D, 1994] An Introduction to Materials Science and Engineering, 3rd Edition. John Wiley and Sons, New York.

[Campion. R, 2003] Durability Review of Elastomers for Severe Fluid Duties, Rubber Chemistry and Technology, vol 76, pg 719

[Carleo. F, 2018] Modelling the Viscoelastic Behaviour of Rubber, PhD Thesis Queen Mary University of London

[Dal, H. Badienia, Y. Acikgoz, K. and Denli, F. A, 2019] A comparative study on hyperelastic constitutive models on rubber: State of the art after 2006, Constitutive Models for Rubber XI, pg 239

[Dassault Systemes, 2014] Dassault Systemes, 2014, Abaqus/CAE User's Guide. Abaqus v6.14 Documentation. Providence.

[De, D. K, 1994] The effect of particulate fillers on the strain energy function and the crack growth in rubbers, PhD Thesis Queen Mary University of London.

[Doi. M and Edwards. S. F, 1986] Theory of Polymer Dynamics, Clarendon Press

[Dluzneski. P. R, 2001] Dluzneski. P.R, 2001, Peroxide vulcanization of elastomers, Rubber Chemistry and Technology, vol 74, pg 451

[Dyna-Drill, 2010] Elastomers Brochure, Dyna-Drill® Technologies

[Dyna-Drill, 2013] Elastomer Temperature Compatibility Guide, Dyna-Drill® Technologies

[Dyna-Drill, 2015] DXT Product Sheet, Dyna-Drill® Technologies

[Eduard. T, Erich. K, 1934] Rubber like masses from butadiene hydrocarbons and polymerizable nitriles, US1973000A.

[Fernandez-Berridi, M, Gonzalez, N, Mugica, A. and Bernicot, C, 2006] Pyrolysis-FTIR and TGA techniques as tools in the characterization of blends of natural rubber and SBR, Thermochimica Acta, vol 444, pg 65

[Flory. P. J, 1953] Principles of Polymer Chemistry, Cornell University Press

[Gent. A. N et Al, 2001] Engineering with rubber. How to Design Rubber Components, 2nd Edition,

[Gent, A.N, Lindley, P.B and Thomas, A.G, 1964] Cut growth and fatigue of rubbers. I. The relationship between cut growth and fatigue, Journal of Applied Polymer Science, vol 8, pg 455

[Gent, A.N and Henry, A.W, 1967] On the tear strength of rubbers, Proceedings of the International Rubber Conference, pg 193

[Gent, A.N. and Tompkins, D.A, 1969] Nucleation and growth of gas bubbles in elastomers, Journal of Applied Physics, vol 40, pg 2520

[Gent, A. N, Razzaghi-Kashani, M, and Hamed, G. R, 2003] Why Do Cracks Turn Sideways?, Rubber Chemistry and Technology, vol 76, pg 122

[Gent. A. N, 2001] Engineering with Rubber: How to Design Rubber Components, 3rd ed., Carl Hanser Verlag GmbH & Co. KG

[Gough. J, 1805] Gough. J, 1805, A description of a property of Caoutchouc, or Indian rubber, Memories of the Literacy and Philosophical Society of Manchester, vol 1, pg 288

[Gough. J, 2000] Stress-Strain Behaviour of Rubber, PhD Thesis Queen Mary University of London

[Greensmith, H.W. and Thomas, A.G, 1955] Rupture of rubber. Part III. Determination of tear properties, Journal of Polymer Science, vol 18, pg 189

[Greensmith, H.W. 1956] Rupture of rubber IV. Tear properties of vulcanisates containing carbon black, Journal of Polymer Science, vol 21, pg 175

[Greensmith, H.W, 1960] Greensmith. H.W, 1960, Rupture of rubber. VIII. Comparisons of tear and tensile rupture measurements, Journal of Applied Polymer Science, vol 3, pg 183

[Groenewoud, W. M, 2001] Differential Scanning Calorimetry, Characterisation of Polymers by Thermal Analysis, pg 10

[Griffith. A. A, 1920] The Phenomena of Rupture and Flow in Solids, Philosophical Transactions of the Royal Society A

[Han. C et al, 2014] Thermal failure of rubber bushing of a Positive Displacement Motor: A study based on thermo-mechanical coupling, Applied Thermal Engineering, vol 67 pg 489

197

[Hamed, G. R, 2005] Tearing of Vulcanized Rubber, Rubber Chemistry and Technology, vol 78, issue 3, pg 548

[Hayashi, S, Sakakida, H, Oyama, M, and Nakagawa, T. 1991] Low-Temperature Properties of Hydrogenated Nitrile Rubber (HNBR), Rubber Chemistry and Technology, vol 64, pg 534

[Higuchi. T, Leeper. H.M and Davies. D.S, 1948] Determination of Tensile Strength of Natural Rubber and GR-S, Analytical Chemistry, vol 20, pg 1029

[Houwink, R, 1956] Slipping of molecules during the deformation of reinforced rubber, Rubber Chemistry and Technology, vol 29, pg 888.

[ISO, 1382:2012, 2012] ISO, 1382:2012, Rubber-Vocabulary, 2012

[Jerrams, S, Hanley, J, Murphy, N, Ali, H, 2008] Equi-Biaxial Fatigue of Elastomer: The Effect of Oil Swelling on Fatigue Life, Rubber Chemistry and Technology, vol 81, pg 638

[Joule. J.P, 1858] On some thermo-dynamic properties of solids, Philosophical Transactions of the Royal Society of London, vol 149, pg 91

[Kawabata. A and Kawai. H, 1977] Advanced Polymer Science, vol 24, pg 89

[Kadir, A, and Thomas, A. G, 1981] Tear Behaviour of Rubbers over a Wide Range of Rates, Rubber Chemistry and Technology, vol 54, pg 15

[Kim, D. Y, Kim, G. H, Nam, G. M, Kang, D. G and Seo, K. H, 2019] Oil Resistance and Low-Temperature Characteristics of Plasticized Nitrile Butadiene Rubber Compounds, Journal of Applied Polymer Science, vol 136, issue 32, pg 47851

[Kobatake, T, Kodama, K, and Hayashi, S, 1997] Improvement of Low-Temperature Flexibility of Hydrogenated Nitrile-Butadiene Rubber, Rubber Chemistry and Technology, vol 70, pg 839

[Kraus, G, Childers, C and Rollmann, K, 1966] Stress softening in carbon black reinforced vulcanizates. Strain rate and temperature effects, Rubber Chemistry & Technology, vol 39, pg 1530

[Lake, G.J. et al, 1969] Fracture mechanics of rubber, Proceedings 2nd International Conference on Fracture.

[Lake, G. J, 1970] Application of fracture mechanics to rubber articles, with particular reference to tyres, Proc. Int. Conference of Yield, Deformation and Fracture of Polymers.

[Lake, G. J, 1983] Aspects of fatigue and fracture of rubber, Progress of Rubber Technology, vol 45, pg 89

[Lake, G. J, 1995] Fatigue and Fracture of Elastomers, Rubber Chemistry and Technology, vol 68, pg 435

[Lake, G. J, 2003] Fracture mechanics and its application to failure in rubber articles, Rubber Chemistry and Technology, vol 76, pg 567

[Lake, G.J. and Thomas, A.G, 1967] The strength of highly elastic materials, Proceedings of the Royal Society A, vol 300, pg 108

[Lake. G. J, and Yeoh. O. H, 1987] Effect of Crack Tip Sharpness on the Strength of Vulcanized Rubbers, Journal of Polymer Science, vol. 25, pg 1157

[Lou, W, Zhang, W, Liu, X, Dai, W. and Xu, D, 2017] Degradation of hydrogenated nitrile rubber (HNBR) O-rings exposed to simulated servo system conditions, Polymer Degradation and Stability, vol 144, pg 464

[Mattson, B., Stenberg, B, Persson, S. and Ostman, E, 1990] Thermo-oxidative degradation of thick-walled rubber materials studied by IR-technique and computer X-ray topography scanning, Rubber Chemistry and Technology, vol 63, issue 1, pg 23

[Mattson, B. and Stenberg, B, 1992] Electrical conductivity of thermo-oxidatively-degraded EPDM rubber, Rubber Chemistry and Technology, vol 65, issue 2, pg 315

[Memmler. 1934] The Science of Rubber, Reinhold, New York

[Miehe. C, 1995] Discontinuous and Continuous Damage Evolution in Ogden-Type Large Strain Elastic Materials, European Journal of Mechanics, A/Solids 14

[Mooney, M. 1940] A theory of large elastic deformation, Journal of Applied Physics, vol 11, pg 582

[Mooney, M, and Wolstenholme, W. E, 1952] Modulus and Relaxation of Elastomers in Torsion At Low Temperatures, Rubber Chemistry and Technology, vol 25, pg 412

[Mooney, M, Wolstenholme, W. E, and Villars, D. S, 1944] Drift and relaxation of rubber, Journal of Applied Physics, vol 17, pg 576

[Mullins. L, 1947] Effect of stretching on the properties of rubber, Journal of Rubber Research, vol 16, pg 275

[Narynbek, U. K, Dragicevic, M, Albouy, P, Huneau, B, Beranger, A. and Heuillet, P, 2017] Strain-Induced Crystallization Ability of Hydrogenated Nitrile Butabiene Rubber, The 10th European Conference on Constitutive Models for Rubber (ECCMR X)

[Ogden. R. W, 1986] Recent Advances in the Phenomenological Theory of Rubber Elasticity, Rubber Chemistry and Technology, vol 59, pg 361

[Ogden. R. W and Roxburgh. D. G, 1999] A Pseudo-Elastic Model for the Mullins Effect in Filled Rubber, Proceedings: Mathematical, Physical and Engineering Sciences, vol 455, pg 2861

[O'Rourke, 2008] Reactive Ester Plasticizer for Elastomers, Rubber World, vol 239, pg 16

[Papadopoulos, I. C, 2006] Predicting the Fatigue Life of Elastomeric Components, PhD Thesis Queen Mary University of London

[Papadopoulos, I. C et al, 2008] Rate Transitions in the Fatigue Crack Growth of Elastomers, Journal of Applied Polymer Science, vol 109, pg 1900

[Rivlin. R. S, 1948] Large Elastic Deformations of Isotropic Materials, Philosophical Transactions of the Royal Society of London. Series A, Mathematical and Physical Sciences, vol 240, pg 459

[Rivlin. R. S and Thomas. A. G, 1953] Rupture of Rubber. Part 1. Characteristic Energy for Tearing, Journal of Polymer Science

[Schlumberger, 2004] PowerPak Steerable Motor Handbook, Schlumberger

[Severe, G and White, J. L, 2000] Physical properties and blend miscibility of hydrogenated acrylonitrile-butadiene rubber, Journal of Applied Polymer Science, vol 78, pg 1521

[Stenberg, B., Peterson, L.O., Flink, P. and Bjork, F, 1986] Effect of butyl rubber coating on accelerating aging of NR, Rubber Chemistry and Technology, vol 59, pg 70

[Tao, Y, 2018] Predicting the fatigue life and introducing structural health monitoring in cord reinforced rubber composites, PhD Thesis Queen Mary University of London

[Thomas. A. G, 1955] Rupture of rubber. Part II. The strain concentration at an incision, Journal of Polymer Science, vol 18, pg 177

[Thomas, A.G, 1958] Rupture of rubber. Part V. Cut growth in natural rubber vulcanizates, Journal of Polymer Science, vol. 31, pg 467

[Thomas, A.G, 1960] Rupture of Rubber. Part VI. Further experiments on the tear criterion, Journal of Applied Polymer Science, vol 3, pg 168

[Treloar. L. R. G, 1975] The Physics of Rubber Elasticity, 3rd Edition, Clarendon Press Hanser Gardner Publications Inc.

[Tsunoda, K, 2001] The role of visco-elasticity on the crack growth behaviour of rubber, PhD Thesis Queen Mary University of London

[Tunnicliffe. L, 2015] Particulate Reinforcement of Elastomers at Small Strains, PhD Thesis Queen Mary University of London

[Tunnicliffe. L and Busfield. J. J. C, 2015] Characterisation and Constitutive Modelling of Rubber Materials for Mud Motor Application, Report for Schlumberger Gould Research

[Van Amerongen, G. J, 1964] Diffusion in elastomer, Rubber Chemistry and Technology, vol 37, pg 1065

[Weitao, L., Weifang, Z., Xuerong, L., Wei, D. and Dan, X, 2017] Degradation of Hydrogenated Nitrile Rubber (HNBR) O-rings exposed to Simulated Servo Systems Conditions.

[Windslow. R. J and Busfield, J. J. C, 2017] Service life prediction under combined cyclic and steady state tearing, ECCMR X 2017, pg 295

[Windslow. R. J, 2018] Computational Modelling of Fracture Processes in Elastomeric Seals, PhD Thesis: Queen Mary University of London.

[Yeoh. O. H, 1990] Characterisation of Elastic Properties of Carbon Black Filled Rubber Vulcanizates, Rubber Chemistry and Technology, vol 63, pg 792

[Zhang. J et al, 2014] Failure analysis and finite element simulation of key components of PDM, Engineering Failure Analysis, vol 45, pg 15